U.S. DEPARTMENT OF ENERGY | Energy Efficiency & Renewable Energy

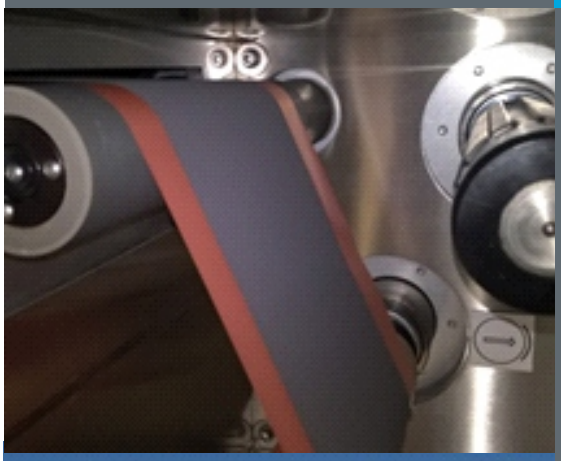

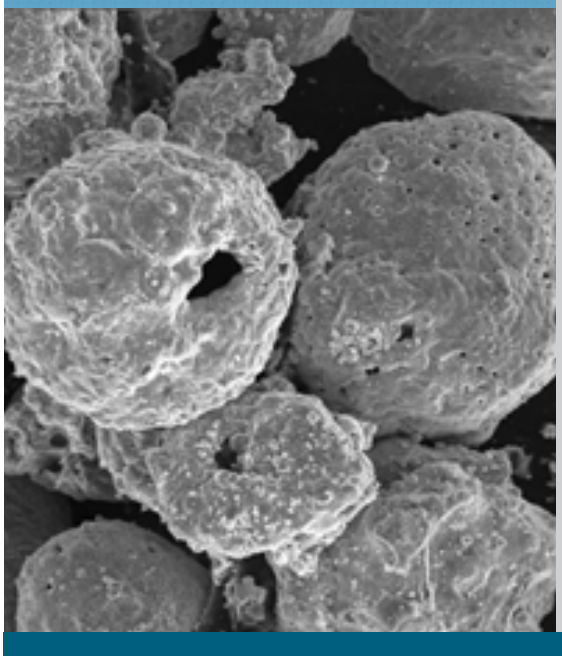

# FY 2016 Annual Progress Report for Advanced Batteries

August 2017

# CONTENTS

# FIGURES

# TABLES

# I. Introduction

## I.A. Vehicle Technologies Office Overview

The Department of Energy's (DOE's) Vehicle Technologies Office (VTO) develops advanced transportation technologies that would reduce the nation's use of imported oil. Technologies supported by VTO include electric drive components such as advanced energy storage devices (batteries and ultracapacitors), power electronics and drive motors, advanced structural materials, energy efficient mobility systems, advanced combustion engines, and fuels. VTO is focused on funding high-reward/high-risk research conducted by national laboratories, universities, and industry partners and promising improvements in critical components needed for more fuel efficient (and consequently, also cleaner-operating) vehicles.

During the past year, the U.S. government continued research and development (R&D) support of plug-in electric vehicles (PEVs) such as plug-in hybrids, extended range electric vehicles, and all-electric vehicles. One of the objectives of VTO is to enable U.S. innovators to rapidly develop the next generation of technologies that achieve the cost, range, and charging infrastructure necessary for the widespread adoption of PEVs. Significant penetration of PEVs into the transportation sector could reduce U.S. dependence on foreign oil, cut back on emissions and mitigate the negative economic impacts associated with crude oil price fluctuations, thus enhancing U.S competitiveness in the world.

Key stakeholders for the VTO R&D activities include universities, national laboratories, other government agencies and industry including automakers, battery manufacturers, material suppliers, component developers, private research firms, and small businesses. VTO works with key U.S. automakers through the United States Council for Automotive Research (USCAR)—an umbrella organization for collaborative research consisting of Fiat Chrysler LLC, the Ford Motor Company, and the General Motors Company. Collaboration with automakers through the US DRIVE (Driving Research and Innovation for Vehicle Efficiency and Energy Sustainability) Partnership enhances the relevance and the potential for success of the overall research platform.

An important prerequisite for the electrification of the nation's light duty transportation sector is development of more cost-effective, longer lasting, and more abuse-tolerant PEV batteries. In fiscal year 2016 (FY16), the DOE VTO battery R&D funding was $103 million. The R&D focus continued to remain on the development of high-energy batteries for PEVs and very high-power devices for hybrid vehicles. This document summarizes the progress of VTO battery R&D projects supported in FY 2016. An electronic version of this report is accessible at https://energy.gov/eere/vehicles/vehicle-technologies-office-annual-progress-reports.

VTO competitively awards funding through funding opportunity announcement (FOA) selections, and projects are fully funded through the duration of the project in the year that the funding is awarded. The future direction for direct□funded work at the national laboratories is subject to change based on annual appropriations.

## I.B. Vehicle Technologies Battery R&D Overview

### I.B.1. DOE Battery R&D Goals and Technical Targets

To meet current VTO objectives, batteries, power electronics, motors, lightweight materials and vehicle structures must see dramatic advances. Accordingly, performance and cost targets have been established for all the key technical areas associated with a PEV. Achieving those targets will meet the needs for a range of vehicle types – including plug-in hybrids as well as short and long range all-electric vehicles. Some of the technology targets, derived from computer modeling as well as from hardware-in-the-loop simulation of batteries operating in PEVs under multiple drive cycles, are shown in Figure I-1.

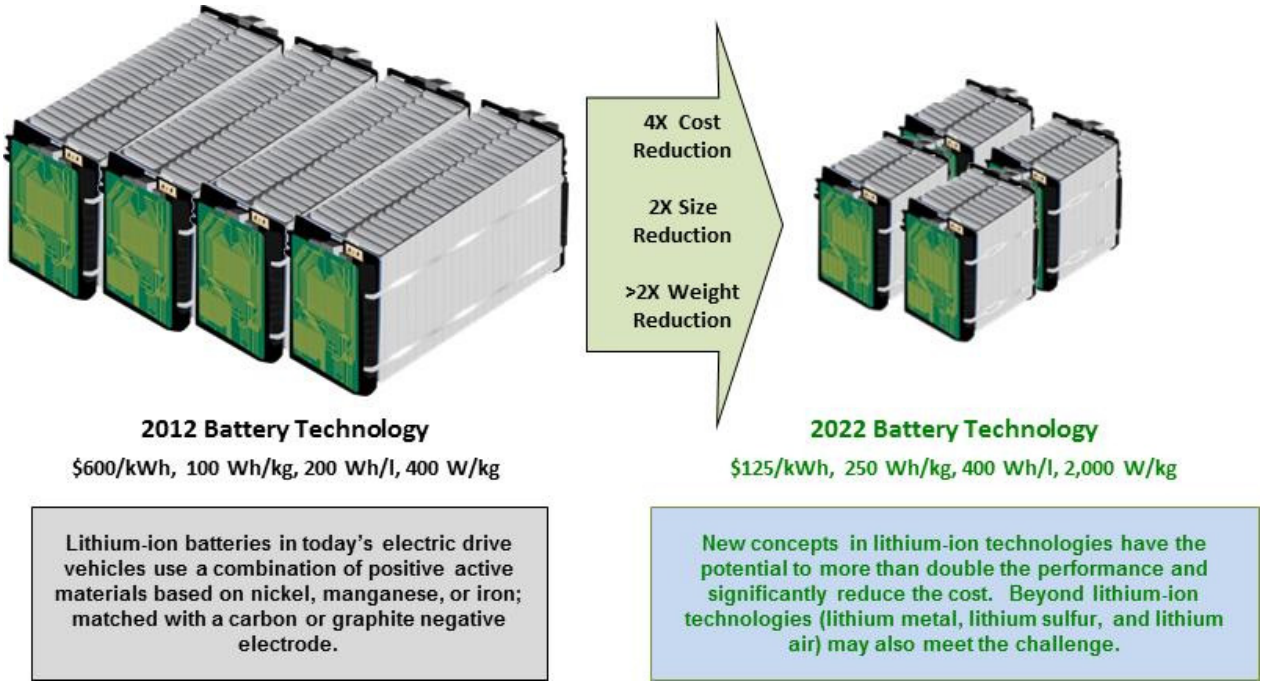


Figure I-1: Battery advancements needed to enable a large market penetration of PEVs

## I.B.2. DOE Battery R&D Plans

The VTO battery R&D effort attempts to advance battery development to improve the market penetration of electric vehicles. Program targets accordingly focus on overcoming technical barriers. Those targets include: (1) a significantly reduced battery cost, (2) increased battery performance (power, energy, and durability), (3) reduced battery weight and volume, and (4) increased battery tolerance to abusive conditions such as short circuit, overcharge, and crush.

Current battery technology performs far below its theoretical limits. For example, in the near term, even with existing lithium-ion technology, there is an opportunity to more than double the battery pack energy density (from 125 Wh/kg to 250 Wh/kg) by using new high-capacity cathode materials, higher voltage electrolytes, and high capacity silicon or tin-based intermetallic alloys to replace graphite anodes. Despite some recent promising advances, more R&D is needed to achieve the performance and lifetime requirements for deploying those advanced technologies in PEVs.

Over the longer term, battery chemistries "beyond lithium-ion" – i.e., solid state, lithium metal, lithium-sulfur, magnesium-ion, lithium-air, and certain other advanced chemistries – offer the possibility of specific energy levels significantly greater than those of current lithium-ion batteries and also offer potentially reduced battery costs. However, major shortcomings in cycle life, power density, energy efficiency, and/or other critical performance parameters (as well as cost) currently hinder the commercial introduction of state-of-the-art "beyond lithium-ion" battery systems. Innovative breakthroughs would be needed for those new battery technologies to enter the market. To facilitate such breakthroughs, VTO launched a new initiative entitled the "Battery500 Consortium" in 2016. The VTO Battery500 Consortium's goal is to develop and demonstrate technologies that achieve 500 Wh/kg and 1000 electric vehicle (EV) charging cycles.

Increases in energy density described above are crucial to achieving VTO cost and performance targets. Additional R&D efforts, including those related to pack design optimization and simplification, manufacturing improvements at cell/pack levels, reduced production cost for battery materials, and novel thermal management technologies will also help reduce battery cost. The associated technical challenges and potential solutions to those challenges are listed in Table I- 1.

### Table I- 1: Major Lithium-Ion Technology Technical Challenges and Potential Pathways

| Barrier/Challenge | Potential Solutions |
|---|---|
| • Reduce cost and improve the performance of lithium-ion battery technology | • Improve material and cell durability<br>• Improve energy density of active materials<br>• Reduce inactive material<br>• Improve design tools/design optimization<br>• Improve manufacturing processes |
| • Develop higher energy battery technology such as next generation lithium-ion, solid state, lithium metal, lithium-sulfur and lithium-air<br>• Issues with these materials include poor cycle life, low power, low efficiencies, and safety | • Improve electrolyte/separator combinations to reduce dendrite growth for Li metal anodes<br>• Advanced material coatings<br>• New ceramic, polymer, and hybrid structures with high conductivity, low impedance, and structural stability<br>• Establish a consortium of industry, universities, and national laboratories to collaboratively investigate innovative solutions |
| • Improve abuse tolerance performance of battery technology | • Non-flammable electrolytes<br>• High-temperature melt integrity separators<br>• Advanced materials and coatings<br>• Improve understanding of reactions<br>• Modeling and simulation for safer designs<br>• Battery cell and pack level innovations such as improved sensing, monitoring, and failure-avoidance strategies such as thermal management systems |
| • Reduce recharge time and increase utility of EVs through Extreme Fast Charging (XFC) | • Higher power density and lower cost active materials and electrode designs for XFC applications<br>• Active battery materials tolerant to high temperatures<br>• New cell and pack designs optimized for XFC<br>• Innovative cooling systems<br>• Innovative/adaptive battery charging algorithms to preserve and prolong life |

## I.B.3. Energy Storage R&D Programmatic Structure

VTO's energy storage effort includes multiple activities, ranging from focused fundamental materials research to prototype battery cell development and testing. The R&D activities can involve either shorter-term pre-competitive research by commercial developers or exploratory materials research generally spearheaded by national laboratories and universities. These consist of five major program elements which are inter-related and complementary, namely:

- Advanced Battery Development

- Battery Testing, Analysis, and Design
- Applied Battery Research (ABR)
- Manufacturing and Process Development
- Advanced Battery Materials Research (BMR)

The *Advanced Battery Development* R&D activity focuses on the development of robust battery cells and modules to significantly reduce battery cost, increase life, and improve its performance. It takes place in close partnership with the automotive industry, partially through a cooperative agreement with the United States Advanced Battery Consortium (USABC). In FY 2016, the USABC supported nine cost-shared contracts with developers to further the development of batteries for PEVs and Hybrid Electic Vehicles (HEVs). DOE also works in close collaboration with USABC to develop battery and ultracapacitor requirements for various vehicle types[1] and test procedures.[2] In addition to the USABC projects, DOE often directly supports battery and material suppliers via contracts administered by the National Energy Technology Laboratory (NETL). In FY 2016, NETL managed 20 such battery R&D contracts. (In this report, Chapter II focuses on the battery development program.)

The *Battery Testing, Analysis, and Design* activity is complementary to the battery development program. High level projects pursued in this area include performance, life and abuse testing of contract deliverables, laboratory- and university-developed cells, and benchmark systems from industry; thermal analysis, thermal testing and modeling; development of new test procedures and maintenance of current test procedures; development of tools for the computer aided engineering of batteries; requirements analyses; cost modeling; other energy storage use and life studies; and recycling studies of core materials. Battery technologies are evaluated according to USABC-stipulated Battery Test Procedures. The manuals for the relevant applications (PEV and HEV) are available online[3,4,5]. Benchmark testing of an emerging technology is performed to remain abreast of the latest industry developments. (In this report, Chapter III focuses on the Battery Testing, Analysis, and Design activity.)

The *Applied Battery Research* (ABR) activity is focused on the optimization of next generation, high-energy lithium-ion electro-chemistries that incorporate new battery materials. It emphasizes identifying, diagnosing, and mitigating issues that impact the performance and lifetime of cells constituted of advanced materials. It investigates the interaction between cell components (cathodes, anodes, electrolytes, binders, conductive additives, and separators) as they impact performance and life. Typical issues associated with incorporating newly developed material into working PEV cells can include: (1) inadequate power capability needed to meet PEV requirements, (2) insufficient cycle life stability to achieve the 1,000 to 5,000 “charge-depleting” deep discharge cycles, and (3) poor performance at lower temperatures. ABR is conducted by a team that includes six national labs and several universities. (In this report, Chapter IV lists all the projects under this activity.)

The Battery *Manufacturing and Process Development* activity complements the ABR activity. It involves R&D at the national labs on systematic material engineering and customized scaled processes to produce high quality material at kilogram-levels. It also involves in-line analysis methods of quality control to detect electrode flaws and contaminants and development of new atomic layer deposition techniques which would be more amenable to high-volume manufacturing. It also includes industry partnerships to develop novel electrode/cell manufacturing technologies utilizing proven as well as emerging battery chemistries, reducing the ratio of inactive materials to active materials, higher process yields, cost-effective drying, novel separator coatings, commercially scalable prelithiation methods, and novel battery architectures. (The projects in this activity are also listed within Chapter IV.)

---

[1] See http://uscar.org/guest/article_view.php?articles_id=85

[2] See http://uscar.org/guest/article_view.php?articles_id=86

[3] Battery Test Manual for Electric Vehicles, U.S. Department of Energy, Vehicle Technologies Office, Revision 3, INL/EXT-15-34184, June 2015. See http://www.uscar.org/commands/files_download.php?files_id=405

[4] FreedomCAR Battery Test Manual For Power-Assist Hybrid Electric Vehicles, October 2003, DOE/ID-11069. See http://www.uscar.org/commands/files_download.php?files_id=58

[5] United States Council for Automotive Research, RFP and Goals for Advanced Battery Development for Plug-in Electric Vehicles. See http://www.uscar.org/guest/teams/12/U-S-Advanced-Battery-Consortium

The *Advanced Battery Materials Research* (BMR) activity addresses fundamental issues of materials and electrochemical interactions associated with lithium batteries. It develops new/promising materials and uses advanced material models to discover them and their failure modes, as well as scientific diagnostic tools/techniques to gain insight into why they fail. Battery chemistries are monitored continuously with periodic substitution of more promising components based on input from activity participants, outside experts, and from the overall assessment of world-wide battery R&D. This work is carried out by a team of researchers located at several national labs, universities, and commercial entities. It also studies issues critical to the realization of beyond lithium-ion technologies, such as solid-state technology, lithium metal systems, lithium sulfur, and lithium air. Some of the main areas of focus include new methods to understand and stabilize lithium metal anodes; to contain Li polysulfides to enable the use of sulfur cathodes; and to develop electrolytes that support lithium air and Li/sulfur cells. The newly-started VTO *Battery500* projects are to be managed in conjunction with this program element. (In this report, Chapter V lists all the projects that are part of the Advanced Battery Materials Research (BMR) activity and Chapter VI introduces the *Battery500* program.)

The *Extreme Fast Charging (XFC)* activity was initiated in FY 2016 as a means to understand the cost and technical barriers associated with implementing the 350kW direct current fast-charging of EVs. It is necessary to reduce EV refueling time through XFC to levels comparable with internal combustion engine vehicles (ICEVs) to enable the widespread adoption of battery EVs. The convenience brought to consumers by XFC technology leads to the increased utility of EVs, which in-turn provides consumers with greater choices. A team from three national laboratories, in consultation with automakers, battery developers, EVSE manufacturers, and utilities has identified R&D needs for XFC. Those R&D areas include (but are not limited to) battery materials research, advanced electrode design, advanced cooling systems, enhanced interoperability of vehicle to electric vehicle supply equipment (EVSE), and infrastructure planning. (Because this activity is just starting during FY2017, its projects will be reported in the next year's annual progress report.)

Several *Small Business Innovation Research* (SBIR) contracts are also supported by VTO, in addition to the R&D described above. SBIR projects have been the source of new ideas and concepts. These SBIR projects are focused on the development of new battery materials and components. (A short list of the energy storage SBIR project-starts is included at the end of Chapter II.)

The Electrochemical Energy Storage Roadmap describes ongoing and planned efforts to develop electrochemical storage technologies for PEVs and can be found at the EERE Roadmap page http://energy.gov/eere/vehicles/downloads/us-drive-electrochemical-energy-storage-technical-team-roadmap.

VTO has established extensive and comprehensive ongoing coordination efforts in energy storage R&D across all of the DOE complex and with other government agencies. Coordination within DOE and with other government agencies is a key attribute of the VTO energy storage R&D efforts. VTO coordinates efforts on energy storage R&D with the DOE Office of Science, and the DOE Office of Electricity. Coordination and collaboration efforts also include membership and participation in the Chemical Working Group of the Interagency Advanced Power Group (IAPG), active participation in program reviews and technical meetings sponsored by other government agencies, and participation of representatives from other government agencies in the contract and program reviews of DOE-sponsored efforts. DOE also coordinates with the Department of Army's Advanced Vehicle Power Technology Alliance, the Department of Transportation/National Highway Traffic Safety Administration (DOT/NHTSA), the Environmental Protection Agency (EPA), and with the United Nations Working Group on Battery Shipment Requirements. Additional international collaboration occurs through a variety of programs and initiatives. These include: the International Energy Agency's (IEA's) Hybrid Electric Vehicles Technology Collaboration Program (HEV TCP), the G8 Energy Ministerial's Electric Vehicle Initiative (EVI), and bilateral agreements between the U.S. and China.

## I.B.4. Recent Advanced Battery R&D Highlights

- **The world's leading market for EVs:** U.S. is a leading market for EVs and is producing some of the most advanced PEVs available today. Consumer excitement and interest in PEVs are growing, despite recent drops in gasoline prices. In 2016, the U.S. PEV sales jumped 37% from 2015 levels and there were 30 PEV models being offered for retail sale. There were 560,000 PEVs on U.S. roadways at the end of 2016.

- **Successful commercial applications:** VTO has a successful track record of planning and executing R&D on critical battery technologies that move into commercial applications. Hybrid and electric vehicles on the market from GM, Ford, Fiat Chrysler, BMW, Mercedes, and Land Rover are using lithium-ion technologies which were developed under DOE VTO projects.
- **Lithium-ion capacitors (Maxwell Technologies Inc./USABC):** In 2016, Maxwell Technologies announced the first commercial application of lithium-ion capacitors (LIC) for rapid energy regeneration in a trolley system for the largest Chinese rail manufacturer (the China Railway Rolling Stock Corporation). This technology was initially developed under a USABC program and is based on an asymmetric supercapacitor LIC, in which one electrode stores charge exclusively like a classical capacitor while the other stores lithium ions like in a battery. This hybrid of two technologies provides several times the capacity of a normal supercapacitor while also retaining excellent power capabilities. (See Figure I-2.) The USABC project also launched Maxwell to start in the making of large-scale supercapacitors in a pouch format. Maxwell's K2 2.85V 3400F cells, available since 2014, offer 17% more power and 23% more energy than contemporary state of the art cells. The K2 2.85V ultracapacitor was recognized as one of EDN's Hot 100 Products of 2014 and now has found commercial application in transportation.

**Figure I-2: LICs provide better energy density than conventional supercapacitors. Where energy is important this can reduce the storage device's volume. The unit on the right, developed in the USABC project, is half the size/weight, but twice the power and three times the energy of the standard pack to the left**

- **Battery Cost Reduction:** The 2016 DOE PEV battery cost reduction milestone of $250/kWh was accomplished. DOE-funded research has helped reduce the current cost projection for an EV battery (for three DOE-funded battery developers) to an average $245 per kilowatt-hour of useable energy. This cost projection is derived by inputting material costs and cell and pack designs from those developers into ANL's peer-reviewed public domain Battery Production and Cost model (BatPaC). The cost projection is based on a production volume of at least 100,000 batteries per year. The cost is derived for batteries meeting DOE/USABC system performance targets. The battery development projects focus on high voltage and high capacity cathodes, advanced alloy anodes, and process improvements. Details of the cost model inputs are available in spreadsheets and also included in DOE quarterly reports. DOE's goal is to continue to drive down battery cost to $125/kWh by 2022.
- **Advanced Cell Development (Amprius/USABC):** Silicon has significant potential as a new anode material since it offers nearly 10 times the theoretical capacity of graphite which is currently used in lithium-ion batteries for PEVs. However, when intercalated with lithium ions, silicon swells upto four times its volume, causing mechanical and chemical failures and an inadequate cycle life. Amprius, Inc. of Palo Alto, California has developed a unique silicon structure – nanowires grown directly on the current collector without binders – which addresses swelling by enabling silicon to expand and contract internally. In a multi-year USABC project Amprius is developing cells sized for PEV applications that are expected to meet DOE targets for energy density and possibly cycle life. The project's first-year 2 Ah cells completed more than 550 cycles and exceeded many of the USABC's power and energy targets. (See Figure I-3.)

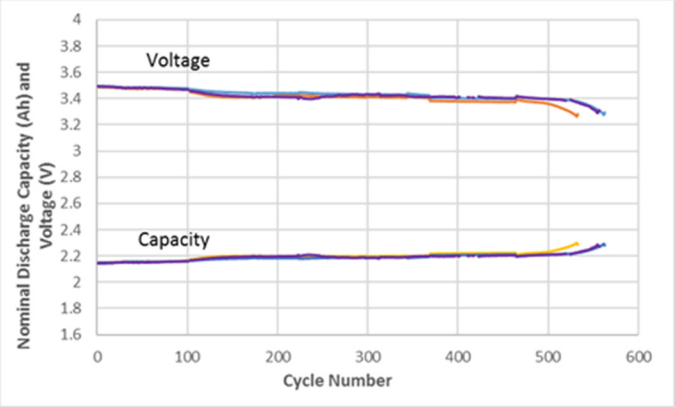


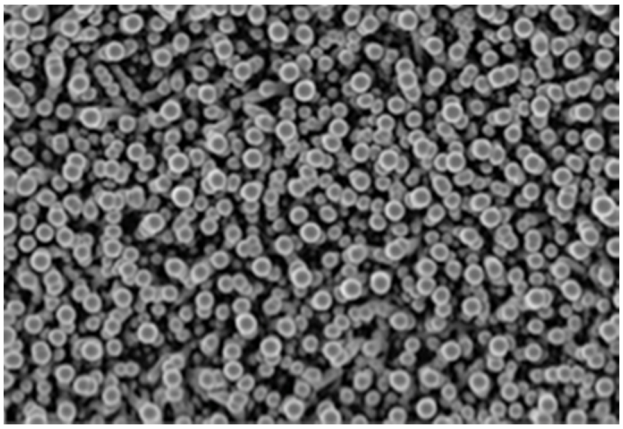

**Figure I-3: Amprius cell performance: (top) the voltage drift past 500 cycles was less than 4%, and (bottom) a top-down microscopic view of Amprius silicon nanowire structure**

- **Advanced Anode R&D (XG Sciences, Inc):** In another R&D effort to utilize the high capacity of silicon anodes while improving their generally poor cycling stability, XGS Sciences of Anne Arbor, Michigan has developed XG SiG™, a Si/graphene composite anode material that features a nano-structured material design and low-cost, scalable manufacturing process utilizing graphene to mitigate the cycling stability issues of Si in lithium-ion batteries. XGS' optimization of the Si/graphene composite structure delivers high capacity (600 mAh/g), high first cycle efficiency (~85%), and cycling stability of >85% at 1,000 cycles in 2 Ah cells with an NCA cathode produced and tested at A123 Systems. (See Table I-2). Scalable Si/graphene dispersion and coating processes and the low cost XGS manufacturing process were thus ready for transition to mass production. (See Figure I-4.)

### Table I-2: 2 Ah Pouch Cell Cycling Data (600 mAh/g Si/Graphene Anode/NCA Cathode, 165 Wh/kg)

| Cycle | 0 | 250 | 500 | 750 | 1,000 |
|---|---|---|---|---|---|
| % Capacity | 100% | 90% | 88.5% | 87.5% | 87% |

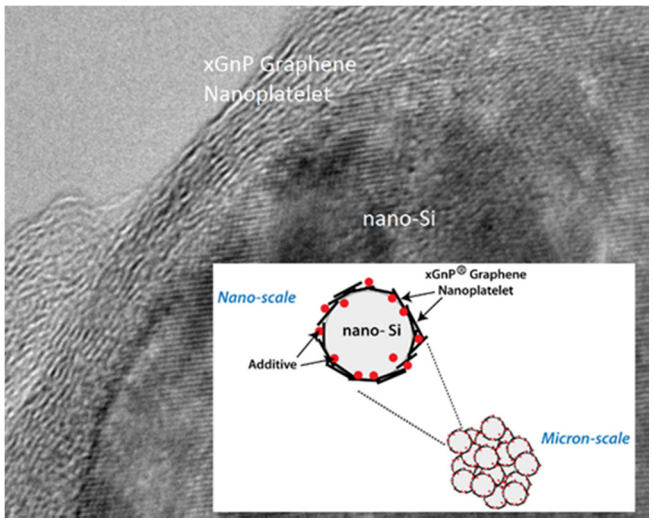


Figure I-4: Transmission electron microscope image showing Si/graphene composite material in the region of the graphene Si interface and graph illustrating nano-structured material design (inset)

- **Lower Cost, Enhanced Safety Separator Technology (ENTEK Membranes/USABC):** Separator membrane is an essential component of lithium batteries allowing ion transport while keeping the positive and negative electrodes from touching. Separators impact performance, safety, and cost. To enhance the features of the separator, ENTEK of Portland, Oregon has developed an innovative approach of incorporating nanoparticle filler into the bulk structure of the separator and applying an alumina nanoparticle coating on top of the separator. Figure I-5 illustrates that this nanoparticle alumina coating approach requires 60% less coating mass compared to conventional coatings (with ~0.5 µm diameter particles) to achieve high temperature dimensional stability (i.e., less than 5% shrinkage in the separator at temperatures above the melting point of the base polyolefin separator). The nanoparticle alumina coatings enhance safety features, improve energy density, and reduce cost. Additionally, ceramic coatings may allow for a higher voltage stability (up to 4.9 V), which will improve the energy density of lithium-ion cells. ENTEK is collaborating with Farasis Energy Inc. to demonstrate this advanced separator technology in high voltage lithium-ion PEV batteries.

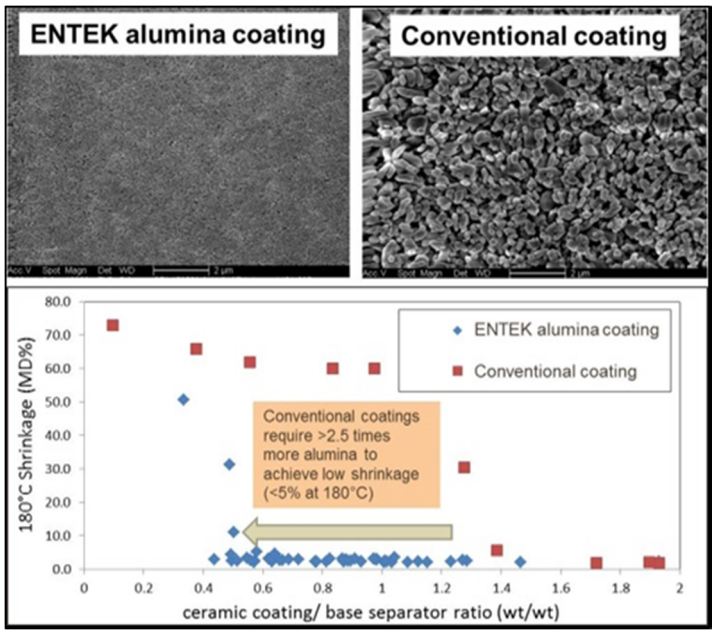


Figure I-5: Coating with nano-alumina allows for a substantial reduction in coat weight required to achieve high temperature dimensional stability which may improve safety features in the separator, reduce cost, and improve energy density

- **Advanced Processing R&D (Oak Ridge National Laboratory)**: For making lithium-ion batteries, the formation of electrolyte wetting and anode passivation film (called solid electrolyte interphase, or SEI) are necessary, but expensive due to long wetting and SEI formation periods. It is estimated that

the wetting/formation cycling cost at $7.5/kWh is much higher than $2.2/kWh for electrode processing. This process may take up several days, depending on the cell manufacturer, require large number of cyclers, large footprint, and intense energy consumption for the cyclers and environmental chambers. Researchers at Oak Ridge National Laboratory (ORNL) have developed a new fast formation method to generate the SEI in lithium-ion batteries consisting of graphite and $LiNi_{0.5}Mn_{0.3}Co_{0.2}O_2$ as the anode and cathode, respectively. The new formation method is shown in Figure I-6 (top, orange line) and is compared with a baseline method (top, blue line). The baseline method consists of a series of full charge and discharge cycles at a constant C-rate without any interruption between the lower and upper cut-off voltages (2.5 – 4.2 V). The new method, however, involves repeated cycling within a high state-of-charge region (4.2 – 3.9 V) after the first charge until the last cycle where a full discharge takes place. Compared to the baseline, the new method reduced formation time from more than 9 days to less than a day. The new method at ORNL resulted in similar capacity retention compared to the baseline (Figure I-6, bottom). Thus, the new method not only reduced the formation time greatly, it also resulted in similar cell capacity retentions, which could significantly increase production throughput and reduce capital equipment savings for new battery plants.

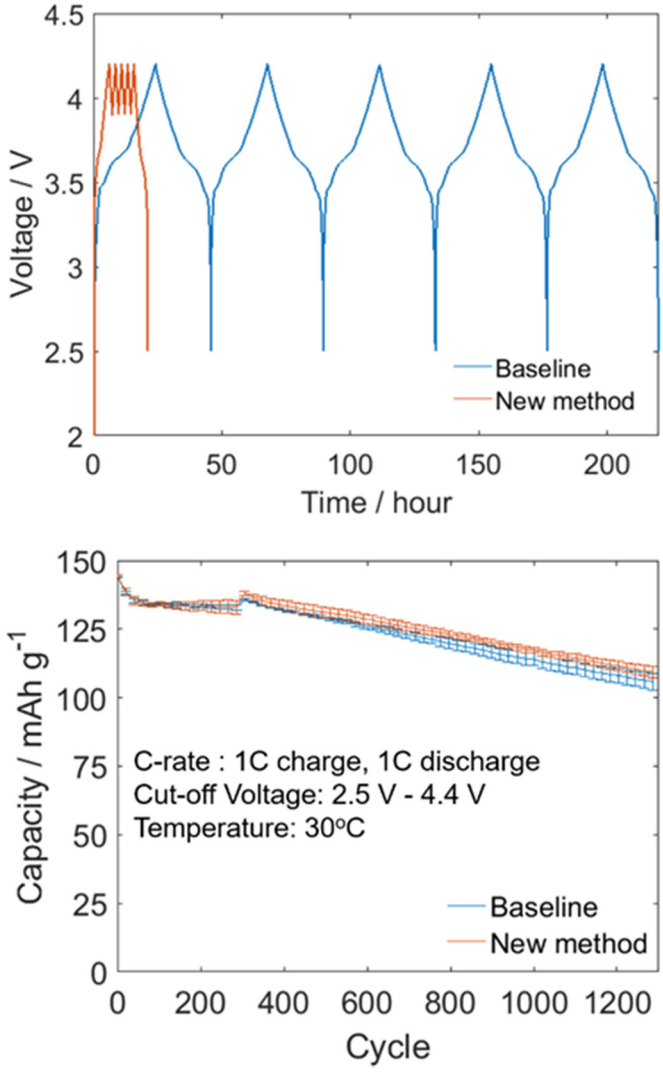


**Figure I-6: Top graph portrays the baseline and new formation method illustrated as voltage profiles, showing ten times faster formation time for the new method. Bottom graph exhibits capacity after the new formation retained more than one after the baseline. The error bars correspond to 90 percent confidence intervals**

- **Battery Safety R&D (National Renewable Energy Laboratory):** NREL's Battery Internal Short Circuit (ISC) Device, the first sensor able to accurately simulate an internal short circuit within a lithium-ion cell, received the prestigious R&D 100 Award in 2016. Internal short circuits in lithium-ion batteries, usually caused by latent flaws during manufacturing that can escape detection during

normal screening. While these defects enter the battery cell coming off the assembly line, significant time can elapse before a defect surfaces as internal short circuit and later fails catastrophically via thermal runaway (e.g., the Boeing Dreamliner and Samsung Note 7 battery failures). To evaluate if new battery designs and materials can improve tolerance to internal short circuits, the battery industry uses external methods not representative of internal short circuit. The NREL device, shown in Figure I-7, allows battery developers to evaluate the effectiveness of new materials and cell designs to assess and address their hazards and bring safer batteries to market. CT imaging (Figure I-8) provides unprecedented insights into the failure mechanisms in 18650 cells after initiation of the NREL ISC Device. An improved version of battery ISC Device has been used by five battery manufacturers to evaluate the stability of lithium iron phosphate cathodes, combustion gas evaluation after an internal short circuit, effectiveness of non-flammable electrolytes and shut-down separators, fusible tabs, vent designs, and propagation testing. In 2016, NREL received over 1,000 orders from NASA and three different battery manufacturers for the ISC Device to improve safety of lithium-ion batteries.

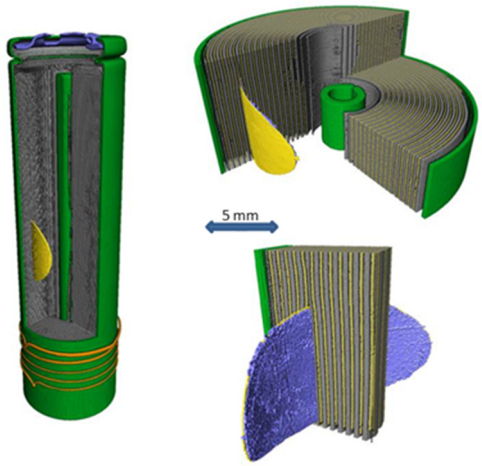


**Figure I-7: Computerized tomography (CT) rendering of Battery ISC Device inside a lithium-ion battery. The yellow and blue portion of the image is the ISC device in an 18650 cell. Courtesy: Donal Finegan, University College of London**

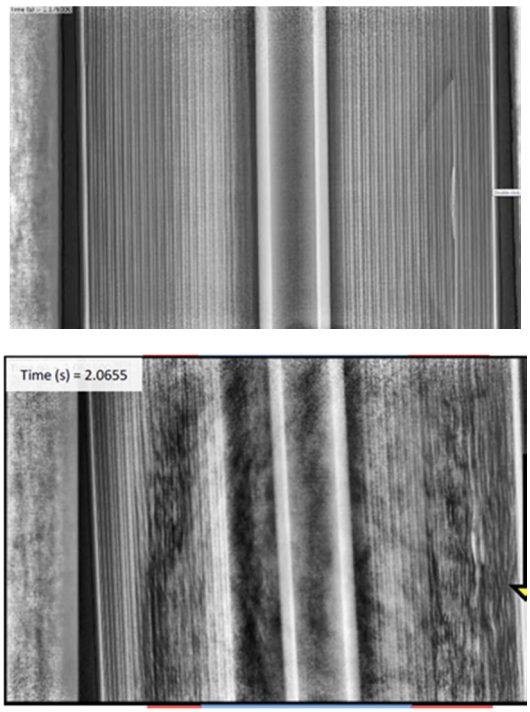


**Figure I-8: Computerized tomography scan of 18650 cell, with the Battery ISC Device implanted on the right side of the cell, shows cell before going into thermal runaway (top) and while going into thermal runaway (bottom)**

- **Advanced Cathode R&D (TIAX, LLC):** TIAX has developed long-life lithium-ion cells which exceed DOE energy and power targets (200 Wh/kg and 800 W/kg pulse power, respectively) for PHEV40 battery cells. The technology pairs a high capacity version of TIAX's proprietary high energy and high power CAM-7® cathode material with a blended anode containing Si and graphite materials. Prototype 18650 cells, with CAM-7 and the Si-based blended anode were built and tested, delivering higher specific energy and power than baseline cells employing CAM-7/graphite. (See Figure I-9.) The specific energy for the program deliverable cell is projected to reach 220 Wh/kg upon scaling to state-of-the-art 18650 cell hardware and to 250 Wh/kg upon scaling to 15 Ah pouch cells, which is substantially higher than the 100-160 Wh/kg typical of current PHEV lithium-ion cells. Moreover, these cells also achieved excellent cycle life, with 85% capacity retention after 1000 cycles in on-going cycle life testing. By simultaneously meeting the PHEV40 power and energy targets and providing long life (although below the 5,000 cycle DOE/USABC cycle life target), resulting in a lithium-ion battery system that can be smaller, lighter, and less expensive than current state-of-the-art lithium-ion batteries.

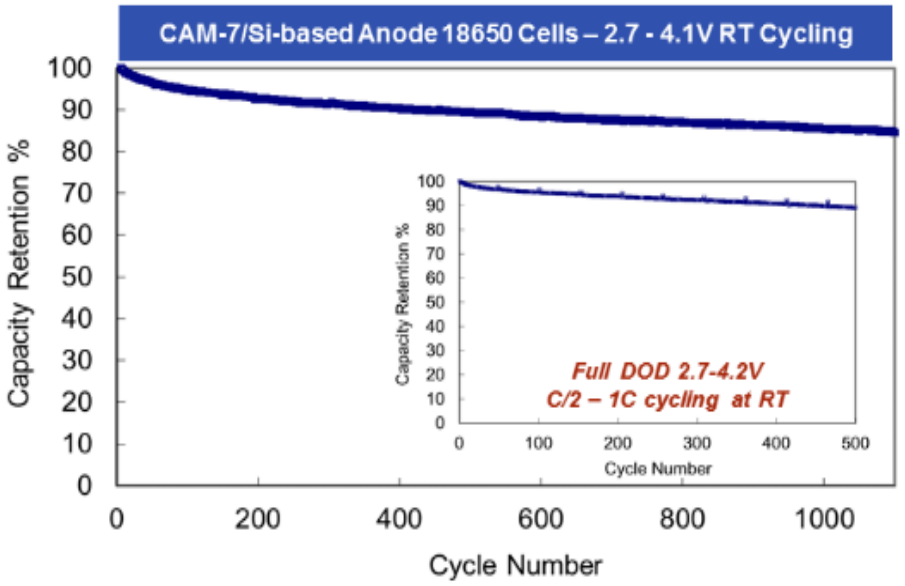


Figure I-9: Excellent cycle life was achieved in the program demonstration 18650 cells with higher capacity CAM-7 and blended Si-based anode

- **Advanced Electrolyte R&D (Daikin Industries of North America):** The electrolyte is an important component in lithium-ion batteries impacting cost, performance, energy density, life and safety. Increasing the voltage window of state-of-the-art lithium-ion cells increases energy density, but negatively impacts the cell's life and safety. Daikin has shown that a typical hydrocarbon electrolyte is not suitable for battery operation above 4.35 V due to gassing and decomposition of the electrolyte. Daikin development has led to the introduction of fluorocarbons into the conventional electrolyte, allowing it to cycle up to 4.5 V in 1 Ah NMC(111)/graphite cells. Cycle life testing (25°C) was initiated in multiple cell chemistries to determine whether cell failures at higher voltages occur independent of cell chemistry. Figure I-10 shows the cycle life of hydrocarbon and fluorocarbon electrolytes in 1 Ah NMC/Graphite cells at 4.2, 4.35, and 4.5 V. Both the hydrocarbon and fluorocarbon electrolytes are stable at 4.2 V, the hydrocarbon electrolyte at 4.35 is not stable after 150 cycles while the fluorocarbon electrolyte is stable at 4.35 V beyond 250 cycles. At 4.5 volts, the hydrocarbon electrolyte is not stable while the fluorocarbon electrolyte is stable beyond 250 cycles. When cycling NMC/graphite cells at 4.5 V, a capacity increase of about 15% is realized, but the hydrocarbon electrolyte begins to fail after several cycles while more than 250 cycles were achieved with the fluorocarbon electrolyte with 80% capacity retention.

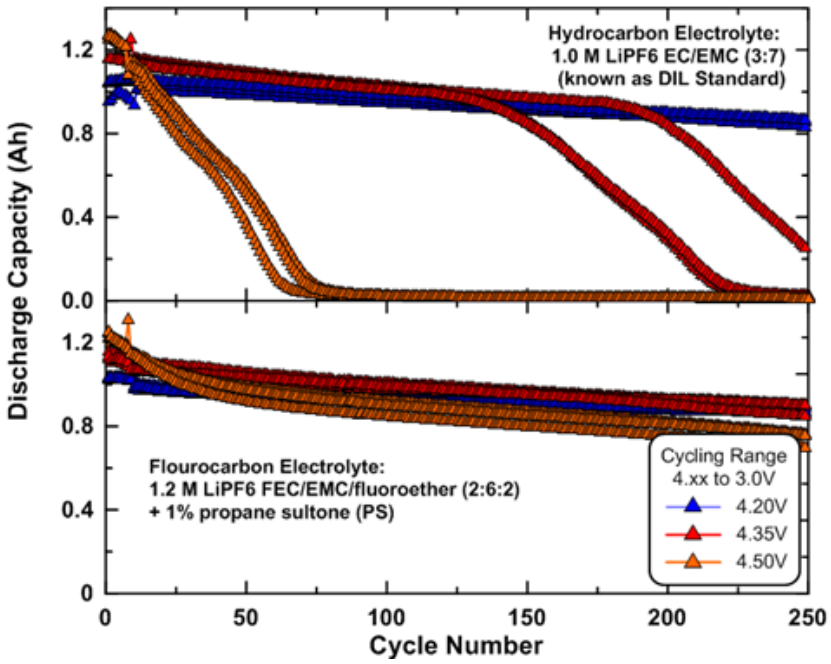


**Figure I-10: Cycle life showing capacity of 1Ah NMC/graphite cells with both standard carbonate (top) and fluorinated (bottom) electrolytes at cycled at a Vmax of 4.2, 4.35, and 4.5V**

- **Advanced Electrolyte R&D (Silatronix):** All automotive lithium-ion batteries use electrolytes that contain lithium hexafluorophosphate ($LiPF_6$). Although $LiPF_6$ has many advantages, a major disadvantage is that under both high temperature and high charge voltage conditions, in the (inevitable) presence of water, $LiPF_6$ in traditional carbonate solvents decomposes and creates highly reactive and destructive compounds. When carbonate/$LiPF_6$ electrolytes break down inside of a battery, it leads to gas generation, side reactions, and electrolyte consumption – thus reducing life and capacity. Silatronix of Madison, Wisconsin, improving upon technology licensed from Argonne National Laboratory, has developed a commercially available organosilicon material called OS3. This material has proven to inhibit $LiPF_6$ breakdown. OS3 benefits are particularly notable during high temperature operations when traditional electrolytes decompose. OS3 provides benefits to lithium-ion batteries in concentrations of just 2-5%. The minimal amount of material needed to impact cell performance makes OS3 cost-effective for all lithium-ion applications. Tests have demonstrated that OS3 material can reduce cell swelling in a lithium-ion nickel-manganese-cobalt (NMC) cell. Figure I-11 shows how adding OS3 material can significantly extend battery life during high temperature operations in lithium-cobalt-oxide (LCO) cells. OS3 material is currently under evaluation for use by most major lithium-ion battery manufacturers. Silatronix continues to develop organosilicon chemistry to enable the next generation of high voltage, high energy density EV batteries.

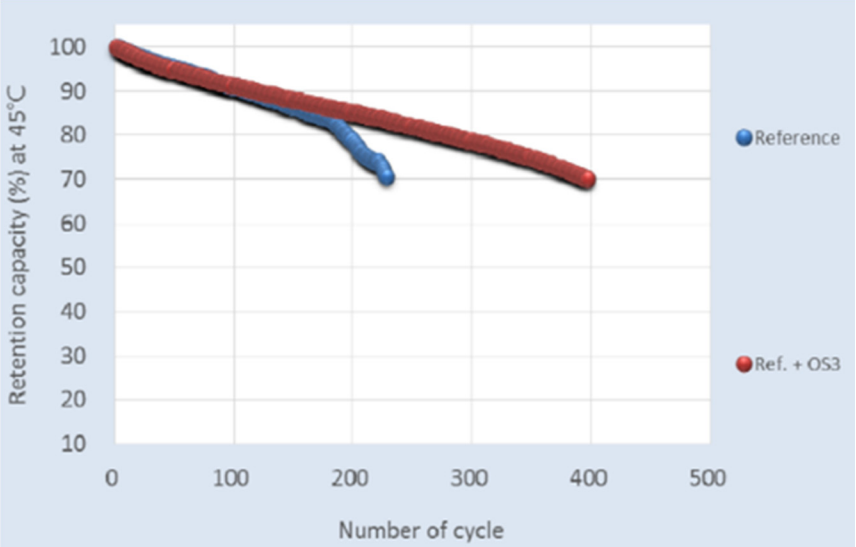


**Figure I-11: 4.45 V lithium-ion LCO pouch cell battery. Reference cell represents a standard battery. Ref. +OS3 contains 3% OS3 material. Test conditions: Charge to 4.45 V at 1 C, current cut-off 1/20 C, rest 10 min, discharge to 3.0 V at 1 C, rest 10 min at 45 °C**

- **Advanced Electrolyte R&D (Argonne National Laboratory):** Conventional electrolytes for lithium-ion batteries, typically comprised of mixtures of various carbonates electrolytes with $LiPF_6$ salt, decompose above 4.5 V vs. $Li^+/Li$ leading to a low Coulombic efficiency, rapid capacity fade, and severe self-discharge, which worsens at elevated temperatures. To address the stability of the carbonate electrolytes, scientists at Argonne National Laboratory have developed a new class of electrolytes based on fluorinated carbonate solvents. A variety of fluorinated carbonates (both cyclic and linear) were synthesized and the superior voltage stability was examined using density functional theory calculation and electrochemical cyclic voltammetry. Figure I-12 shows the cycling performance of the new electrolyte in a 5 V lithium-ion battery using $LiNi_{0.5}Mn_{1.5}O_4$ as a 5 V cathode and graphite as the anode. Compared with conventional electrolytes, the fluorinated electrolyte shows much improved performance both in Coulombic efficiency and capacity retention at 55°C. Another desirable property of the new electrolyte is its non-flammability which is also imparted by the fluorination, and was demonstrated by lack of any flame or fire after igniting the electrolyte-soaked testing specimen (glass wool stick) by a torch. Next steps in this work include estimating the production cost of the fluorinated compounds, and further improving the long-term anode stability.

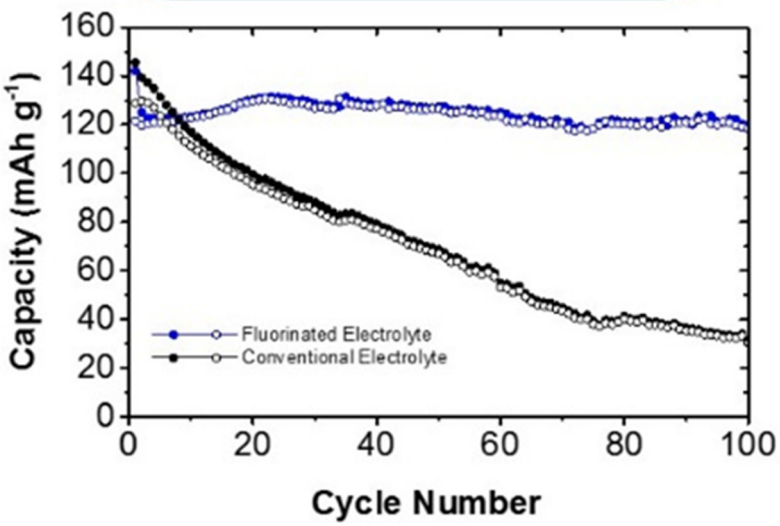


**Figure I-12: Capacity retention of $LiNi_{0.5}Mn_{1.5}O_4$ /graphite cells cycled at 55 °C with F-electrolyte compared with conventional electrolyte at C/3. (Cutoff voltage: 3.5-4.9 V)**

- **Solid State Electrolyte Research (University of Maryland):** Through modification of interfacial layers obtained via computational modeling and controlled interfacial structures by 3D printing, the University of Maryland has achieved a low interfacial resistance in cells with a solid ceramic electrolyte comparable to commercial flammable liquid electrolyte batteries. This solves the "large interfacial resistance" problem, a significant issue for solid-state batteries. The research team used atomic layer deposition to place a thin film of aluminum oxide on top of the solid ceramic structure (Figure I-13a and b). With a chemically engineered garnet-based ceramic electrolyte, the team showed there was a "negligible interface resistance" between the Li metal anode and the ceramic electrolyte interface: the garnet/Li interfacial resistance was reduced by three orders of magnitude to 1 Ohm*cm$^2$ (Figure I-13d). They also decreased the cathode/garnet interfacial resistance to 7.5 Ohm*cm$^2$, which is a dramatic improvement over the >3000 Ohm*cm$^2$ resistance without surface modification (Figure I-13c). Finally, 3D garnet surface structures were printed to increase the effective surface area relative to the planar areal surface area, forming structured ion-conductive pathways with varying line spacing. Resultant interfacial resistance decreased linearly with increased surface area, achieving a 52% resistance decrease. The battery community is thus getting closer to delivering high energy, high power, and nonflammable batteries using solid electrolytes.

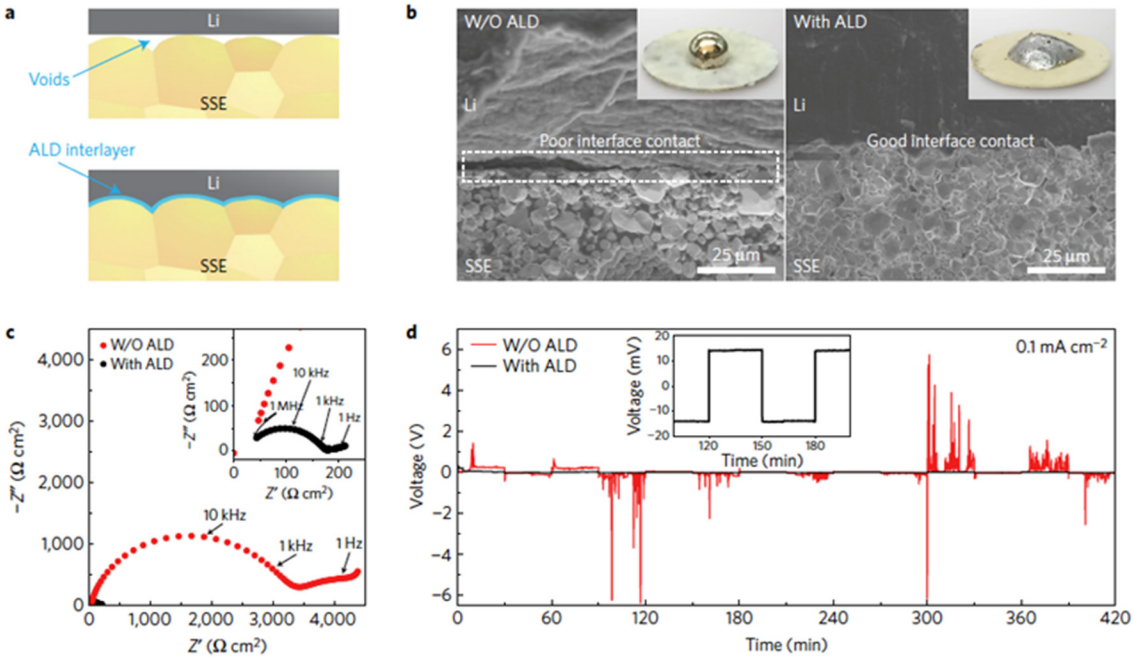


**Figure I-13: a: Schematic diagram of the wetting behavior of garnet surface with molten Li. b: SEM images of the garnet solid-state electrolyte/Li metal interface. With and without ALD-$Al_2O_3$ coating; insets are photos of melted Li metal on top of the garnet surface clearly demonstrating classical wetting behavior for the ALD-treated garnet surface. c: Comparison of EIS profiles of the symmetric Li non-blocking garnet cells. Inset shows the much lower impedance curve of for the ALD-treated garnet cell. d: Comparison of cycling for symmetric cells of Li/bare garnet/Li (black curve) and Li/ALD-treated garnet/Li (red curve) at a current density of 0.1mAcm$^2$. The inset is the magnified curve of the ALD-treated cell**

- **Beyond Lithium-ion Research (Stanford University):** Lithium metal anode is often known as the "holy grail" of battery technologies not only due to its high capacity (which is up to ten-fold higher than commercial graphite anodes materials), but also its challenges. Mainly, there are two such challenges: lithium dendrite growth, which may result in internal short circuits and possibly thermal runaway, and a poor cycling stability that shortens cycle life. Stanford University has developed a new principle on designing Li metal anodes, constructing a "stable host" to reduce the anode's volume change during cycling. To achieve this goal, an advanced nanotechnology structure is utilized as shown in microscopic images (a-c) in Figure I-14. Here, the designed structure consists of stacked graphene layers with uniform nanoscale interlayer gaps. The gaps provide room for storing Li metal. This layered stacking nanostructure offers several important advantages: (1) due to the graphene "host", the volume change can be significantly mitigated to <20%; (2) the large surface area of the host can enable uniform Li deposition; (3) the graphene layers provide surface protection to reduce side reactions on highly-reactive Li metal. This construct successfully suppresses Li dendrites, while

at the same time allows good cycling. Cells with commercial $LiCoO_2$ (LCO) cathode further exhibit high-power output, with <6 minute charging time.

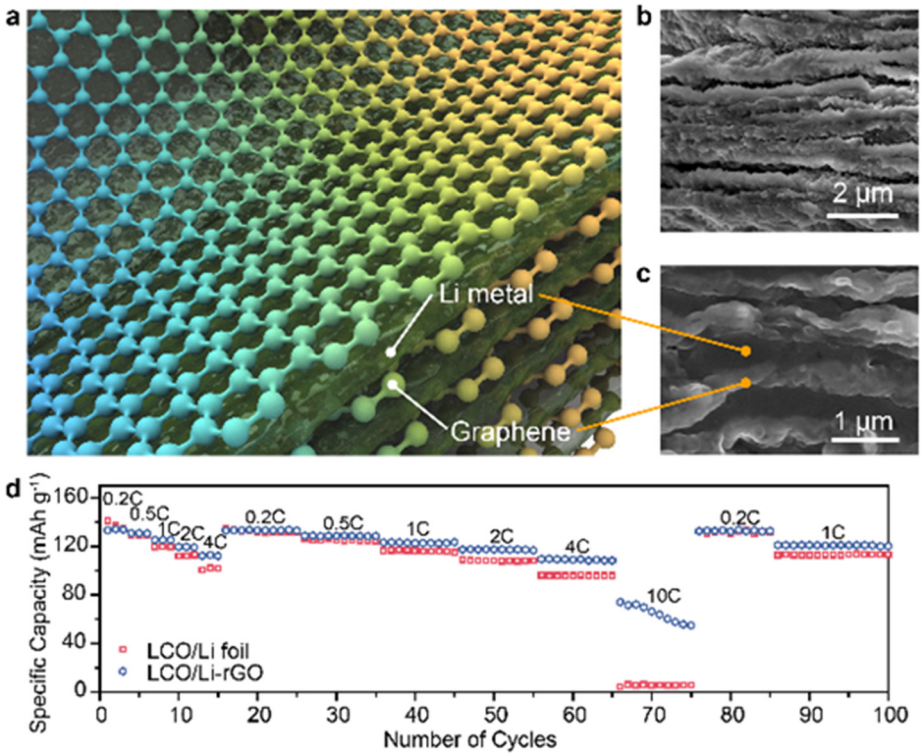


**Figure I-14: Schematic of the Li metal anode with "stable host", which exhibits layered stacking of Li metal and graphene. (b,c), Scanning electron microscopy (SEM) images of the Li metal anode in cross-section view. (d) Cycling stability of Li–rGO and Li foil symmetric cells at 1 mA cm-2 and 1 mAh cm-2**

- **Beyond Lithium-ion R&D (Pennsylvania State University):** Pennsylvania State University (PSU) has identified an alternate reaction pathway with a new functional electrolyte to enable high performance lithium-sulfur (Li-S) batteries. In Li-S batteries, the dissolution of lithium polysulfide intermediates and an irreversible formation of solid $Li_2S$ in conventional ether-based electrolytes leads to a significant capacity loss and use of a large amount of the electrolyte, thus greatly reducing cell energy density and cycle life. To address this problem, PSU researchers developed a functional electrolyte system using dimethyl disulfide (DMDS) as a co-solvent for Li-S batteries. DMDS promotes the discharge of sulfur through an alternate electrochemical reaction pathway by formation and subsequent reduction of dimethyl polysulfide species (Figure I-15a-c). The new reaction pathway not only boosts cell capacity, but also improves electrochemical kinetics and reduces electrolyte amount. As a result, sulfur cathodes with unparalleled performance are achieved: a stable capacity of around 1,000 mAh/g sulfur at a very low electrolyte/sulfur ratio of 5 mL/g using practical, high-sulfur-loading (4 mg S/cm) cathodes, which is almost double the capacity obtained with conventional electrolytes under the same conditions (Figure I-15d,e). This work represents a major step towards lowering the electrolyte amount in Li-S batteries in order to increase future energy-density of Li-S batteries.

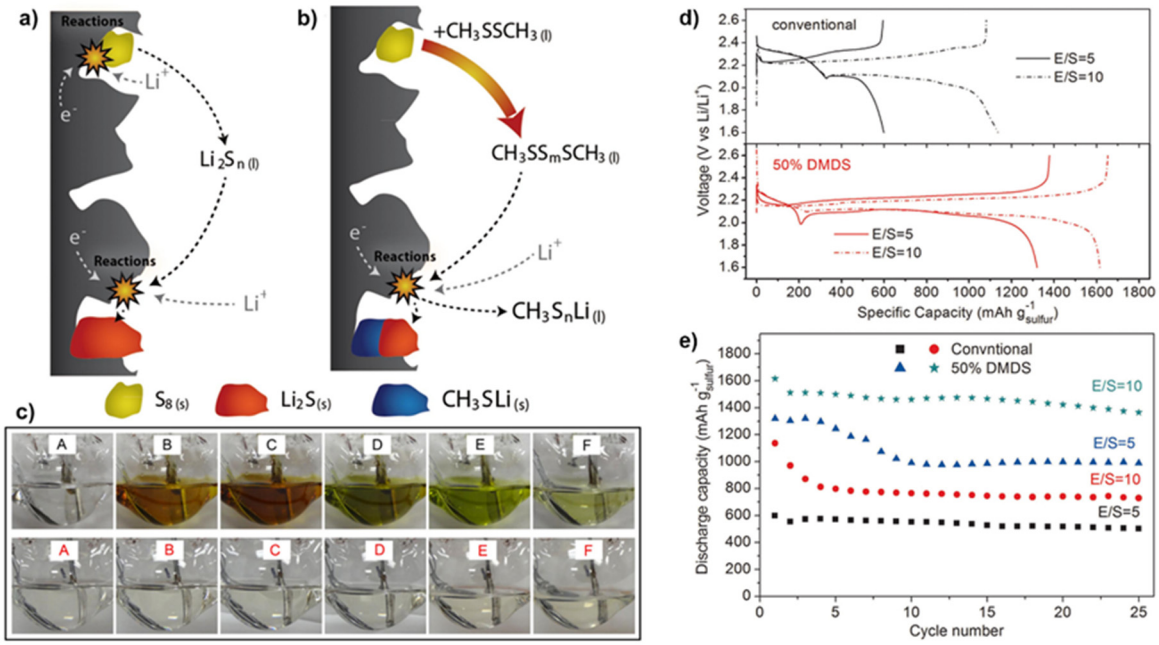


**Figure I-15: Schematic diagrams of the discharge mechanism of (a) conventional ether-based and (b) DMDS-containing Li-S electrolytes, and (c) photos showing the electrolyte color changes during discharge from A to F in conventional (upper) and DMDS-containing (lower) electrolytes. (d, e) Electrochemical performance of high-sulfur-loading cathode with low electrolyte to sulfur (E/S) ratios of 10 and 5 mL g-1 in conventional and DMDS-containing electrolyte**

- In 2016, VTO awarded 14 advanced batteries projects totaling $16.4 million in the areas of high-voltage electrolytes, solid-state electrolytes, lithium metal protection, advanced characterization techniques and advanced battery material modeling—(See Table I- 3). Initiated in FY 2017, these projects will be covered in greater detail in the next year's annual report.

### Table I- 3: FY 2016 Vehicle Technologies Program-Wide Funding Opportunity Announcement: List of Awardees

| Applicant | Location | Project Title/ Description | Federal Cost Share[6] |
|---|---|---|---|
| Development of Advanced High-Voltage Electrolytes and Additives, Conformable and Self-Healing Solid State Electrolytes, and Lithium Metal Protection (Area of Interest 6) | | | |
| University of Pittsburgh | Pittsburgh, PA | Utilize a novel approach to mitigate lithium dendrite formation by designing a composite lithium anode | $1,250,000 |
| Massachusetts Institute of Technology | Cambridge, MA | Conduct fundamental studies of an alkali halide based solid-electrolyte to demonstrate self- healing properties to overcome low cycle life and safety concerns associated with dendrite formation for lithium metal | $1,250,000 |
| Rutgers, The State University of New Jersey | Piscataway, NJ | Design a 3-D metal fluoride all solid-state battery that has the potential for extremely high specific and volumetric energy densities (600 Wh/Kg, 1,400 Wh/L). | $1,077,074 (jointly funded) |
| Daikin America, Inc. | Decatur, AL | Develop fluorine containing carbonate solvents that will allow existing lithium-ion batteries to operating above 4.5 V thereby increasing energy density while maintain performance and safety. | $1,250,000 (jointly funded) |

[6] Through the Advanced Vehicle Power Technology Alliance between the Department of Energy and the Department of the Army, the Army is contributing $2.21 million co-funding in several areas where there are joint development opportunities.

| Applicant | Location | Project Title/ Description | Federal Cost Share[6] |
|---|---|---|---|
| Penn State University Park | University Park, PA | Develop protective, self-healing layers for lithium metal anodes that will allow high cycling efficiency (> 99.7%) and dendrite-free cycling. | $1,139,319 |
| University of Washington, Seattle | Seattle, WA | Design a novel gel electrolyte that possesses a self-healing property to suppress dendrites at the lithium metal electrode and traps polysulfides that are detrimental to Li-S battery cycle life. | $1,250,000 |
| West Virginia University Research Corporation | Morgantown, WV | Develop solid-state electrolytes that integrate a highly-conductive inorganic nano-fibrous network with a conductive polymer matrix composite to suppress dendrites in lithium-metal batteries. | $1,244,012 |
| The Research Foundation for the SUNY Stony Brook University | Stony Brook, NY | Investigate lithium-metal batteries with a solid state, self-healing electrolyte/separator with improved electrolyte conductivity and cycling efficiency. | $1,065,975 |
| University of Maryland | College Park, MD | Design self-healing, 3-D conformal solid state electrolytes to prevent dendrite formation and achieve in high battery cycle life. | $1,250,000 |
| Development of Advanced Battery Material Characterization Techniques (Area of Interest 7) | | | |
| General Motors LLC | Warren, MI | Develop a comprehensive set of diagnostic techniques that enable the understanding of the mechanical/chemical degradation of the solid electrolyte interface layer to improve the performance and cycle life of current lithium-ion batteries. | $1,452,676 |
| University of California - San Diego | La Jolla, CA | Develop advanced microscopy and spectroscopy tools to understand and optimize the oxygen evolution that impacts the performance of current lithium ion cathodes. | $1,080,000 |
| Advanced Battery Materials Modeling (Area of Interest 8) | | | |
| Texas A&M Engineering Experiment Station | College Station, TX | Develop a multi-scale modeling approach to study the chemical structures of electrolytes and the solid electrolyte interface layers. | $1,200,000 |
| University of California - Berkeley | Berkeley, CA | Develop a comprehensive model to identify promising materials candidates for all solid state lithium batteries. | $891,000 |
| Michigan State University | East Lansing, MI | Develop an electrochemical-mechanical model to design artificially solid electrolyte interface coatings. | $999,943 |

## I.B.5. Organization of this Report

This report covers all the FY 2016 projects that were ongoing (or had started up) as part of the advanced battery R&D (i.e., energy storage R&D) effort in VTO. Chapter II through V contain descriptions and account of the progress of various R&D projects supported through VTO funding. A list of individuals who contributed to this annual progress report (or who collaborate with the energy storage R&D effort) appears in Appendix A. A list of acronyms is provided in Appendix B.

We are pleased with the progress made during the year and look forward to continued work with our industrial, government, and scientific partners to overcome the remaining challenges to delivering advanced energy storage systems for vehicle applications.

**David Howell**

VTO Deputy Director and Program Manager for Hybrid and Electric Systems

Vehicle Technologies Office

**Tien Q. Duong**

Manager, Advanced Battery Materials Research and VTO Battery500 Consortium

Vehicle Technologies Office

**Peter W. Faguy**

Manager, Applied Battery Research and Advanced Processing R&D

Vehicle Technologies Office

**Brian Cunningham**

Manager, Battery Development; and Battery Testing, Analysis and Design; and Small Business Innovation Research for Batteries

Vehicle Technologies Office

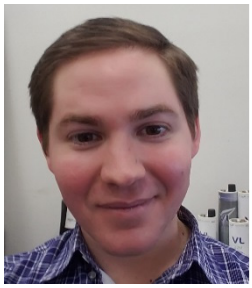

**Samuel Gillard**

Technology Development Manager, Battery Testing, Analysis and Design

Vehicle Technologies Office

# II. Advanced Battery Development

## II.A. USABC Battery Development & Materials

### II.A.1. High Energy Lithium Batteries for Electric Vehicles (Envia Systems)

**Herman Lopez, Principal Investigator**
Envia Systems
7979 Gateway Blvd., Suite 101
Newark, CA 94560
Phone: 510-962-3687; Fax: 510-510-7012
E-mail: hlopez@enviasystems.com

**Oliver Gross, USABC Program Manager**
Fiat Chrysler Automobiles
800 Chrysler Drive East
Auburn Hills, MI 48326
Phone: 248-219-3011; Fax: 248-944-3035
E-mail: oliver.gross@fcagroup.com

Start Date: June 2014
End Date: July 2017

**Abstract**

#### Objectives

- Develop high capacity silicon-based anode composite electrodes capable of supporting long cycle life by controlling electrode pulverization, lithium consumption and conductivity loss.
- Develop high capacity cathode blend composites capable of supporting the energy, cycle life, calendar life, power, safety, and low/high temperature cell requirements.
- Develop a manufacturable and cost-effective pre-lithiation process that enables the fabrication of large-format high-capacity pouch cells.
- Screen and down-select best electrolyte formulation and separator type for meeting USABC performance, cost and safety cell targets.
- Design, build, test and deliver large format pouch cells integrating high capacity Si-based anode and cathode composites along with optimized electrolyte, separator and pre-lithiation process that meet USABC EV cell goals.

#### Accomplishments

- Achieved >700 cycles from 20Ah pouch cells before reaching 80% capacity retention integrating down-selected $SiO_x$-based anode and Ni-Co-Mn-based cathode blend.
- Screened various $SiO_x$, n-Si, and Si alloy materials and based on capacity, cycle life, irreversible capacity loss, processability and manufacturability, down-selected $SiO_x$ as the anode material to integrate in future cell builds.
- Evaluated different Mn-, Ni-, and Co-rich cathode blends in order to maximize specific capacity, average voltage, electrode density, loading, DC-resistance, and cycle life.
- Nanoscale successfully built and qualified their large roll-to-roll pre-lithiation machine, currently being used for the anode pre-lithiation development.

- Improved cell cost model with more reliable cost numbers.

### Future Achievements

- Complete iteration #2 cell build integrating down-selected and optimized anode, cathode, electrolyte, separator and pre-lithiation process.
- Complete final cell build integrating down-selected and optimized anode, cathode, electrolyte, separator and pre-lithiation process.
- Deliver cell to the National Laboratories for independent cell testing.
- Validate final cell cost model.

## Technical Discussion

### Background

In order to reduce our dependence on imported fossil fuels (and in the process decrease greenhouse gas emissions), electric vehicles (EVs) have received intense attention as a possible solution. One of the main barriers to widespread adoption of EVs relates to the lack of available high energy, low cost and safe energy storage devices. Lithium-ion batteries (LIBs) are presently the best energy storage solution used in currently sold EVs. Further improving the performance of LIBs by integrating high capacity active materials, novel passive components and unique cell designs will be critical for the success and mass adoption of EVs.

### Introduction

This project is developing a new battery system based on novel high-capacity Ni-Co-Mn (NCM) cathode blends and high capacity silicon-based anode composites that could meet the USABC EV cell performance targets for 2020. In order to enable high Si-content anodes, a manufacturable and cost effective pre-lithiation process will need to be developed to compensate for the high irreversible capacity loss (IRCL) of the anode. At the conclusion of the program, Envia will demonstrate LIBs with usable specific energy greater than 350 Wh/kg and usable energy density greater than 750 Wh/l while maintaining other performance requirements of EV cells, including power, calendar life, cycle life, safety and cost. This will be achieved through a collaborative effort across several organizations, where each organization provides expertise on specific components of the material, processing and cell. Ultimately, large format cells meeting USABC goals will be built and delivered to the National Laboratories for testing.

### Approach

Envia is utilizing a system-level approach to screen, develop and optimize critical cell components (cathode, anode, electrolyte, separator), pre-lithiation processes (process, dose), cell design (N/P ratio, electrode design) and cell formation and testing protocols that will enable meeting the USABC EV cell level goals for the year 2020. The development will consist of integrating high capacity Ni-Co-Mn cathode blends, pre-lithiated silicon-based high capacity anodes, high voltage electrolyte and ceramic-coated separator into large capacity (10-60 Ah) pouch cells. The developed cells will exhibit high energy density and power, good cycle life and calendar life and acceptable low-temperature performance while meeting cell level cost and safety targets. Cells will be delivered and tested by the following National Laboratories: Idaho National Laboratory (INL), Sandia National Laboratories (SNL) and National Renewable Energy Laboratory (NREL).

Envia is leveraging its material, process and cell development expertise to develop, modify and engineer material and cell-level solutions to meet the cell specifications. During this project, Envia has partnered with leading companies like Daikin America (electrolyte), Asahi Kasei (separator), Nanoscale Components (pre-lithiation processing), A123 Venture Technologies (cell manufacturing), 3M (Si alloys), and DuPont (n-Si composites), to develop the best materials, processes and cells practicable. Having the proper partnerships will increase the probability of meeting the USABC project goals by leveraging the strength of each of the partner, with Envia mainly focusing on its core strengths of cathode and anode development, and cell design. Partnering with large chemical and cell partners also ensures that any developed technology will have a clear path to high volume production and commercialization.

The program has been structured so that as it progresses throughout its 3 years, the cell targets increase in difficulty with respect to specific energy, energy density, cycle life and cell cost (see Figure II-1). The program consists of 5 cell builds that include the baseline and final program cell build intended to track the projected cell development timeline.

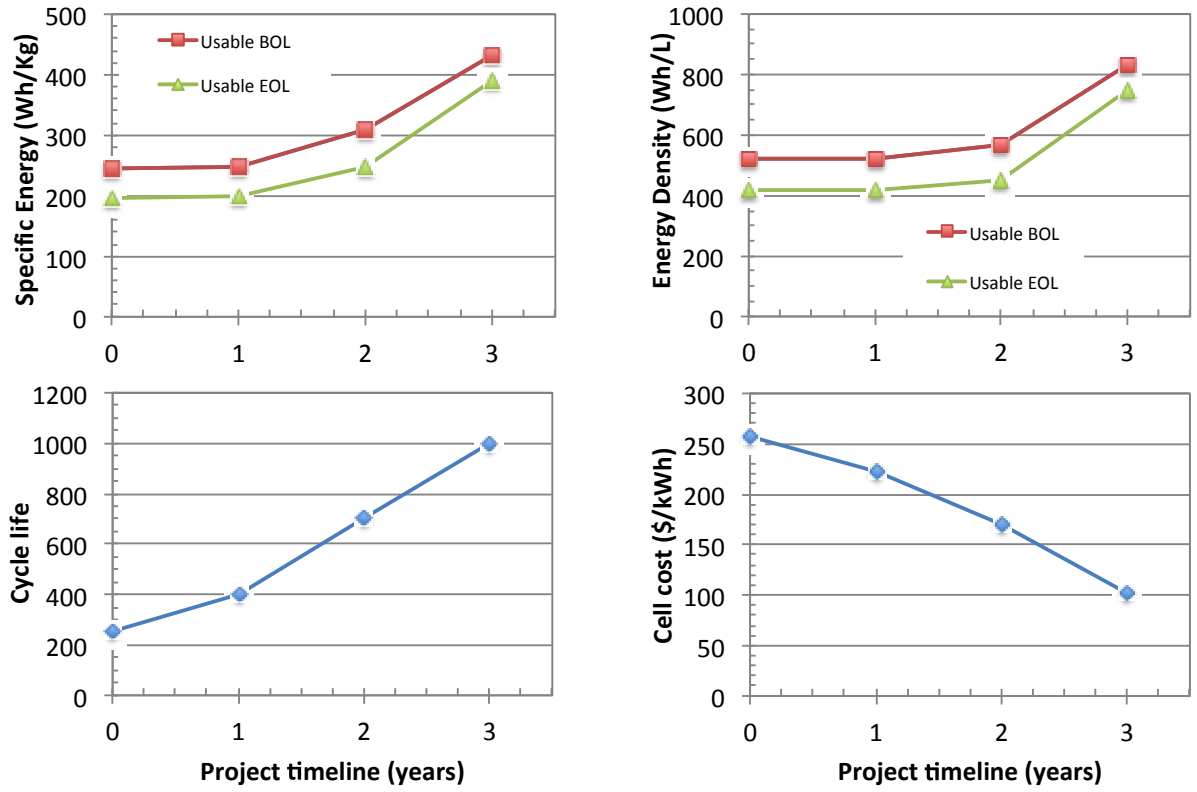


**Figure II-1: Projected high energy cell development timeline**
*Envia Systems*

## Results

**Anode Development:** Envia has screened multiple high capacity silicon-based anode materials from 3M, DuPont, and various commercial vendors. Screening of various nano-silicon (n-Si), silicon-based alloys and silicon oxide ($SiO_x$) composites was performed and evaluated based on capacity, cycle life, irreversible capacity loss, processability and manufacturability. During the material screening, the materials were tested following vendor recommendations and by applying Envia's own electrode formulation, processing and coating know-how in an attempt to further improve the performance of the silicon materials. In general, n-Si was tested at various active percent levels, passivated by a variety of coatings and blended with other graphitic-based active materials and in all cases cycle life was compromised. Si-based alloys showed improved cycled life compared to n-Si, but showed lower capacity and poor cycle life compared to $SiO_x$-based anode materials. After evaluating the various Si-based materials, Envia has down-selected $SiO_x$-based materials as the material of choice to meet the challenging USABC cell targets. $SiO_x$-based materials continue to have challenges with respect to cycle life and development will continue to further improve the performance.

Upon completion of year 2 of the program, Envia has integrated Si-$SiO_x$-based carbon composite anodes into the baseline, iteration #1 and multiple internal cell development cell builds. Anode material development has focused on optimizing the anode composition, electrode formulation and material coating. The composite has been formed by engineering the precise amount of carbon, type of carbon and processing (see Figure II-2). Additional anode surface coatings and electrode designs continue to be explored to further improve the cycling and energy performance of the cells.

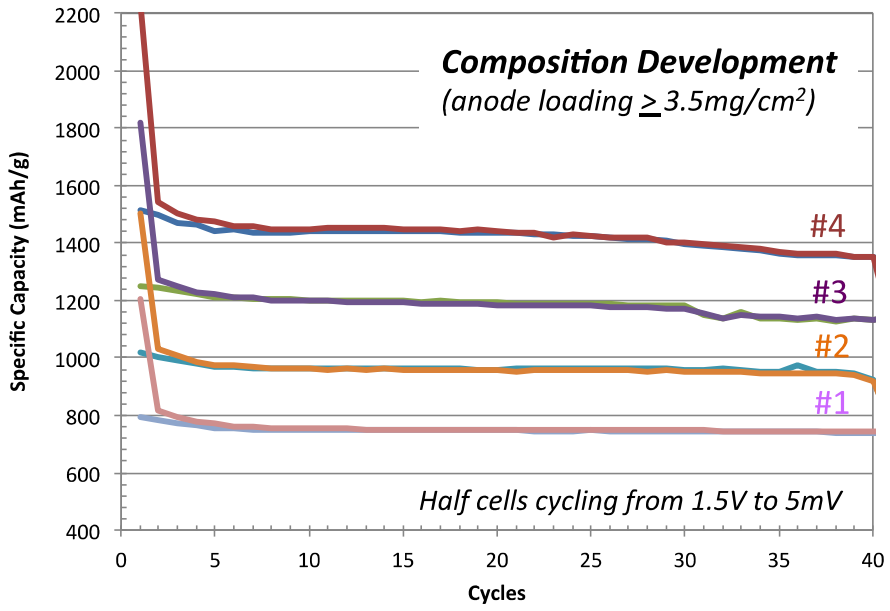


**Figure II-2: Half-cell electrochemical performance of various $SiO_x$-Si-C anode composites**
*Envia Systems*

**Cathode Development:** Envia has down-selected a lithium-rich manganese-rich cathode composition, dopant and surface coating based on capacity, average voltage, DC-resistance, usable energy and cycle life. The down-selected cathode material (C#24) has shown ~800 cycles to 80% energy retention in graphite cells when cycled at a C/2 rate at the voltage window of 4.35-2.2 V (see Figure II-3). To further optimize the performance of the cathode, different Mn-rich, Ni-rich and Co-rich cathode blends have been explored to leverage the advantages of each of the components and will be used in future cell builds.

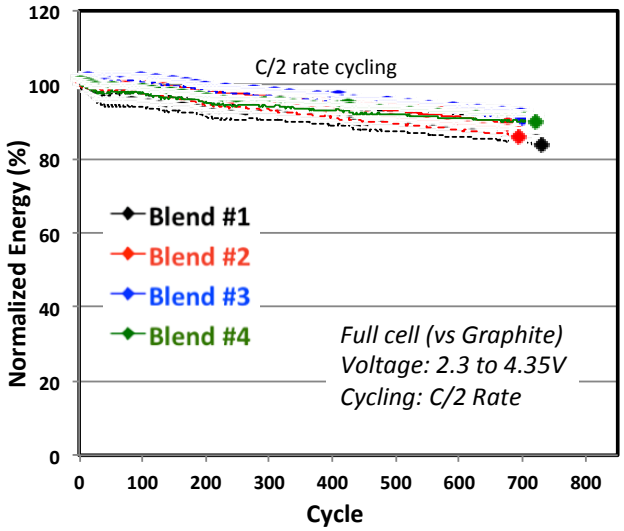


**Figure II-3: Half-cell electrochemical performance of various Ni-Co-Mn-based cathode blends**
*Envia Systems*

**Pre-lithiation Development:** A consequence of working with high capacity silicon-based anodes, and especially with $SiO_x$-based materials, is an inherent high irreversible capacity loss. In order to compensate for this loss, pre-lithiation is a requirement. Envia has partnered with Nanoscale Components, which pre-lithiates anodes via a scalable, manufacturable and cost effective roll-to-roll electrochemical process. Early in the program, Nanoscale successfully pre-lithiated and delivered silicon-based anode electrode (A#7) to support 1Ah capacity build #1 cells. Other anode formulations and compositions have been attempted and will continue to be optimized during the program to develop a pre-lithiated anode capable of meeting USABC EV cell targets.

Nanoscale completed its larger pilot scale pre-lithiation line, which is now able to pre-lithiate electrodes for large format pouch cells. The new pilot line has the following attributes: 1) 50x larger than the initial line; 2) 5x wider to support a 300 mm anode width with 10x longer length for faster throughput; and 3) designed for near production levels of automation. The new pilot scale line is currently being used for pre-lithiation trials of Envia's high capacity anode formulations. Once the pre-lithiation of Envia's current A#14 anode formulation is successful, material will be integrated in cell build #2.

As Nanoscale's pre-lithiation process is optimized, Envia continues its large capacity cell development utilizing SLMP (stabilized lithium metal powder) from FMC Lithium as the pre-lithiation material. Using the SLMP process Envia has routinely made 1, 10 and 20 Ah pouch cells to optimize and down-select the cell components, design and testing protocols.

**Cell Development:** In order to meet USABC EV cell targets, multiple high capacity cell builds have taken place and are scheduled throughout the remainder of the program. Currently, 1, 10 and 20 Ah pouch cells have been built and tested by incorporating promising active and passive materials, cell components, and cell designs. Cell build iteration #1 served as the first time that cells were assembled, integrating materials and a cell design from Envia, pre-lithiation from Nanoscale and cell assembly from A123.

In parallel, smaller cell builds consisting of fewer cells have taken place and will continue to be built to evaluate and down-select the best electrolyte, separator, cathode, anode, cell design, and testing conditions that will feed the larger builds. Currently Envia has achieved >700 cycles from 20 Ah cells before reaching 80% capacity retention (see Figure II-4). The high capacity (20 and 10 Ah) and high-energy (245 and 265 Wh/kg) cells integrate the down-selected Ni-Co-Mn cathode blend, high $SiO_x$ content anode composite, SLMP-type pre-lithiation and optimized electrolyte, separator and cell design. Similar cells are expected to be built in the upcoming iteration #2 cell build. Iteration #3 cell build will target specific energies >300 Wh/kg while integrating similar anode and cathode materials.

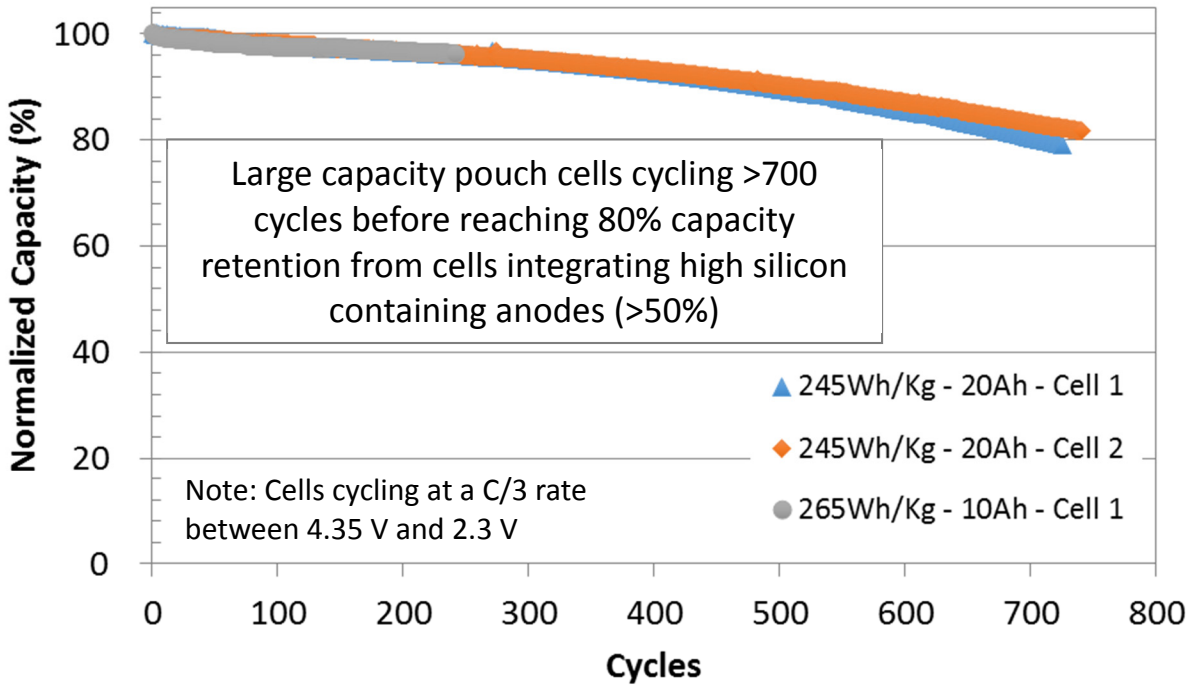


**Figure II-4: Cycle life performance from 20 Ah and 10 Ah cells cycling at a C/3 rate and voltage of 4.35-2.3 V**
*Envia Systems*

## Conclusions

Envia has shown >700 cycles before reaching 80% capacity retention from 20 Ah capacity pouch cells integrating a Ni-Co-Mn cathode blend, high $SiO_x$ content anode composite, SLMP-type pre-lithiation and optimized electrolyte, separator and cell design. 20 Ah cells just finished cycling and tear-down and failure analysis is planned to understand the failure modes and further improve the cell performance.

Envia will continue to use a system-level approach to further develop and optimize the critical material and cell components (cathode, anode, electrolyte, separator), pre-lithiation, cell design (N/P ratio, electrode design) and cell formation and testing protocols that will enable meeting the USABC EV cell targets. Development will continue with the goal of down-selecting the best materials, components and processes to integrate in the upcoming cell build iteration #2 and #3. Close interaction with all development partners and careful postmortem analysis will be central to the effort, and critical to the success of the project.

### Products

## Presentations/Publications/Patents


1. “High Energy Lithium Batteries for Electric Vehicles”, ES247_Lopez_2015_p, US DOE Vehicle Technologies Program Annual Merit Review, AMR, 2015.
2. “High Energy Lithium Batteries for Electric Vehicles”, ES247_Lopez_2016_p, US DOE Vehicle Technologies Program Annual Merit Review, AMR, 2016.

# II.A.2. Development of a High Energy Density Cell and Module for EV Applications (LG Chem Power, Inc.)

**Mohamed Alamgir, Principal Investigator**
LG Chem Power, Inc.
1857 Technology Drive
Troy, MI 48083
Phone: 248-291-2375
E-mail: alamgir@lgchem.com

**Chulheung Bae, USABC Program Manager**
Ford Research & Innovation Center
2101 Village Road
Dearborn, MI 48121
Phone: 313-410-1398; Fax: 313-248-4077
E-mail: cbae@ford.com

Start Date: February 2015
End Date: January 2018

## Abstract

### Objectives

- Development of a high energy density, low-cost cathode material to meet the requirements of the USABC targets for long-range EV battery.
- Development of a high capacity Si-based anode that is capable of long cycle-life.
- Understanding/Optimization of high capacity electrode structures that will enable the manufacturing of low-cost, long-life EV batteries.
- Fabrication and testing of modules comprising high capacity cathodes and Si-based anodes using a suitable thermal management system. Since cells using Si anodes are expected to undergo considerable volume changes, the objective is to develop a mechanical structure that will be effective in retaining the cells as well as thermally managing them to prolong life and abuse-tolerance.

### Accomplishments

- Studies were carried out to improve the durability of Mn-rich cathode materials using scaled-up ALD coating and doping. This included work to eliminate first cycle inefficiency and gassing especially when charged to high voltages using chemical activation.
- Preliminary studies to use high Ni-content cathode materials have been performed. The use of ALD coating leads to improved durability.
- Comprehensive studies to characterize Si-based anode materials, including development of appropriate binders, conductive additives and electrolytes, are currently in progress.
- Two batches of baseline cells have been fabricated and delivered to the USABC for testing.
- Studies of electrode structures were carried out with the goal of developing high loading electrodes.

### Future Achievements

- Work will focus on improving the durability of Ni-rich cathode using surface coatings and electrolyte optimizations.
- Cycle-life issue of high loading Si-based anodes will be addressed using optimized electrolytes and electrode structure.

- Cells made using the most optimized cathode/anode from the above studies will be built into modules to characterize their thermo-mechanical behavior in order develop an optimized mechanical and thermal management system that will be robust with respect to life and abuse-tolerance.

## Technical Discussion

### Background

Mass-scale commercialization and adoption of EVs critically depends on the development of high energy-density, low-cost EV batteries. This is a 3 year program that aims to advance the EV battery technologies to help achieve this overall objective.

### Introduction

The development of high energy density, low-cost EV battery meeting USABC requirements necessitates the use of very high capacity cathodes as well as of high energy density anodes. A survey of the current crop of cathode and anode materials having the potential for meeting the performance, life and cost targets show that high energy density cathodes such as Li rich NCM or high Ni-content NCM and Si-based anodes are the most attractive choices for this purpose. The current program is aimed at utilizing these electrode materials for achieving those objectives.

### Approach

In order to achieve the program objectives, the following key approaches are being pursued.

- Use of high capacity NCM cathodes. This entails both Mn rich as well as high Ni content cathode materials.
- Use of high capacity Si-based anode that has the best cycle-life at a high loading level.
- Development of high loading electrode to realize high energy density.

### Results

The following is a summary of the progress made this year.

#### Cathode Development

We have been pursuing dual approaches to develop a high capacity and long-life cathode material. These are:

- Use of Mn-rich NCM
- Use of Ni-rich NCM

Although the Mn-rich NCM has a very high capacity (~250 mAh/g), when charged to voltages as high as 4.6V, it encounters several well-known drawbacks such as inferior life, gassing, voltage fade as well as a high resistance value at low SOCs. We have pursued multiple avenues such as ALD coating, doping, chemical activation as well as various electrolyte additives to solve these issues. While these approaches yielded relatively good improvement, the data shown below indicate that the magnitude of improvement was not large enough to warrant continued studies with this material in this program. For example, Figure II-5 shows the data for a cell built using our most optimum Mn-rich cathode and a high loading Si-based anode we prepared as our first baseline deliverable. The data show considerable impact on the delivered capacity as the function of upper voltage cutoff of 4.4 and 4.6V. The cycle-life of the cell was, however, considerably poor as the capacity faded to less than 80% after 25 cycles at room temperature. More dramatic fade was observed during storage at 60°C and SOC=80%. Structural evolution, Mn dissolution and thick SEI formation are attributed to such rapid decay in cell performance. Given those poor life characteristics, studies with this cathode material were discontinued.

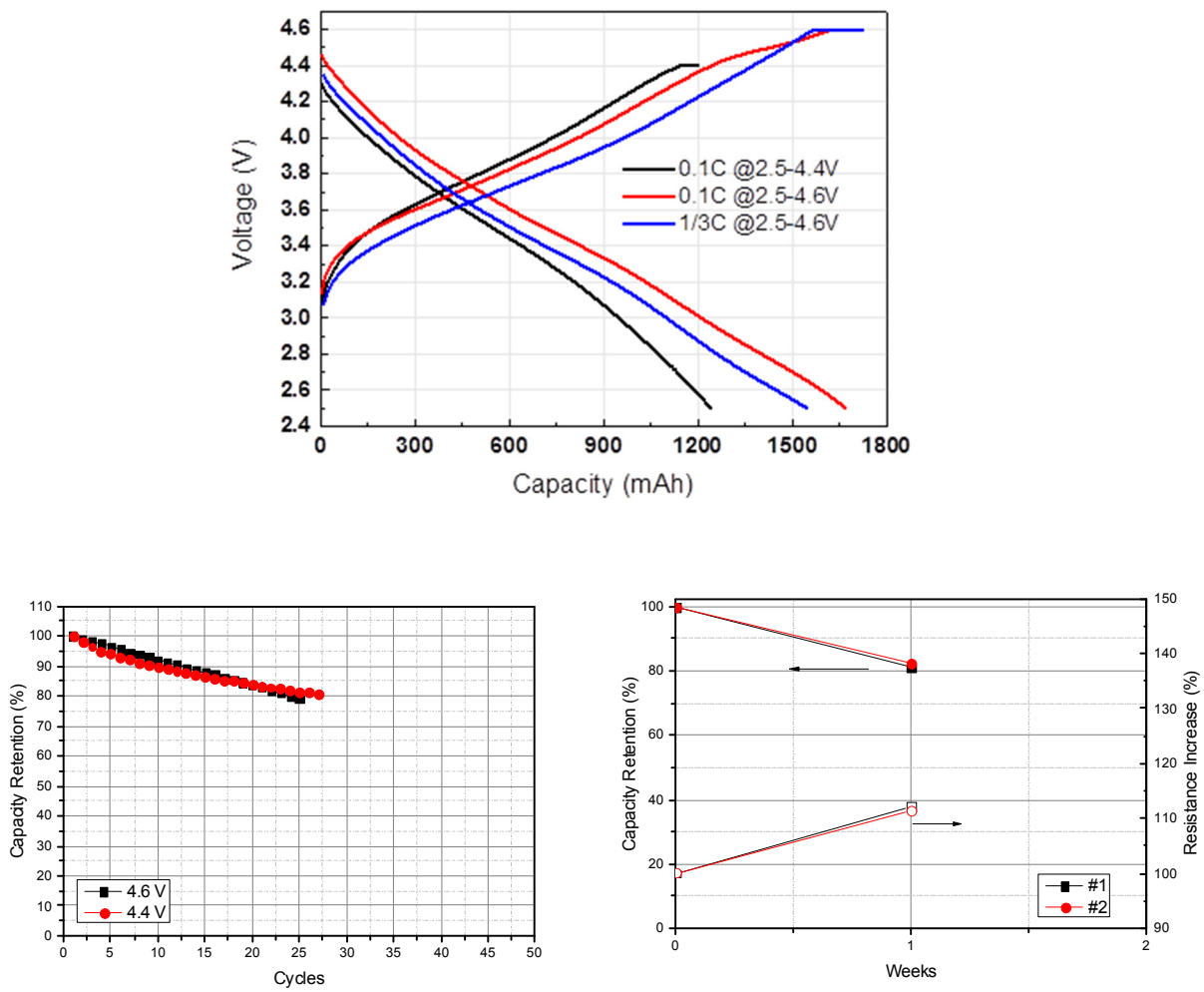


**Figure II-5: Results from a Mn-rich cathode/high loading Si-anode cell. Top) effect of charge voltage on delivered capacity; Bottom left: cycle-life of the cell at room temperature at the C/3 discharge rate and C/10 charge rate. Bottom right) Storage at 60 °C and 80% SOC**

Consequently, Ni-rich NMC was selected as our primary path for the cathode chemistry. We selected ALD coating as one of the routes for improving the durability of the cathode. Data showed that the capacity and the rate capability of the cathode are not adversely affected by the coating and, in fact, it showed a slightly higher capacity and better capacity retention compared to its untreated counterpart (see Figure II-6).

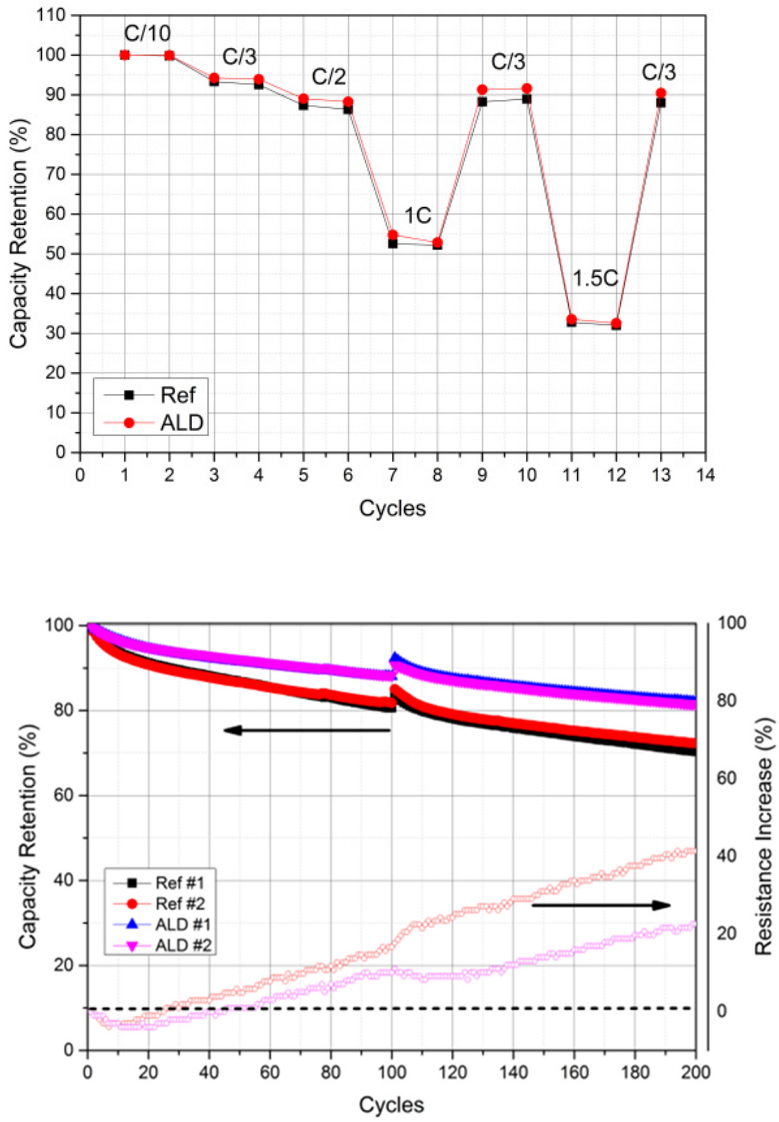


**Figure II-6: Top) Rate Capability of ALD-coated Ni-rich cathode/graphite cells. Bottom) Capacity retention and resistance increase during charging and discharging between 2.5 and 4.2 V at room temperature at C/3**

Cells using the highest amount of Si-anode loading (30%) and Ni-rich cathode were then built to test their performance. The data show considerable monotonously increasing resistance rise below SOC 70%. However, unlike their Mn-rich counterparts, these cells showed considerably better cycle-life. They showed close to 80% capacity retention after 100 cycles compared to the 80% capacity retention after 25 cycles for the Mn-rich cathode cells (see Figure II-7, Figure II-8). In addition, the Mn-rich based cells vented after 60 cycles due to excessive gassing.

Higher temperature cycling at 45°C leads to a further fade in the capacity with a concomitant rise in cell resistance. Studies will be carried out to stabilize the interface and suppress the side reactions that lead to this capacity fade and resistance rise. Although there is a larger fade of these cells at 45°C, we note here that these data are significantly superior to those we obtained using the Mn-rich cathode.

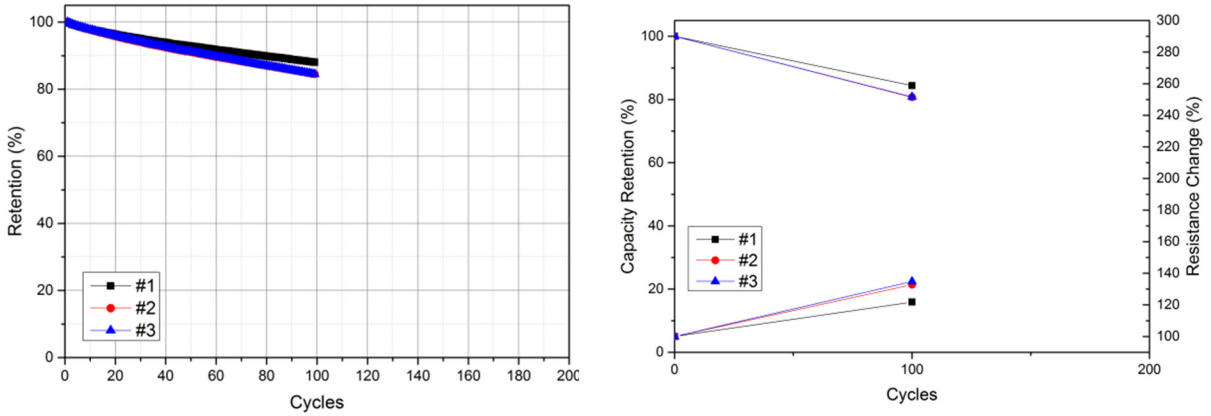


**Figure II-7: Cycle-life results at 25 °C for high loading Si-anode/Ni rich cells. Cells cycled between 2.5 and 4.2 V at C/3**

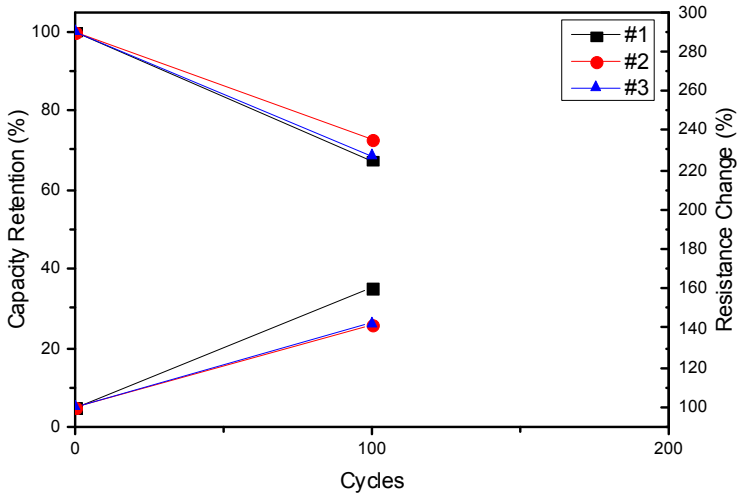


**Figure II-8: Cycle-life results at 45 °C for high loading Si-anode/Ni rich cells. Cells were cycled between 2.5 and 4.2 V at C/3**

## Conclusions

Extensive studies involving doping, surface treatment and electrolyte optimization, among others, did not lead to any significant improvement in the durability of Mn-rich cathode cells. Consequently, work on this cathode was discontinued in favor of the Ni-rich cathode which showed a much superior performance. ALD coating appears to improve the durability of the cells. Preliminary studies with high loading of Si-based anode showed reasonably good cycling at room temperature but the capacity fade and resistance rise at elevated temperature are still unsatisfactory. Future studies will be focused on improving the durability of this cell by further optimizing the electrodes and electrolyte.

# II.A.3. Advanced High-Performance Batteries for Electric Vehicle (EV) Applications (Amprius)

**Ionel Stefan, Principal Investigator**
Amprius, Inc.
225 Humboldt Court
Sunnyvale, CA 94089
Phone: 800-425-8803; Fax: 866-685-7420
E-mail: ionel@amprius.com

**Matthew Denlinger, USABC Program Manager**
Ford Research & Innovation Center
2101 Village Road
Dearborn, MI 48121
Phone: 313-390-4505; Fax: 313-337-2408
E-mail: mdenling@ford.com

Start Date: January 2015
End Date: January 2018

## Abstract

### Objectives

- Amprius is engaged in a three-year, anode-focused USABC project to develop and deliver vehicle-size cells that meet USABC's technical requirements. Throughout the project, Amprius will improve its silicon nanowire anode material and cell performance in a baseline cell, and then transfer learnings to larger cells. At project's end, Amprius will deliver ~40 Ah cells with end of life specific energies of 350 Wh/kg and energy densities of 750 Wh/L.
  - The project addresses the key performance and production challenges to the commercialization of high-capacity cells and batteries with silicon nanowire anodes. The barriers addressed include:
    - Energy: Low Wh/kg and Wh/L
    - Cycle Life: <1,000 Cycles
    - Size: Small Anodes and Cells
    - Cost: High $/kWh
- Amprius' goal is to deliver cells that meet USABC's EV battery goals. Amprius will deliver high-capacity pouch cells at the conclusion of the project's first, second and third years. Idaho National Laboratory will independently test the performance and safety of Amprius' cells according to USABC's test protocols.
  - Specific technical targets:
    - Available Energy Density @ C/3 Discharge Rate: 750 Wh/L
    - Available Specific Energy @ C/3 Discharge Rate: 350 Wh/kg
    - DST Cycle Life: 1,000 Cycles
    - Peak Discharge Power Density, 30 s Pulse: 1500 W/L
    - Peak Specific Discharge Power, 30 s Pulse: 700 W/kg
    - Peak Specific Regen Power, 10 s Pulse: 300 W/kg
    - Calendar Life: 15 Years
    - Selling Price @ 100K units: $100
    - Operating Environment: -30°C to +52°C
    - Normal Recharge Time: < 7 Hours
    - High Rate Charge: 80% ΔSOC in 15 min
    - Peak Current, 30 s: 400 A

- Unassisted Operating at Low Temperature: > 70% Useable Energy @ C/3 Discharge Rate at -20°C
- Survival Temperature Range, 24 Hr: -40°C to+ 66°C
- Maximum Self-discharge: < 1%/month

## Accomplishments

- Designed the project's interim, Year 2 cells, to achieve a target capacity of ≥ 10 Ah. Began to make hardware changes to prepare for building larger anodes and the project's interim, Year 2 cells.
- Built Silicon-NCM cells with average capacities of 10.5 Ah, specific energies of 336 Wh/kg, and energy densities of 826 Wh/L.
- Tested the DST cycle life of the project's baseline, Year 1 cells, all with capacities ≥ 2 Ah. The Silicon-NCM cells that Amprius tested achieved more than 550 cycles.
- Exceeded numerous USABC performance goals. Amprius' ≥ 2 Ah Silicon-NCM cells exceeded USABC's targets for Peak Discharge Power Density, Peak Specific Discharge Power, Peak Specific Regen Power, High Rate Charge, Unassisted Operation at Low Temperature (-20°C), Maximum Self-Discharge. Amprius' cells also met USABC's targets for Operating Environment and Survival Temperature Range (24 Hour).
- Reduced the main gap in performance, cycle life, by tuning anode structure and identifying electrolyte additives that improve Solid Electrolyte Interphase (SEI) stability and extend cycle life.
- Sourced and tested advanced cell components (e.g. separators) and cathode materials.

Designed the project's final, Year 3 cells, to achieve a target capacity of ≥ 40 Ah. Began to design fixtures to prepare for building larger anodes and the project's final, Year 3 cells.

## Future Achievements

- Test the cycle life of the project's interim, Year 2 cells with capacities ≥ 10 Ah.
- Deliver to Idaho National Laboratory cells with capacities ≥ 10 Ah.
- Continue to extend cycle life by tuning anode structure and identifying electrolyte additives that improve Solid Electrolyte Interphase (SEI) stability.
- Build the project's final, Year 3 cells, with capacities ≥ 40 Ah.

## Technical Discussion

### Background

Today's lithium-ion cells have limited room to improve specific energy or energy density; their active materials – a graphite anode paired with one of several commercially available cathodes – are used at energy capacities close to their fundamental limits and their packaging has already been optimized. New active materials are needed to boost performance and extend driving range.

### Introduction

Silicon has significant potential as a new anode material; silicon offers nearly 10 times the theoretical energy capacity of graphite. However, when charged with lithium ions, silicon swells up to four times its volume, causing capacity fade and mechanical failure. Because of swelling, conventional approaches to silicon anodes have not produced cells with the long cycle life required for electric vehicle applications.

## Approach

Amprius has innovative silicon technology – an anode made of silicon nanowires – that is capable of addressing silicon swelling, unlocking silicon's potential, and meeting USABC's commercialization criteria.

Amprius' technology is unique in three respects: (1) material, (2) structure, and (3) results. First, Amprius' anode material is made of silicon rather than graphite or a graphite-silicon composite. Second, Amprius' anode structure is composed of nanowires rather than particles. Third, Amprius has demonstrated both high energy and long cycle life in full cells with silicon nanowire anodes.

Amprius' unique, patent-protected material and structure – nanowires that are "growth-rooted" (i.e. grown directly on the current collector, without binders) – addresses swelling by enabling silicon to successfully expand and contract internally. Because the nanowires are attached to the current collector, Amprius does not rely on particle-to-particle contact and is able to achieve not only long cycle life, but also high electrical conductivity and power.

Before the USABC project, Amprius achieved >700 Wh/L at start of life and >400 C/2 cycles at 100% depth of discharge (DOD). To meet USABC goals, Amprius will during the project:

- Increase specific energy and energy density by tuning anode structure and using advanced components (e.g. thinner substrates and separators). Amprius will also transition from LCO to NCM.
- Extend cycle life by optimizing anode structure and identifying and/or developing electrolyte formulations that improve the solid electrolyte interphase (SEI) stability and cell performance.
- Increase anode and cell size by developing methods for (1) handling larger anodes; (2) improving the uniformity of silicon growth and deposition technologies; (3) reducing defect density; and (4) utilizing manufacturing methods that inherently scale to larger dimensions.

## Results

Amprius designed the project's interim, Year 2 cells, to achieve a target capacity of ≥ 10 Ah. Amprius began to make hardware changes to prepare for building larger anodes and the project's Year 2 cells.

Amprius doubled the length and depth of the baseline, Year 1 cells, to achieve Year 2's target capacities (see Figure II-9).

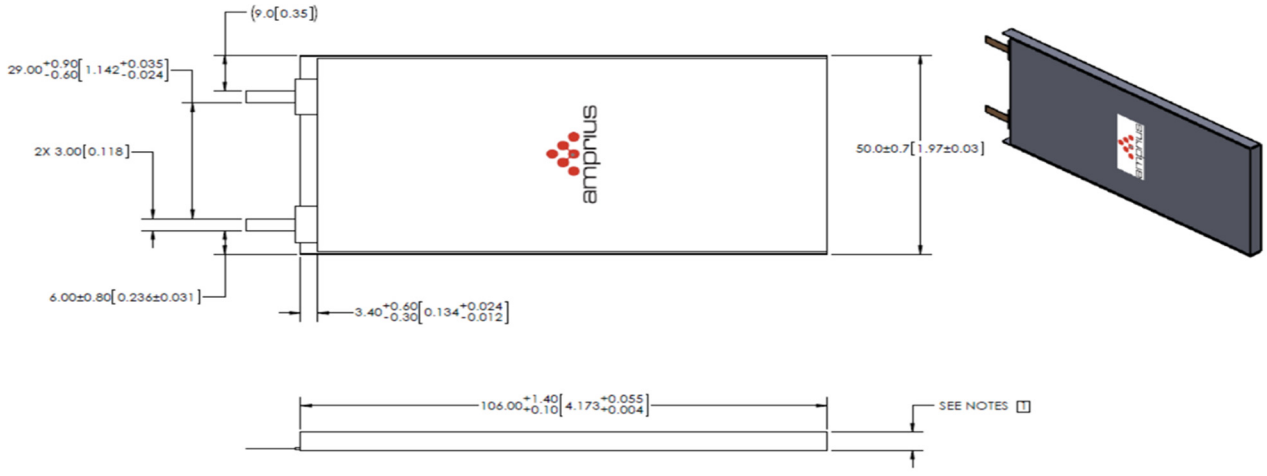


**Figure II-9: Amprius designed the project's Year 2 Silicon-NCM cells to achieve capacities ≥ 10 Ah**

Amprius built Silicon-NCM cells with average capacities of 10.5 Ah, specific energies f 336 Wh/kg, and energy densities of 826 Wh/L.

Amprius substantially increased the energy per unit of weight and volume of its silicon anode-based cells (see Table II-1).

### Table II-1: Amprius' Year 2 Cells Achieved High Specific Energies and Energy Densities

| Cell | Ah | Wh | Wh/L | Wh/kg |
|---|---|---|---|---|
| 1 | 10.5 | 34.2 | 838 | 336 |
| 2 | 10.5 | 34.1 | 814 | 337 |

Amprius evaluated the cycle life of the project's baseline, Year 1 cells, all with capacities ≥ 2 Ah. The Silicon-NCM cells that Amprius tested achieved more than 550 cycles.

Amprius demonstrated long DST cycle life. Voltage drift during cycling past 500 cycles was less than 4%. After an average of 553 cycles, Amprius' cells could not deliver the initial Available Energy within the operating voltage range (see Figure II-10).

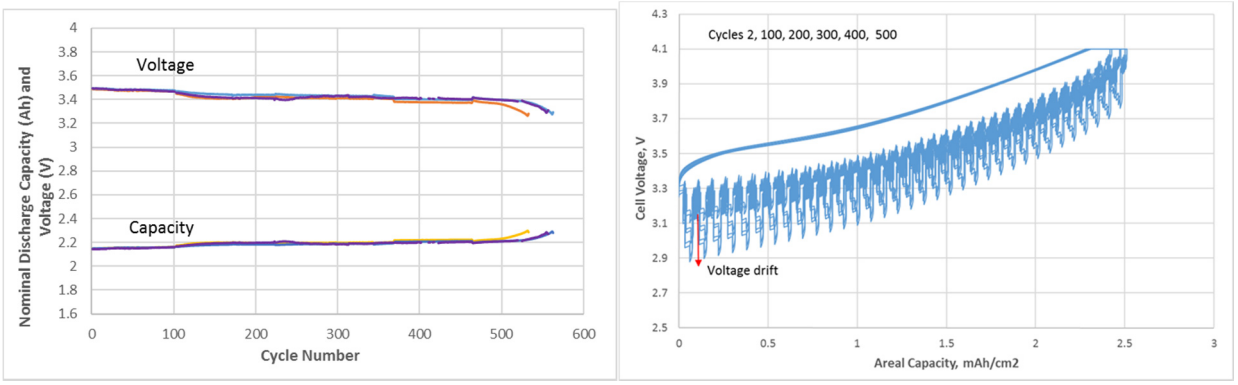


Figure II-10: Nominal voltage and capacity plot (left) and Potential vs. Capacity plot for cycles number 2, 100, 200, 300, 400 and 500 during DST cycle life evaluation of Amprius' Silicon-NCM cells

Amprius' cells exceeded several USABC performance goals.

- Amprius' ≥ 2 Ah Silicon-NCM cells exceeded USABC's targets for Peak Discharge Power Density, Peak Specific Discharge Power, Peak Specific Regen Power, High Rate Charge, Unassisted Operation at Low Temperature (-20°C), Maximum Self-Discharge. Amprius' cells also met USABC's targets for Operating Environment and Survival Temperature Range (24 Hour) (see Table II-2).

### Table II-2: Amprius' Silicon-NCM Cells Exceeded USABC Performance Goals

| Characteristics at 30°C and End of Life | Units | USABC Goals – Cell Level | Amprius > 2Ah Cells (NCM-523) Cell Level |
|---|---|---|---|
| Peak Discharge Power Density, 30 s Pulse | W/L | 1,500 | 2,089/2,368 |
| Peak Specific Discharge Power, 30 s Pulse | W/kg | 700 | 906/1,025 |
| Peak Specific Regen Power, 10 s Pulse | W/kg | 300 | 646 at 1% DOD |
| Operating Environment | °C | -30 to +52 | -30 to 52 |
| High Rate Charge | Minutes | 80% ΔSOC in 15 min | 86% ΔSOC in 15 min |
| Unassisted Operating at Low Temperature | % | > 70% Useable Energy @ C/3 Discharge Rate at -20°C | > 72% Useable Energy @ C/3 Discharge rate at -20 °C |
| Survival Temperature Range, 24 Hr | °C | -40 to +66 | -40 to +66 |
| Maximum Self-discharge | %/mon | < 1 | 0.2% |

- Amprius reduced the main gap in performance, cycle life, by identifying electrolyte additives that improve Solid Electrolyte Interphase (SEI) stability.

For example, in Q6, Amprius screened 15 electrolyte formulations made with a previously selected group of four additives. In Q7, Amprius evaluated the best of those formulations and new ones at high temperature (50°C). For screening, Amprius measured the relative capacity retention after either storing the cells at full charge at 50°C or after cycling the cells at 50°C for a number of cycles. For concentration optimization, Amprius used a design of experiment methodology to reduce the number of combinations. In cycling, Amprius used a typical test method: CC-CV at C/2 rate with 10% current taper and C/2 discharge rate, over the full voltage range (2.85-4.25V).

A sample set of results are shown in Figure II-11. The corresponding formulations are highlighted in the formulations matrix. Formulation ELY241 was developed in Year 1 and was used in Amprius' Year 1 cell deliverables. A few of the formulations screened in Q7 better or significantly better cycle life compared to ELY241. In particular, ELY243 gave the best cycle life at room temperature.

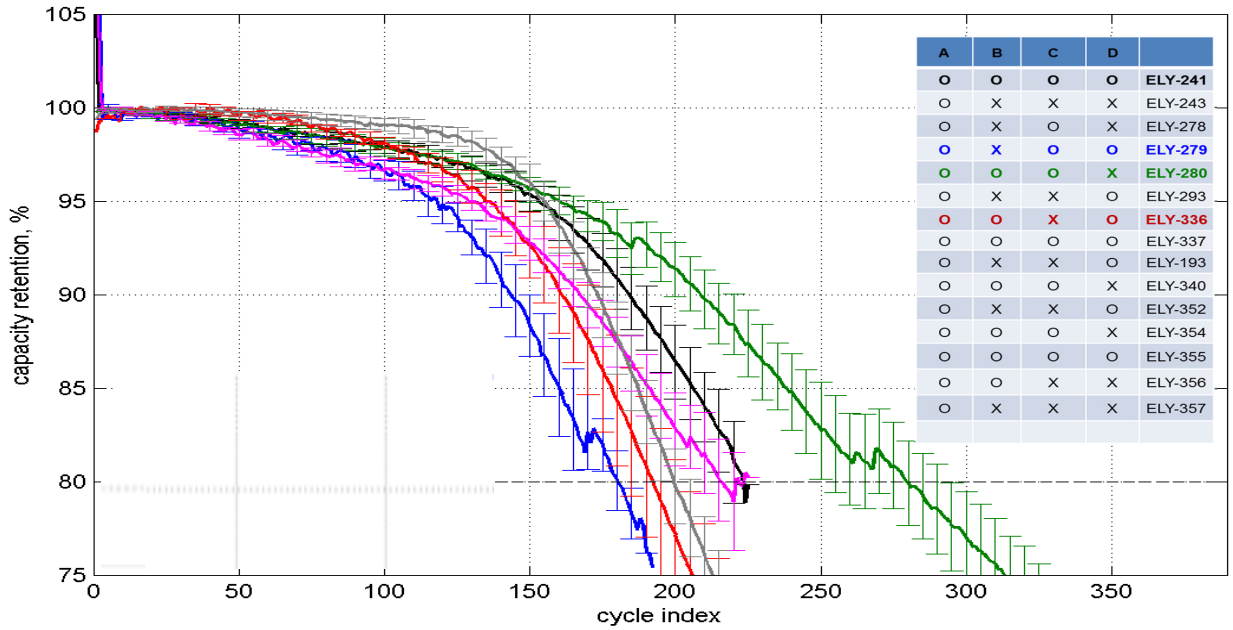


**Figure II-11: Accelerated cycle life evaluation of electrolyte formulations in a screening design of experiment**

Amprius designed the project's final, Year 3 cells, to achieve a target capacity of ≥ 40 Ah. Amprius also began to design fixtures to prepare for building larger anodes and the project's final, Year 3 cells.

Amprius selected the VIFB—/99/300 form factor for ≥ 40Ah cells. This cell is a pouch cell with tabs on opposite sides. Amprius will use cell components (e.g. separator, pouch material and electrolyte) selected and/or optimized in smaller Year 1 and Year 2 form factors. Amprius modeled the following cell specifications:

- Rated Capacity: 40 Ah at C/3 rate
- Vmax100 = 4.2V
- Vmin0 = 2.5V
- Cell weight = 382 g
- Cell size = 5.0x99x300 mm
- 348 Wh/kg and 902 Wh/L

## Conclusions

During the project's second year, Amprius continued to make significant progress increasing cell energy, extending cell cycle life, and demonstrating that its silicon nanowire anode-based cells exceed USABC's goals. In January, Amprius will build and deliver ≥ 10 Ah cells for independent testing at Idaho National Laboratory.

During Year 3, Amprius will continue to (1) increase cell energy by optimizing anode structure and exploring advanced components, (2) extend cell cycle life by tuning anode structure and testing new electrolyte formulations, and (3) finish making hardware changes and start building larger anodes and the project's final cells with capacities ≥ 40 Ah.

## Products

## Presentations/Publications/Patents

1. "Advanced High-Performance Batteries for Electric Vehicle (EV) Applications", ES41_Stefan_2016, US DOE Vehicle Technologies AMR, 2016.

## References

None

# II.A.4. Development of Advanced High-Performance Batteries for 12V Start-Stop Vehicle Applications (Maxwell Technologies)

**Scott Jorgensen, USABC Program Manager**
DE-EE0006250 Recipient: Maxwell Technologies
GM R&D Center
Mail Code 480-106-160
30500 Mound Road
Warren, MI 48090-9055
Phone: 586-986-1915
E-mail: scott.w.jorgensen@gm.com

**Shaw Lynds, Principal Investigator**
Maxwell Technologies, Inc.
3888 Calle Fortunada
San Diego, CA 92123
Phone: 858-503-3474
E-mail: slynds@maxwell.com

Start Date: October 2014
End Date: November 2016

## Abstract

### Objectives

The objective of this program is to develop a hybrid lithium ion/ultracapacitor energy storage system that meets or exceeds all USABC technical and economic goals for 12V Start-Stop vehicles applications.

### Technical Barriers:

In order for 12V stop start systems to achieve mass adoption they must be affordable, have excellent performance, and be easy to integrate into vehicles. The barriers addressed include:

- Performance: Cold cranking.
- Integration: Mass and volume.
- Cost: $/pack.

### Technical Targets:

- Cold Cranking: Withdrawal of 360Wh followed by cold soak to -30°C, and then perform 3 successive crank cycles of 0.5 seconds at 6kW, 4 seconds at 4kW, and 10 seconds at rest.
- Mass: 10kg.
- Volume: 7L.
- Cost: USABC ultimate goal $180 (not-under hood application), contracted project goal $230.

### Accomplishments

- Baseline Ultracapacitor pouch cells delivered to ANL for testing and currently on RPT8.
- Final delivery Ultracapacitor pouch cells delivered to ANL for testing and currently on RPT0.
- Proof of Concept (POC) modules delivered to ANL for testing and currently on RPT0.
- Proof of Concept (POC) modules delivered to NREL and have completed thermal testing.
- Proof of Concept (POC) modules delivered to Sandia for abuse testing.

- Failure Analysis (FA) completed on risk reduction POC cold crank failure.

## Technical Discussion

### Introduction

There is a strong technical and economic case developing in the energy storage industry for the hybrid combination of ultracapacitors and batteries in a variety of applications. It is a natural fit for applications that share a healthy requirement for both energy and power and for those applications that are required to function at very low temperatures. The emerging hybrid electric vehicle market is such an application.

The growing proliferation of start-stop or micro hybrid technology in mainstream passenger vehicles demonstrates the value, benefit and ease of adoption of such an electrical hybrid configuration. As the costs of battery cells and ultracapacitors continue to fall, the value proposition of that combination in the micro hybrid market becomes even more compelling.

This 19-month program will determine the technological and economic feasibility of adopting a hybrid energy storage system consisting of lithium-ion batteries and Maxwell ultracapacitors to an automotive start-stop application as specified by USABC and the Department of Energy. The proposed Maxwell 12V Start-Stop system consists of a single pack containing lithium-ion battery cells and the "to be developed" optimized Maxwell UCAP cells controlled by a single electronic management system.

Ultimately, the program failed to produce a module that fully met USABC gap chart goals. Some initially promising results had to be re-evaluated in light of Failure Analysis conducted on an early risk reduction module late in the program, resulting in a final prototype design that missed gap chart targets in both cost, mass, and volume. Nevertheless, the program did provide insight into how to best hybridize different forms of energy storage technologies for compact, high performance, and cost effective solutions, which provide both cost and weight advantages over a baseline battery only design.

### Approach

The program was conducted via two parallel development tracks. The first track (Task 1) used a proof-of-concept module to study the electrical, life cycle and control/communication performance of the hybrid pack. The second track (Task 2) included the development of the optimized configuration of the Maxwell ultracapacitor: needed for weight, volume and cost conformance. When combined, the results of each of these development tracks provide a complete, verified comparison of the proposed system's performance and cost against the USABC 12V Start-Stop Gap Chart.

### Results

#### Task 1

#### Design and build of the POC modules

The first task was to design and build a working ultracapacitor and LFP module to evaluate a direct parallel hybrid system against USABC goals. These POC modules consisted of off-the-shelf components including Maxwell 3000F ultracapacitors and A123 20AH LFP batteries. As shown in Figure II-12, the design utilized separate LFP and ultracapacitor packs connected together via bus bars in a Group 31 form factor. In addition, a combined battery and capacitor monitoring board was included to maintain balance in each of the cell strings and report health status. The baseline POC design was finished in the first half of the year, and then built and tested to USABC 12V start-stop requirements. Figure II-13 shows the baseline POC module as packaged prior to shipping to ANL for testing.

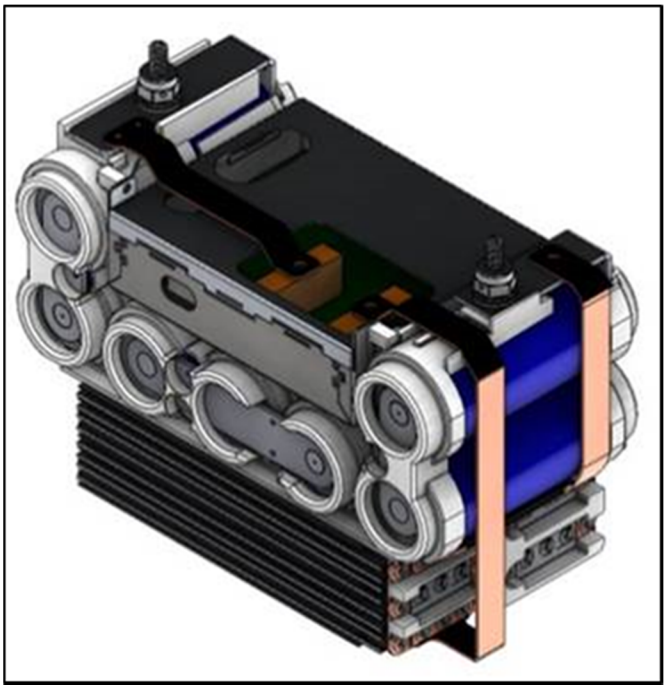

Figure II-12: The baseline POC module design


Figure II-13: The baseline POC module deliverable

### Testing and model optimizations of the POC modules

A Matlab Simulink model of the hybrid system was built using parameters measured from HPPC testing of individual UCAP and LFP cells. This model, shown in Figure II-14, was able to replicate HPPC results over temperature as well as permitted prediction of cold crank performance at both beginning and end of life.

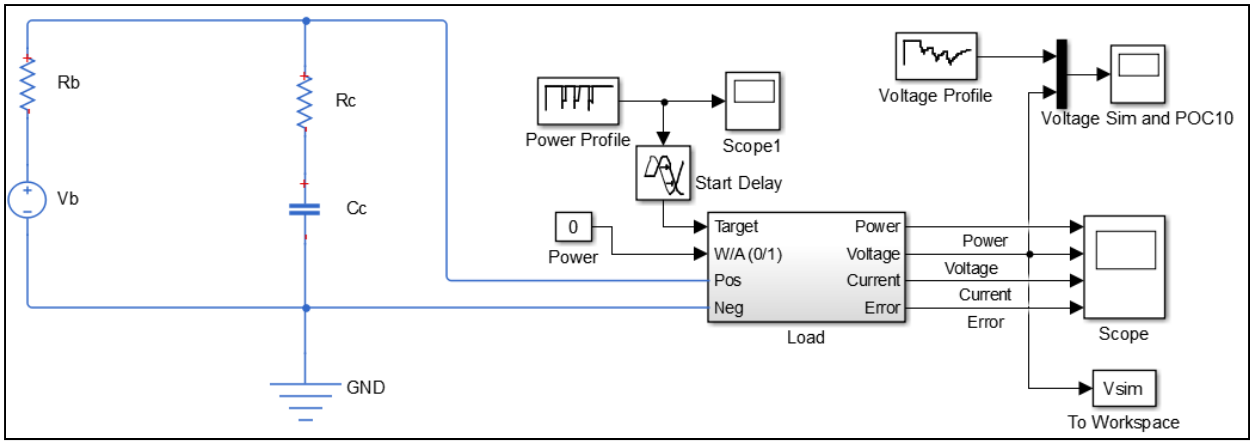


Figure II-14: The Simulink model of the hybrid system

## Risk reduction testing and FA

The initial sizing of the POC modules using this module indicated that a pack of 8 20Ah LFP cells in parallel with a single string of 6 3000F Ucap cells would meet the program goals. However, after RPT2 of risk reduction testing at Maxwell, a POC built to this configuration failed to meet the cold crank test. A full FA was preformed resulting in a resizing final prototype module to a dual string of 6 3600F Ucap cells. A mockup of this larger module passed the cold crank test at -30°C, as shown in Figure II-15.

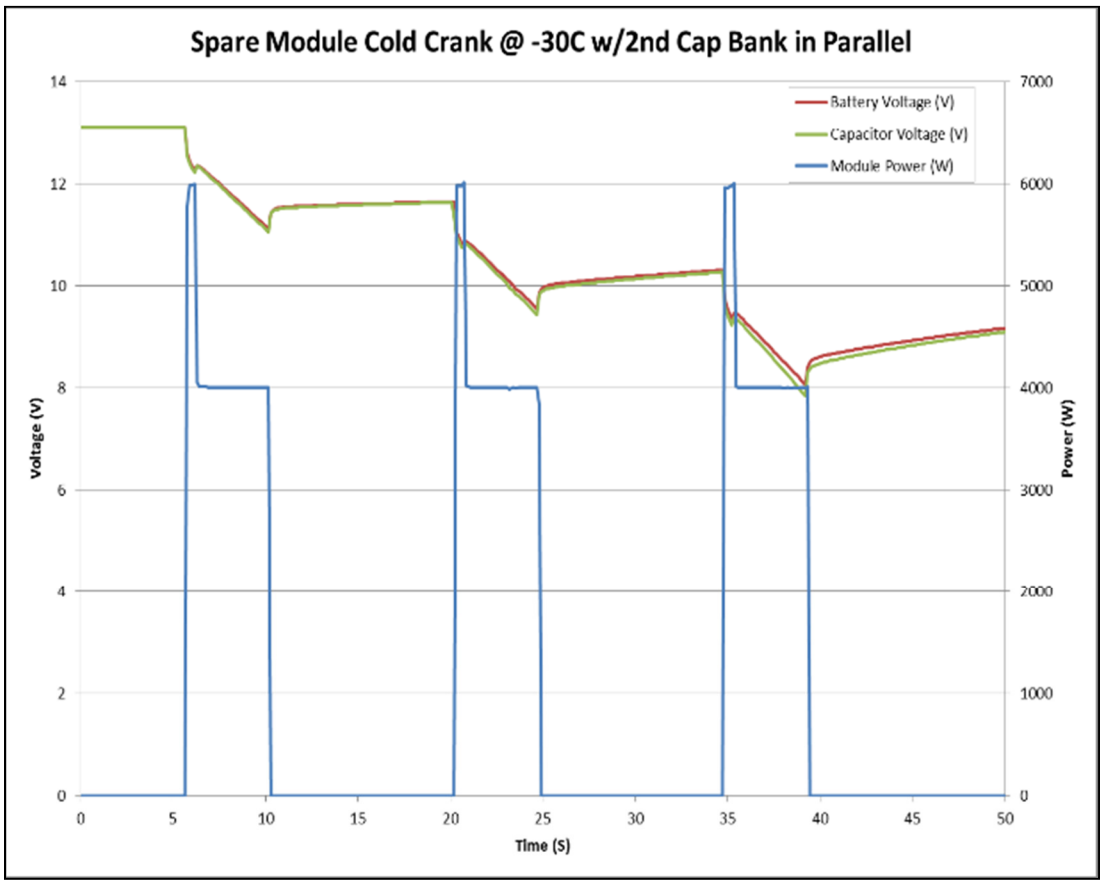


Figure II-15: Cold crank of the mockup post FA duel string module

### The prototype CAD model

This large module was reflected in the prototype CAD shown in Figure II-16, whose size and weight were used for the final program gap chart numbers

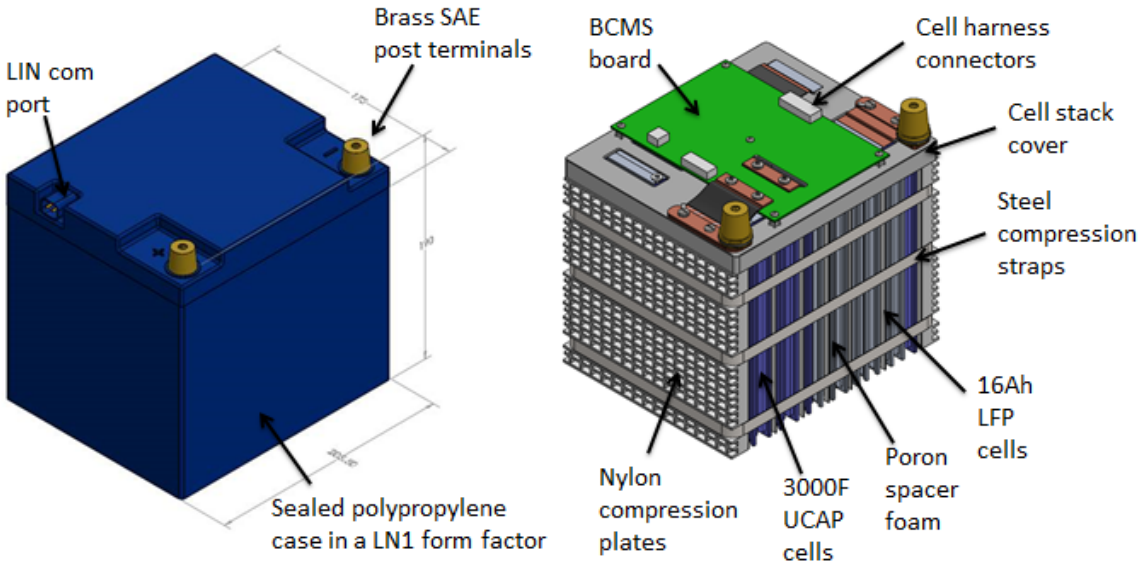


Figure II-16: The prototype module CAD

## Task 2

### Optimized Ucap Cells

To optimize cell cost and packing volume, the program target was to achieve a pouch cell ultracapacitor. Early research identified the key hurdle to achieving a pouch cell ultracapacitor was reduction of cell gassing, as pouch cells are not as gas tolerant as can cells. Figure II-17 shows the gas analyses of Ucap cells at increasing voltages. Based on these results, it was determined that the reaction shown in Figure II-18 was the dominant cause of gas generation that needed to be addressed. Developments under this program achieved a 3X reduction in gassing for the final pouch design configuration as shown in Figure II-19.

| | 2.5V 65°C MC2600 | 2.7V 65°C MC2600 | 2.85V 65°C MC2600 | 3V 65°C MC2600 |
|---|---|---|---|---|
| Hydrogen ($H_2$) | 65.01 | 78.95 | 89.51 | 92.81 |
| Methane ($CH_4$) | 0.20 | 0.22 | 0.13 | 0.12 |
| CO | 31.29 | 17.54 | 7.67 | 3.94 |
| $CO_2$ | 0.61 | 0.44 | 0.13 | 2.09 |
| 1,1,1 TFE ($CH_3CF_3$) | 0.04 | 0.22 | 0.13 | 0.93 |
| Acetonitrile ($CH_3CN$) | 2.84 | 2.63 | 2.43 | 0.12 |

Figure II-17: Gas analysis of Ucap cells

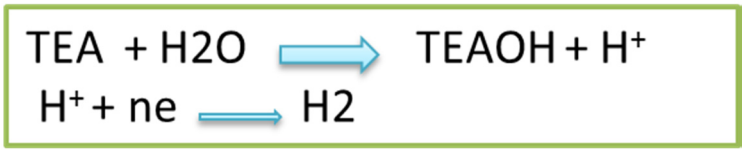


Figure II-18: The reaction between TEABF4 and water

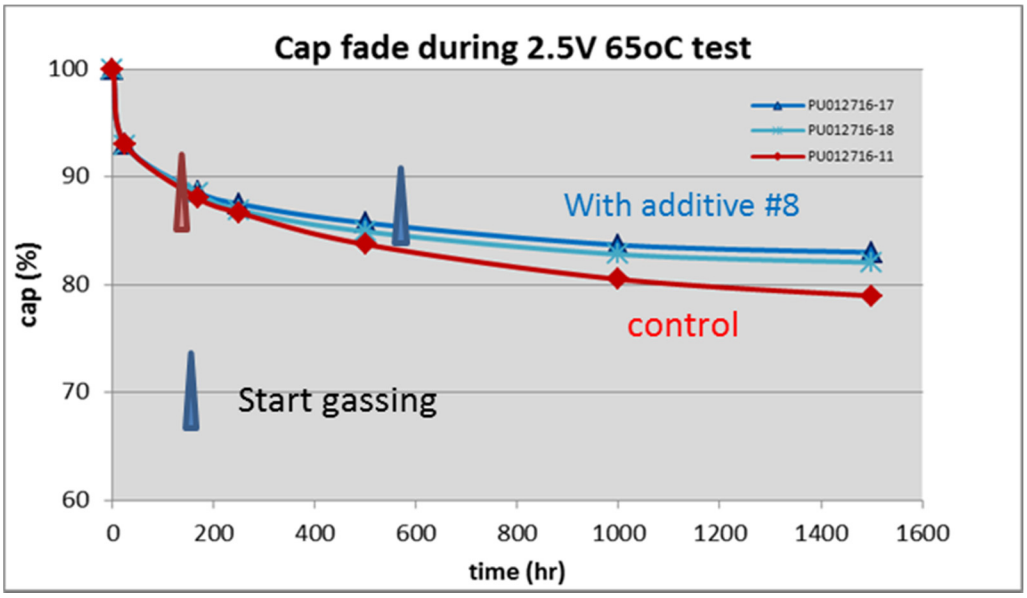


| | Control Design | Final Pouch Design |
|---|---|---|
| Electrode | Maxwell UCAP electrode | Maxwell UCAP electrode with thickness defined |
| Electrolyte | TEABF4/AN | TEMABF4/AN+additive#8 |
| Separator | Control separator | Separator #1 |
| Cell Format | Pouch | Pouch |

Figure II-19: The final pouch cell deign configuration and test results

## Conclusions

As shown in the final program gap chart projections shown in Table II-3, this project was unable to fully meet all the USABC gap chart requirements. However, the developments under this have substantially progressed the state of the art with regards to Ultracapacitor gas management as well as hybrid energy storage systems. The final prototype design represents a significant improvement in the hybrid supercapacitor - battery system. Maxwell is continuing work on both gas reduction, in the hopes of achieving higher temperature rated cells rather than pouch format cells, as well and hybrid start stop solutions, though no longer in an integrated module format. It is expected that the developments in these areas started under this program will yield commercial stop start products within the next few years.

### Table II-3: The Final Program Gap Chart Projections

| End of Life Characteristics | Units | USABC - Not under hood | SOW proposal | Results of the FA test | Final deliverable results |
|---|---|---|---|---|---|
| Discharge Pulse, 1s | kW | 6.0 | 6.5 | 14 | 14 |

| End of Life Characteristics | Units | USABC - Not under hood | SOW proposal | Results of the FA test | Final deliverable results |
|---|---|---|---|---|---|
| Max current, 0.5s | A | 900 | 1200 | 2000 | 1000 |
| Cold cranking power at -30°C (three 4.5s pulses, 10s rests between pulses at lower SOC) | kW | 6kW for 0.5s followed by 4kW for 4s | 3 Cranks | 3.0 Cranks | 1.5 Cranks |
| Min voltage under cold crank | Vdc | 8.0 | 8.2 | 8.0 | 8.0 |
| Available energy (750W accessory load power) | Wh | 360 | 360 | 450 | 450 |
| Peak recharge rate, 10s | kW | 2.2 | 2.6 | 2.6 | 2.6 |
| Sustained recharge rate | W | 750 | 750 | 750 | 750 |
| Cycle life, every 10% life RPT with cold crank at min SOC | engine starts/miles | 450k/150k | 450k | 3200k | 3200k |
| Calendar life at 30°, 45°C if under hood | Years | 15 at 30°C | 15 at 30°C | 23 | 23 |
| Minimum round trip energy efficiency | % | 95 | 95 | 97 | 97 |
| Maximum allowable self-discharge rate | Wh/day | 2.0 | 1.7 at 30°C | 1.3 at 30°C | 1.3 at 30°C |
| Peak operating voltage, 10s | Vdc | 15 | 15 | 14.4 | 14.4 |
| Sustained Operating Voltage - Max | Vdc | 14.6 | 14.6 | 14.0 | 14.0 |
| Minimum operating voltage under Autostart | Vdc | 10.5 | 10.5 | 11.8 | 11.8 |
| Operating temperature range (available energy to allow 6 kW (1s) pulse) | °C | -30 to +52 | -30 to +52 | -30 to +52 | -30 to +52 |
| +30 to +52 | Wh | 360 | 360 | 460 | 460 |
| 0°C | Wh | 180 | 180 | 440 | 440 |
| -10°C | Wh | 108 | 108 | 420 | 420 |
| -20°C | Wh | 54 | 54 | 400 | 400 |
| -30°C | Wh | 36 | 36 | 220 | 220 |
| Survival temperature range (24 hours) | °C | -46 to +66 | -46 to +66 | - | - |
| Maximum system weight | kg | 10.0 | 9.6 | 10.2 | 7.2 |
| Maximum system volume | L | 7.0 | 7.0 | 10.4 | 6.8 |

| End of Life Characteristics | Units | USABC - Not under hood | SOW proposal | Results of the FA test | Final deliverable results |
|---|---|---|---|---|---|
| Maximum system selling price (@250k units/year) | $ | $180 | $230 with path to $199 | $437 | $297 |

**Products**

## FY 2016 Publications/Presentations

1. 2016 DOE Annual Peer Review Meeting Presentation.

# II.A.5. A 12V Start-Stop Li Polymer Battery Pack (LG Chem Power, Inc.)

**Mohamed Alamgir, Principal Investigator**
LG Chem Power, Inc.
1857- Technology Drive
Troy, MI 48083
Phone: 248-291-2375
E-mail: alamgir@lgchem.com

**Scott Jorgensen, USABC Program Manager**
GM R&D Center
Mail Code 480-106-160
30500 Mound Road
Warren, MI 48090-9055
Phone: 586-986-1915
E-mail: scott.w.jorgensen@gm.com

Start Date: January 2015
End Date: December 2016

## Abstract

### Objectives

- The goal of this program is to develop a low-cost, abuse-tolerant 12V Start-Stop lithium-ion battery that will be capable of meeting the life, cold-cranking and cost targets of USABC.
- Technical Barriers
  - In order for 12V lithium-ion-based Stop-Start battery systems to achieve mass adoption they must be affordable, have excellent performance, and easy to integrate into vehicles.
  - Barriers addressed:
    - Performance: Cold cranking.
    - Integration: Mass and volume.
    - Cost.
- Technical Targets
  - Cold Cranking: Withdrawal of 360 Wh followed by cold soak to -30°C, then perform 3 successive crank cycles of 0.5 seconds at 6 kW, 4 seconds at 4 kW, and 10 seconds at rest.
  - Mass: 10 kg.
  - Volume: 7 L.
  - Cost: USABC goal: $220 (underhood application) project goal: $240.

### Accomplishments

- LMO and LTO having different morphologies, surface properties and compositions using various conductive additives in the electrodes were evaluated for power, durability and manufacturability.
- Cathodes and anodes having different porosities were studied with respect to cell performance and durability.
- Considerable focus has been placed on work to minimize gassing at high temperatures.
- Cells show outstanding thermal performance and abuse-tolerance.
- Several iterations of cells have been delivered to the National Labs for testing/validation.
- A battery pack with a simple mechanical and thermal design and simplified BMS has been developed and will be delivered to USABC for testing and validation.

## Technical Discussion

### Introduction

12V Start-stop batteries are gaining increasing attention as cost-efficient solution for reducing carbon emission on a global scale. To achieve this objective, Lithium-ion batteries offer promising alternative to lead-acid batteries because of their much higher specific energy and longer life. Key challenges for realization of this objective are cold-cranking power and cost. The objective of this proposal is to address these key issues.

### Approach

To achieve the above objectives, the following approaches were pursued.

- Develop a long-life, abuse-tolerant cell using LTO/LMO active materials.
- Manipulate cathode and anode material properties such as morphologies/surface area to increase power.
- Optimize cathode and anode compositions, their porosities as well as electrolyte compositions, with respect to life and power.
- Develop a low-cost battery pack using including a simple BMS.

### Results

The following summarizes the progress LGCPI has made in this program.

#### Optimization of the Cathode

Three generations of cells have been developed in course of this program. In order to develop high power cells, we evaluated different types of LMO cathode materials. These materials had different particle sizes, surface area, dopings and doping levels as well as surface coatings. Further, we also evaluated cathodes having different compositions by varying type and amount of conductive agents and binder. These characteristics were optimized to lower electrode resistance and increase cell power. Approaches similar to these were also pursued to develop a high power LTO anode. A number of electrolyte compositions as well as separators of different thickness and porosities were also examined.

In addition to varying the electrode material properties, we also carried out studies to improve processing conditions such as electrode manufacturing and aging. For example, LTO is a nano-material and has the propensity to adsorb moisture that is deleterious for cell performance such as life and swelling. Thus, appropriate processing conditions need to be developed that ensures well-functioning LTO electrode.

The above studies have led to considerable improvements in the cell life and power. Data in Figure II-20 show the continuous improvement in performance we were able to achieve in course of this program. While the preliminary sample faded rapidly at 60°C and 70% SOC, the A1 sample showed considerable improvement in the storage characteristics of the cell.

One of the key challenges of lithium-ion batteries for Start-Stop applications is meeting the cold-cranking power requirement of the USABC. While the first generation cells achieved the cold-cranking power at 100% SOC, the various modifications we have brought about in the cell have resulted in significantly improving the cold-cranking power capability. For example, the data below in Figure II-21 display the improvement we have achieved via the optimization of the separator. As the data show, we currently meet the cold-cranking power using the proposed cell at 70% SOC. These are beginning-of-life data and cold-cranking power at end-of-life will be verified.

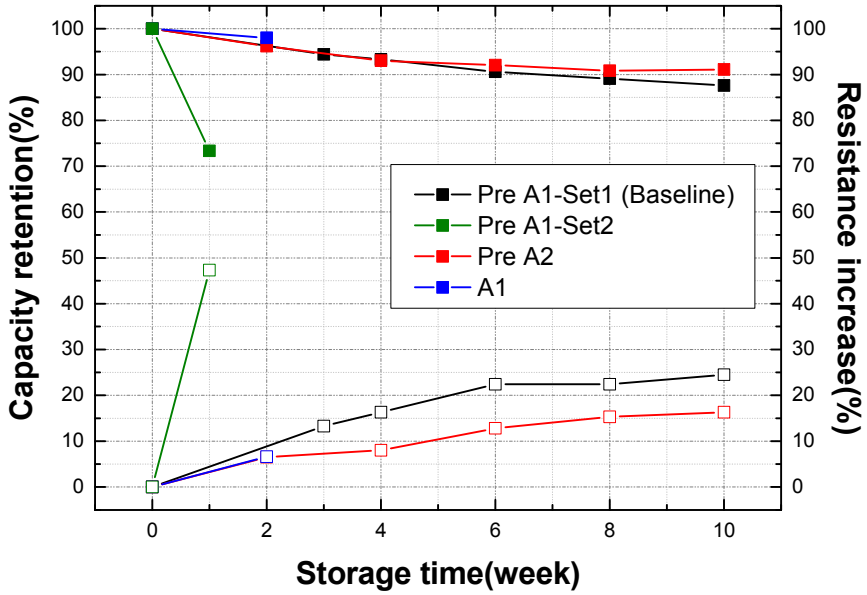


Figure II-20: The storage properties of the cells improved as improvements were achieved in the material and processing conditions of the LTO/LMO cells

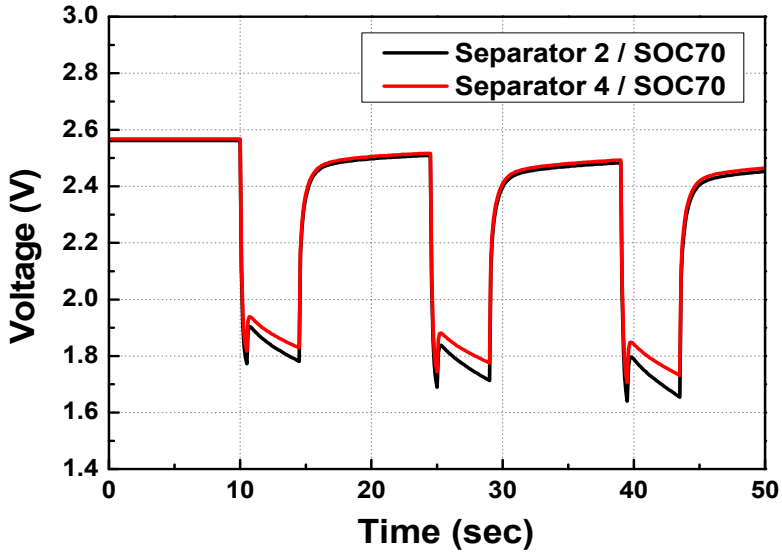


Figure II-21: The storage properties of the cells improved as improvements were achieved in the material and processing conditions of the LTO/LMO cells

The cells we developed in this program demonstrate outstanding abuse tolerance. A summary of the test data acquired per USABC test protocols is given in Table II-4. The data show that even during the 32A overcharge (Figure II-22), there was only venting of the cells, without any smoke, indicating the high level of safety of this cell. None of the test results exceeded an EUCAR hazard level of 4, and only during the thermal stability test to 250°C was smoke observed.

## Table II-4: Summary of Test Data Acquired Per USABC Test Protocols

| LGChem cell ID | Test | Condition | End Condition | Notes | EUCAR |
|---|---|---|---|---|---|
| 0022 | Thermal Ramp | 100% SOC heated at 5°C/min | 250°C, hold for 15 min, or failure | Venting and smoking, no self-ignition | 4 |
| 0023 | Thermal Ramp | 100% SOC heated at 5°C/min | 250°C, hold for 15 min, or failure | Venting and smoking, no self-ignition | 4 |
| 0021 | Overcharge | 1C (12A), room temperature | 250°C, hold for 15 min, or failure | Vent, no smoking | 4 |
| 0028 | Overcharge | 32A, room temperature | 250°C, hold for 15 min, or failure | Vent, no smoking | 4 |
| 0029 | Blunt rod, into face | 3 mm rod, 0.1 mm/s, 55°C, 100% SOC | Failure, ≥100 mV drop, or full penetration | No vent or outgassing: full penetration achieved | 2 |
| 0030 | Blunt rod, into face | 3 mm rod, 0.1 mm/s, 55°C, 100% SOC | Failure, ≥100 mV drop, or full penetration | No vent or outgassing: full penetration achieved | 2 |

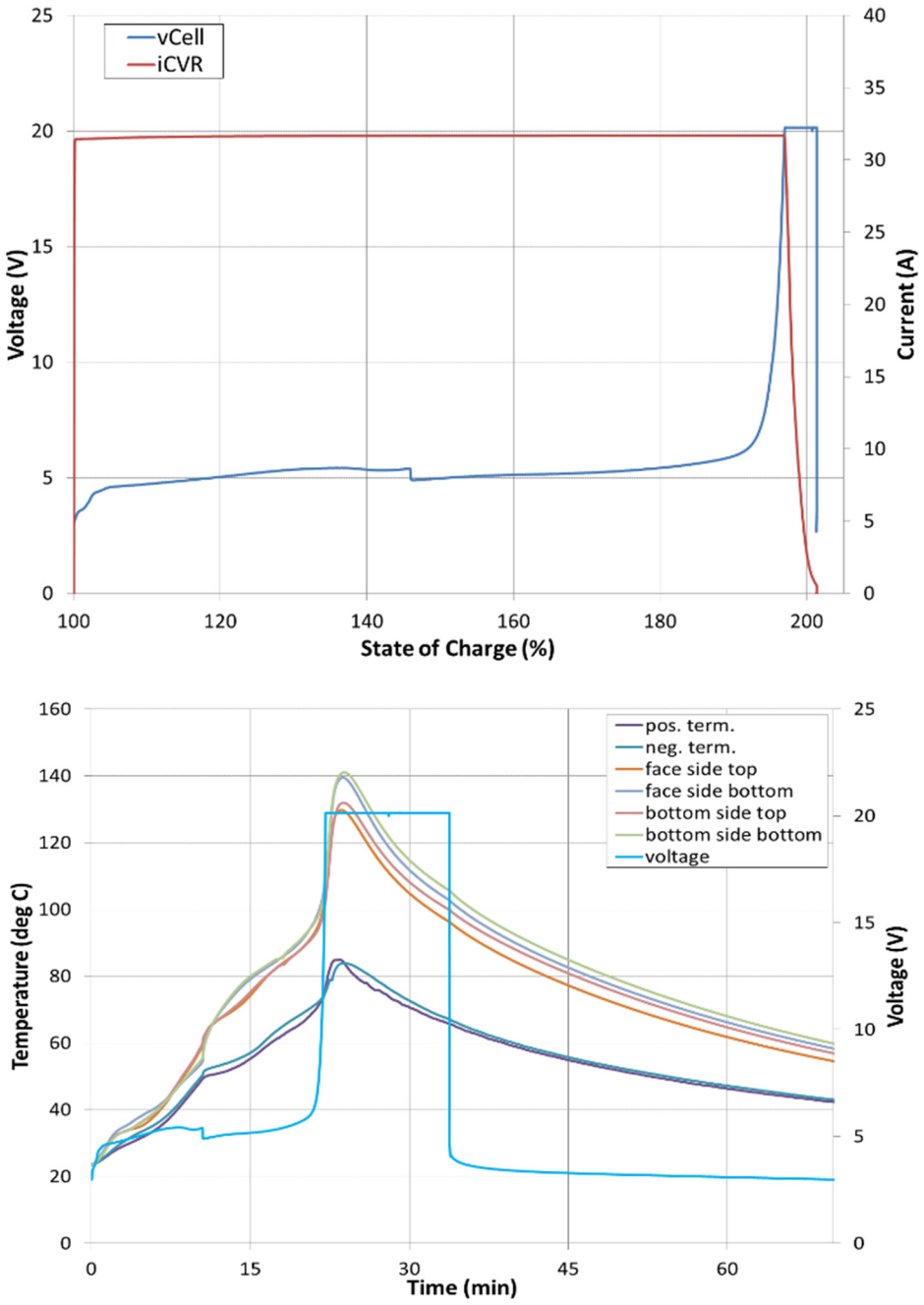


Figure II-22: Overcharge test for 32 A

## Development of the 12 Battery Pack

The focus of our battery pack design was to efficiently package and thermally manage the 12V battery pack as well as develop a simplified BMS system in a cost effective manner. A number of options to hold the cells in a mechanically robust manner were evaluated for down-selection. Several approaches that can efficiently shield the cells from exterior heat while being able to shed heat from the cells during operation were also studied. Illustrative simulations were carried out to estimate the amount of heat generated during typical operation. For example, experimental data acquired from the pack at 75°C for 4 hours agreed quite well with these estimations indicating that the cells remain below 50°C during this storage.

At the end of 2016, a number of packs will be built for delivery to the national labs for testing and validation according to USABC protocols. Figure II-23 shows the schematic of such a pack.

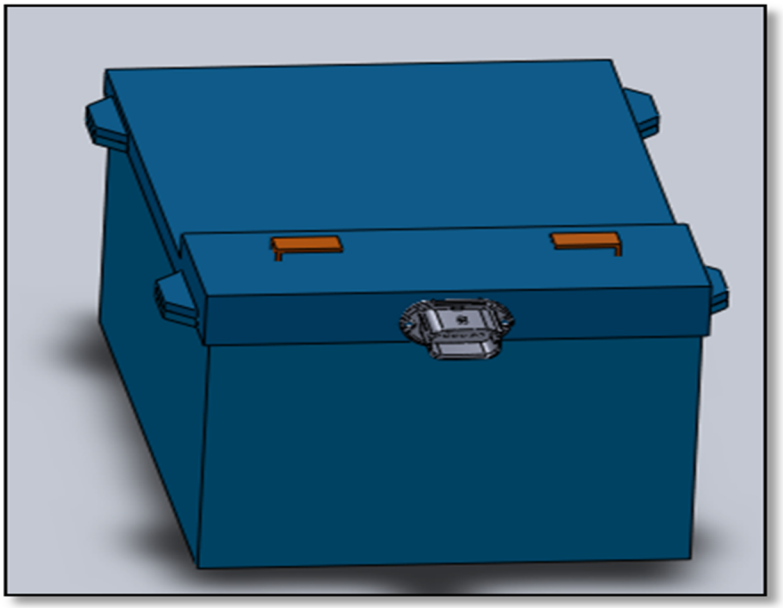

Figure II-23: Schematic of the 12 V lithium-ion Start-Stop battery pack developed in this program

## Conclusions

LG/LGCPI developed a 12V Start-Stop lithium-ion battery pack using an LTO/LMO cell chemistry. Modifications primarily to the cathode, anode and the separator resulted in significant improvement in the cold-cranking power of the battery. The packs will be delivered to the USABC for full characterization, life and abuse-tolerance tests.

There is, however, still a gap to the USABC target of meeting the cold-cranking power at the bottom of the SOC, and a gap in cost. Further development work is needed to bridge these gaps. Scaling up the battery size, however, enables us to meet the target power albeit with a battery cost that is higher than the USABC target.

### Products

## Presentations/Publications/Patents

1. “A 12V Start-Stop Li Polymer Battery Pack”, ES249_Alamgir_2016_p, US DOE Vehicle Technologies AMR, 2016.

# II.A.6. Development of 12V Start-Stop Microhybrid Batteries (Saft)

**Ian O'Connor, PD/Principal Investigator**
Saft America, Inc.
13575 Waterworks Street
Jacksonville, FL 32221
Phone: 904-861-2320; Fax: 650-331-2199
E-mail: ian.oconnor@saftamerica.com

**Harshad Tataria, USABC Program Manager**
General Motors
30003 Van Dyke Avenue
Warren, MI 48092
Phone: 248-836-7894; Fax: 586-492-4420
E-mail: harshad.s.tataria@gm.com

Start Date: June 2015
End Date: December 2017

## Abstract

## Objectives

- Saft proposes to develop an advanced, high-performance battery module for 12V Start-Stop (12VSS) vehicle applications. This technology is based on Saft's proprietary LTO lithium-ion battery technology and will advance the work undertaken in the first Phase development project with USABC.
- Technical Barriers
  - A number of key technical barriers need to be overcome to achieve both a commercial product and widespread adoption. The cost of a lithium-ion battery product is generally the most challenging requirement for deployment in the automotive industry. With this in mind Saft has proposed to undertake a novel design to eliminate numerous features that contribute to the overall cost of a battery whilst retaining the performance and lifetime characteristics that are necessary for an automotive application.
  - Barriers addressed:
    - Achieving cold-crank requirements
    - Extending the lifetime performance of the technology through alternative chemistries
    - Optimization of system control for communication and cell balancing
- Technical Targets
  - Minimize gas generation by electrochemical methods.
  - Reduce impedance growth at high temperature to meet cycle life requirements, whilst retaining low temperature (-30°C) performance characteristics.
  - The overall performance targets outlined by the USABC for the final battery are shown in Figure II-24 below.

| First Cell Deliverables | Gap Analysis Chart | | |
|---|---|---|---|
| End of Life Characteristics | Units | Under Hood Target | RPT2, 46,000 cyc |
| Discharge Pulse, 1 s | kW | 6 | 10.5 |
| Max discharge current, 0.5 s (minimum design) | A | 900 | 1000 |
| Cold cranking power at -30 ºC (three 4.5 s pulses, 10 s rests between pulses at min SOC) | kW | 6 kW for 0.5 s | 6 kW |
| | kW | 4 kW for 4 s | |
| Min voltage under cold crank | Vdc | 8 | 7.4 |
| Available energy (750 W accessory load power)* | Wh | 360 | 493 |
| Sustained Recharge Rate | W | 750 | 750 |
| Cycle life, every 10% life RPT with cold crank at min SOC | Engine starts/ miles | 450 k/150 k at 45 ºC | 46,000 |
| Calendar life at 30 ºC, 45 ºC if under hood | Years | 15 at 45 ºC | |
| Minimum round trip energy efficiency | % | 95 | |
| Maximum allowable self-discharge rate | Wh/day | 2 | 0.11 |
| Peak Operating Voltage, 10 s – Max | Vdc | 15 | 15 |
| Sustained Operating Voltage – Max | Vdc | 14.6 | 14.6 |
| Minimum Operating Voltage under Autostart | Vdc | 10.5 | 10.5 |
| Operating Temperature Range – to allow 6 kW (1s) pulse | ºC | -30 to 75 | -10ºC to 75 ºC |
| 30 ºC – 52 ºC | Wh | 360 | 502 |
| 0 ºC | Wh | 180 | 437 |
| -10 ºC | Wh | 108 | 139 |
| -20 ºC | Wh | 54 | |
| -30 ºC | Wh | 36 | |
| Survival Temperature Range (24 hours) | ºC | -46 to 100 | |

Figure II-24: USABC targets and initial Saft results

## Accomplishments

- Identification of an electrolyte blend system giving promising results for low temperature conductivity.
- Further analysis of electrolyte blends to investigate gas evolution, with identification of potential methods of significant gas reduction.

## Technical Discussion

### Introduction

This project will result in the development and delivery to USABC of fully functional prototype modules with cells in prismatic format as part of a 12 V start-stop battery system. The cells will be placed in series which also incorporates battery management electronics.

### Approach

**Innovative Approach:** This project is primarily focused on developing a low cost lithium-ion product for the automotive industry. Ultimately, we aim to provide to USABC deliverable modules in the form of multiple,

fully functional prototypes. In addition, Saft proposes to include other innovative design, development, and process improvement ideas which will reduce cost, reduce formation time several-fold, and provide simple, robust battery monitoring electronics.

- Design and manufacture a single monoblock while matching the mechanical limitations required by USABC. In particular the focus will be on achieving the performance characteristics within the 7 liter volume provided for the final module.
- Achieve cold crank performance at a temperature of -30°C as defined in the USABC test manual. This will be achieved by coupling an LTO negative electrode with a LMO based positive electrode. The electrolyte selection is also key to achieving good conductivity at low temperatures.
- Achieve increased high cycle-life/calendar life of up to 450 k cycles by limiting the impedance growth over time and preventing/accommodating significant gassing.
- Achieve a cost target of <$220/monoblock incorporating a system control unit capable of preventing overcharge on the battery and communicating with the vehicle for voltage/temperature monitoring.

## Results

The project efforts were initiated in January 2016 and we have achieved the following progress:

### Electrode Development

A number of variables were optimized on the electrodes in order to meet cold crank performance and mitigate gassing.

Further testing on the LTO electrode using different material suppliers and carbon concentrations were carried out. The results of this testing is consolidated into the data table shown in Figure II-25 below. In it we can see a snapshot of different materials that were reviewed and their impact on cold-crank performance. In general, a higher 1st 6kW pulse voltage is represented in green and offers the best opportunity for success. Supplier 4 grade 1 with graphite and carbon black as percolating network give the best cold crank performance. Moreover, with a mix of graphite and carbon black, the overall gas generation of the cell should be reduced.

| | Voltage at 0.5S first pulse | | | | | | | | | | | |
|---|---|---|---|---|---|---|---|---|---|---|---|---|
| | 95% SOC | | 70% SOC | | 55% SOC | | 40-45% SOC | | 30-25% SOC | | 15% SOC | |
| Supplier 4 grade 1 + 4% carbon 2 | 1.89<br>1.85<br>1.84 | 1.86 | 1.85<br>1.80<br>1.80 | 1.82 | 1.83<br>1.79<br>1.78 | 1.80 | 1.84<br>1.79<br>1.77 | 1.80 | 1.82<br>1.77<br>1.75 | 1.78 | 1.68<br>1.55<br>1.59 | 1.61 |
| Supplier 1 + 4% carbon 2 | 1.86<br>1.76<br>1.85 | 1.82 | 1.51<br>1.70<br>1.64 | 1.62 | | | 1.47<br>1.62<br>1.56 | 1.55 | | | 1.41<br>1.32<br>1.48 | 1.40 |
| Supplier 4 grade 2 + 1% carbon + 3% graphite1 | 1.73<br>1.89<br>1.83<br>1.86 | 1.82 | 1.65<br>1.80<br>1.72<br>1.76 | 1.73 | 1.57<br>1.73<br>1.64<br>1.70 | 1.66 | 1.51<br>1.68<br>1.57<br>1.61 | 1.59 | 1.45<br>1.61<br>1.45<br>1.53 | 1.51 | 1.33<br>1.51<br>1.31<br>1.42 | 1.39 |
| Supplier 4 grade 1+ 1% carbon 2 + 3% graphite 1 | 1.87<br>1.86<br>1.87 | 1.87 | 1.82<br>1.76<br>1.80 | 1.79 | 1.75<br>1.67<br>1.71 | 1.71 | 1.67<br>1.55<br>1.63 | 1.62 | 1.59<br>1.43<br>1.54 | 1.52 | | |
| Supplier 1 + 1% carbon + 3% graphite1 | 1.65<br>1.68<br>1.63<br>1.73 | 1.66 | 1.48<br>1.52<br>1.46<br>1.61 | 1.49 | 1.46<br>1.48<br>1.42<br>1.58 | 1.46 | 1.41<br>1.45<br>1.39<br>1.53 | 1.42 | 1.38<br>1.40<br>1.34<br>1.48 | 1.37 | 1.27<br>1.27<br>1.24<br>1.38 | 1.26 |
| Supplier 1 + 2% carbon + 2% graphite1 | 1.66<br>1.33<br>1.28 | 1.42 | 1.477<br>1.231<br>1.099 | 1.27 | 1.446<br>1.179<br>1.080 | 1.24 | 1.274<br>0.876<br>0.968 | 1.04 | | | | |

Figure II-25: LTO supplier screening and changes in electrode formulations

LMO material supplier screening showed that supplier 1 grade 2 offers some improvement at lower SOC. Furthermore it was possible to reach 30% porosity for the LMO electrode at lab scale. A 30% porosity for the LMO does not compromise cold crank performance and should be targeted from now on.

Moving forward, Saft will continue to utilize the highest performance materials. With regards to the separator, there is a wide selection of separators available and the inter-electrode distance can be critical to the performance of the cell. This is especially true at cold temperatures, where the electrolyte has a more significant impact on the cell impedance. Ultimately, through testing we were able to identify that the PP with a thickness of 12 µm had the best performance and this was chosen as the best separator for the first cell deliverables as well as the most likely candidate for the monoblock.

## Electrolyte Development

The level of gassing from blends of acetonitrile without additives were far too high. However, even with the additive it was above the level of gassing which we considered acceptable. Furthermore when we carried out cold crank testing on cells prepared with the acetonitrile + 2% additive we found the performance was severely affected. We also carried out testing with zeolite to absorb excess moisture, but found no benefit as the water just desorbed again under higher temperatures.

It was decided that the focus of electrolyte development would transition toward our other electrolyte composition, ester-based blend for which we had looked at two separate but chemically similar blends containing solvents A, B or C.

These compositions do not have any nitrile electrolyte and should offer significantly better stability than the acetonitrile blend. We can also see from Figure II-26 that the performance of solvent A- and B-based electrolyte still gives reasonable performance down to about 25% SOC, which should give a good opportunity to pass the cold crank performance.

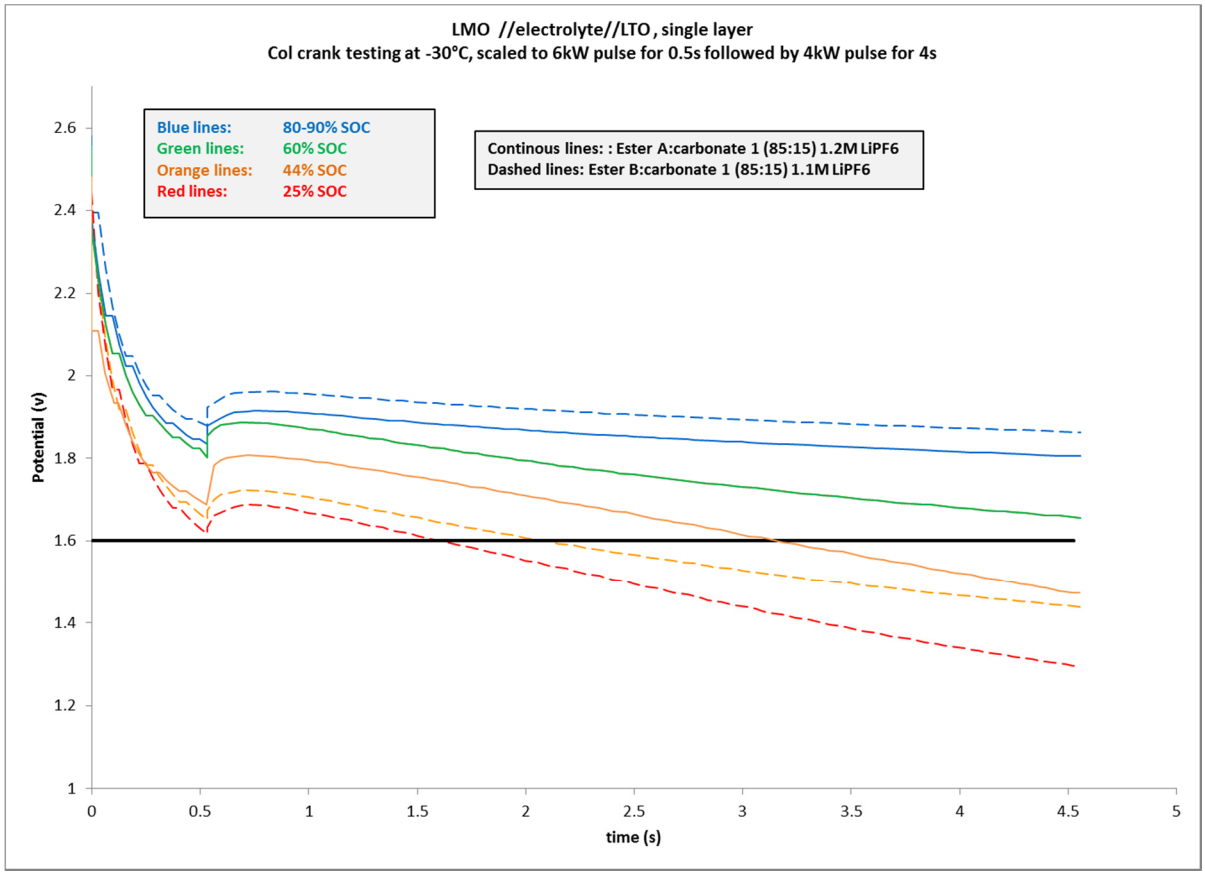


Figure II-26: Comparing Ester A and Ester B based electrolyte blends on cold crank performance

In order to select the best electrolyte to pass cold crank performance, ionic conductivity at -30°C was measured by Soulbrain for ester A, B and C blends with carbonate 1 and 2 using different volume ratios. As depicted in Figure II-27, ester C based electrolytes have the highest conductivity. Soulbrain's DOE also showed no major difference in ionic conductivity using $LiPF_6$ or LiFSi salt. LiFSi salt should help decrease gassing according to scientific articles. Saft will be testing gassing and stability of ester C based electrolyte blends.

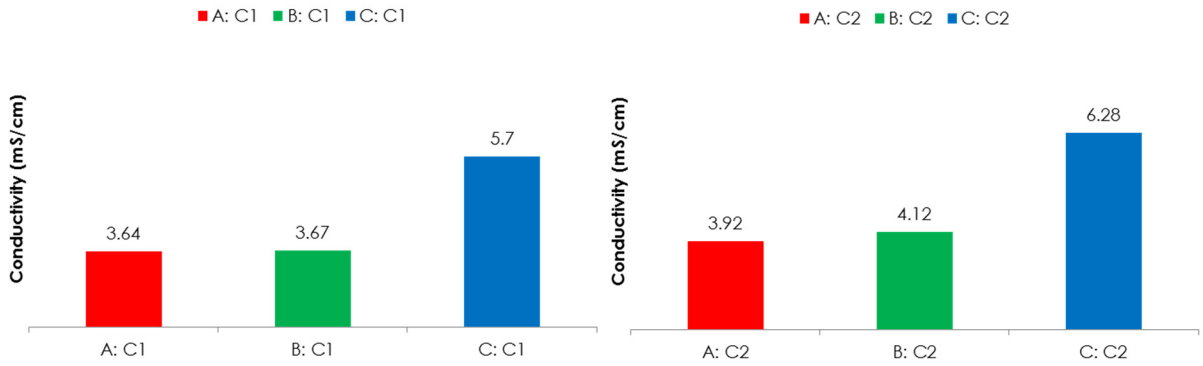


Figure II-27: Soulbrain ionic conductivity for ester A, B and C based blends at -30 °C

## First cell deliverable

The first cell deliverables were manufactured and shipped to INL. However, Saft also retained a number of cells for in-house testing. Cells had an average of 1.5Ah capacity. Initial self-discharge testing was also carried out with the results demonstrating reasonable self-discharge whereby the cells had an average of 0.11Wh/day. The final testing profiles carried out were for the cell impedance and again we found an average of 0.77mΩ impedance. The gassing results of this testing for three different cells manufactured with the same cell composition are shown in the Figure II-28. The data is very consistent between cells and it is expected that increasing the carbonate content should decrease the gassing rate to a value closer to the target.

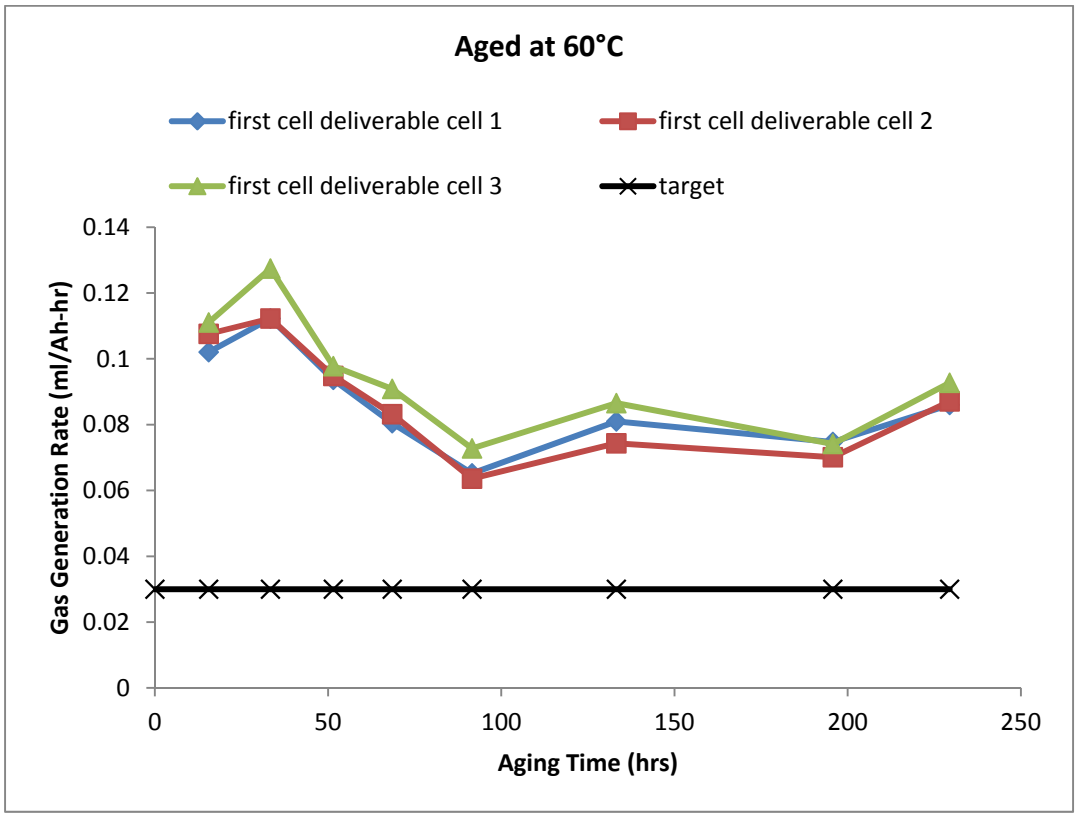


Figure II-28: Gassing rate of 3 different cells manufactured as part of 1st deliverable batch and filled with 85:15 ester: carbonate electrolyte blend; Target rate is 0.03 ml/Ah-hr

The three cells filled with 1.2M $LiPF_6$ ester A: carbonate 1 (85:15) passed the 0.5s scaled 6kW pulse for the three consecutive pulses as can be seen in Figure II-29. There is no loss in capacity at 45°C, 55°C and 65°C after 2 months calendar life testing at 50% SOC. Impedance increases during calendar life testing but the power capability of the cells at 45°C, 55°C and 65°C remain above the 6kW discharge pulse and 2.2kW charge pulse requirements as shown in Figure II-30.

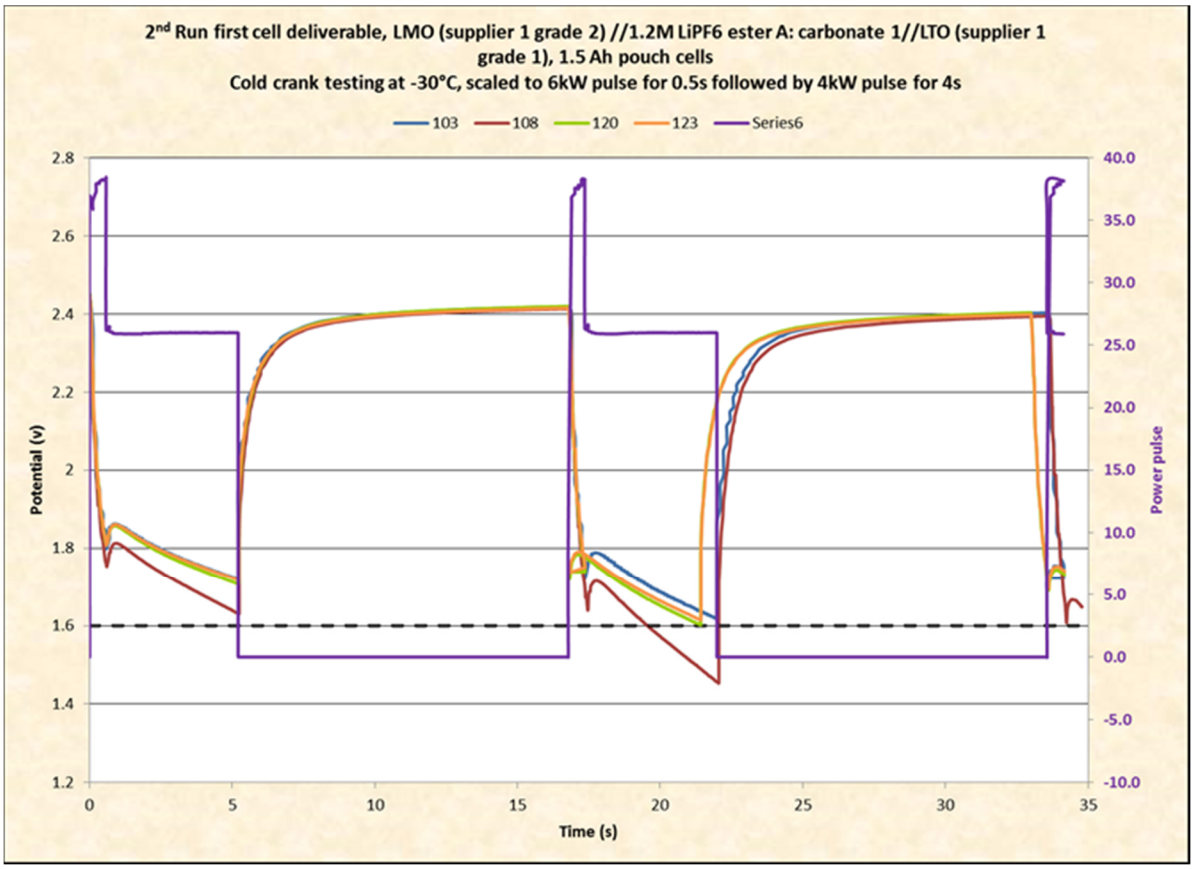


Figure II-29: Cold crank performance of cells manufactured as part of 1st deliverable batch and filled with 85:15 ester: carbonate electrolyte blend

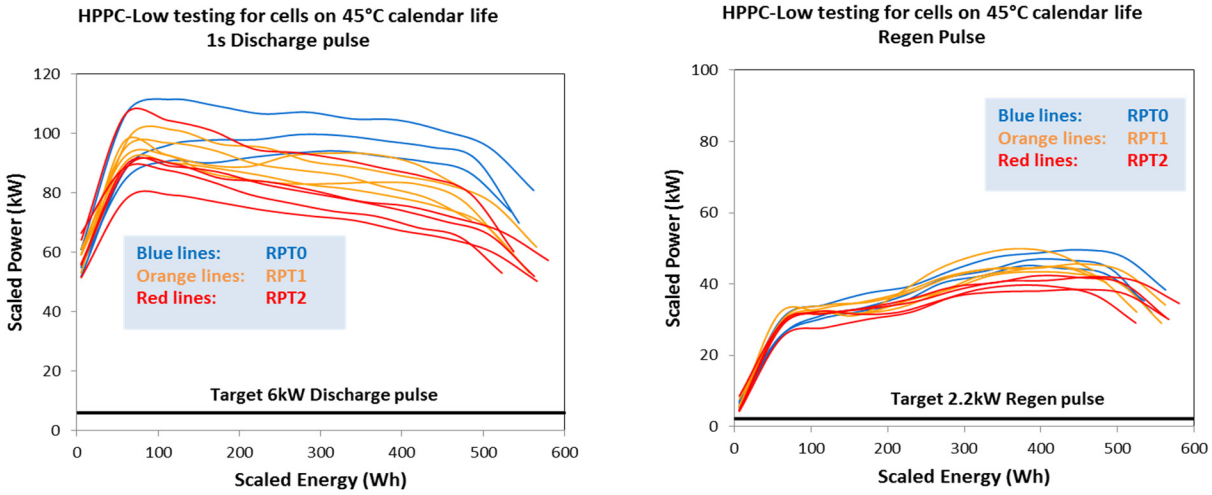


Figure II-30: Discharge capacity of the first cell deliverable before testing, after 1 month and after 2 months testing

The cells passed thermal performance testing down to -10°C taking into account the degradation imposed on the cells when tested in the specific order of 75°C, 30°C, 0°C and -10°C. Saft modeled the survivability testing conditions to determine the environment the cells would be subjected to. Cells will be tested at 70°C instead of 105°C.

The cells pass cold crank performance for the first two 6kW pulses at RPT0. For RPT1 and RPT2 the cells don't pass the 6kW pulses.

### Cell/Module Development

Over the course of 2016, Saft investigated numerous polymer types to determine whether they would be successful at acting as a barrier to moisture penetration into the electrolyte. It was determined that the overall risk to the lifetime of the module was too high and therefore it was decided to pursue alternative case construction for the module design. The overall goal is still to manufacture a prototype module at 46 Ah, and achieve all of the performance-based requirements from the gap analysis above. The final assembly will include an integrated, cost-effective battery monitoring system. An analysis of the functions required to adequately manage the electrochemical system has been initiated.

## Conclusions

### Electrode/Electrolyte Development

For the electrolyte studies, we will continue to investigate gassing and electrolyte conductivity and the impact on cold crank performance. Additional electrolytes and blends will be studied which combine good conductivity with reduced gas generation. Additives and coatings will also be investigated to reduce gassing. C-size full cell studies will be carried out with multi-layer electrodes with cold crank performance testing. Additionally, electrode optimization studies will be initiated with work on optimizing positive and negative electrode formulation (binder, percolating network etc.)

### Cell/Module Development

Saft will continue to optimize the different cell formats to achieve a more precise understanding of potential module performance and cost. Saft will identify the PCB specifications and determine appropriate industry standards to follow for circuit design, with a focus on the target cost. Additionally, we will focus on the interconnection design and determine the optimal solution for packaging, reliability, and cost for connections between the cells/busbars and the PCB.

# II.A.7. Advanced Polyolefin Separators for Lithium-ion Batteries Used in Vehicle Applications (AMTEK Research, LLC)

**Robert Waterhouse & Weston Wood, Project Manager & Principal Investigator**
AMTEK Research LLC
250 N. Hansard Avenue
Lebanon, OR 97355
Phone: 541-259-3901; Fax: 650-331-2199
E-mail: wwood@entek.com

**Brian Cunningham, DOE Technology Development Manager**
U.S. Department of Energy
Vehicle Technologies Office
1000 Independence Avenue, SW
Washington, DC 20585
Phone: 202-287-5686
E-mail: Brian.Cunningham@ee.doe.gov

Start Date: June 2015
End Date: June 2017

## Abstract

### Objectives

To develop advanced separators with improved high voltage oxidation resistance, safety features (high temperature dimensional stability, lower shutdown temperature), and lower cost for lithium-ion batteries for electrified vehicle applications.

### Technical Barriers

One of the main technical challenges in this project is the development of lithium-ion batteries with voltage stability up to 5 V. This technical barrier applies to the whole system, in which the proper electrodes, electrolyte additives and advanced separator must be properly selected so that the integrated system meets the high voltage requirements. The other main challenge is finding a solution to the proposed USABC targets that is both technically feasible and cost effective. The proposed work suggests adding value to the separator in terms of cell performance, high-voltage oxidation resistance, safety (low shrinkage, shutdown), while simultaneously reducing cost.

### Technical Targets

- Voltage tolerance: 4.5 - 5.0 V
- Air permeability: Gurley less than 250s/100cc
- Electrical resistance: MacMullin Number < 9
- High temperature dimensional stability: shrinkage less than 5% at 180°C
- Shutdown Temperature: 105°C (stretch goal)
- Wetting rate: >20% improvement compared to baseline
- Cost: <$1/$m^2$

### Accomplishments

- Produced separator with moderate loading of inorganic filler in the bulk resulting in higher porosity, lower impedance and improved wetting characteristics.

- Demonstrated enhanced shutdown with low-melting polymer wax coating.
- Developed higher voltage (4.4 V) 18650 cell with enhanced stability electrolyte during cycle life and storage testing.

## Technical Discussion

### Introduction

ENTEK has proposed to develop an advanced separator with high voltage oxidation resistance, improved safety features, and reduced cost to meet the EV requirements given by the USABC Program. The current program consists of three phases: Phase I develops and incorporates the desired features into the separator; Phase II develops approaches for reducing cost; and Phase III proves out the technology in large format, high voltage cells built by Farasis Energy.

### Approach

Phase I is based on our existing process technologies (extrusion-extraction of base films together with coatings on these base films), to incorporate value-added features (such as improved wettability, lower temperature shutdown, reduced thermal shrinkage, and improved oxidation resistance) into the separator.

In Phase II, we investigate incorporation of these features into separators by using lower cost, in-line technologies compatible with our existing manufacturing process. In-line process capability, as opposed to an off-line secondary process, will be critical for achieving the lowest possible cost structure.

In both Phase I and phase II, the developmental separator materials will be thoroughly characterized for their mechanical, chemical, and electrical properties, including cycling in coin cells and 18650 cells built by Farasis. The 18650 cells will be tested for electrochemical performance (cycle life, power (HPPC), and calendar life) and thermal abuse.

In Phase III, the best candidate separator films from Phase II will be delivered to Farasis Energy for incorporation into larger format (25 Ah) lithium-ion batteries with high voltage spinel positives and graphite negatives. These cells will be delivered to USABC/DOE for testing. Prior to building the 25 Ah deliverable cells, there will be a prototype build of 2 Ah pouch cells, to confirm the performance of the high voltage chemistry in a pouch cell design and to provide the data for a Go/No Go decision with USABC, on whether to proceed with the final deliverables.

### Results

The main tasks for January 2016 through October 2016 were:

- Production and characterization of separator with moderate loadings of inorganic filler.
- Investigation and characterization of coatings with lower temperature shutdown.
- Development of improved 18650 cell design and chemistry for improved 60ºC storage test results at a higher charge voltage (4.4 V).

#### Inorganic filler formulation trials

Two production trials were conducted in efforts to investigate the potentially improved properties from the addition of moderate levels of inorganic filler particles to the base sheet formulation:

Trial #4: Inorganic fillers were incorporated into the base separator for improving wetting, increasing porosity, and controlling pore size. All separators were prepared with 2.5% filler by volume. The fillers were fumed silica and fumed alumina, both plain and with a hydrophobic silane treatment.

Trial #5: Silica filler loading levels from 2.25wt% to 20wt% were investigated. Both untreated and hydrophobic, silane-treated silica were used in this investigation. Additionally, the silica was fed to the

extruder in two different forms: as a powder and as a pellet. The separator processing conditions were maintained constant throughout the trials for all the filler compositions.

A summary of the physical properties of selected samples from each trial is shown in Table II-5. The commercial ENTEK 20 EPH separator (20 µm nominal thickness, ~48% porosity) was used as a control sample for comparison.

**Table II-5: Physical Properties of Samples Selected from Inorganic Filler Trials #4 and #5**

| Sample Description | Porosity % | EMVECO Thickness µm | Basis weight g/m2 | Gurley s/100cc | MacMullin Number Dim'less | Puncture gf |
|---|---|---|---|---|---|---|
| 20 EPH Control, 20µm | 48.1 | 21.0 | 9.9 | 179 | 7.5 | 571 |
| Trial #4: 2.5% alumina, treated | 52.4 | 21.4 | 10.1 | 123 | 6.3 | 481 |
| Trial #4: 2.5% silica, untreated | 54.0 | 25.7 | 11.1 | 114 | 6.0 | 495 |
| Trial #4: 2.5% silica, treated | 52.1 | 21.7 | 10.1 | 131 | 7.1 | 516 |
| Trial #5: 5% silica, treated | 50.4 | 20.7 | 9.9 | 154 | 7.5 | 533 |
| Trial #5: 10% silica, treated | 54.9 | 21.9 | 9.2 | 121 | 4.5 | 511 |
| Trial #5: 10% silica, untreated | 59 | 21.9 | 8.7 | 95 | 3.6 | 440 |
| Trial #5: 20% silica, untreated | 65.3 | 21.5 | 7.8 | 75 | 3.2 | 393 |

Table II-5 shows that increasing levels of filler resulted in greater porosity, higher air permeability (lower Gurley test seconds) and lower electrical resistance (MacMullin Number). While the puncture strength decreased with increasing filler level (consistent with the decrease in polymer volume fraction in the separator), the puncture strength was still higher than the values specified in the USABC separator Gap Chart.

Thermal and mechanical properties of the control and trial samples are shown in Table II-6. For Trials 4 and 5, separator shrinkages increase and mechanical properties decrease with increasing filler content. The decreased mechanical strength is consistent with the higher porosity and reduced polymer volume fraction. The increase in shrinkage is also a direct result of the increase in porosity. Application of a ceramic coating to the filled separator will be required to control the shrinkage at high temperatures.

## Table II-6: Thermal and Mechanical Properties of Samples Selected from Inorganic Filler Trials

| Sample Description | 120°C shrinks 30 min MD% | 120°C shrinks 30 min XMD% | MD Tensile kg/cm$^2$ | XMD Tensile kg/cm$^2$ | MD Elongation (%) | XMD Elongation (%) |
|---|---|---|---|---|---|---|
| 20 EPH Control | 9.0 | 4.0 | 1190 | 763 | 109 | 286 |
| Trial #4: 2.5% alumina, treated | 7.5 | 4.8 | 1371 | 594 | 87 | 300 |
| Trial #4: 2.5% silica, untreated | 8.5 | 2.3 | 907 | 542 | 93.5 | 365 |
| Trial #4: 2.5% silica, treated | 8.9 | 4.5 | 1509 | 596 | 67.5 | 353 |
| Trial #5: 5% silica, treated | 14.8 | 9.6 | 1154 | 722 | 75 | 263 |
| Trial #5: 10% silica, treated | 15.6 | 13.1 | 1142 | 725 | 81.3 | 238 |
| Trial #5: 10% silica, untreated | 16.2 | 11.9 | 815 | 722 | 72.8 | 198 |
| Trial #5: 20% silica, untreated | 17.4 | 14.0 | 803 | 532 | 57 | 241 |

Shutdown testing was conducted on control and trial samples under constant heating rate and pressure. The electrolyte used for shutdown testing was 1M LiTFSI in 1:1 v:v ratio of polyethylene carbonate: triethylene glycol dimethylether. This electrolyte was chosen because of its lack of flammability and its high boiling temperature. The separator was wetted in the electrolyte, sandwiched between graphite sheets, and heated at a rate of 60°C/min under a pressure of 450 psi. The electrical ac impedance of the separator was measured as a function of temperature. "Shutdown temperature" was defined as the temperature at which the impedance increased to 1000x the impedance at 100°C.

Shutdown testing was conducted on control and trial samples under constant heating rate and pressure. Shutdown results are shown in Table II-7. Separators prepared with 10wt% inorganic filler show similar shutdown curves to that of control samples. When increasing the silica loading level to 20wt%, samples still display shutdown characteristics, although the slope of the impedance/temperature curve decreased considerably, resulting in a higher measured shutdown temperature.

## Table II-7: Thermal and Mechanical Properties of Samples Selected from Inorganic Filler Trials

| Sample Description | Impedance at 100°C Ohms | 1000x Shutdown Temperature °C |
|---|---|---|
| 20 EPH Control | 4.7 | 160 |
| Trial #4: 2.5% alumina, treated | 4.4 | 159 |
| Trial #4: 2.5% silica, untreated | NA | 163 |
| Trial #4: 2.5% silica, treated | NA | 156 |
| Trial #5: 5% silica, treated | 4.1 | 162 |
| Trial #5: 10% silica, treated | 3.9 | 162 |
| Trial #5: 10% silica, untreated | 3.5 | 171 |
| Trial #5: 20% silica, untreated | 4.1 | 176 |

The wetting characteristics of the Trial 5 samples were determined using a droplet wetting test. A droplet of controlled volume (5µl) was placed on the separator and the wetted area was measured after 5 minutes for each sample. Propylene carbonate/tri(ethylene glycol)dimethyl ether in proportions of 1:1 by volume was used as the liquid for the wetting experiment. The largest wetting improvement came from the sample with 20wt% untreated silica, which resulted in a 34% improvement in the droplet wetting test relative to the EPH control material. (See Figure II-31.)

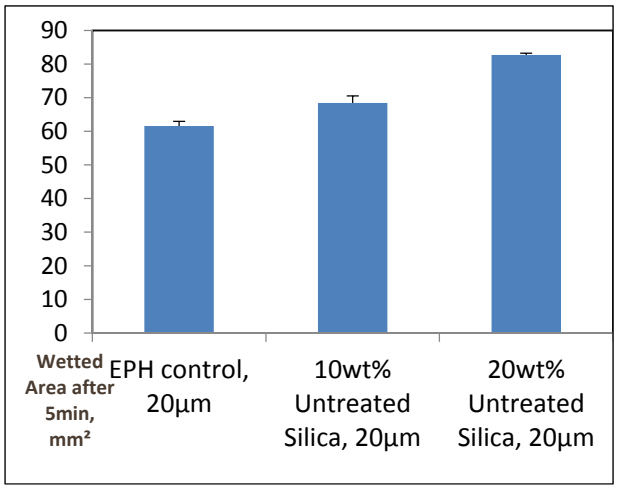


**Figure II-31: Wetting characteristics of selected samples**

## Investigation and characterization of low temperature shutdown coatings

Polymer coatings that will soften in a temperature range higher than the anticipated operating temperature of the battery and lower than the melting point of the polyethylene in the separator film were investigated as a route to reducing the shutdown temperature of the separator. The requirements of the polymer to be used in the coatings are:

- Thermal transition (melting) near 100°C;
- Insoluble in electrolyte solutions at elevated temperatures;
- Must maintain mechanical integrity at elevated temperatures.

Based on these requirements, polyolefins (e.g., PE, PP waxes) were identified as potential candidates for this application. Two polyethylene waxes, with different softening points and particle sizes were investigated. Each grade of polyethylene wax was incorporated into a ceramic based coating at concentrations ranging from 4 to 47 wt%.

Figure II-32 shows shutdown curves of EPH control separator coated with alumina/polyethylene (Wax 1 and 2). The coated separators exhibited a shift to lower shutdown temperatures compared to the EPH control sample. Coated separator incorporating Wax 1 showed a characteristic increase in impedance near 100°C. The magnitude of this peak increased with increasing loading level up to 47wt%. In contrast, Wax 2 did not show this characteristic peak. At the highest loading level of 47wt% for Wax 2, the initial impedance was near 1100 Ohms, and Gurley values were too dense to test. The greatest improvement in shutdown temperature (-13°C) was obtinaed with a coating containing 12% of Wax 2.

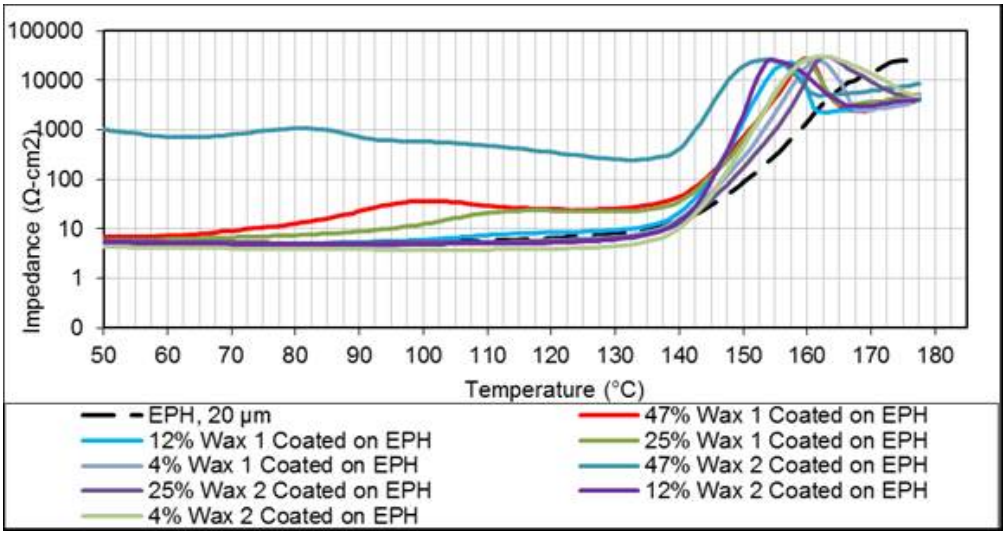


Figure II-32: Wetting characteristics of selected samples

## Improved 18650 cell design for performance characterization of separators

Cylindrical 18650 cells were used for performance evaluation of five different separators in cycle life and storage tests at full charge and elevated temperature (60°C). In storage testing, the cells exhibited a lot of variation within each group and overall poor stability with high rates of self-discharge. Farasis investigated the root cause of the behavior and developed an improved cell design with a more stable electrolyte and higher voltage capability (4.4 V vs. 4.2 V). Seven groups of cells are currently on test with the new cell design. Early results for the 60°C storage test are very promising, as shown in Figure II-33.

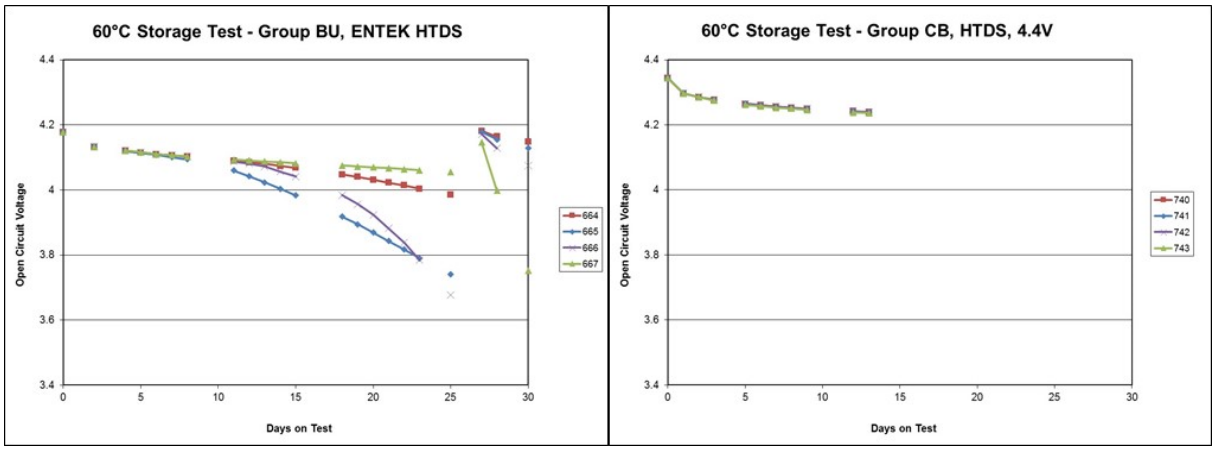


Figure II-33: Wetting characteristics of selected samples

## Conclusions

- The incorporation of moderate amounts of fumed silica into the base sheet yields large improvements in separator porosity and resistance. While the mechanical strength is reduced, it is still acceptable. The shutdown function is preserved, although at a higher temperature.
- Coatings of polyolefin waxes combined with alumina ceramic can be used to lower the shutdown temperature of the separator.
- Farasis has developed an improved 18650 cell design for evaluating the performance of separators developed under this program. The new design operates to a higher voltage of 4.4 V and exhibits good stability and cell-to-cell uniformity. (See Table II-8.)

- Future work will continue the development of coatings for the improved base membrane focusing on high temperature stability, voltage resistance, and cost. New, lower cost methods of applying the coatings will be explored.

## References

- None

### Table II-8: USABC Gap Analysis Chart of Selected Base and Ceramic Coated Membranes

| Parameter | Units | 20 EPH | Trial 5: 10% silica | Trial 5: 20% silica | Advanced Separator Goal | USABC Goal |
|---|---|---|---|---|---|---|
| Nominal Thickness | um | 20 | 20 | 20 | <25 | <25±1 |
| Permeability | s/10cm$^3$ | 14.8 | 9.5 | 6.7 | <25 | <25 (Energy) <11 (Power) |
| MacMullin | None | 7.9 | 4.3 | 3.6 | <9 | <8 (Energy) < 4 (Power) |
| Wettability | None | Wets in electrolyte | Wets in electrolyte | Wets in electrolyte | >20% improvement | Wets in electrolyte |
| Average Pore size | um | <0.2 | <0.2 | <0.2 | <0.2 | <0.2 |
| Puncture | gf/25.4um film | 588 | 506 | 424 | >300 | 300 |
| Thermal Stability | MD% shrink, 90°C (1 h) | 2.4 | 2.8 | 2.8 | <3 | <5 |
| Tensile Strength | MD% shrink, 180°C (30 min) | >60 | >60 | >60 | <5 | - |
| Cost | PSI at 2% offset | 7040 | 4509 | 4850 | >3000 | 1000 psi at 2% offset |
| Shutdown Temperature | $/m² | - | <1.20 | <1.20 | 1.00 | 0.60 |
| High Voltage Resistance | °C | 160.0 | 170 | 170 | 10°C Less than baseline* | 105 |

# II.A.8. Rapid Commercialization of High Energy Anode Materials (SiNode Systems)

**Cary Hayner, Principal Investigator**
SiNode Systems
3440 S. Dearborn Street, #113N
Chicago, IL 60616
Phone: 612-220-3846
E-mail: caryhayner@sinode-systems.com

**Francis Wang, Ph.D., Program Manager**
SiNode Systems
3440 S. Dearborn Street, #113N
Chicago, IL 60616
Phone: 312-894-9809
E-mail: francis@sinode-systems.com

Start Date: May 2016
End Date: October 2018

## Abstract

### Objectives

The project entitled "Rapid Commercialization of High Energy Anode Materials" has been established with the aim of extending, benchmarking and demonstrating the performance of SiNode System's advanced silicon-based anode materials in battery form factors and designs relevant for electric vehicle applications.

### Accomplishments

- SiNode has achieved an 80% first cycle efficiency and a 99.4% average coulombic efficiency for initial material stabilization trials.
- Manufacturing scale-up has begun internally with current production rates of ~1kg/month.
- Materials production is on track to exceed 2kg/month in Q4 (early 2017).
- Cell prototype development with A123 systems has begun and is on track for 1Ah cell delivery in Q5 (~April–May 2017).

## Technical Discussion

### Background

As the global popularity of electric vehicles steadily increases, so have its power and energy requirements to meet mainstream needs. Performance trajectories of traditional lithium-ion technology, despite an annual 3–5% improvement in energy density since inception, suggest that long term electric vehicle needs will not be met without an evolution beyond traditional energy storage materials (i.e., graphitic anodes). SiNode Systems has developed a novel Si-based, negative-electrode materials technology which can enable a quantum leap in battery energy and power density, and can significantly impact battery weight and run-times that burden today's electric vehicles. Herein, we report the technical highlights and accomplishments from the first seven months of the USABC project entitled: "Rapid Commercialization of High Energy Anode Materials".

## Introduction

The market adoption of silicon-based anodes has been primarily challenged by rapid cycle life degradation, a result of extreme anode volume changes during charge and discharge. Cycle life degradation in silicon-based alloys is well understood and can be broken down into two fundamental failure modes: a. electrical disconnection and b. unstable solid electrolyte interface (SEI).

The electrical disconnection of electrochemically active particles occurs as a consequence of extreme anode volume changes, and is evidenced as irreversible capacity losses. Researchers have leveraged SEM and electrochemical characterization techniques to demonstrate that these irreversible losses can occur either by particle fracture and/or isolation from conductive supports (i.e., carbon black conductive additives etc.) In either case, irreversible capacity losses due to electrical disconnection are not readily solved by the addition of excess conductive agents, binders or traditional coatings.

Cycle life degradation in alloy anode systems is also a function of SEI instability. In the absence of a stabilized interface, lithium is continually consumed at the active surface, ultimately impacting available lithium ion redox transport. Interface stability is particularly challenging in alloy anode systems, as new surfaces are continuously exposed during expansion-fracture. As in the case of electrical disconnection, irreversible losses due to SEI instability are not readily solved by traditional methods (i.e., low surface area coatings) due to the large volume changes during charge and discharge.

## Approach

SiNode Systems has demonstrated a novel high energy density (>300 Wh/kg) Si-based negative-electrode materials technology that has the long-term potential to replace graphite-based anodes in lithium-ion batteries. SiNode's technology uses a proprietary silicon alloy-graphene material architecture to achieve: i) category-leading performance and ii) solutions to long-standing Si anode technical hurdles. The proprietary combination of silicon-based alloys and a flexible 3D graphene network helps stabilize the active material during charge and discharge (see Figure II-34) by providing an interfacial barrier between the active material and the electrolyte which can accommodate large volumetric changes through a laminar graphene sliding mechanism. The 3D graphene-silicon architecture results in: a. minimization of capacity losses due to electrical disconnection, b. significantly improved active utilization (mAh/g) and c. partial stabilization of the SEI interface with a flexible physical barrier between electrolyte and active material.


Figure II-34: Si-anode failure mechanisms (left), SiNode graphene-wrapped advanced silicon anode architecture (right)

SiNode has made continuous improvements against key USABC advanced electrode metrics, demonstrating an attractive trajectory towards USABC advanced electrode goals. The program goal is the advancement and commercialization of advanced silicon-based active materials for high energy/high power EV batteries. Specifically, the program aims to demonstrate that SiNode technologies can: a. exceed USABC electric vehicle performance targets in USABC-recognized cell form factors, b. produce at-scale by commercially viable methods and c. reach USABC cost targets at scale. To this end, a set of tasks were developed to address the core technology gaps and associated barriers: Task 1: Materials Stabilization and Analysis, Task 2. Manufacturing Scale-Up, Task 3. System Cost Reduction, Task 4. Cell Prototype Evaluation, Task 5. Downstream Cell Process Optimization and Task 6. Cell Characterization and Performance Evaluation.

## Results

**Task 1 - Materials Stabilization and Analysis:** It has been recognized that SEI stabilization is one of the key technological challenges in achieving USABC cycle life objectives (i.e., 1000 cycles). First cycle efficiency (FCE) and average coulombic efficiency (CE) are two of the commonly referenced key performance indicators (KPIs) for cycle life. SiNode, in collaboration with strategic commercial partners, is pursuing several technical routes to achieve USABC performance targets, including graphene wrapping optimization, silicon alloy compositions (i.e., Si:O), active material surface modifications, electrolyte additives and physical mixtures with graphite anode materials.

Figure II-35 highlights the pace of innovation for average CE and FCE for the program to date. First cycle efficiencies have shown a 9.6% improvement (Q2 FCE=80%) from program start, and have been achieved by optimizing the graphene type and composition at the active material:electrolyte interface. Average CE has been improved from 98.6% to 99.4%, and has been achieved by altering the average Si:O ratio. Although both average CE and FCE require further improvements, an attractive pace of innovation to extend SiNode cycle life capabilities and meet USABC goals has been demonstrated.

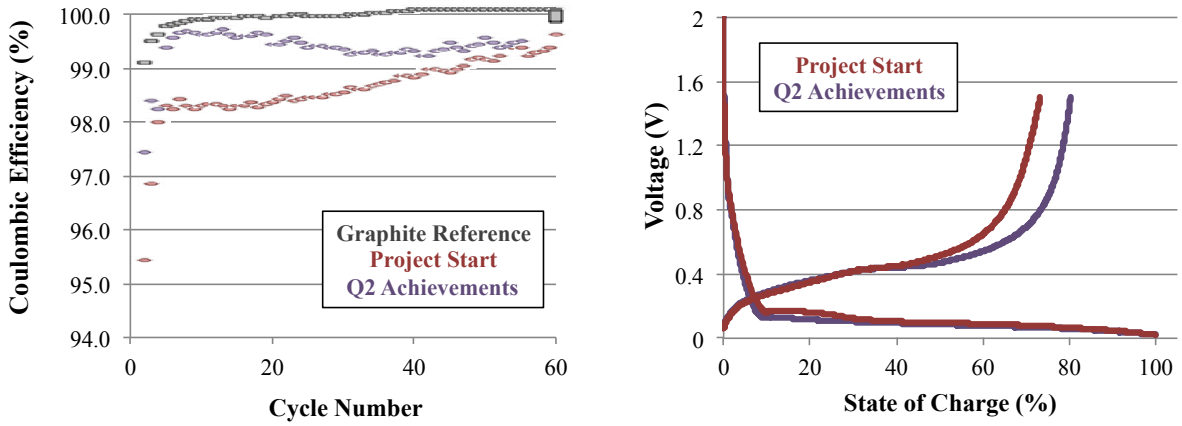


Figure II-35: Average Coulombic Efficiency vs Cycle Number (left), First Cycle Efficiency (Right)

**Task 2 – Manufacturing Scale-Up:** Task 2 addresses the production readiness of SiNode's anode technology. Activities involve commercial partnerships to demonstrate scalable products using commercially viable methods. Over the next several quarters, materials production will be ramped up and will transition from lab-scale operations to pilot scale operations by Q1 2017. Figure II-36 summarizes the latest forecast from August 2016 to April 2017. The introduction of additional production throughput will come on-line in early 2017 to keep excess production work shifts to a minimum. Partners are expected to transition operations internally by early Q1 2017. Product validation will be regularly addressed to insure both quality and scale.

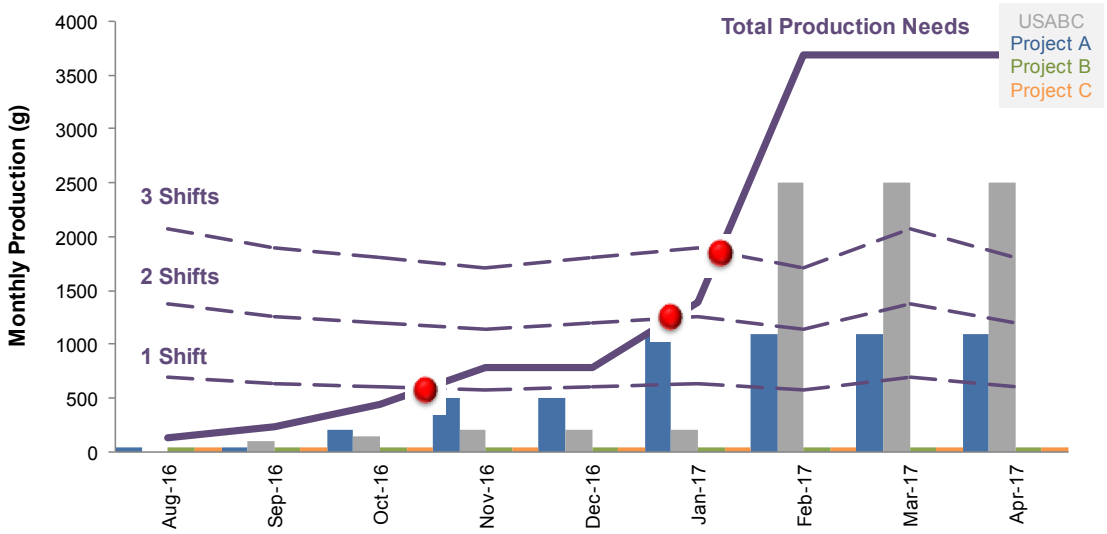


Figure II-36: SiNode Active Material Production Ramping Forecast (Q4 2016 – Q1 2017)

## Conclusions

SiNode has entered the 7th month of this 30-month-long project. Over the next quarter, manufacturing scale-up and cell prototype production will begin to ramp to our 1Ah pouch-cell deliverables. This will be a major milestone for SiNode, and successful demonstration of performance in commercially relevant cells will mark the achievement of a minimum viable product.

Several challenges face the project over the coming year, including consistent improvements of the average coulombic efficiency, electrode expansion, multi-kilogram production, successful battery electrode design and line-of-sight on materials cost reductions (i.e., graphene and silicon).

SiNode has demonstrated a cadence of innovation and product development over the past 7 months, and looks optimistically towards demonstration of viable performance in commercially relevant EV cells.

### Products

## Presentations/Publications/Patents

1. "Advanced Silicon-Graphene Composites for High Performance Applications," C. Hayner, J. Lau, S. Ha, J. McKinney, F.P. Wang, S. Mayekar, International Meeting on Lithium Batteries, Chicago, Illinois, June 21, 2016.
2. "High Energy Anode Material Development for Lithium-ion Batteries," C. Hayner, Department of Energy Annual Merit Review, Washington, D.C., June 7, 2016.

### References


1. McDowell, M. T.; Lee, S. W.; Nix, W. D.; Cui, Y. Adv. Mater. 2013, 25, 4966.
2. Zhang, W.-J. J. Power Sources 2011, 196, 877.
3. Park, C.-M.; Kim, J.-H.; Kim, H.; Sohn, H.-J. Chem. Soc. Rev. 2010, 39, 3115.
4. Larcher, D.; Beattie, S.; Morcrette, M.; Edström, K.; Jumas, J.-C.;Tarascon, J.-M. J. Mater. Chem. 2007, 17, 3759.
5. Kasavajjula, U.; Wang, C.; Appleby, A. J. J. Power Sources 2007,163, 1003.
6. Huggins, R. A. J. Power Sources 1999,1−82, 13.
7. Besenhard, J. O.; Yang, J.; Winter, M. J. Power Sources 1997, 68, 87.
8. Winter, M.; Besenhard, J. O. Electrochim. Acta 1999, 45, 31.
9. M. N. Obrovac and V. L. Chevrier, Chem. Rev. 2014, 114, 11444−11502

# II.A.9. Hybrid Electrolytes for PHEV Applications (NOHMs Technologies)

**Surya Moganty, Principal Investigator**
NOHMs Technologies, Inc
1200 Ridgeway Avenue
Rochester, New York, 14467
Phone: 607-379-5444
E-mail: surya@nohms.com

**Zoe Zhou, USABC Program Manager**
Ford Research & Innovation Center
2101 Village Road
Dearborn, MI 48121
Phone: 313-248-1896; Fax: 313-621-0646
E-mail: qzhou18@ford.com

Start Date: August 15, 2015
End Date: February 14, 2017

## Abstract

Rechargeable lithium-ion batteries are promising energy storage options for plug-in-hybrid electric vehicles (PHEVs) and all-electric vehicles (EVs). However, among other requirements for lithium-ion batteries to be viable for transportation applications, a high energy density cathode is required. High voltage cathodes have the potential to provide a solution for low cost, longer-range electric vehicles. This new class of electrode material can deliver capacity >250 mAh $g^{-1}$, that is ~65% higher than that delivered by current state-of-the-art cathodes. To access this high capacity, one has to operate the cell at a higher potential >4.5 V vs Li/Li+, whereas conventional lithium ion cells do not exceed 4.2 volts. Conventional lithium-ion battery electrolytes, however, are NOT stable above 4.2 Volts and complementary development of electrolytes that are stable at these higher voltages is critical to make use of this class of high voltage cathodes. An electrolyte innovation that enables temperature-stable 5V cell operation would transform the industry and enable rapid growth of new market segments.

Research and Development at NOHMs has resulted in a family of novel electrolyte formulations, which include ionic liquids to improve energy density, safety, and high temperature durability of Plug-In Hybrid Electric Vehicle ("PHEV") lithium-ion batteries. NOHMs' proprietary functional ionic liquids in-development for lithium-ion battery electrolytes have displayed excellent electrochemical and thermal stability compared to state-of-art lithium-ion battery electrolytes, and when compared with previously reported ionic liquid electrolytes demonstrate improved stability against graphite-containing anodes and high voltage cathodes, as well as improved rate capability and low temperature performance.

To meet the USABC long term criteria for electrolytes (1) cost (2) high-voltage stability (3) low-temperature performance, and (4) abuse tolerance, NOHMs is partnering with A123 Systems (A123) for manufacturing and testing commercial-grade cells as well as with a chemical consultant company (Xerox) to develop and scale a low-cost, high-purity synthesis process for its ionic liquid electrolytes.

The objective of this program is to develop functional ionic liquid based electrolyte combinations with appropriate co-solvent combinations that exhibit high ionic conductivity, excellent cathodic and anodic stability and high thermal stability for applications in 5V lithium-ion batteries. The proposed work will build on the success of NOHMs electrolytes to create optimized electrolyte formulations that are non-flammable and simultaneously overcome traditional barriers, effective SEI layer formation and cation co-intercalation in graphite associated with ILs. The final goal of this project is to demonstrate the feasibility of these ionic liquid electrolyte systems in 2Ah and 10Ah Graphite//$LiMn_{1.5}Ni_{0.5}O_4$ (LNMO) and Graphite//$Li_{1.2}Mn_{0.55}Ni_{0.15}Co_{0.1}O_2$ (NMC532) full cells.

## Objectives

To achieve these goals, we propose to pursue the following technical objectives during the proposed electrolyte development:

- Functional ionic liquid design and synthesis (NOHMs)
- "5.0 V" Electrolyte formulation and optimization (NOHMs and A123)
- Prototype cell assembly and testing (A123 and NOHMs)
- Design and cost study of electrolyte production (NOHMs and Xerox)
- Building 2Ah and 10 Ah pouch cells for USABC deliverables (A123 and NOHMs)

## Accomplishments

- Identified stable functional ionic liquid with both cathodic and anodic stability
- Developed electrolyte formulations showing high voltage stability (>4.5V)
- Delivered 2Ah NMC532 cells (30 pcs) for independent testing at national labs (INL, SNL)
- Developed insights into working mechanism of NOHMs electrolyte formulation at 4.5V against NMC532 cathode using various analytical methods (EIS, FTIR, XPS)

## Future Achievements

- Delivery of 2 Ah LNMO pouch cells (30 pcs) for national lab testing
- Delivery of 10 Ah NMC532 pouch cells (30 pcs) for national lab testing
- Delivery of 10 Ah LNMO pouch cells (30 pcs) for national lab testing
- Cost estimation of electrolyte formulations
- Fundamental understanding of electrolyte working mechanism

## Technical Discussion

### Background

Because the energy density of a battery is proportional to the cell potential and the power density is proportional to the square of the cell potential, it is understood that electrode couples capable of operating at higher voltages provide synergistic benefits. Therefore, new strategies for designing lithium-ion batteries with higher energy and power demand alternative high potential cathode materials with superior capacities, in comparison to standard oxides ($LiCoO_2$, $LiMn_2O_4$) and olivine phosphates ($LiFePO_4$) type electrodes in current use. Among various insertion cathode materials, $LiMn_{1.5}Ni_{0.5}O_4$ (LNMO) spinels, layered $Li_2MnO_3$ stabilized $LiMO_2$ (M = Mn, Ni, Co) oxides (NMC), and $LiMPO_4$ olivines (M= Mn, Mn and Fe, Co) are actively investigated as next generation cathode materials for high voltage applications. To access the high capacity from any of these high voltage cathodes, one has to electrochemically activate the cathodes by charging to a potential >4.5 V vs Li/Li+. Conventional lithium-ion battery electrolytes, however, are not stable above 4.2 Volts and complementary development of electrolytes that are stable at these voltages is critical to safely use this class of high voltage cathodes.

### Introduction

Recent progress in synthesis and electrochemical analysis of room temperature ionic liquids (ILs) has established the promise of this unique class of materials as electrolytes for next-generation lithium batteries. ILs are organic salts having melting points below 100°C and generally consist of a bulky cation and an inorganic anion. The large cation size allows for the delocalization and screening of charges, resulting in a reduction in the lattice energy and thereby the melting point or glass transition temperature. Because of their unique combination of physicochemical properties, such as negligible vapor pressure, non-flammability, good room-temperature ionic conductivity, wide electrochemical window, and favorable chemical and thermal

stability, ILs possess many synergistic attributes that make electrolytes based on ILs viable materials of choice for lithium batteries. The vast range of anion and cation chemistries that can be combined to create ILs tailor-made or explicitly designed to complement a specific combination of electrode chemistries also provide a largely untapped materials library that can address important concerns about battery safety.

## Approach

Research and Development at NOHMs has resulted in a family of novel electrolyte formulations containing pyrrolidinium-based ionic liquids showing excellent high voltage stability. Ethylene carbonate (EC) is the main functional component of the state-of-the-art electrolyte due to its excellent SEI film forming ability on carbon-based anode materials. This trait has earned it stature among the other low melting point solvents used in electrolytes for LIBs. Other solvents such as sulfones, fluorinated carbonates and di-nitiriles with excellent high voltage stability and SEI forming ability suffer from high melting temperatures. Hence, to widen the liquidus temperature range of these solvents, we have designed and optimized NOHMs functional ionic liquids that impart desirable traits. By manipulating functional group and amount of ionic liquid, it is possible to adjust the interactions between host solvent molecules and functional ILs. Building on these results, we developed and evaluated novel electrolyte formulations suitable for NMC532 (4.5V) and LNMO (4.9V) cathode materials.

## Results

### Stability against Graphite anode

It has been reported that the cation of the ionic liquid co-intercalate into the graphitic panels and also electrochemically reduce at higher voltages than the lithium-ion co-intercalation potential. NOHMs-designed ionic liquids show excellent stability against graphite anode, Figure II-37 depicts the initial cycle capacity loss or irreversible capacity loss (ICL) measured in Li-Graphite half cells.

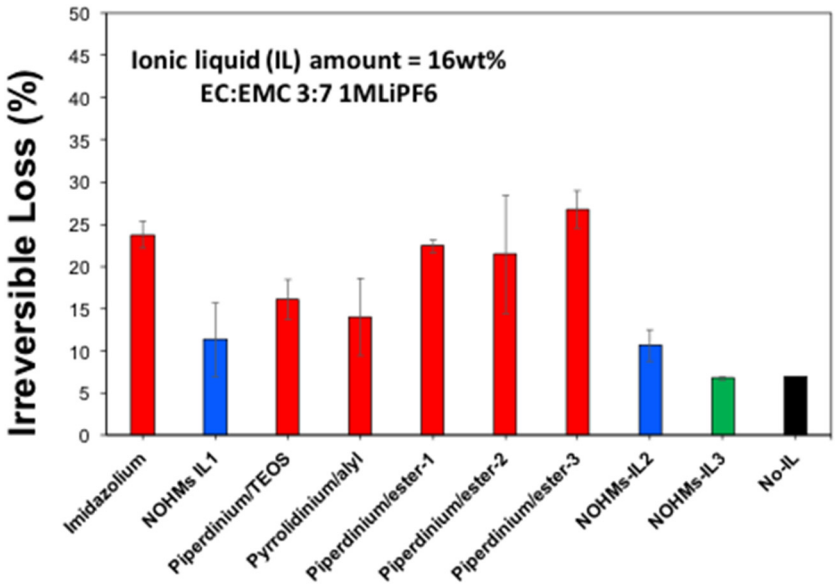


**Figure II-37: Irreversible capacity loss of graphite anode as a function of ionic liquid type. EC/EMC 3:7 1MLiPF6 electrolyte with 16 wt% of ionic liquid was used to measure the capacity loss. Among the various ionic liquids investigated NOHMs designed ionic liquids showed excellent stability against graphite anode. Graphite anodes were supplied by A123**

ICL provides insight into the SEI formation and stability of ionic liquids. Variety of ionic liquids at 16 wt% were added to the baseline electrolyte (EC:EMC 3:7 1M LiPF6). As shown in Figure II-38, NOHMs designed ionic liquids show a very low iCL comparable to base line electrolyte (No-IL). This confirms the stability of NOHMs ionic liquid even at very high concentration (16 wt%).

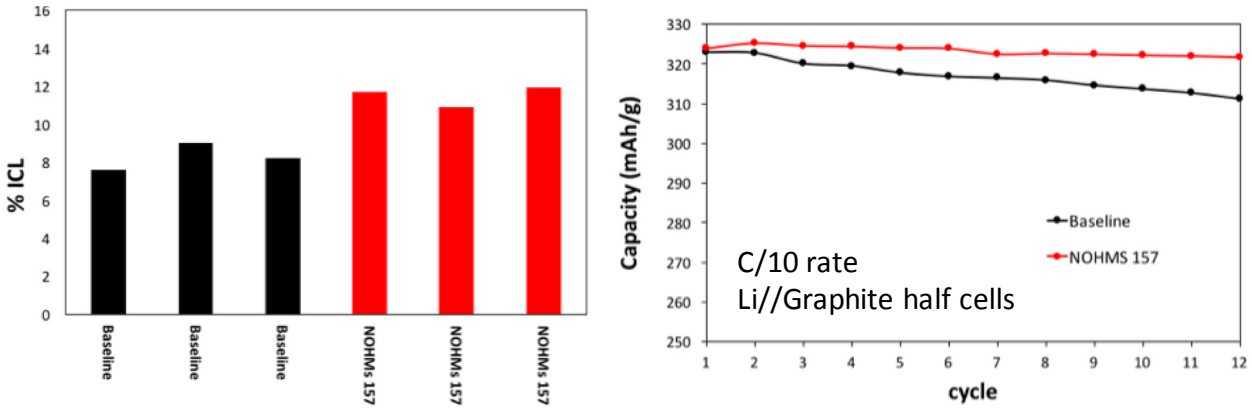


Figure II-38: Comparison of ICL for base line electrolyte and NOHMs electrolyte HVE157. Li-Graphite half-cell cycling data showing the stability of NOHMs designed ionic liquid

## High voltage stability

Building on these screening results, we developed electrolytes and evaluated high voltage stability against NMC532 and LNMO using floating voltage measurements. Figure II-38 compares the measured ICL and Li-Graphite half cell cycle life. The NOHMs electrolyte showed excellent stability against graphite anode.

High voltage stability of NOHMs electrolyte formulation HVE157 was measured using floating voltage measurements. Figure II-39 compares the measured leak current density of LNMC532-Li half cells containing baseline and NOHMs electrolyte formulations. Low leak current density indicates reduced oxidation at the specified voltage. NOHMs designed formulations showed excellent oxidative stability.

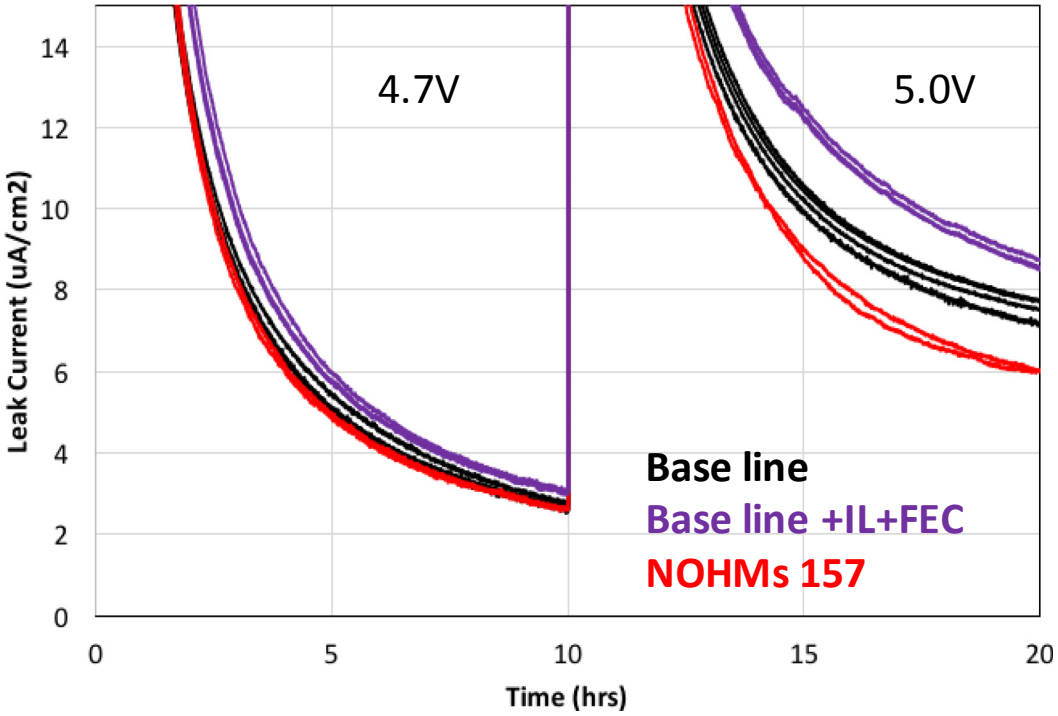


Figure II-39 Floating voltage profiles of NMC532|Li coin cells. The voltages are held for 10 hrs at 4.7V & 5.0V for NMC532. Leak current describes the severity of the oxidative reactions with the cathode surface

NOHMs HVE157 electrolyte formulation showed excellent stability at Graphite anode and NMC532 cathode. Figure II-40 compares the ionic conductivity of NOHMs HVE157 with baseline electrolyte. We found that conductivity values are comparable over a wide temperature range.

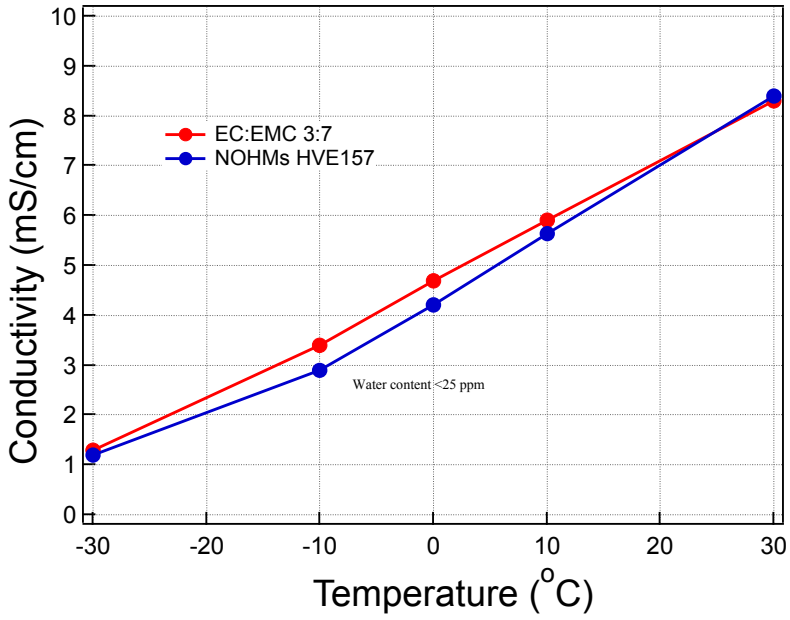


**Figure II-40: Ionic conductivity of base line electrolyte and NOHMs HVE157 electrolyte over a wide temperature range**

## 2 Ah NMC532 cells

Based on promising results for single layer pouch cells, we selected HVE157 as the electrolyte candidate for 2 Ah NMC532-Graphite cell build. A123 systems delivered 30 2Ah cells to DoE labs (Idaho and Sandia) for independent testing. Figure II-41 compares the 1C discharge profiles for 2 Ah cells. The cells showed very minimal cell to cell variation.

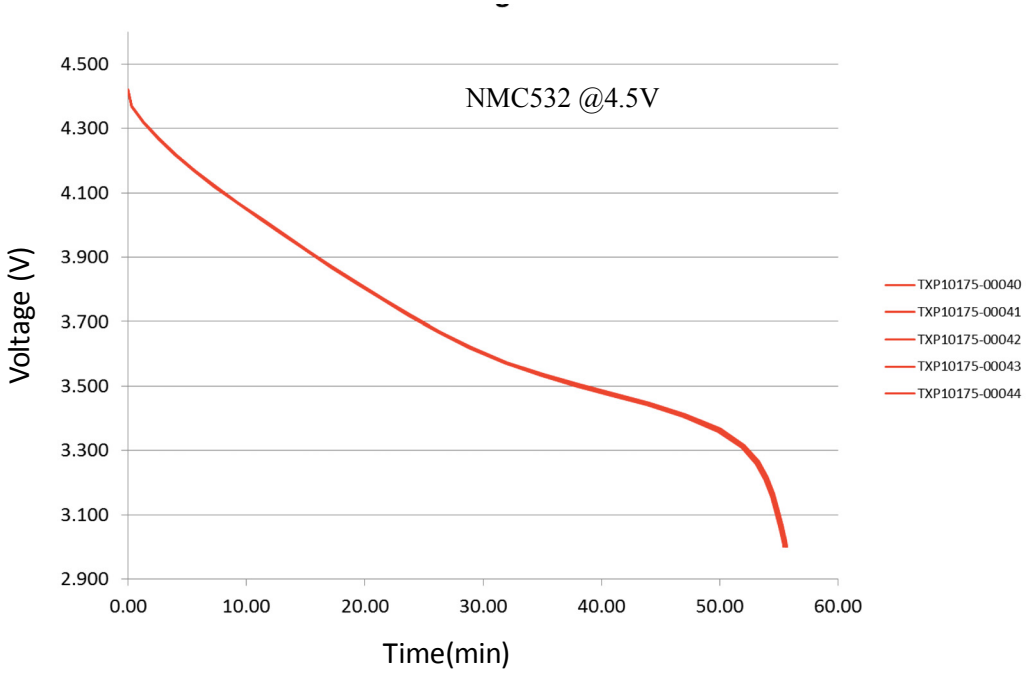


**Figure II-41: Discharge profiles of five 2 Ah NMC532 cells. Discharge profile were collect at 1 C rate. Very minimal cell to cell variation was observed**

A123 has started testing the 2 Ah pouch cells constructed with graphite anodes and NMC 532 cathodes for HPPC, cold crank, and high temperature storage. Results for HPPC and cold crank tests are summarized in below Figure II-42). A battery scaling factor (BSF) of 1620 was calculated, extrapolating from available information in the HPPC curves, and has been used for the cold crank and charge depleting cycle life.

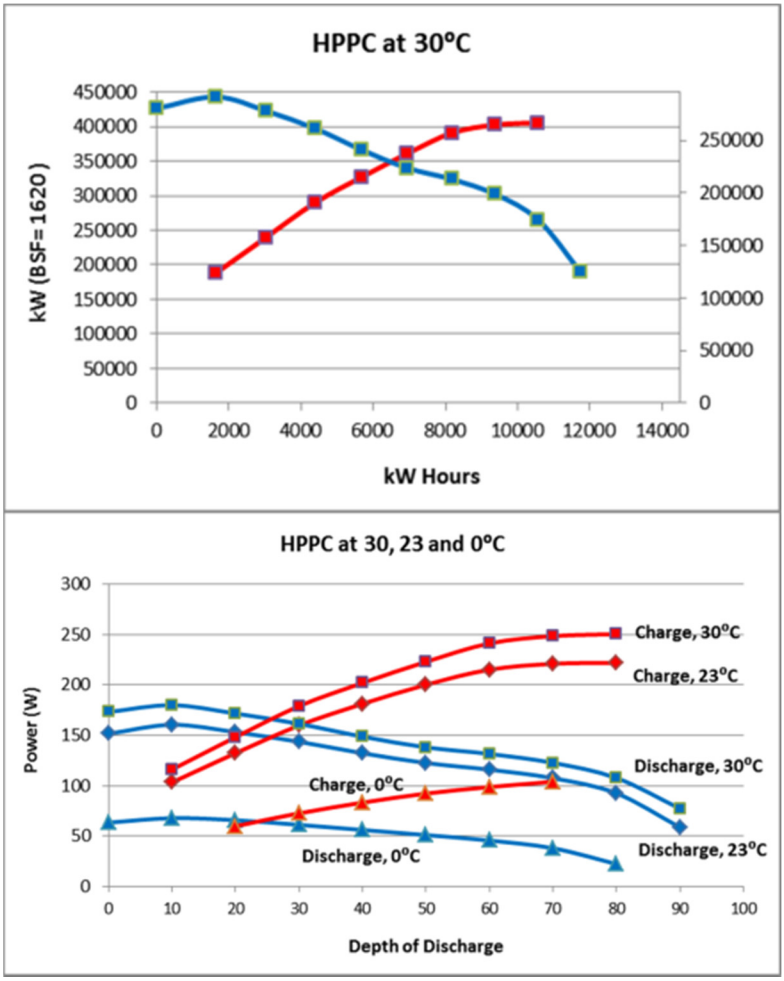


Figure II-42: HPPC testing of 2 Ah NMC532 pouch cells using NOHMs electrolyte

BOL cold crank testing, using the BSF of 1620 and at 50% SOC, provided results well above the cutoff. Figure II-43 shows the cold crank test results. The initial results are looking very promising.

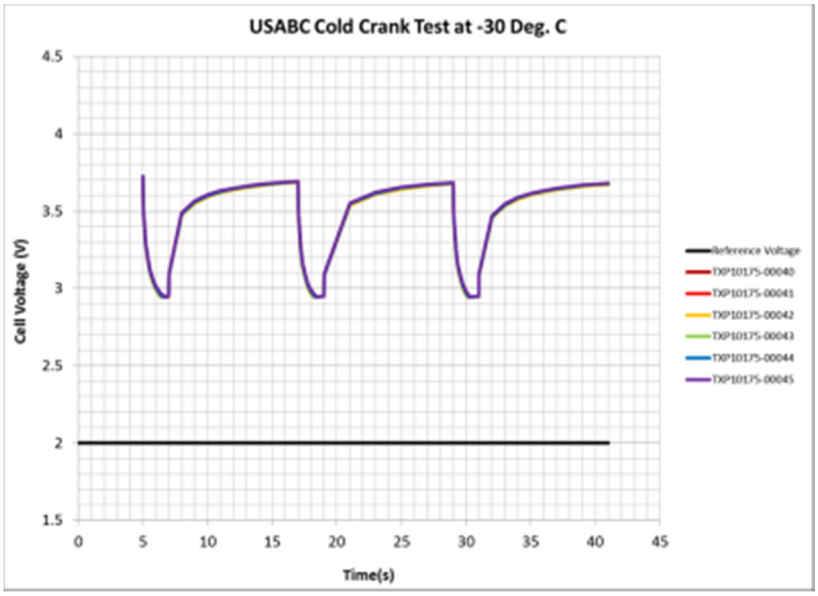


Figure II-43: Cold crank results from testing of 2 Ah NMC532 cells @ 50% SOC

The charge-depleting cycling test is ongoing and initial results are looking very promising. Figure II-44 shows the ongoing cycling test results for 2Ah cells.

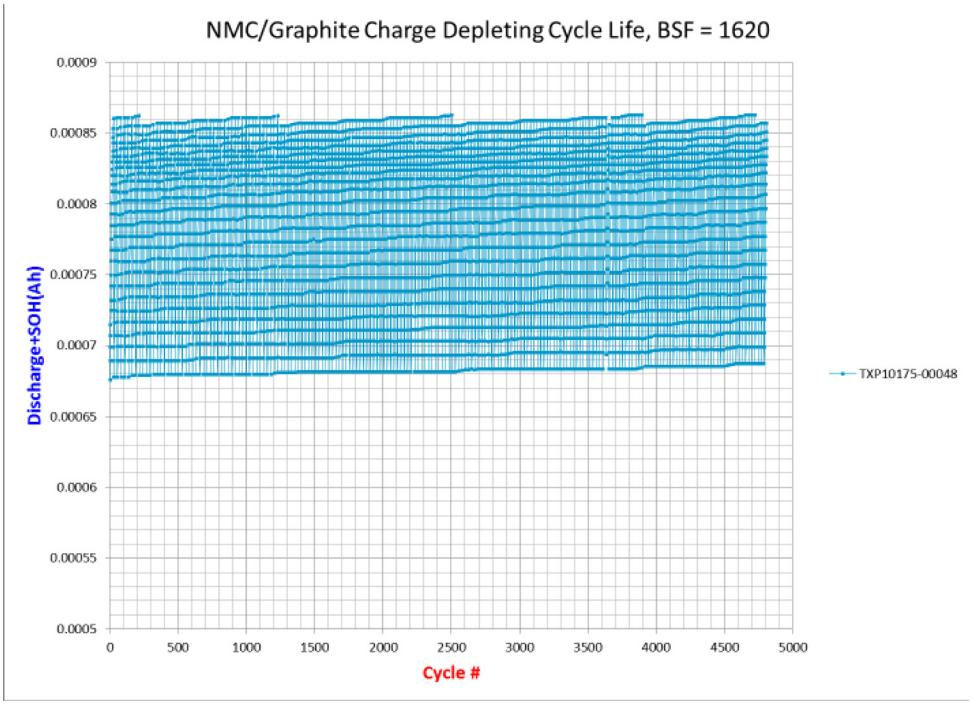


**Figure II-44: Charge depleting cycle life test for 2 Ah NMC532 cells containing NOHMs electrolyte**

## Mechanistic understanding of the high stability of NOHMs HVE 157 electrolyte

Groups of 29 mAh NMC532|Graphite single layer pouch (SLP) cells were constructed and activated with (30:70) EC:EMC 1M$LiPF_6$ (Baseline) and HVE 157. The two electrolytes were cycled using an upper cut-off voltage of either 4.1V or 4.5V. The cells underwent a C/10 constant current and C/20 constant voltage two cycle formation, followed by a C/3 cycling, and utilizing a 3V lower voltage cut-off. During the formation and every 10 cycles thereafter, an impedance measurement (EIS) was collected using a potentiostat.

Cells cycled at 4.5V generated an additional ~50 mAh/g initial capacity when compared to their counter-part at 4.1V. A capacity retention profile (Figure II-45) reveals an expected increase in capacity decay associated with the 4.5V when compared to 4.1V samples, regardless of electrolyte. When focusing specifically at 4.5V cells, samples with HVE157 show greater capacity retention, and a 5% increase at 100 cycles. At 4.1V, both sample groups appear stable with little decay. The differentiation between the HVE157 and baseline in Figure II-45 at 4.1V appears to have been instigated during the rest steps for impedance collection, but not demonstrative of capacity fade. Given these outcomes, the HVE157 appears to specifically contribute toward higher voltage stability. It offers little benefit in fade characteristics at the lower 4.1V cut-off used for commercial electrolytes.

Impedance analysis was used as a method for monitoring the electrochemical reactions involved in the capacity fade. There are multiple interpretations that can be applied to interfacial impedance changes; however, a continuous growth over a cycling period is a good indicator of a continuously reactive surface.

Unlike the 4.5V cells, the 4.1V baseline cells demonstrated no significant growth in interfacial impedance. (Figure II-46(a)) This confirms that the voltage cut-off is indeed safe for the commercial electrolyte, as expected. The electrolyte HVE 157 initiates with slightly higher interfacial impedance post formation and grows slight after 10 cycles, but then decreases at 40 cycles and even further at 60 cycles. When looking at the 4.5V for HVE 157 (Figure II-46 (b)), although it remains relatively unchanged there are small decreases in interfacial impedance witnessed during cycling.

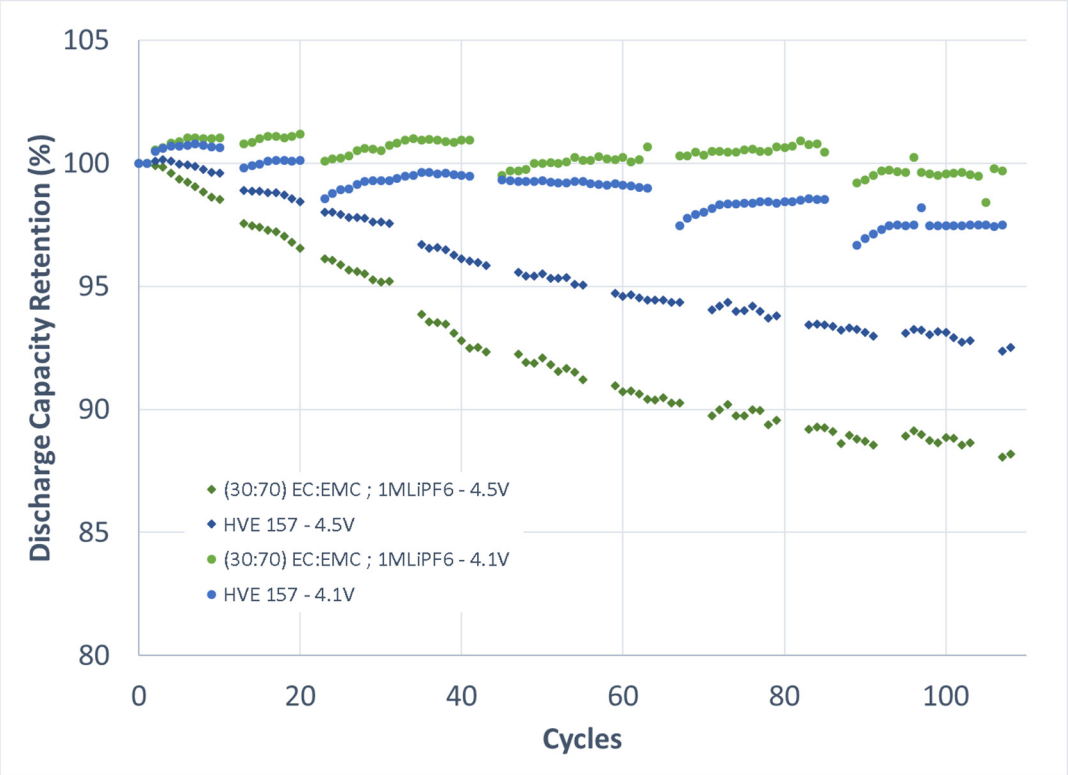


**Figure II-45: Capacity retention plots for base line electrolyte and NOHMs HVE157 electrolyte cycled at 4.1 V and 4.5 V cutoff voltages. Cycling was conducted at room temperature using C/3 rate**

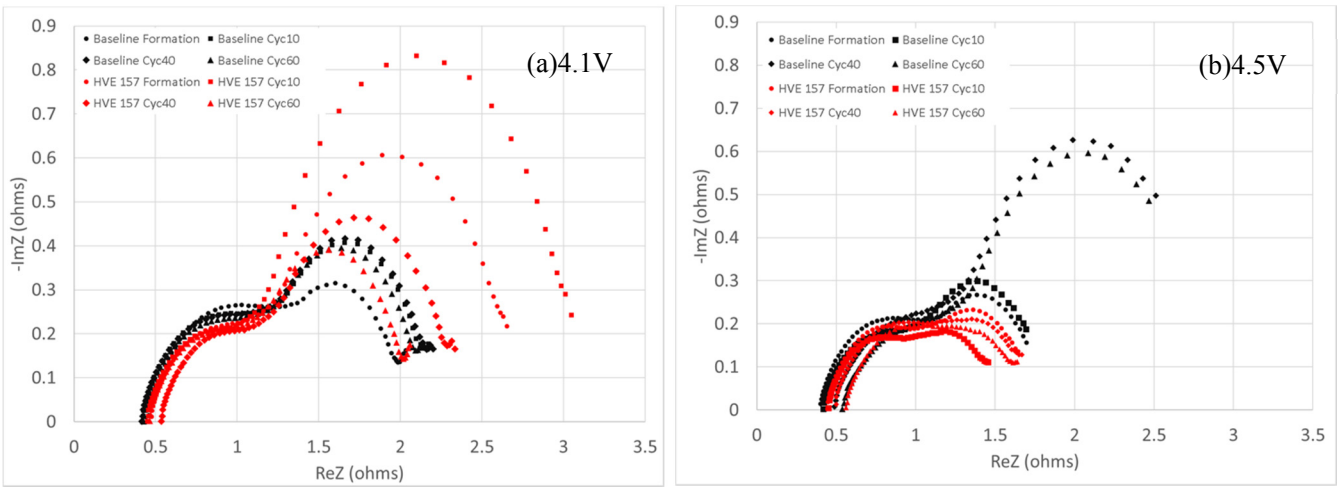


**Figure II-46: EIS spectra of NMC532-Graphite 29mAh SLP cells after being charged to 3.8 V. (a) cycled using 4.1 V upper limit and (b) cycled using 4.5 V upper limit. Impedance data collected from 0.1 Hz to 1 MHz**

Hence, the impedance growth in case of baseline electrolyte explains the rapid capacity fade at the elevated charge cutoff voltage and the stable impedance for NOHMs designed HVE157 electrolyte formulation confirms the high voltage stability along with excellent SEI characteristics on Graphite anode as well.

To further understand the working mechanism of HVE157, X-ray photoelectron spectroscopy (XPS) was employed on the cycled NMC532 cathodes. These XPS results have helped us identify a potential surface film on the cathode unique to HVE157 samples. The surface film thickness appears to be exceed that of the baseline sample and contains a composition with lower carbon and higher oxygen, phosphorus, and lithium concentrations. The oxygen, phosphorus, and carbon are also slightly different in molecular assembly inferring additional or separate decomposition species depending on electrolyte.

XPS allows us to analyze the elemental composition of the electrode surface and/or any surface films that may exist. This information can in turn be used to identify electrolyte species involved in the electrochemical reactions. XPS was completed using an Al source on a Kratos Ultra DLD. Samples were briefly exposed to atmosphere (120 sec) prior to pulling vacuum on the XPS chamber. A glovebox entrance was made operational for future analyses to ensure no atmospheric exposure going forward. A survey scan (broad resolution) was completed on all samples followed by regional scans (narrow resolution) on particularly significant elements identified during the survey scans. No surface treatments or etching were completed on the samples. Two replicates per group were completed and found to be remarkably close in elemental composition.

Our findings suggest that the NOHMs additive in HVE157 undergoes a decomposition at the cathode surface, leaving behind remnants of the original molecule. This is supported by the lack of Si, but presence of higher P and O concentrations in HVE157 samples when compared to baseline. (Figure II-47 b,c)

The absence of Mn, reduction in Ni, and increased presence of Li in the HVE157 compared to the baseline, reveals a thicker film formation in samples containing HVE157 (Figure II-47 b, c). This is further defended by the drastic changes in O, P, F, and C compositions along with shifts in their binding energies compare to the pristine NMC bare sample. Lastly, a key shift in the F binding energy reveals an absence of PVDF (cathode binder) in HVE157, but not in baseline electrolyte.

The majority of the F on the cycled cathodes can be identified as LiF via a 685eV marker (Figure II-48d). Little involvement from the ionic liquid cation is suspected as there were no identified changes in nitrogen concentrations or shifts in binding energy. The P in baseline aligns with a phosphite molecule inferred from $LiPF_6$ involvement in the electrochemical reactions. The same phosphite peak is found in HVE157 samples, but an additional second peak reveals a molecule with a $P_xO_y$ – Phosphate structure (Figure II-48 c). This molecule is presumed to be a decomposition of the NOHMs additive, based on its attributes.

The rich presence of O and shifts in binding energy for O and C elude to the presence of carbonate solvent decomposition. The specific shift at C for HVE 157 fits neatly with O-C=O molecules. Complementary, the shifts at O for the same correspond with R-CO2 type molecules (Figure II-48 a). There appears to be a stronger carbonate involvement in HVE157 samples than in the baseline.

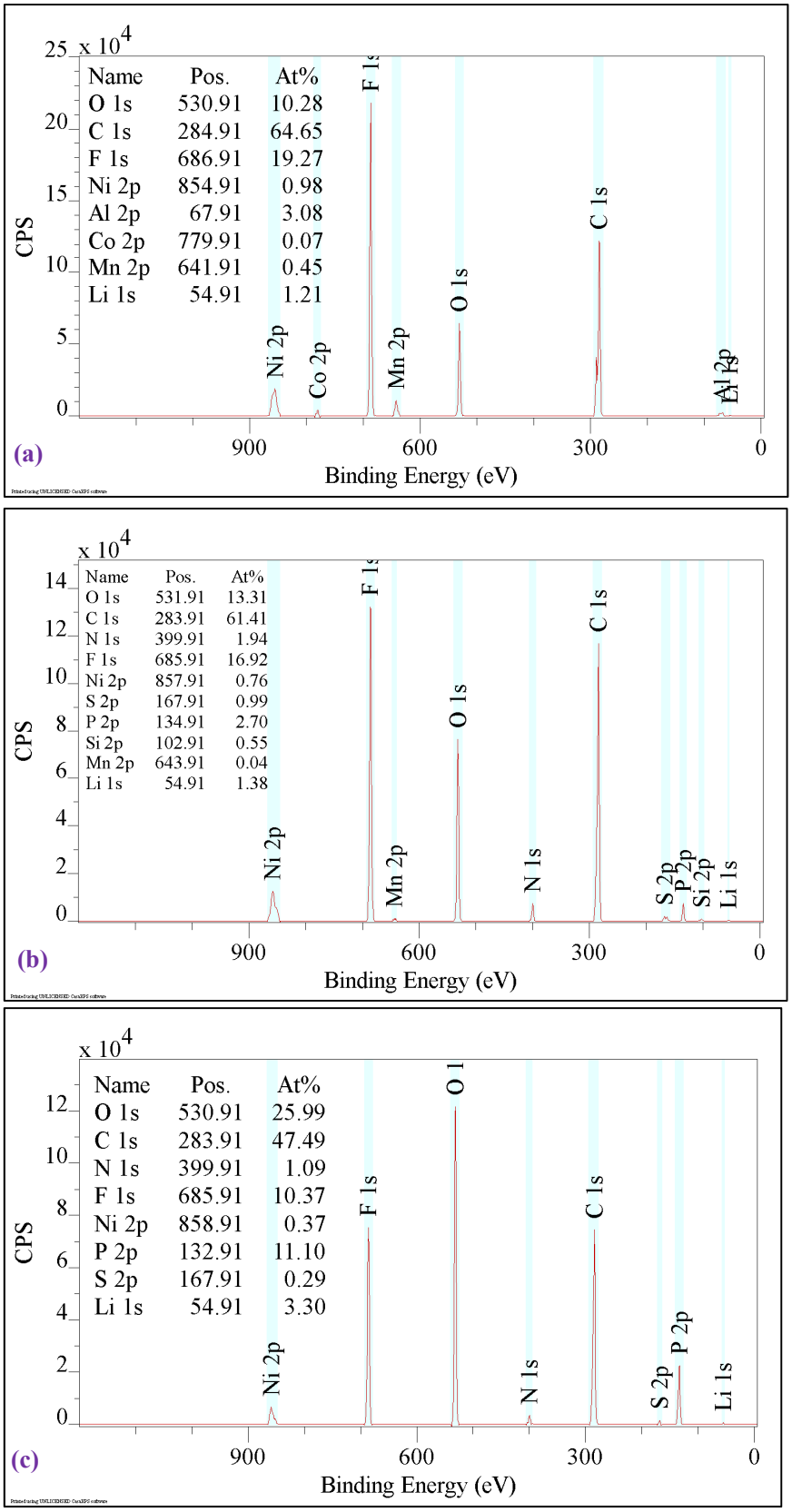


**Figure II-47: XPS board scans of cathode surface. An elemental selection and backgrounding process yields the sharp peak views. The table reveals the element (Name), binding energy (Pos.), and Composition (At%). (a) Bare Pristine NMC cathode (b) Post Cycling NMC Cathode with Baseline Electrolyte (c) Post Cycling NMC Cathode with HVE157 Electrolyte**

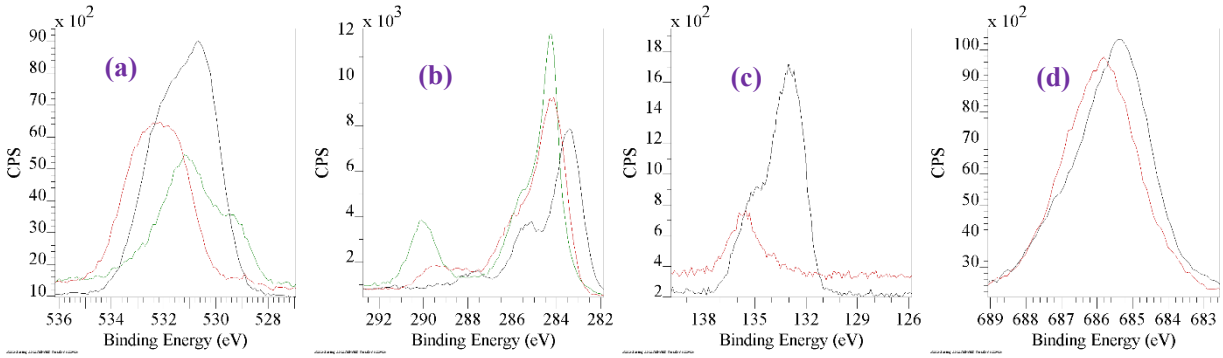


**Figure II-48: XPS element specific scans of cathode surface. Curves are coded as follows: Pristine NMC (green), Baseline Electrolyte (red), HVE157 (black). (a) Oxygen 1s (b) Carbon 1s (c) Phosphorus 2p (d) Fluorine 1s**

## Conclusions

Variety of functional ionic liquids were synthesized and screened against graphite anode and high voltage cathodes (NMC532, LNMO) for both cathodic and anodic stability. Based on numerous screening tests (both at NOHMs and at the A123 facility), we developed the HVE157 electrolyte formulation and delivered thirty 2 Ah for testing to DoE labs. Initial results conducted on the delivered 2Ah 4.5V NMC532 cells at A123 facility shows promise.

Fundamental understanding of the working mechanism of NOHMs designed electrolytes is ongoing to optimize the electrolyte composition to meet the USABC PHEV goals.

In collaboration with A123, we will be delivering thirty 2Ah LNMO (4.9V), thirty 10Ah NMC532 and finally thirty 10Ah LNMO cells for independent testing.

Cost studies are ongoing for the functional ionic liquid molecule to estimate the cost of the electrolyte formulations developed during the course of this study.

## Presentations/Publications/Patents

1. Hybrid electrolytes for PHEV applications, Surya Moganty et al., DOE Annual merit review meeting, June 2016.

# II.A.10. A Closed Loop Recycling Process for End-of-Life Electric Vehicle Lithium-ion Batteries (Worcester Polytechnic Institute)

**Yan Wang, Principal Investigator**
Worcester Polytechnic Institute
100 Institute Road
Worcester, MA 01609
Phone: 508-831-5453; Fax: 508-831-5178
E-mail: yanwang@wpi.edu

**Renata Arsenault, DOE Program Manager**
Ford Research & Innovation Center
2101 Village Road
Dearborn, MI 48121
Phone: 313-805-5133; Fax: 313-248-4077
E-mail: rarsena4@ford.com

Start Date: February 2, 2016
End Date: January 15, 2018

## Abstract

### Objectives

The objective of this program is to scale up and demonstrate Worcester Polytechnic Institute's (WPI) novel and efficient lithium-ion battery recycling process, verify its claim of no or minimal sorting, and develop PHEV cell designs with a lower cost structure for improved industry sustainability.

### Accomplishments

Confirmed that:

- Different discharge methods do not affect WPI recycling process.
- The purity of recovered NMC111 is comparable with commercial control powder.
- The tap density of NMC111 synthesized with recycled materials has reached ~2.6 g/cc (target is ≥2.30 g/cc).
- The recovered NMC111 shows good electrochemical properties, as confirmed by tests conducted by A123 Systems.
- The recovery efficiencies of each of Ni, Mn and Co are over 80% (efficiency target ≥ 80%).
- The recovery efficiency of Li is over 70% (efficiency target ≥70%).

### Future Achievements

- Finalize the precursor and cathode synthesis parameters to obtain NMC111 with ~10µm (D50)
- Increase the concentration of spent battery materials during co-precipitation reaction
- Shred FCA casing material and incorporate it into the recycling stream
- Synthesize NMC111 with recovered $Li_2CO_3$
- Deliver recovered NMC111 material to A123 Systems for testing with coin cells
- Scale up to 3kg and 10kg experiments (measured by mass of incoming shredded battery materials) to be used for 2Ah and 25Ah cells

## Technical Discussion

### Background

Prof. Wang's team at WPI has developed a patent pending recycling process to generate new $LiNiMnCoO_2$ (NMC) cathode materials from spent lithium-ion batteries. The process recovers new NMC cathode materials from a mixture of lithium-ion batteries and does not need the incoming stream of lithium-ion batteries to match the stoichiometry of the recovered NMC material. Additionally, copper, steel, aluminum, graphite, and plastics are also recovered. In the USABC project, WPI is partnering with A123 Systems, an expert in cell manufacturing for EV/HEV/PHEV applications, to recycle spent lithium-ion batteries from EVs, HEVs and PHEVs and generate new cathode materials for new PHEV cells. By completing the research, not only will the team provide a path towards lowering the cost of PHEV batteries but also will contribute to improved industry sustainability.

### Introduction

The purpose of this USABC project is to successfully recycle multiple 10 kg size batches of end of life EV batteries consisting of different incoming cathode chemistries via the recycling process developed at WPI and, produce PHEV format cells of a single chemistry using the recovered NMC111 cathode. Over the course of the two year development program, WPI/A123 systems will improve the performance of the recovered cathode materials so that they exhibit performance equivalent to current commercial materials, as confirmed by A123 and National lab testing using USABC PHEV test procedures. Other materials including steel, copper, aluminum, etc. will also be recycled. The recycling process and recovery of cathode materials will follow a patent pending process developed at WPI. To date, this process has been conducted on a laboratory scale (up to 1kg) at WPI and the resulting recovered cathode materials have low impurity concentrations, dense particles, and electrochemical properties closely approaching those of new commercial materials. The USABC development program will advance the WPI recycling technology through the completion of three major tasks: 1) optimize synthesis parameters of the recovered $LiNi_{0.33}Mn_{0.33}Co_{0.33}O_2$ (NMC111) cathode materials to improve particle density and electrochemical performance; 2) improve the recycling efficiency of cathode materials and lithium and 3) scale the process from the existing 1 kg scale to the 10 kg scale. Figure II-49 below provides a schematic representation of the program in terms of the hardware that will support evaluations at each of the three main stages.

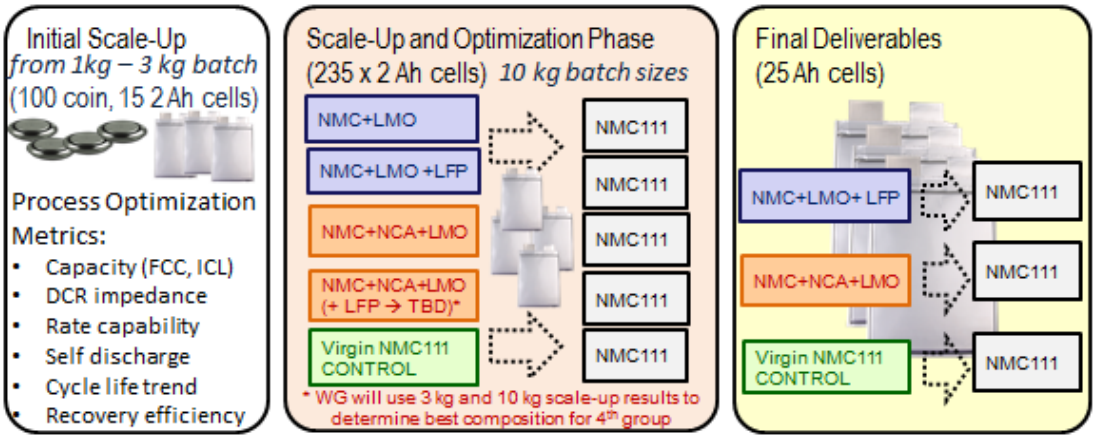


| Test Article | Total Made | Groups | USABC/ ANL | A123/ WPI | Comments |
|---|---|---|---|---|---|
| 2 Ah NMC111/ gr cells | 250 | 5 | (5x10) 50 total | 200 | Majority of testing by A123/WPI to inform optimization |
| 25 Ah NMC111/ gr cells | 60 | 3 | (3x10) 30 total | 30 | |

Figure II-49: WPI program overview

## Approach

The project goals will be achieved through execution of the key tasks detailed below:

**Improve the electrochemical performance of NMC111.** One of the major tasks of the program is to increase the capacity and expected life of NMC111 that is recovered from a mixture of PHEV/HEV/EV batteries to be equivalent to commercially available cathode material, or show no more than 5% difference in the metrics being tracked. WPI will further refine the ability to tailor the Ni, Mn and Co stoichiometry to consistently deliver the 1:1:1 product regardless of incoming chemistry variations. The project will advance from current status involving coin cell testing through an intermediate 2Ah cell to final deliverable 25Ah cells. To improve the electrochemical performance, WPI will work with A123 systems to evaluate and improve the properties of the recovered cathode material. By optimizing process parameters such as precipitation time and stirring rate, it is believed that WPI can increase the particle density and specific capacity, which are key to successful commercialization of the recycling technology. The project will strive to increase the reversible capacity of the recycled cathode from 150mAh/g to 155mAh/g. That said, project emphasis will be on the relative difference between cells made with recovered material and commercial NMC versus absolute performance of both, as the latter can be affected by many factors tangential to our focus.

**Improve the recovery efficiency.** There are two facets to recovery efficiency: minimizing losses of desirable components in the various processing steps and minimizing the quantity of virgin materials required to supplement the incoming stream of spent batteries. Both aspects will be addressed in order to deliver the most favorable economics. To maximize the recovery efficiency of Ni, Mn, and Co as $Ni_{1/3}Mn_{1/3}Co_{1/3}(OH)_2$, the pH will be closely monitored and controlled. The most important step is the impurity removal step in which Al, Cu and Fe impurities are removed as hydroxides. The amount of Ni, Mn and Co lost depends upon two primary factors: their concentration in solution and the pH. The lowest pH which can be obtained while maintaining impurity levels below targets will be determined, so as to allow for the maximum recovery efficiency. To maximize the recovery efficiency of lithium carbonate, the amount of water that is evaporated will be strategically tuned. By determining the concentration of the impurities ions present in solution (Na, $SO_4$) from measured concentrations of sodium and sulfur, the exact volume point at which sodium sulfate becomes insoluble can be calculated using the Ksp of sodium sulfate at the temperature in question. This will be used to optimize the water added and subsequently evaporated, along with other purification and temperature related refinements to minimize unnecessary dilution and maximize yield.

**Scale-up.** The significant challenge of going from 1kg to 10kg experiments will be accomplished by conducting the scale-up in stages. First, the work will proceed from 1kg experiments to 3kg (increase factor of 3), and then to 10kg (increase factor of 3.3). The process used will be similar to that already demonstrated on the 1 kg scale. The following steps will be optimized for maximum efficiency: (a) demonstrate safe discharge and shredding of the batteries. This project will demonstrate that entire shredded modules can be recycled. (b) separate any casing and metallic module components using magnetic separation, (c) separate copper and aluminum by density separation, (d) demonstrate complete leaching of cathode materials, (e) efficiently remove any impurities, (f) achieve the optimized precipitation conditions for $NMC(OH)_2$ in the larger chemical reactor, (g) synthesize NMC cathode materials. At each scale (1 kg, 3 kg, 10 kg), recovered material properties will be compared against commercial cathode material using both powder and resultant cell attributes in clearly defined, measureable Milestones.

## Results

**NMC111 Synthesis.** Figure II-50 shows the SEM images of the NMC111 precursor ($NMC(OH)_2$) synthesized from recycled lithium-ion batteries. At 10 hours, the particles are uniformly spherical. At 20 hours, small particles begin to form. At 30 hours, a bimodal distribution is observed. From the image with higher magnification, the particles are dense and spherical. The synthesized NMC111 cathode material is shown in Figure II-51 and, like the precursor, exhibits a dense morphology and a bimodal distribution in particle size. The tap density is >2.5 g/cc, as tested at A123 Systems, which is higher than the target tap density (2.3 g/cc). Measured impurity levels of synthesized NMC111 precursor and cathode materials are comparable to the commercial NMC111, as confirmed by Inductive Coupled Plasma (ICP). In addition to feeds consisting of GM Volt batteries (same cells as Ford Focus Electric Vehicles), FCA Fiat 500-e batteries were also processed, and similar results were obtained. For example, Figure II-52 shows the synthesized NMC111 from different feeds

including two separate batches of GM Volt batteries and one batch of FCA Fiat 500-e batteries. Very similar tap density (~2.7 g/cc) and morphology (spherical shape) of NMC111 was obtained from all three batches, clearly demonstrating the flexibility of the recycling approach for different recycling streams.

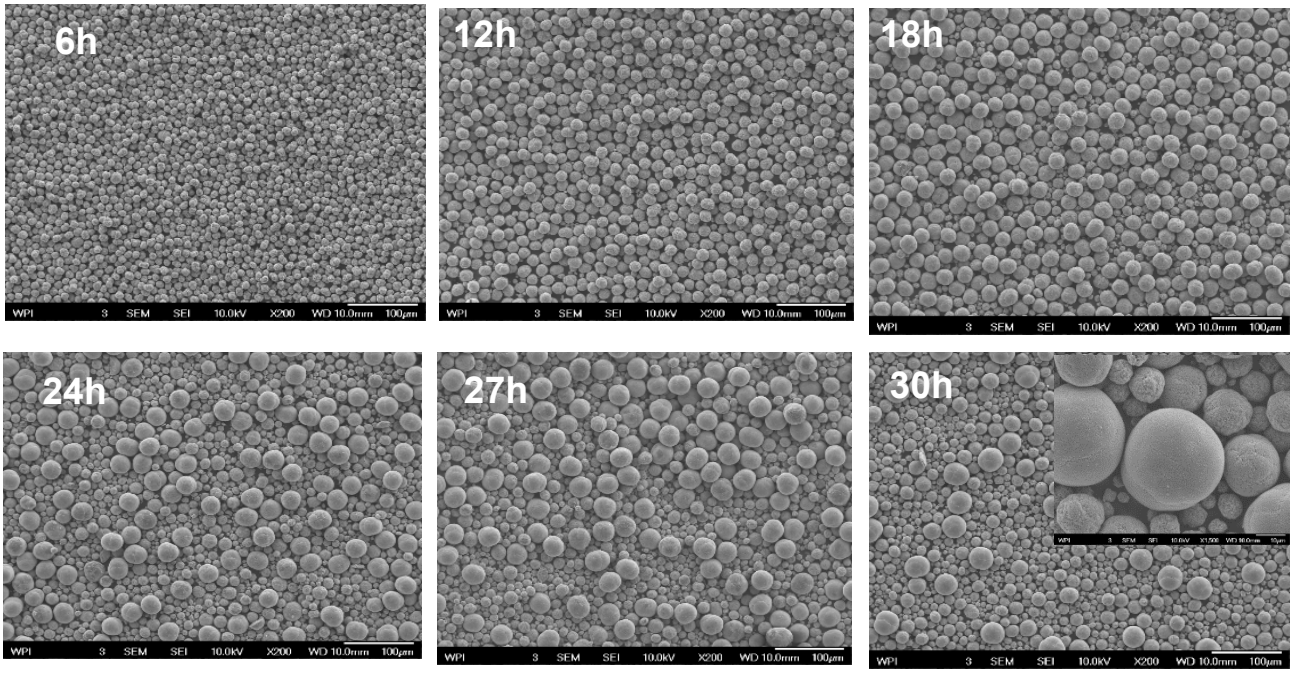


**Figure II-50: The morphology of NMC111 precursor with reaction time**

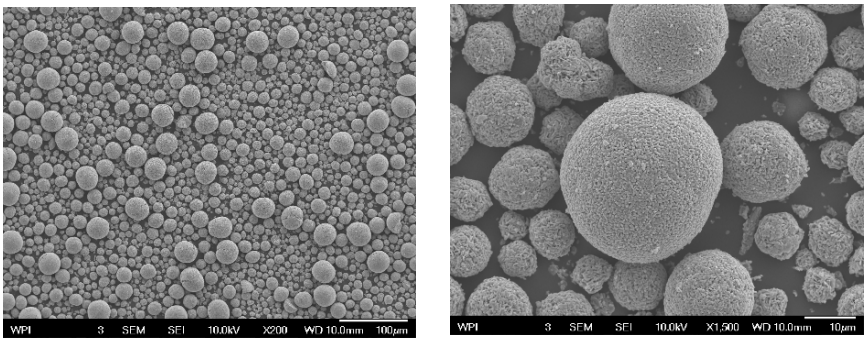

**Figure II-51: The morphology of NMC111 cathode material**

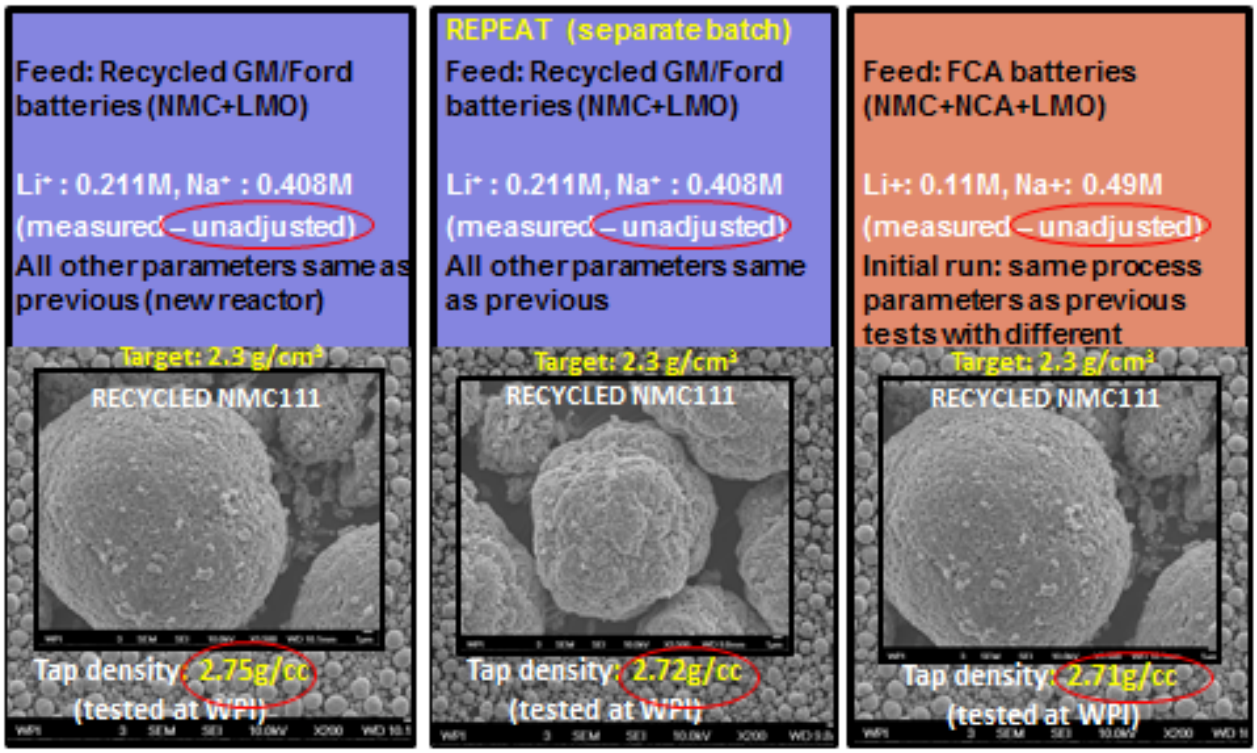


Figure II-52: The synthesized NMC111 cathode material from different feeds

**Optimize Recycling Process to Improve the Recycling Efficiency.** The efficiency which we are focusing on is cathode recovery efficiency. For elements of Ni, Mn, and Co, there are four possible loss points for cathode materials including shredding and sieving L1, leaching process L2, removal of impurities L3, and co-precipitation reaction L4. The following equation is used to calculate efficiency.

$$\text{Efficiency} = (1\text{-}L1) \times (1\text{-}L2) \times (1\text{-}L3) \times (1\text{-}L4)$$

Experiments conducted thus far have enabled quantification of loss parameters for each stage, L1 through L4. The loss of cathode materials during shredding and sieving (L1) is about 2%. There is no detectable loss during the leaching (L2) and co-precipitation (L4) steps. Loss during removal of impurities L3 is shown in Table II-9. Therefore, the efficiency of Ni, Co and Mn is 80.1%, 85.0% and 89.7%, respectively, which is above the target efficiency (80%). Similarly, the recovery efficiency for lithium was determined to be 70.07%, which is also above the target efficiency (70%). Subsequent work will focus on minimizing the use of purchased raw materials and maximizing yield of the process overall.

### Table II-9: The Loss of Ni, Mn and Co During Removal of Impurities

| | Before removing impurities | After removing impurities | Loss (L3) |
|---|---|---|---|
| Volume(L) | 1.60 | 2.02 | |
| Ni (mol/L) | 0.17 | 0.110 | 18.3% |
| Mn (mol/L) | 0.60 | 0.435 | 8.5% |
| Co (mol/L) | 0.16 | 0.110 | 13.3% |

**Electrochemical Testing Results.** A123 tested various lots of WPI recovered NMC111 and control powders, and the results are shown in Table II-10. A123's test results demonstrate that synthesized material (for example sample 09212016) from WPI has similar electrochemical performance as the commercial material although the particle size of WPI powder is large. Efforts will continue to improve the recovered material as scale-up

progresses, to reduce particle size and to match high rate power and other performance metrics of the commercial control NMC111.

**Table II-10: Comparison between WPI Synthesized NMC111 with Commercial NMC111**

| Test | Units | Commercial Control Powder | WPI Sample 07292016 | WPI Sample 0817201602 | WPI Sample 08272016 | WPI Sample 09212016 |
|---|---|---|---|---|---|---|
| Tap Density | g/cc | 2.84 | 2.51 | 2.51 | 2.38 | 2.57 |
| D50 Particle Size | um | 9.2 | 16.8 | 14.5 | 16.2 | 22.6 |
| Dry Adhesion (Avg) | f g/in | NA | NA | NA | NA | NA |
| FCC/FDC | mAh/g | 174.7/157.2 | NA | 170.9/150.3 | 177.2/155.4 | 176.8/159.7 |
| Efficiency | % | 90.0 | NA | 88.0 | 87.7 | 90.3 |
| 1C | mAh/g | 130.9 | NA | 110.4 | 121.5 | 130.8 |
| 2C | mAh/g | 119.4 | NA | 95.8 | 107.8 | 117.3 |
| 5C | mAh/g | 40.4 | NA | 32.0 | 33.8 | 30.3 |

## Conclusions

Since the kickoff meeting on February 2, 2016, the WPI/A123 team has made significant progress towards achieving project objectives. Spherical NMC111 with high tap density and purity has been synthesized from both spent GM Volt (Ford Focus) and Fiat 500e batteries. Figure II-53 shows the evolution of tap density and particle size since the program began. These are key attributes that are used to track optimization progress, and the trends in both exemplify WPI's ability to tune the process parameters towards desired technical results. The recovery efficiencies for both cathode material and lithium exceed the target efficiencies subscribed to in the SOW. The electrochemical properties of recovered NMC111 are very close to those of the commercial powder control selected by A123. Future work will strive to reduce the NMC111 particle size, which is directly related to the power, while further scaling the process to the 10 kg batch size required for the final deliverables.

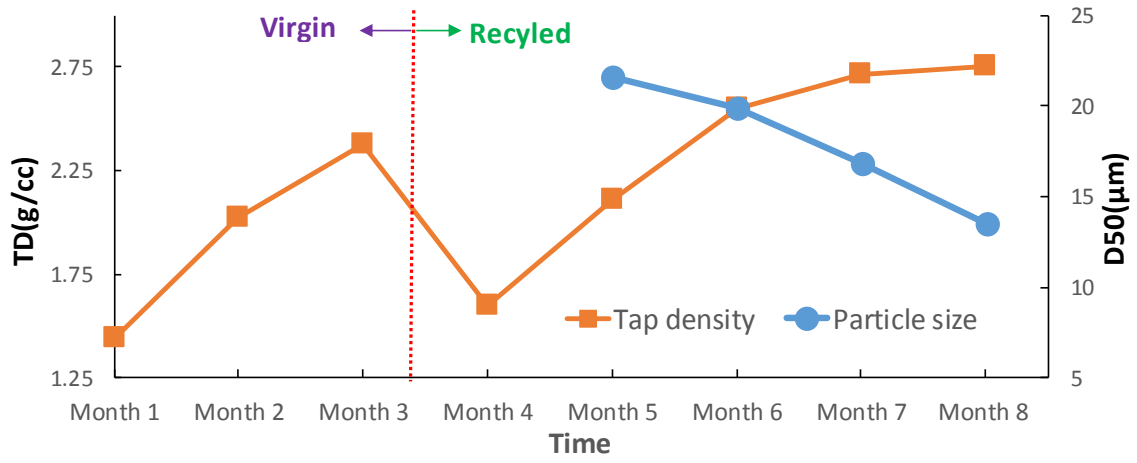


Figure II-53: The Progress of tap density and particle size in the program

## Products

## Presentations/Publications/Patents

1. Joseph Heelan, Eric Gratz, Zhangfeng Zheng, Qiang Wang, Mengyuan Chen, Diran Apelian, Yan Wang, Current and Prospective Lithium-ion Battery Recycling and Recovery Processes, JOM, DOI: 10.1007/s11837-016-1994-y. (JOM Editor's Choice Article)
2. Yan Wang, A Novel Low Temperature Approach to Recycle Lithium ion Batteries with Mixed Cathode Materials, 11th U.S.–China Electric Vehicle and Battery Technology Information Exchange, Denver, CO, April 25-26, 2016.
3. Yan Wang, Zhangfeng Zheng, Qiang Wang, A Closed Loop Process for the End-of-Life Electric Vehicle Lithium-ion Batteries, U.S. DOE 2016 Annual Merit Review and Peer Evaluation Meeting, Washington, D.C., June 6-10, 2016.
4. Yan Wang, Cathode to Cathode Recycling Process for Lithium-ion Batteries, Lithium-Ion Battery recycling Workshop, Argonne National Laboratory, IL, September 28-29, 2016

## References

1. None

# II.A.11. Perform USABC/USCAR Benchmarking Activities (FEV)

**Xiao Guang Yang, USABC Battery Benchmarking Workgroup Lead**
Ford Research & Innovation Center
2101 Village Road
Dearborn, MI 48121
Phone: 313-805-5191, Fax: 313-248-4077
E-mail: xyang11@ford.com

**Tom D'Anna, Principal Investigator**
FEV North America, Inc.
4554 Glenmeade Lane
Auburn Hills, MI 48326
Phone: 248-724-2861, Fax: 248-373-8483
E-mail: danna@fev.com

**Michelbacher Christopher, Brian Cunningham, DOE Program Manager**
Vehicle Technologies Office
U.S. department of Energy
1000 Independence Avenue, SW
Washington, DC 20585
Phone: 202-586-3384
E-mail: Christopher.Michelbacher@EE.DOE.Gov; Brian.Cunningham@ee.doe.gov

Start Date: October 1, 2015
End Date: December 31, 2016

## Abstract

### Objectives

This project is to conduct a complete benchmarking study of the 2015 Volkswagen e-Golf battery electric vehicle including vehicle testing, key component (test stand) testing, and teardown analysis.

### Accomplishments

- After the 2015 VW e-Golf BEV was fully instrumented, the team has completed the following evaluation tests
  - On-road testing
    - Neutral coast down
    - Vehicle acceleration and passing
    - Coast down and recuperation
    - Maximum vehicle speed
    - ABS and stability control events
    - Power analyzer testing and ripple current measurements
  - Fuel economy testing including a number of regulated cycles
    - UDDS, US06, Multi Cycle Test (MCT), SC03, Cold CO
- Vehicle charge capability testing
  - At different temperatures
  - Using Level 1 (L1), Level 2 (L2) and DC fast charge modes
- Test data analysis and knowledge transfer

## Future Achievements

Key component functional test and tear-down/dimensional analysis including e-Motor, transmission, power electronics, and high-voltage battery pack

## Technical Discussion

### Background

The US Advanced Battery Consortium (USABC), USCAR Transmission Benchmark Workgroup (TWG) and Power Electronics Workgroup are interested in evaluating new transmissions, hybrid vehicle, and electric vehicle technologies in production vehicles. FEV North America, Inc. was contracted by the USABC/USCAR to benchmark the 2015 Volkswagen eGolf.

### Introduction

For years, FEV has been one of the competitive benchmarking suppliers for USCAR including the Engine Benchmarking Group (EBG), Transmission Working Group (TWG), and USABC including projects focused on in-vehicle and component-level (test bench) investigations. This specific benchmarking study includes conducting evaluations of the vehicle's fuel economy and performance along with component testing/analysis of the electric motor, power electronics, and high-voltage battery system.

### Approach

FEV procured a representative 2015 VW eGolf vehicle which was equipped with an 85kW AC synchronous permanent magnet electric motor and a single speed transmission. The vehicle is rated with an MPGe of 126 / 105 / 116 (city, highway, combined). The 24.2 kWh lithium-ion battery pack can be recharged by an on-board charger using L1 charging @ 110 V for 20 hours, or L2 charging @ 240 V for 4 hours. The vehicle is also capable of accepting DC fast charging to return 80% capacity in 30 min. Three driver selectable regenerative braking modes and three driving modes (normal, ECO, ECO+) are available for different customer driving preference/needs.

After receiving the new e-Golf, FEV conducted break-in driving and neutral coast-down testing to determine the road load coefficients of the test vehicle. FEV fully instrumented the e-Golf with a CAN bus monitoring system in order to analyze CAN signals of the vehicle buses, together with a set of various discrete sensors and associated data acquisition equipment.

Vehicle-level on-road tests were conducted according to a pre-defined operating condition matrix and driving modes to investigate the vehicle performance and maneuverability. Fuel economy (MPGe) tests were conducted on a chassis dynamometer according to the standard U.S. EPA testing cycles. FEV also performed selected tests with a power analyzer (also on a chassis dynamometer) in order to measure AC power and loss factor. Vehicle charge tests were conducted to evaluate the battery recharge capability and on-board electrical/thermal control strategies throughout a wide range of temperatures. Following the vehicle tests, FEV removed the required components to support the component level investigations/teardown of the E-Motor, transmission, power electronics, and high voltage battery (which are currently ongoing). Upon completion of all vehicle/component testing, FEV will perform a detailed teardown analysis of the EV components.

After the completion of all of the USABC required testing of the vehicle/components, FEV will critically evaluate all data from the vehicle and prepare a final report documenting the test preparation, procedure and results. The report will include FEV's comments on the unique aspects of the design and control strategies captured during the vehicle benchmarking activities.

## Results

Unless noted otherwise, all on-road tests were performed at a test track with flat, smooth surface. Vehicle performance was evaluated on-road under numerous driving conditions. Part of the on-road performance testing included characterization of drive strategies under different drive modes ('normal', 'Eco', Eco+). Figure II-54 shows a comparison of a full load acceleration for the different drive modes.

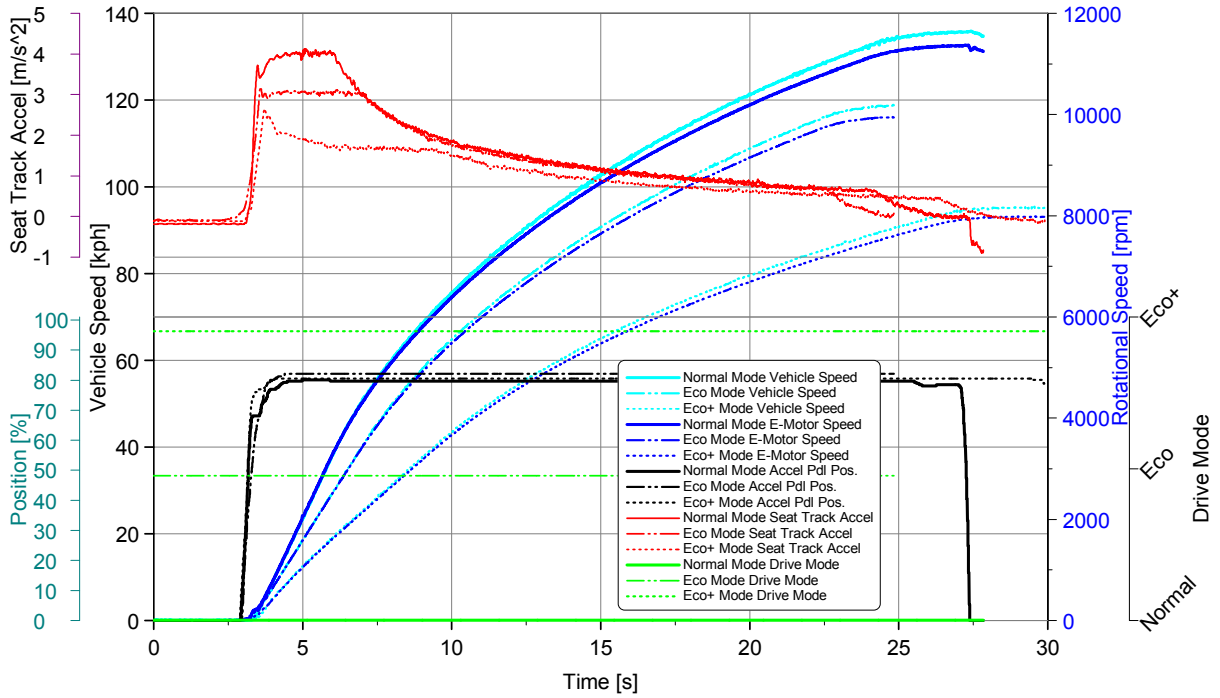


**Figure II-54: Full Load Acceleration (Mode Comparison)**

Figure II-55 shows the vehicle launch behavior in normal mode including the high voltage battery current and voltage among other key measurement signals. The highest current during constant power operation of the E-Motor is around 285A with a voltage of approximately 315V which results in a HV power of approximately 89.7kW.

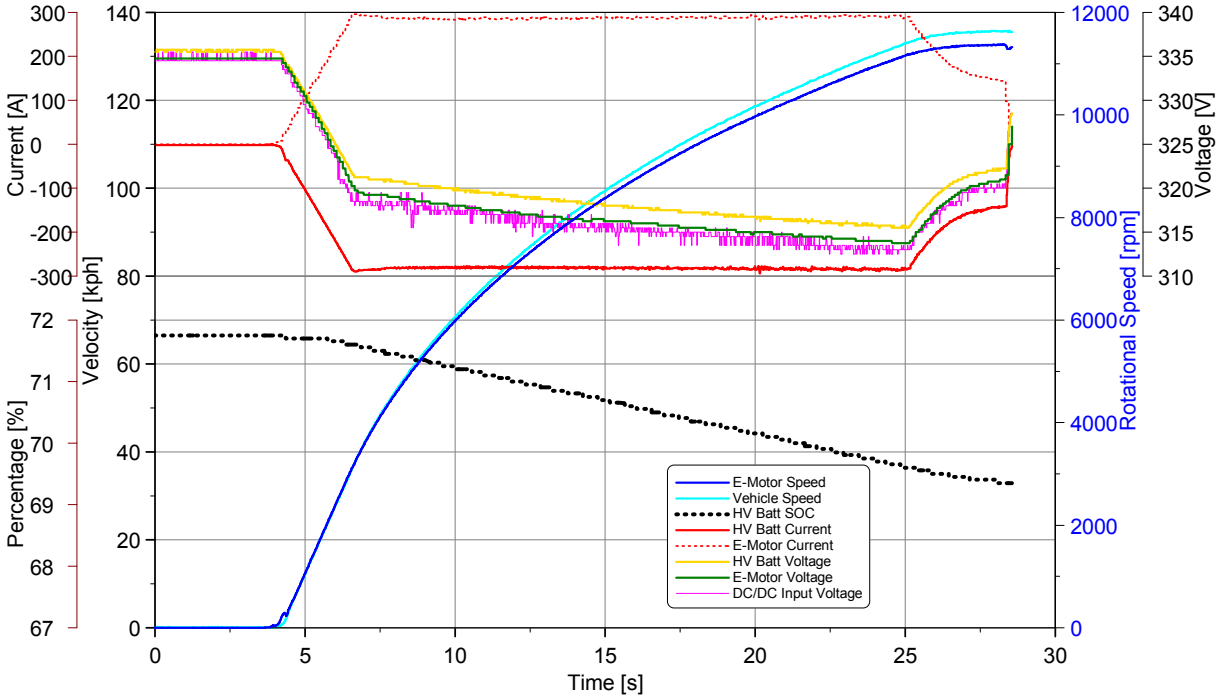


Figure II-55: Full Load Acceleration (HV Signals)

The drive mode comparison shown in Figure II-56 represents a 50-80mph passing maneuver. Vehicle acceleration is reduced in Eco and Eco+ mode. In Eco+ mode, vehicle speed is limited to 56mph unless the kickdown (detent at the accelerator pedal) is applied.

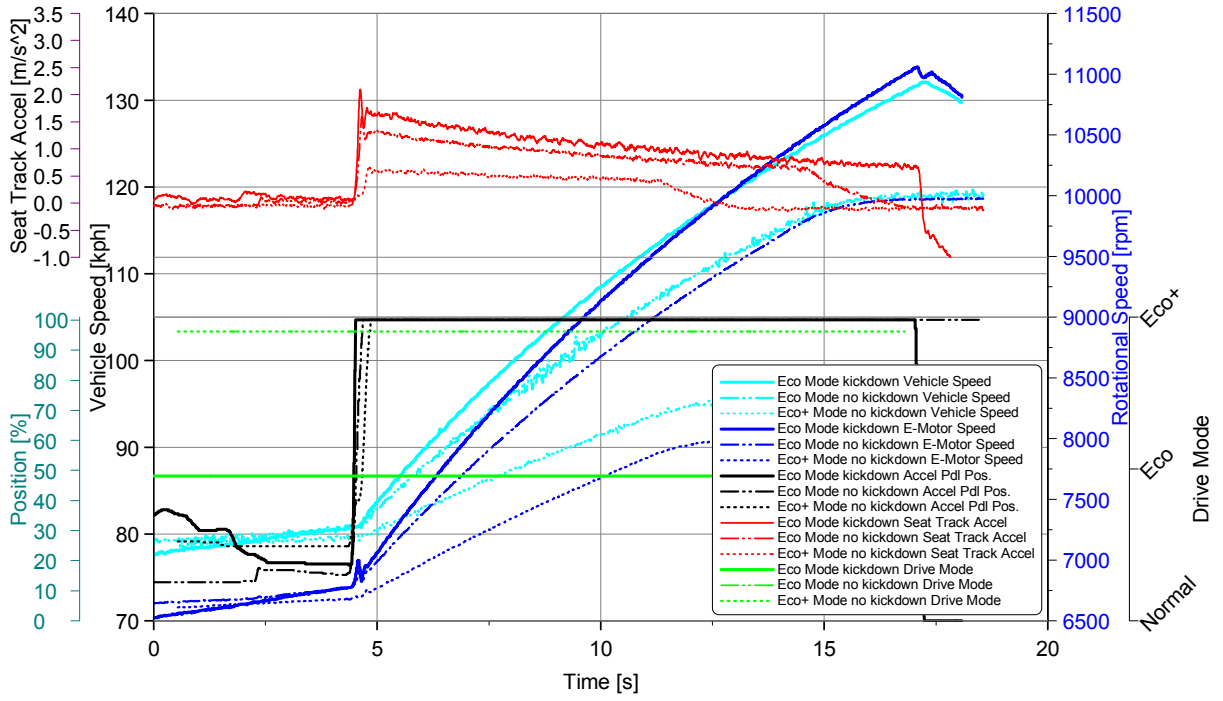


Figure II-56: Passing Maneuver

In a similar way, the vehicle can utilize different mode settings for the regenerative braking (D1 - D3, B). The differences in operation during coast down (no brake pedal applied) are outlined in Figure II-57. The different modes have also been tested during vehicle braking with different deceleration rates.

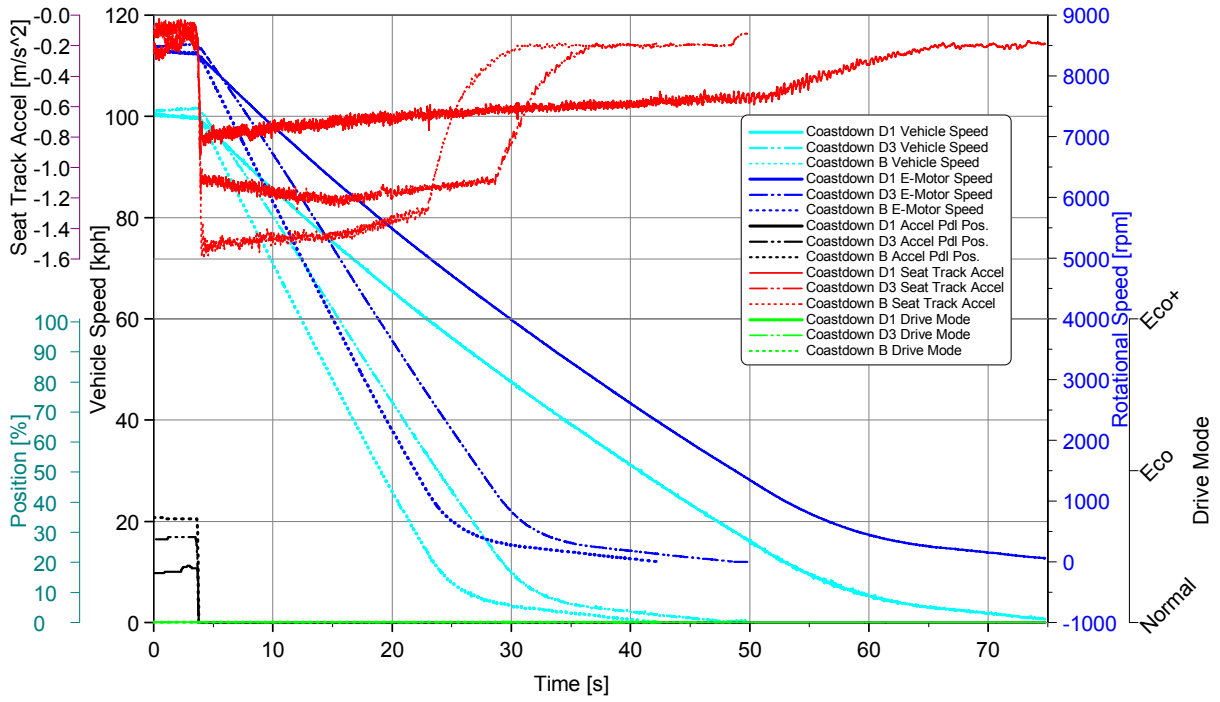


**Figure II-57: Coast Down with Different Regenerative Braking Settings**

Figure II-58 compares the braking with 2m/s$^2$ deceleration rate. Instead of vehicle acceleration, driveline torque is shown in this comparison together with brake pressure to better illustrate the differences in blended braking.

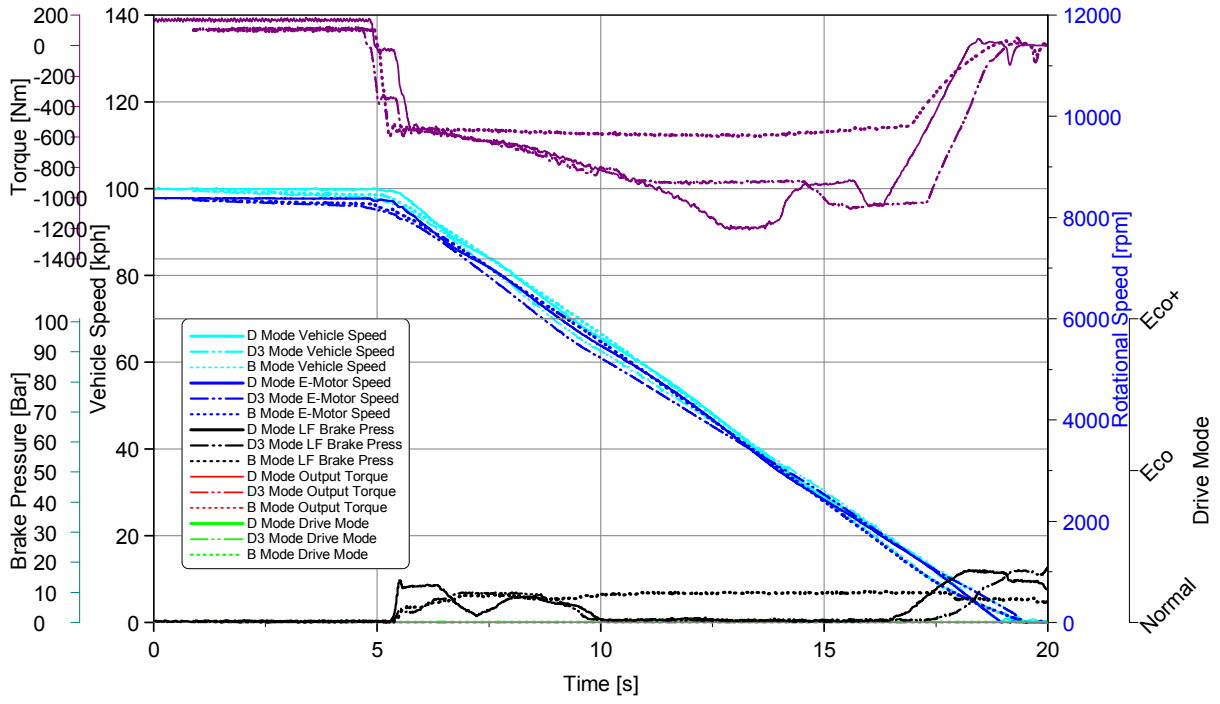


**Figure II-58: Different Regenerative Braking Settings (2 m/s$^2$ Deceleration Rate)**

For completeness, HV battery power for these braking events is shown in Figure II-59.

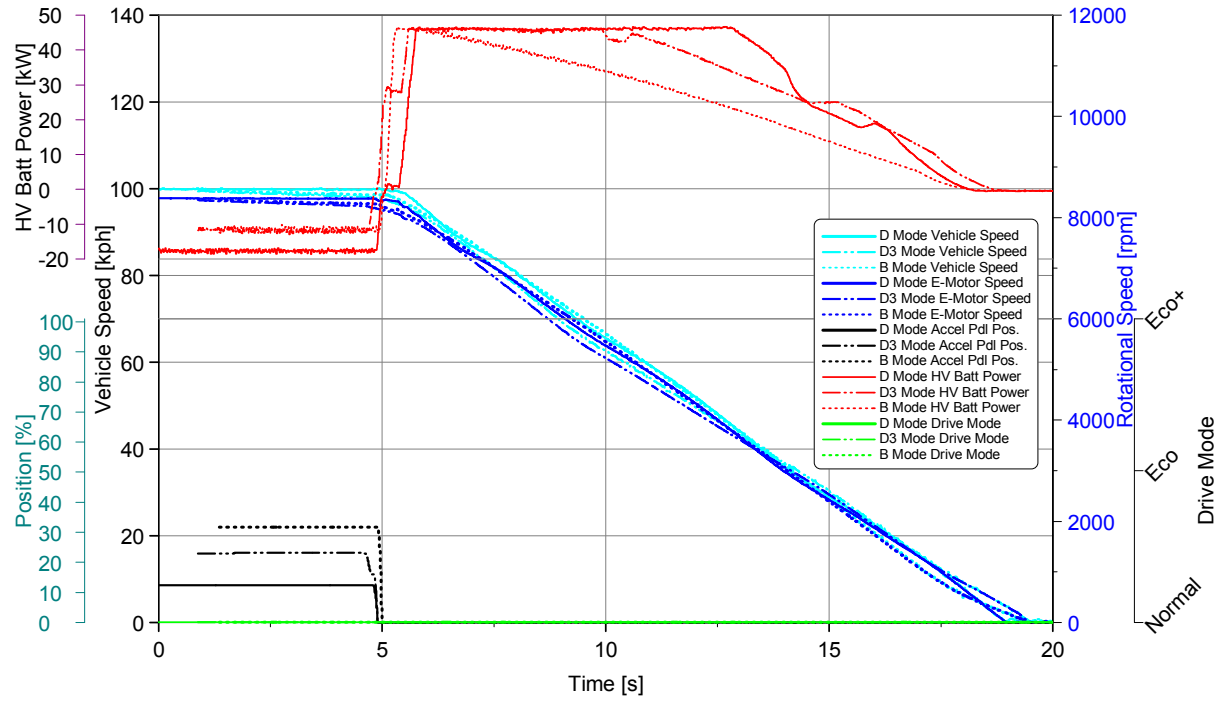


**Figure II-59: Different Regenerative Braking Settings (2 m/s² Deceleration Rate)**

While driving the city profile, 16 UDDS cycles could be completed; during the 17th cycle the vehicle stalled due to a depleted battery. Figure II-60 shows an example of the UDDS cycle together with the energy used (based on HV current and voltage).

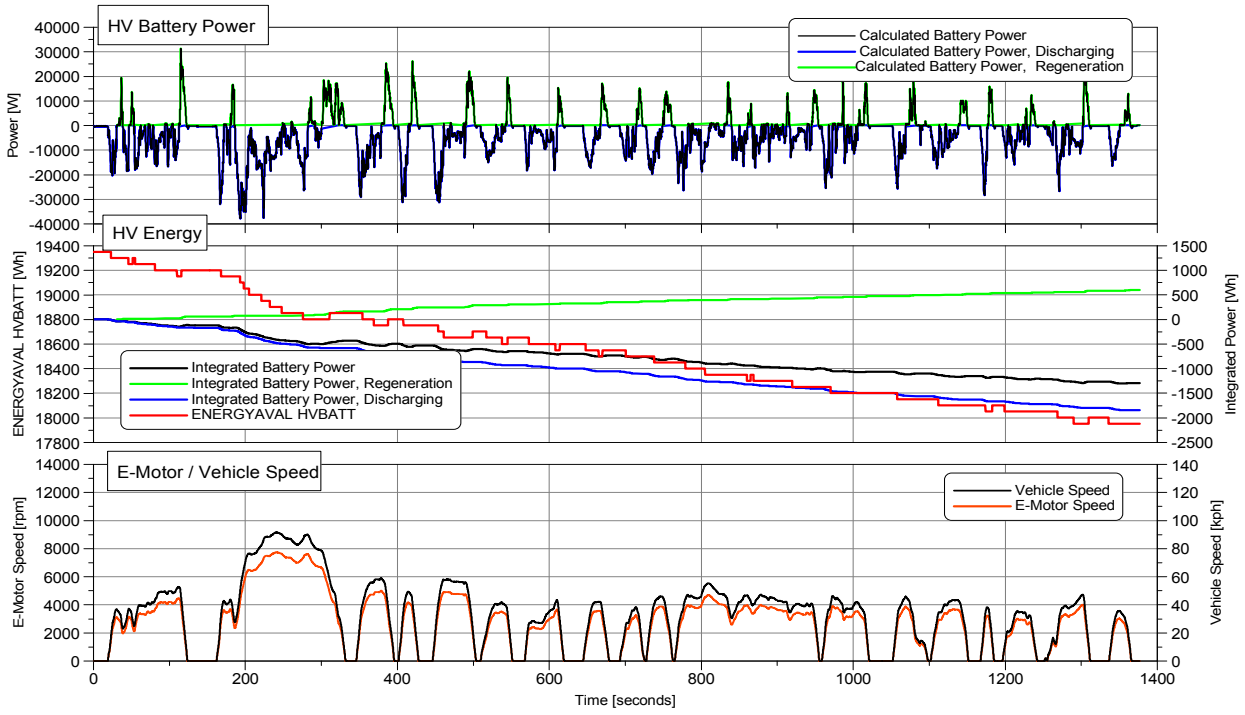


**Figure II-60: Example of the UDDS Drive Cycle**

Below 20% SOC the pedal map of the vehicle changes and it requires a higher pedal input to follow the speed trace of the test cycle, as noted on Figure II-61. During the UDDS testing, this occurred during the 15th test run of the UDDS cycle.

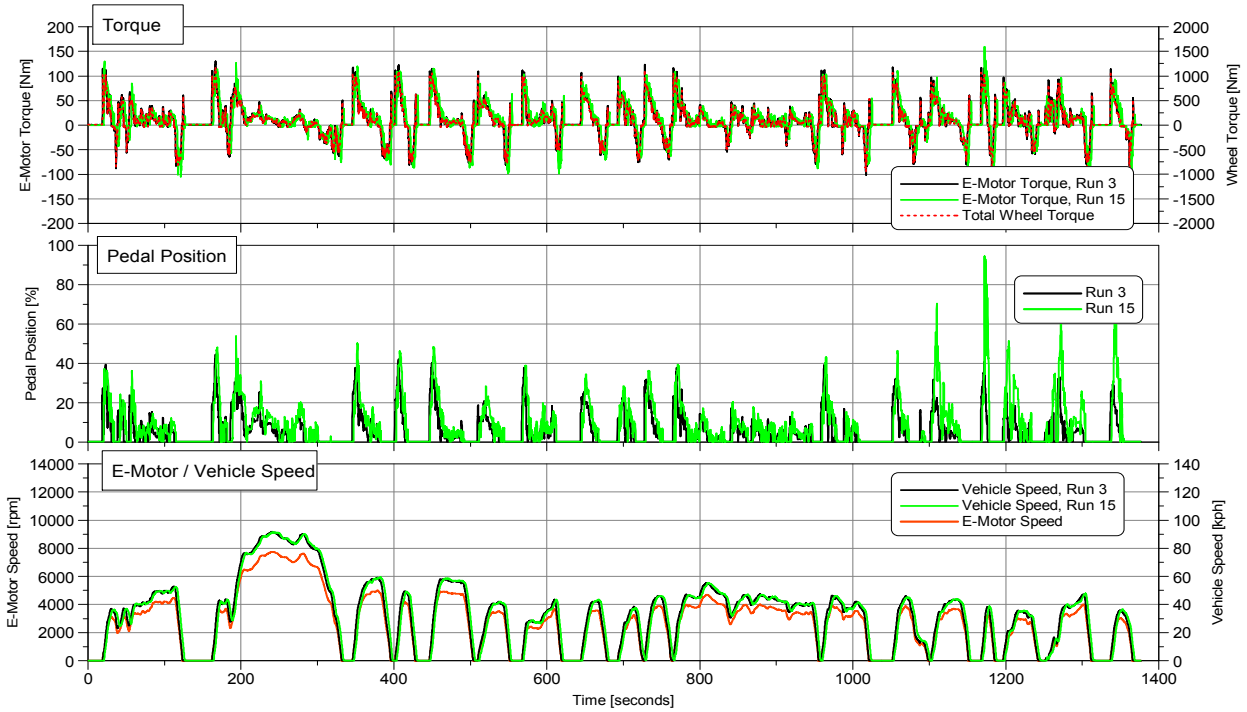


**Figure II-61: Change in Accelerator Pedal Map at 20% SOC**

The operating strategy of the drive modes to the A/C unit was investigated during the SC0 test cycle. While A/C power is limited in Eco mode, the A/C unit is not utilized in Eco+ mode in order to increase the range of the vehicle, see Figure II-62.

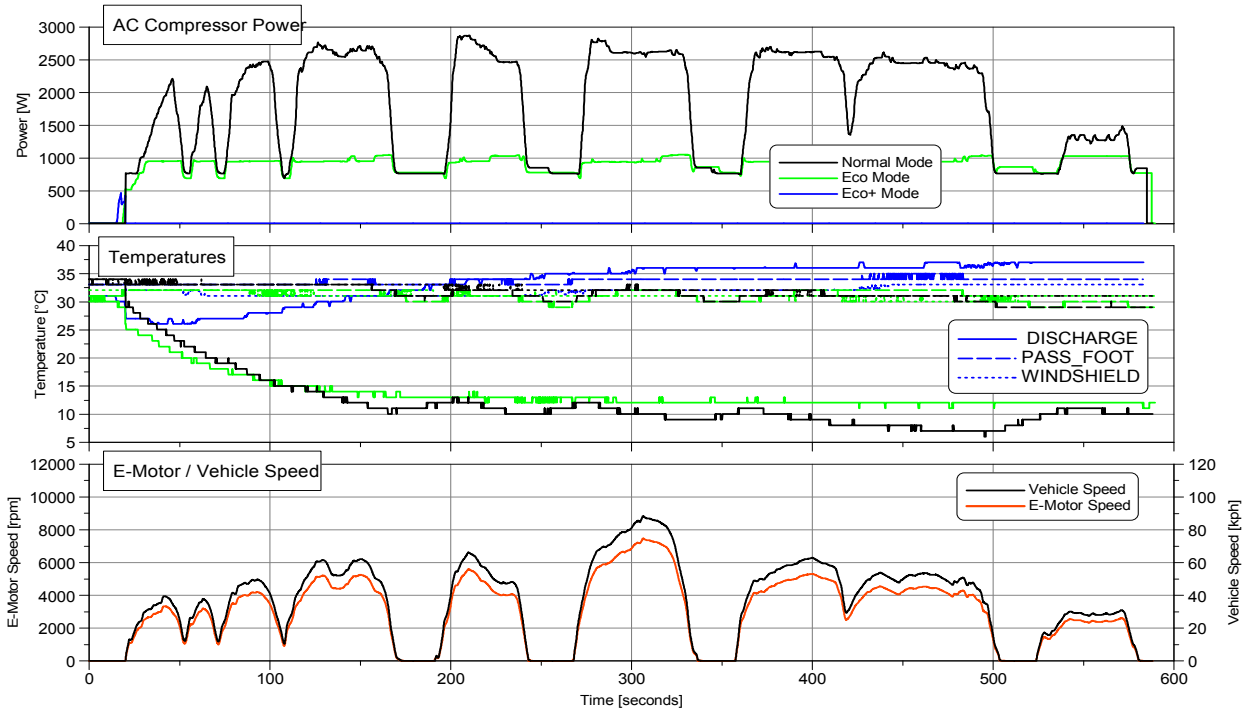


**Figure II-62: A/C Power and Cabin Vent Temp. During SC03 Test Cycle (Different Drive Modes)**

Energy consumption of the HV system is shown in Figure II-63 for these modes when completing the SC03 test cycle.

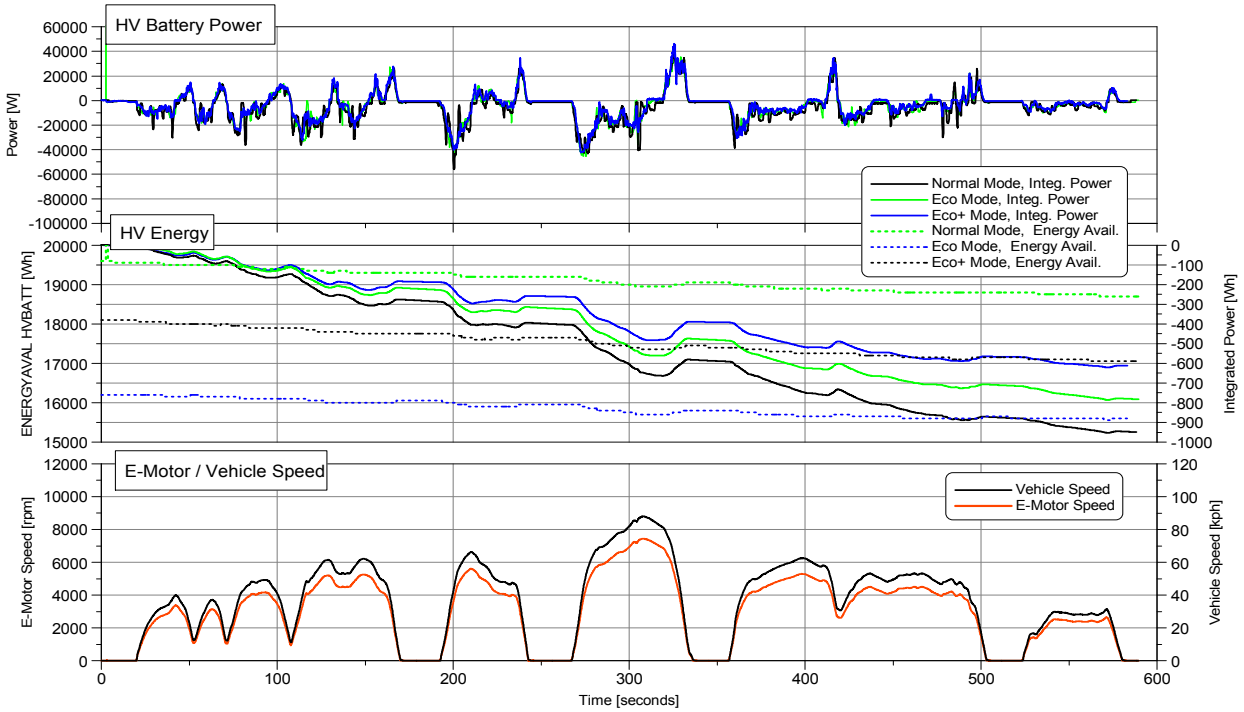


**Figure II-63: HV Power and Energy Usage During SC03 Test Cycle (Different Drive Modes)**

Battery charge testing with the Level 2 charge system was completed at different temperatures as outlined on Figure II-64. Although charge time is increased at cold temperatures (-30°C), charging at this temperatures does not cause any issues/abnormal behavior.

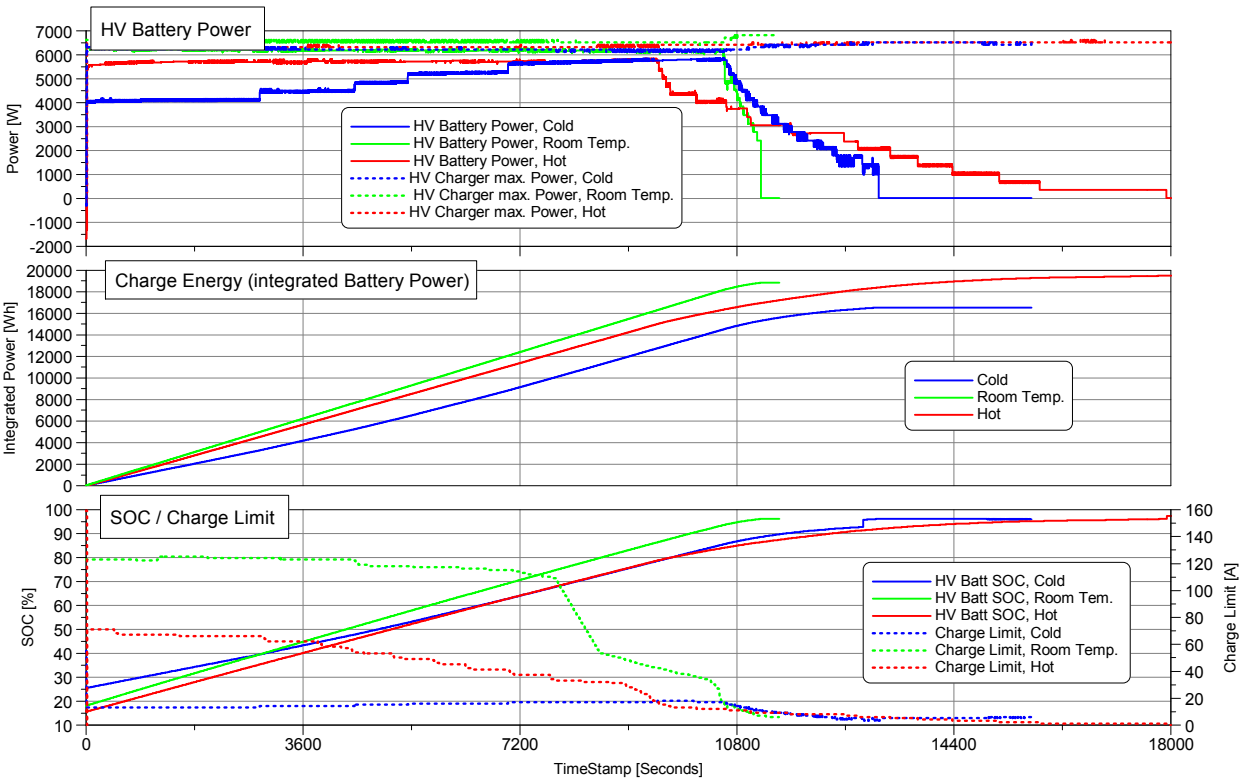


**Figure II-64: Level 2 Vehicle Charging at Different Temperatures**

The VW e-Golf is also equipped with a Level 3 charging option (DC charging); Figure II-65 compares charging time and current for Level 2 and Level 3 charging.

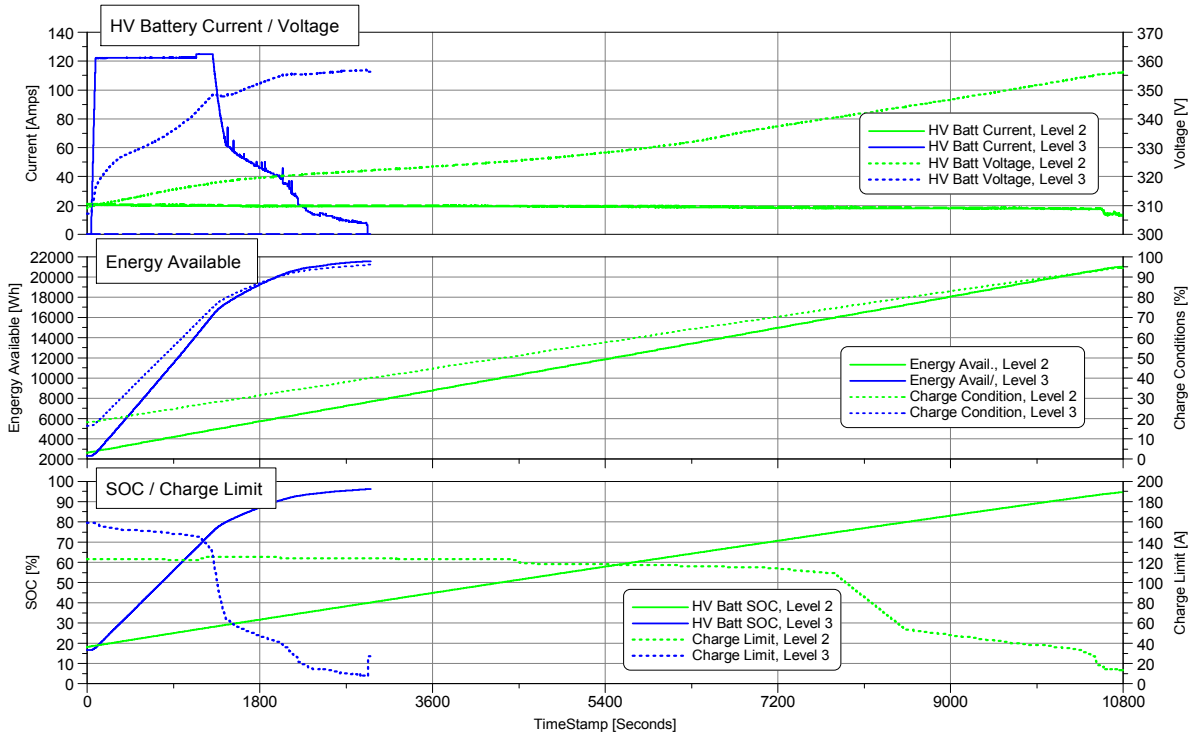


**Figure II-65: Level 2 vs. Level 3 Charging at Room Temperature**

## Conclusions

A summary of the completed VW e-Golf testing is as follows:

- The vehicle uses a synchronous AC permanent magnet motor with 85kW and a fixed gear single speed drive ratio.
- The battery is a 323V, 24.2 kWh lithium-ion pack.
- Temperature spread between individual battery modules of up to 10°C could be witnessed throughout vehicle testing.
- Discharge currents of up to ~280A were recorded during WOT acceleration.
- Up to 0.2V spread between lowest and highest cell voltage could be noticed at high battery loads (e.g. WOT). The spread is reduced with lower battery current draw.
- Drive modes (normal, eco, eco+) affect the accelerator pedal map and max motor performance. When performing a kickdown, drive modes do not limit the maximum output power.
- The vehicle has an optional brake (B) mode, which has higher recuperation during coast downs.
  - Deceleration rates of up to -1.5 m/s$^2$ were measured during coast down in B.
  - The brake lights were found to turn on under these conditions.
  - E-Motor regenerative torque was found to be around -63 Nm.
- The vehicle uses blended braking.
- Up to 45 kW regenerative power was noticed during braking events.
- When coming to a full stop, the vehicle does not apply creep torque when releasing the brake pedal, but launches after initial accelerator pedal tip-in. Once the vehicle is launched and did not exceed ~10 kph, creep torque is applied (e.g., for stop and go traffic).
- A clear linear correlation between used energy and battery SOC was demonstrated.

- The vehicle has a ‘launch assist / hill hold’ function on inclines.
  - The foundation brakes hold the vehicle for up to 3 seconds after brake pedal release.
  - Once rolling back, e-motor torque is increased until the vehicle comes to a full stop.
- The vehicle is rated with a fuel economy of 126/105/116 (city/highway/combined) MPGe and a driving range of 83 miles
- Starting at 20% SOC and below, the vehicle switches automatically into the Eco mode with modified pedal map and reduced AC / heating for extending the driving range.
- DCDC power is reduced at low SOC.
- The usable battery SOC is between 96% and 7%; remaining SOC is about 6.5% when the vehicle does stop due to fully depleted battery.
- Summary and raw data for all vehicle-level tests are delivered. Key component functional testing are on going.

## Products

## Presentations/Publications/Patents

None

## References

None

# II.B. Advanced Lithium Battery Cell Technology

## II.B.1. Development of High-Energy Lithium-Sulfur Battery Cells (Pennsylvania State University)

**Donghai Wang, Principal Investigator**
134 MRL Building
University Park, PA 16802
Phone: 814-863-1287; Fax: 814-863-4848
E-mail: dwang@psu.edu

Subcontractor: EC Power
Subcontractor: Argonne National Laboratory

**Christopher Johnson, Project Manager**
National Energy Technology Laboratory
3610 Collins Ferry Road
Morgantown, WV 26507

Start Date: September 30, 2011
End Date: September 15, 2015

### Abstract

### Objectives

- Develop a novel nanocomposite sulfur cathode for lithium-sulfur batteries with high energy density, efficiency, and cycle life.
- Develop a novel Li-rich composite anode for Li-S batteries to improve cell cycle life.
- Develop novel electrolyte and electrolyte additives for Li-S batteries to improve cell efficiency, stability, and safety.
- Design, fabricate, test, and optimize the design of Li-S batteries using the above new technologies to maximize energy, power, abuse tolerance, and other favorable traits.
- Perform thermal testing of the developed Li-S cells and materials.

### Accomplishments

- Cycled high sulfur content, nitrogen-doped graphene (NG) cathodes with NG-coated separators.
- Optimized the coating thickness and mass loasing of PSU-7/sulfur composite cathodes.
- Studied the cycling efficiency of LiP electrode.
- Fabricated and delivered twenty eight 1 Ah LiP/S pouch cells to Idaho Nation Lab (INL).
- Developed a Li foil anode on copper mesh current collector to greatly decrease anode weight and increase cell specific energy (> 200 Wh/kg) of 2 Ah pouch cells.
- Fabricated and delivered twenty four 2 Ah Li foil / S pouch cells to Idaho Nation Lab (INL).
- Investigated an organo-fluorine compound, 1,1,2,2-tetrafluoroethyl-2,2,3,3-tetrafluoropropyl ether (TTE) as the electrolyte solvent and showed a reduction in the polysulfide shuttle effect.

## Future Achievements

- Deliver baseline cells with energy density 280 Wh/L and 80% capacity retention after 500 cycles at 1C rate.
- Develop carbon-sulfur cathode material composed of at least 85 wt% sulfur with capacity of at least 1300 mAh/g, coulombic efficiency > 95%, and 90% capacity retention in 100 cycles at C/3 charge and discharge rate.
- Develop anode with capacity of 1500 mAh/g and capacity retention of 90% after 100 cycles at C/3.
- Full cell tests with cell irreversible capacity < 15%, coulombic efficiency > 95%, and self-discharge < 0.3% per day.
- Thermal stability characterization of the lithiated electrode via DSC.
- Scale up active material production to the 1 kg level.
- Design pouch cells with energy density > 500 Wh/l, 80% capacity retention after 300 cycles at C/2.
- Nail penetration testing at USABC EUCAR Level 3.

## Technical Discussion

### Background

Lithium-sulfur batteries need to overcome many technical barriers, including the following:

- Polysulfide dissolution and shuttling, combined with degradation of the lithium metal anode and formation of an unstable SEI layer, can severely limit cell lifespan.
- High sulfur loading in the cathode is required for achieving a high energy density; however, high loading often leads to parts of the electrode becoming inaccessible to electrolyte, thereby decreasing energy density and cycle life.
- Cathodes must have high active material loading – however, the low density of sulfur and common composite materials (porous carbon, etc.) make thin, crack-free, high-loading electrodes difficult to achieve.
- Electrolyte modifications that decrease polysulfide solubility or improve SEI layer stability often come at the cost of increased impedance and other issues.

### Introduction

DOE goals require the development of a high-energy, high-power, high-efficiency, long-lasting, low-cost, and safe battery. This project aims to meet these goals by using the extremely promising lithium-sulfur battery chemistry. The Li-S cathode has a theoretical capacity of 1672 mAh/g with a nominal voltage of 2V. In addition, sulfur does not experience any significant size change during lithium insertion/extraction, making it very stable in principle.

Lithium-sulfur's great promise comes with a major challenge. Lithium polysulfides – intermediate charge/discharge states of the cathode – are highly soluble in traditional electrolytes and can move throughout the battery, experiencing redox reactions and thus causing poor efficiency and loss of active material. Additionally, lithium metal commonly used as the anode is vulnerable to mossy lithium and dendrite growth and cannot generally form a stable SEI layer, causing further capacity loss and safety concerns. These, combined with optimization and thermal safety considerations, necessitate a significant body of work to bring the Li-S to the commercialization stage.

## Approach

To design a superior lithium-sulfur battery, we will focus on several aspects of cathode, anode, electrolyte, and whole-cell study and design.

Our sulfur cathode study will hit four main points. To improve volumetric energy density, we will test new methods of generating well-structured carbon frameworks. To improve sulfur loading, we will optimize the pore geometry of our carbon framework and investigate new framework materials and structures. Since mitigating polysulfide dissolution is critical to improving battery stability, we will investigate additives and novel materials that promise to adsorb polysulfides and find an optimal composition and synthesis method. Additionally, with an eye toward commercialization, we will optimize our production methods and conditions, particularly in regards to designing cathode materials that can be easily made into electrodes with realistic active material loading and which can be produced in large batches.

On the anode side, we will investigate promising options for generating lithium powder-based and silicon-based anodes, that we may promote stable SEI formation and prevent dendrite growth. Anode coating methods will also be investigated to this end, and anode-electrolyte compatibility will be studied to ensure excellent whole-cell performance.

Our study of electrolyte options for our sulfur battery will aim to improve SEI stability, decrease active material loss, increase active material utilization, and ensure battery safety. To this end, we will develop new electrolyte systems and additives and test the effects of existing additives on our full battery system, with particular focus on silane/siloxane-based systems and ionic liquid additives.

Additionally, we will optimize cell fabrication and design parameters, such as electrode size and N/P ratio, number of electrodes per stack, etc., to get the most out of our cutting-edge materials. In particular, we will take on the challenge of making electrodes with commercially-viable loadings by optimizing electrode composition and fabrication techniques. Cell modeling and experimental testing will be combined to inform these efforts. The thermal stability and abuse tolerance of our cell components and full cells will also be tested, ensuring safe batteries. Finally, the self-discharge and other half-cell and full-cell properties of the battery system will be fully characterized and optimized.

## Results

### High sulfur content, nitrogen-doped graphene (NG) cathodes with NG-coated separators

Nitrogen-doped graphene (NG) was investigated as an adsorbent of lithium polysulfides and a host for sulfur. Previous studies have shown that nitrogen functional groups enhance the adsorption of lithium polysulfides. Because of nitrogen's strong chemisorption ability, we not only tested this material for use in the cathode, but also on the separator.

NG has a greater surface area and pore volume than nitrogen-doped mesoporous carbon (MPNC), as shown in Table II-11. The nitrogen content in the NG was ~10%. The increased surface area and pore volume can accommodate a higher sulfur content and can ensure a uniform distribution of sulfur in the cathode. Polysulfide intermediates can be kept electrochemically active in both the cathode and on the separator as well.

Nitrogen-doped graphene/sulfur (NG-S) composites with 70% and 80% sulfur content were cycled in coin cells at a C/10 rate for the 1st cycle, then at C/5 for subsequent cycles. A separator with a thin coating of NG (~0.2 mg/cm$^2$) was used in both cycling tests. After initial activitation, the coloumbic efficiency is ~99% for 150 cycles for both NG-S70 and NG-S80. NG can effectively adsorb sulfur and polysulfides, evidenced by the good cycling performance.

**Table II-11: A Comparison between the Surface Area and Pore Volume of NG and MPNC**

| | Surface Area ($m^2/g$) | Pore Volume ($cm^3/g$) |
|---|---|---|
| NG | 920 | 4.2 |
| MPNC | 840 | 1.4 |

## Optimization of PSU-7/sulfur composites

PSU-7/sulfur composite cathode were optimized for coating thickness and electrode composition. The cycling performance for PSU-7 with different coating thickness, and this different sulfur mass loadings, is shown in Figure II-66. The electrode composition of these cells were 7:2:1 (wt) PSU-7 (80 wt% sulfur)/carbon additives/PVDF. All cells were cycled at a C/20 (1C = 1675 mAh $g^{-1}$-sulfur) rate for the first 3 cycles and then at a C/10 rate for all subsequent cycles. Cells with a sulfur mass loading greater than 6 mg $cm^{-2}$ had a capacity decrease between 20% and 35% when switched to the higher cycling rate. At mass loadings under 6 mg $cm^{-2}$, the capacity was more stable. The specific capacity after 15 cycles was nearly equivalent for the 600 µm and 700 µm coating thickness. A 700 µm coating thickness was determined to be optimal for sulfur mass loading and electrochemical performance. An 8:1:1 electrode composition at the optimized coating thickness was also tested, but the specific capacity was about 4-6 times lower than the 7:2:1 cell throughout 15 cycles.

| 70% PSU-7 (80% wt% sulfur), 20% carbon additives, 10% PVDF) | |
|---|---|
| Coating Gap (µm) | Mass loading (mg-sulfur $cm^{-2}$) |
| 600 | 4.08 |
| 700 | 5.54 |
| 800 | 6.59 |
| 900 | 7.15 |

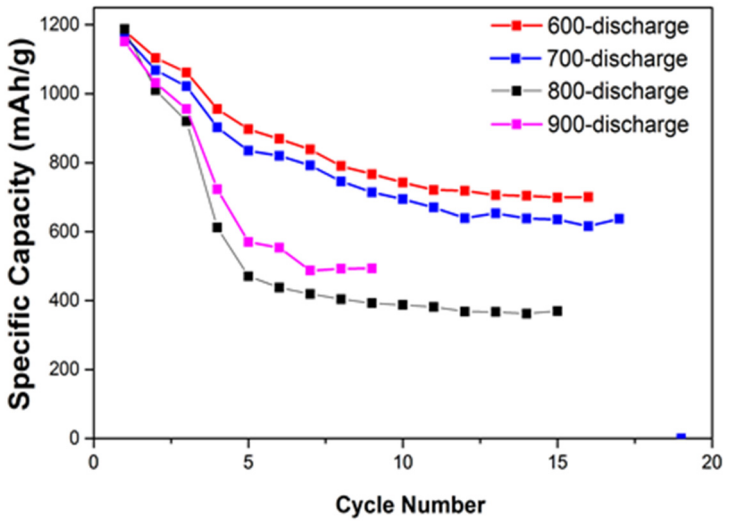


Figure II-66: Cycling performance of PSU-7 electrodes with different coating thicknesses

## Cycling efficiency of LiP electrode

LiP composite anode (Li powder + non-graphite particles) has been developed for high-capacity anode (e.g. 1,000-1,500 mAh/g) in Li-S battery with good cycling performance and feasible fabrication, based on ECP's proprietary Li powder composite anode technology. In this annual report, cycling efficiency of LiP electrode

was studied in coin cells to understand LiP electrode behavior during charge and discharge and its degradation mechanisms.

Three different formulations of LiP electrode were tested in LiP / Li foil coin cells, and they are LiP0: 90 wt% Li Powder + 10 wt% binder; LiP1: 80 wt% Li Powder + 10 wt% additive + 10 wt% binder; LiP2: 60 wt% Li Powder + 20 wt% additive + 20 wt% binder. The electrolyte used was 1.0 M LiTFSI in DME/DOL (1:1 in vol.) with 0.4 M $LiNO_3$. The lithium in LiP electrode was initially dissolved at 0.50 mA/cm$^2$ until cut-off voltage at 1.0 V. Subsequently, Li deposition to LiP electrode at 0.50 mA/cm$^2$ for 10.5 mAh (constant for all cycles) and Li full dissolution from LiP electrode at 0.50 mA/cm$^2$ until 1.0 V were repeated. Accordingly, cycling efficiency is the Li full dissolution amount each cycle divided by the 10.5 mAh of Li deposition amount. As a result, we can obtain lithium loss on LiP electrode during cycling in terms of cycling efficiency and study how content of additive affects cycling efficiency.

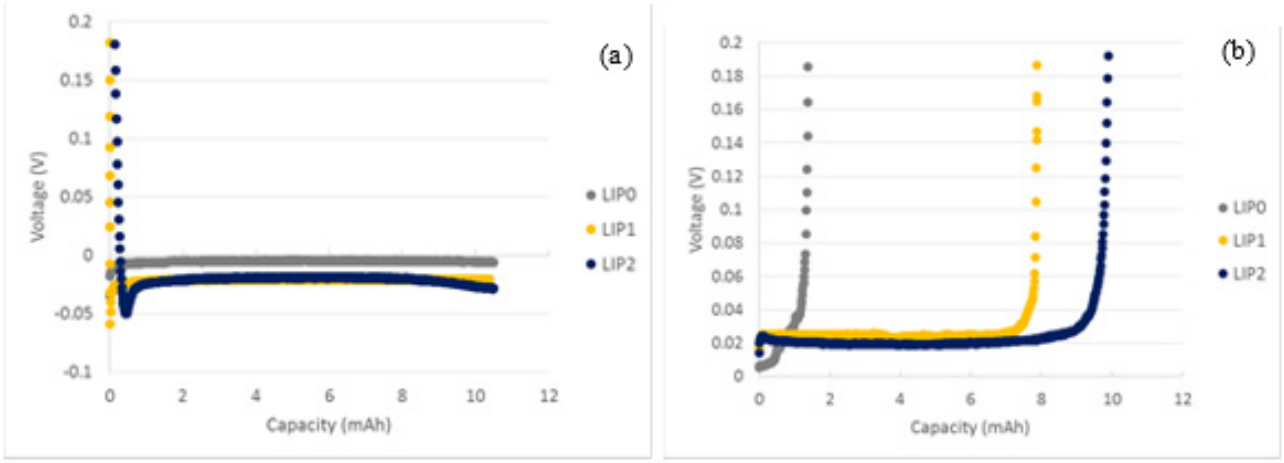


**Figure II-67: Voltage changing with (a) Li deposition amount (mAh) to LiP electrode and (b) Li dissolution amount (mAh) from LiP electrode at the 36th cycle in LiP / Li foil coin cells**

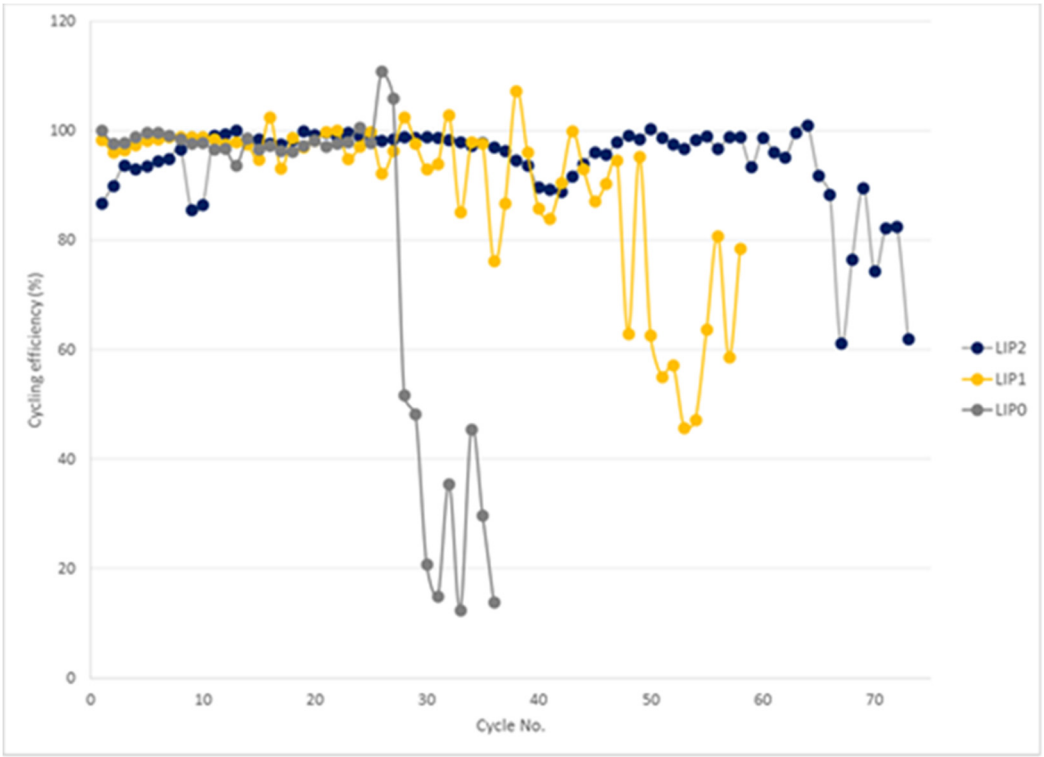


**Figure II-68: Cycling efficiency of LiP electrode in LiP / Li foil coin cells, varying with cycle number**

As shown in Figure II-67(a) for the 36th cycle, when Li deposits to LiP electrode at a constant current (i.e., 0.50 mA/cm$^2$), the voltage of LiP electrode versus Li foil decreases to a negative value and shortly rebounds to a stable voltage (around -20 mV for LiP1 and LiP2 but only about -4 mV for LiP0). Such small voltage (i.e., -4 mV) on LiP0 suggests that micro internal short occur due to lithium dendrite growth.

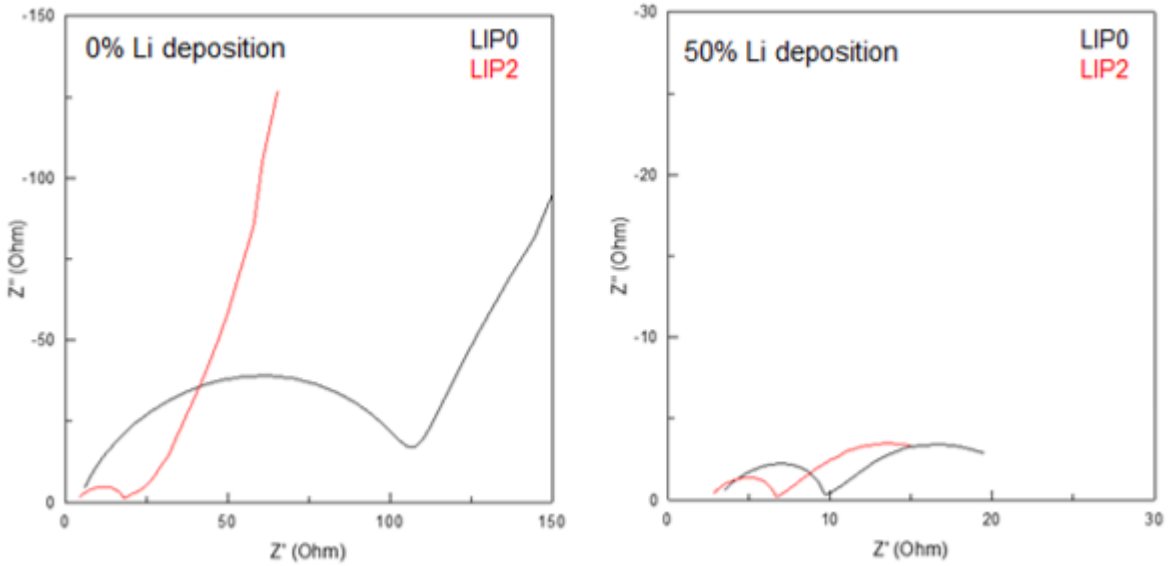


**Figure II-69: Nyquist plots of electrochemical impedance spectra measured at (a) 0% Li deposition (b) 50% Li deposition to LiP electrode at cycle 2 in LiP / Li foil coin cells**

Figure II-67(b) exhibits the voltage profile during Li dissolution from LiP electrode at a constant current (i.e., 0.50 mA/cm$^2$). When the voltage of LiP electrode increases to 1.0 V, Li full dissolution amount is determined: 1.5 mAh for LiP0, 8.0 mAh for LiP1 and 10.2 mAh for LiP2. Thus there is a huge Li loss on LiP0 electrode (i.e., 10.5 mAh – 1.5 mAh = 9.0 mAh loss) and the cycling efficiency is only 14%. The lost Li is wasted for lithium dendrite growth and "dead" Li formation. Whereas, LiP1 and LiP2 have cycling efficiency of 76% and 97%, respectively. Figure II-68 illustrates their cycling efficiency varying with cycle number. The cycling efficiency of LiP2 keeps above 85% for 66 cycles and decreases to 61% at the 67th cycle. LiP1 shows fluctuating cycling efficiency above 76% before decreasing to 63% at the 48th cycle. The cycling efficiency of LiP0 stays above 90% for 27 cycles and falls to 52% after 28 cycles. The sharp decrease of cycling efficiency is at the 67th cycle on LiP2, at the 48th cycle on LiP1 and at the 28th cycle on LiP0, and hence it indicates the additive in LiP1 or LiP2 electrode is beneficial to inhibiting lithium dendrite growth to delay micro internal short.

Nyquist plots of electrochemical impedance spectra (EIS) at cycle 2 are shown in Figure II-69. When the Li deposition amount is 0% in Figure II-69(a), the semi-circular arc on LiP0 electrode (110 ohm wide) is much greater than that on LiP2 (only 16 ohm wide), which suggests that the interfacial resistance on LiP0 (i.e., Cu foil with 0% Li deposition on LiP0) is much higher than that on LiP2 with 20% additive. In Figure II-69(b) at 50% Li deposition amount, the semi-circular arcs on LiP0 and LiP2 become smaller than 0% Li deposition amount, but LiP0 still has higher interfacial resistance than LiP2 (6.6 ohm vs. 4.2 ohm). Figure II-70 shows the ohmic resistance (high frequency intercept at real axis) and the interfacial resistance (mid-frequency semi-circular arc width) obtained from the EIS Nyquist plots, varying with Li deposition amount to LiP electrode at cycle 2. LiP0 has a higher ohmic resistance than LiP2. Accordingly, the 20 wt% additive in LiP2 electrode helps to improve electronic conductivity and reduce the ohmic resistance. Also, the interfacial resistance on LiP2 is lower than LiP0 at all different Li deposition amounts [Figure II-70(b)].

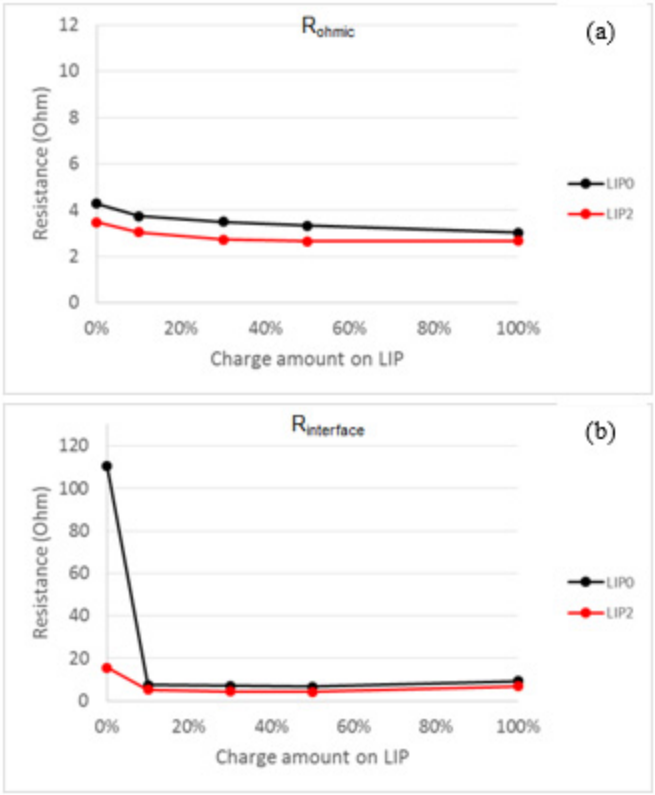


**Figure II-70: (a) Rohmic and (b) Rinterface obtained from Nyquist plots varying with charge amount (Li deposition amount) to LiP electrode at cycle 2 in LiP / Li foil coin cells**

## Fabrication and delivery of twenty eight 1 Ah LiP/S pouch cells

Twenty 1 Ah LiP/S pouch cells were fabricated. Eighteen of them were delivered to Idaho Nation Lab (INL), and the other two cells (#54 and #56) were cycled in EC Power. Figure II-71 is a picture of eighteen pouch cells delivered to INL. Each pouch cell had 6 double-sided LiP anodes, 2 single-sided LiP anodes, and 7 double-sided sulfur cathodes. Each electrode size was 4.4 cm × 5.6 cm. The electrolyte used was 1.0 M LiTFSI in DME/DOL (1:1 in vol.) with 0.4 M $LiNO_3$. The total weight of each pouch cell was ~22 g. Unfortunately, INL found a leaking problem in some pouch cells. Subsequently, EC Power team troubleshot the leaking problem from the pouch sealing process. And then ten 1 Ah LiP/S pouch cells were fabricated and delivered to INL again to make up the leaking pouch cells in the last batch.

## Cycling Performance of 1 Ah LiP/S Pouch Cells

Two 1 Ah LiP / S pouch cells (#54 and #56) were cycled at room temperature. They were charged and discharged at C/20 rate for initial 2 cycles and then C/10 rate between 1.6 V and 2.6 V. The two pouch cells present similar capacity fade with cycling (Figure II-72 and Figure II-73).

Pouch cell #54 shows a stable discharge capacity above 1.3 Ah for 25 cycles while the coulombic efficiency is above 85% (Figure II-72). Subsequently, the discharge capacity decreases to 1.0 Ah after 48 cycles and to 0.8 Ah after 56 cycles. As shown in Figure II-72(b), its S specific capacity is 998 mAh/g at cycle 2 and decreases to 541 mAh/g at cycle 55. Correspondingly, its cell specific energy 144 Wh/kg at cycle 2 and 77 Wh/kg at cycle 56.

Discharge capacity of pouch cell #56 keeps above 1.3 Ah for 27 cycles, and decreases to 1.0 Ah after 50 cycles and then quickly decreases to 0.8 Ah after 55 cycles (Figure II-73). Its S specific capacity is 1080 mAh/g at cycle 2, and its cell specific energy at cycle 2 is 158 Wh/kg.

If we define 0.8 Ah as the cycle life of the 1 Ah pouch cells, the two cells exhibit almost the same cycle life, 55 or 56 cycles.


**Figure II-71: Picture of eighteen 1 Ah LiP/S pouch cells delivered to INL**

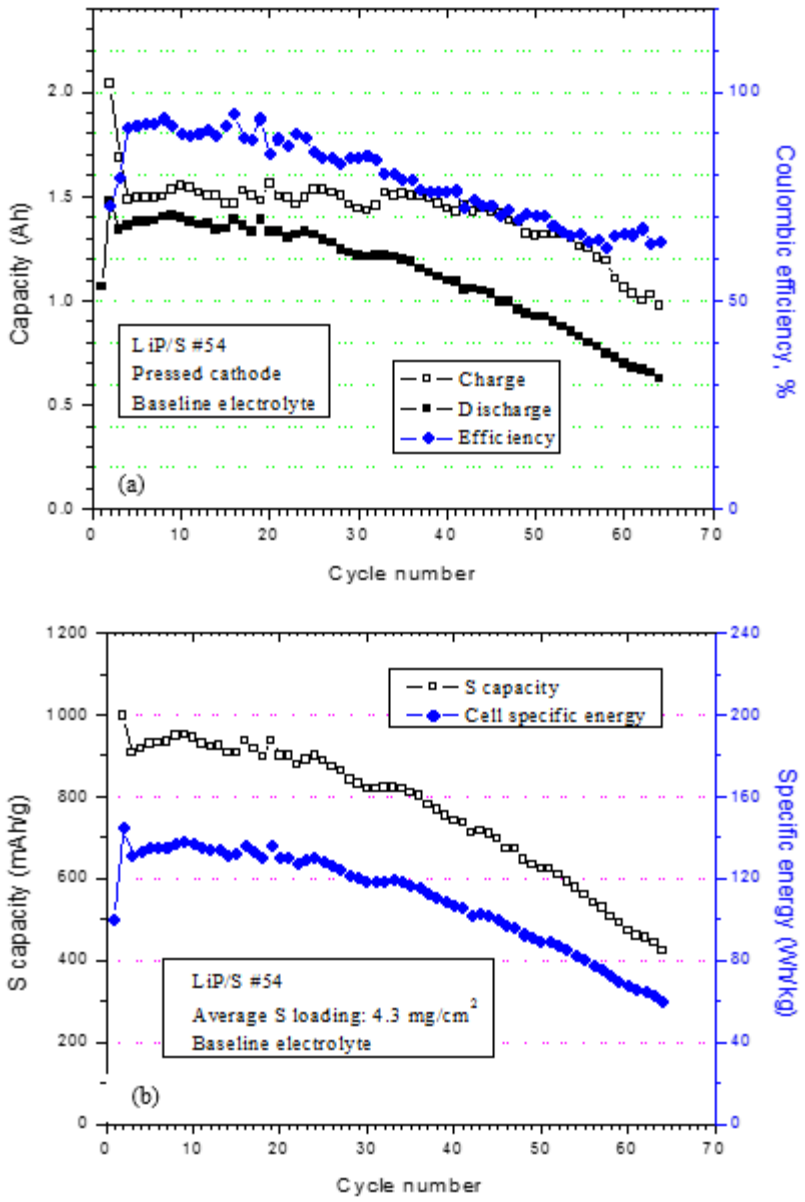


**Figure II-72: Cycling performance of 1 Ah LiP / S pouch cell (#54) (a) Charge and discharge capacity and coulombic efficiency; (b) S specific capacity and cell specific energy**

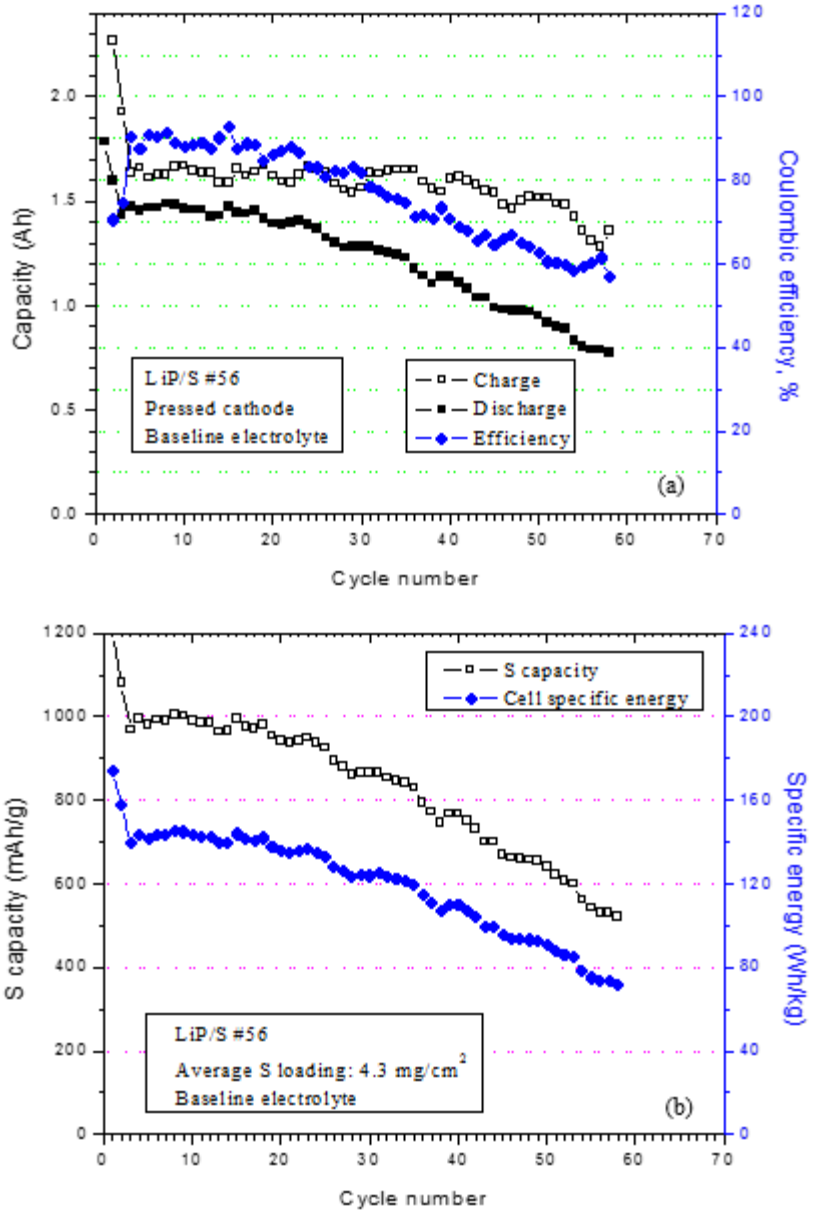


**Figure II-73: Cycling performance of 1 Ah LiP / S pouch cell (#56) (a) Charge and discharge capacity and coulombic efficiency; (b) S specific capacity and cell specific energy**

## High energy 2 Ah Li foil / S pouch cells

In order to increase cell specific energy of pouch cells, the cell weight shall be decreased from anode, cathode and electrolyte amount.

Li foil anode was one layer of 60 µm thick Li foil pressed on both sides of Cu mesh foil (9 µm thick Cu foil with Ø1 mm pores and 40% porosity). The Li foil anode weighed about 43% of the LiP anode used previously for 1 Ah pouch cells.

Electrolyte amount takes a significant part in a pouch cell. Accordingly, different electrolyte amount was attempted in 2 Ah pouch cells to search for the minimum but good electrolyte amount. The electrolyte used was from Argonne National Lab (ANL).

Three Li/S pouch cells with electrolyte amount of 7.2 g, 8.2 g and 9.8 g, respectively, were charged and discharged at C/20 rate for initial 2 or 3 cycles and subsequently C/10 rate between 1.6 V and 2.6 V. As illustrated in Figure II-74, their initial discharge capacity is above 2.0 Ah and their cell specific energy is

above 200 Wh/kg. However, their discharge capacity decreases quickly with cycling. The pouch cell with 9.8 g electrolyte shows better cycling performance than the other two cells with less electrolyte, but its discharge capacity still decreases quickly to 1.5 Ah in 6 cycles.

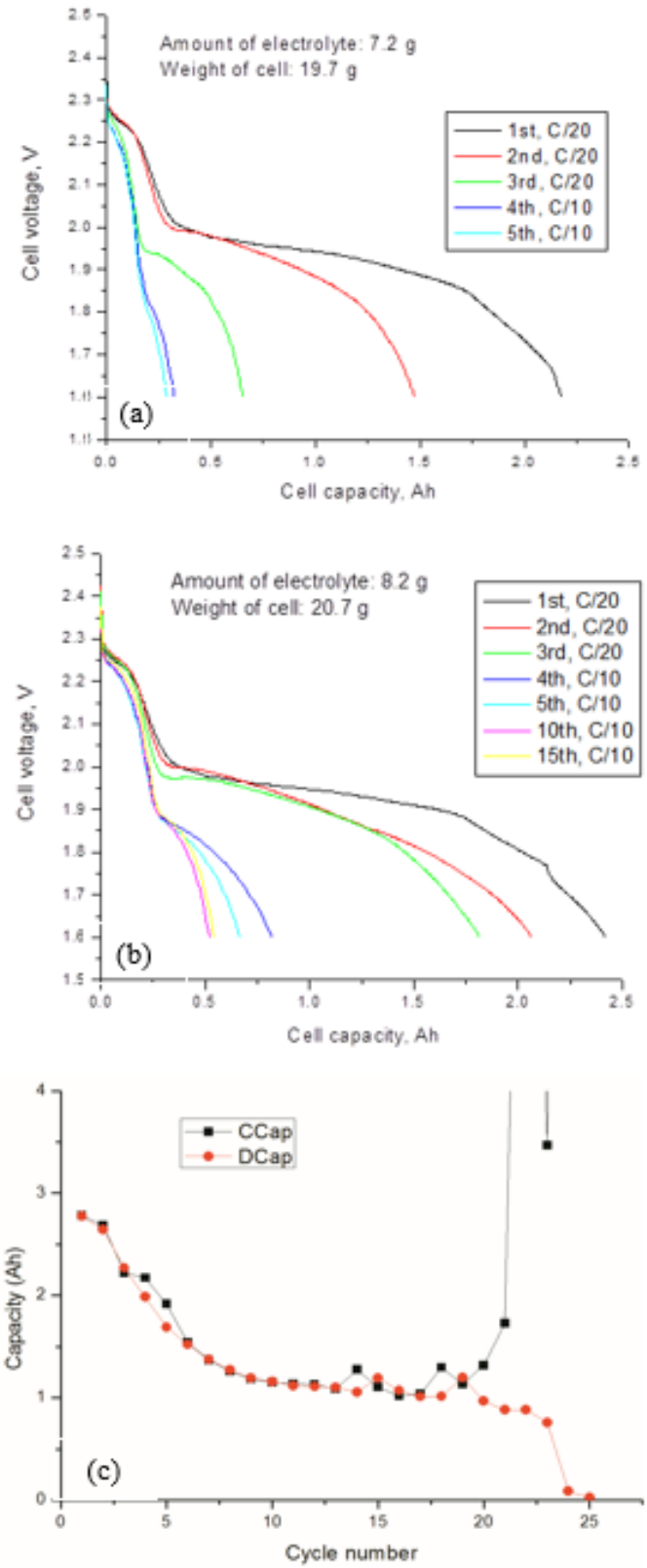


**Figure II-74: Cycling performance of 2 Ah Li foil / S pouch cells (a) 7.2 g electrolyte; (b) 8.2 g electrolyte; (c) 9.8 g electrolyte**

A pouch cell with 12.0 g electrolyte was tested. The cycling C-rate was kept at C/20 rate between 1.6 V and 2.6 V. Its initial discharge capacity is 2.7 Ah and initial cell specific energy is 213 Wh/kg (Figure II-75). Its discharge capacity slowly decreases to 2.3 Ah at cycle 13, but quickly decreases to 1.0 Ah at cycle 14. The quick decrease is likely attributed to micro-shorting due to the growth of Li dendrite during charging.

A pouch cell with thick Li anode was tested. The thick Li anode was two layers of 60 µm thick Li foil pressed on both sides of Cu mesh. The previous pouch cells used a thin Li anode that was one layer of 60 µm thick Li foil pressed on both sides of Cu mesh. The pouch cell with thick Li anode and 12.0 g electrolyte had slightly higher capacity than the one with thin Li anode, but its cycling performance and cell specific energy were similar to the latter one (Figure II-75). Accordingly, the thick Li anode did not defer the quick capacity decrease comparing with the thin Li anode.

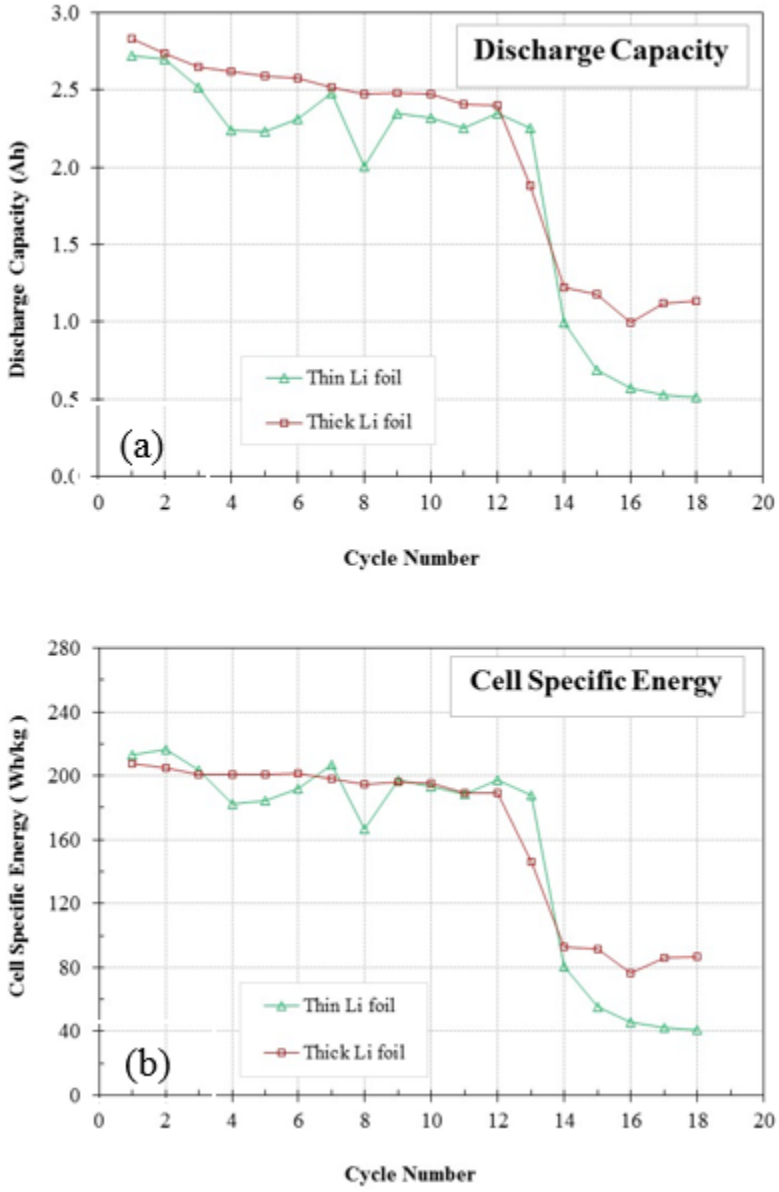


Figure II-75: (a) Discharge capacity, (b) cell specific energy of 2 Ah Li foil /S pouch cells with 12.0 g electrolyte

## Fabrication and delivery of twenty four 2 Ah Li foil / S pouch cells

Twenty six 2 Ah Li foil / S pouch cells were fabricated, and their picture is shown in Figure II-76. They used thin Li anode and 12 g electrolyte. Each pouch cell had 9 double-sided Li foil anodes, 2 single-sided Li foil anodes, and 10 double-sided sulfur cathodes. Each electrode size was 4.4 cm × 5.6 cm. The electrolyte used

was ANL electrolyte with 0.1 M $LiNO_3$. The total weight of each pouch cell was ~23.5 g. Twenty four of them are delivered to Idaho Nation Lab (INL) and the other two cells are being cycled in EC Power and Penn State.

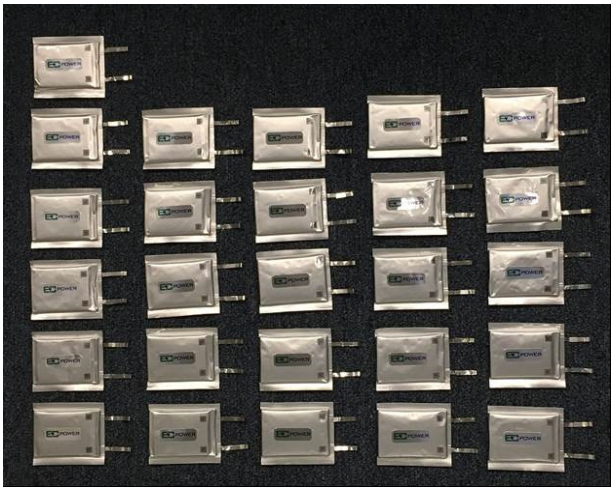

Figure II-76: Picture of twenty six 2 Ah Li foil / S pouch cells

## Cycle performance and coulombic efficiency

An organo-fluorine compound, 1,1,2,2-tetrafluoroethyl-2,2,3,3-tetrafluoropropyl ether (TTE), was investigated for the first time as the electrolyte solvent in the lithium-sulfur battery. The new fluorinated electrolyte suppressed the deleterious shuttling effect and improved the capacity retention and coulombic efficiency in cell tests. In addition, it was found to eliminate the self-discharge of the lithium-sulfur battery.

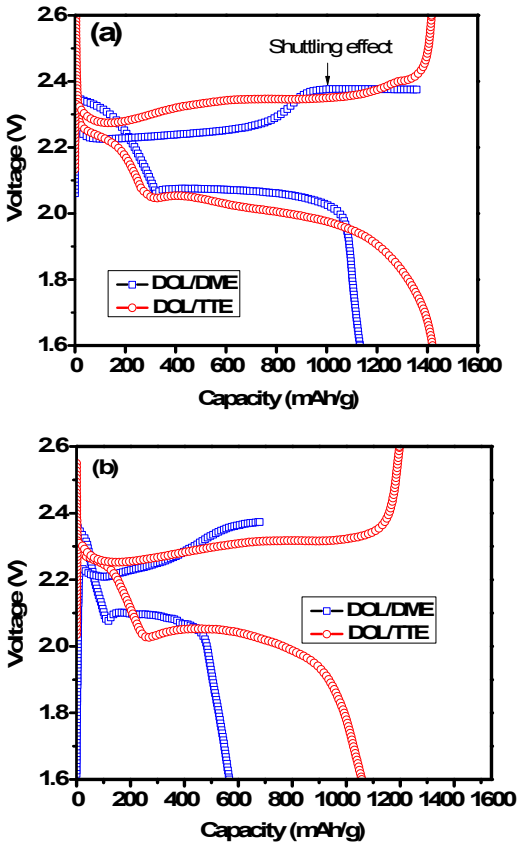


Figure II-77: Galvanostatic potential profiles of Li-S cells with 1.0 M LiTFSI DOL/DME (5/5) and 1.0 M LiTFSI DOL/TTE (5/5) electrolyte at a 0.1C rate

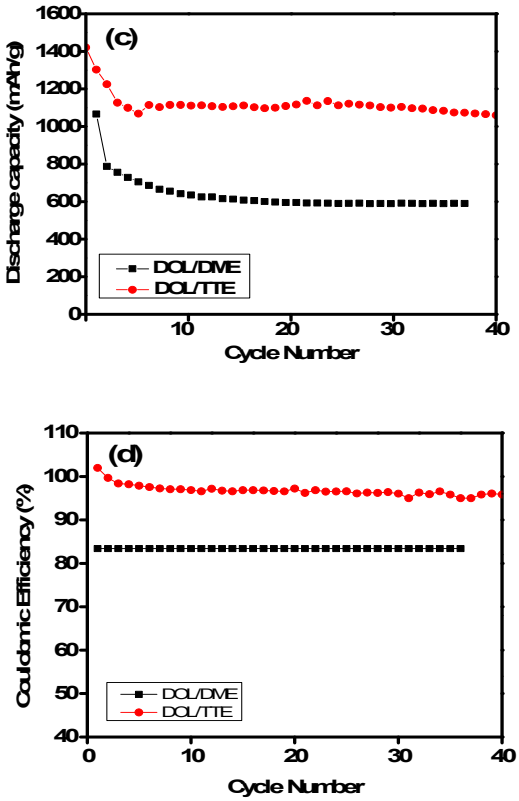


**Figure II-78: Capacity retention (a), and coulombic efficiency (b) of Li-S cells with 1.0 M LiTFSI DOL/DME (5/5) and 1.0 M LiTFSI DOL/TTE (5/5) electrolyte at a 0.1 C rate**

Figure II-77(a) shows the initial voltage profiles of a Li-S cell with the fluorinated electrolyte consisting of 1.0 M LiTFSI DOL/TTE (5/5 volume ratio). These profiles show two plateaus in the discharge. The higher voltage plateau at 2.2~2.4 V is due to the reduction of elemental sulfur to lithium polysulfides (Li2Sx, where x=4-8), and these polysulfides are reduced to lower order species ($Li_2S_2$ and/or $Li_2S$) at the lower voltage plateau, ~2.1~2.0 V. Compared with the Li-S cell using the baseline electrolyte of 1.0 M LiTFSI DOL/dimethoxy ethane (DME) (5/5), the fluorinated electrolyte cell showed a slightly lower voltage and a much higher capacity in the first discharge due to the low viscosity and low conductivity of the fluorinated electrolyte. A significant difference was observed for both cells during the subsequent charge. The TTE-based electrolyte cell displayed a long and flat plateau and a drastic voltage rise at the end of the first charging step without any redox shuttling behavior. The voltage profiles remain unchanged even at deep cycles (Figure II-77(b). The low polarity of the TTE helps reduce the dissolution of polysulfides into the electrolyte as confirmed by the fact that the synthesized $Li_2S_9$ does not dissolve in the TTE solvent. In contrast, the baseline electrolyte cell could not charge completely at each cycle due to the severe shuttling of dissolved polysulfides. The capacity retention and the CE of Li-S cells with two electrolytes are presented in Figure II-78(a) and (b). Low initial capacity and rapid capacity fading with low CE are observed for the Li-S cell using baseline electrolyte due to the dissolution of lithium polysulfide intermediates into the electrolyte, which leads to active sulfur loss and redox shuttle reactions. In contrast, after several formation cycles, the TTE cell maintains a stable discharge capacity of 1100 mAhg-1 for 50 cycles with a CE of 98% (Figure II-78(b)), indicating the effective inhibition of the polysulfide shuttling effect in the fluorinated electrolyte.

Aurbach et al. reported that the shuttle effect can be suppressed by addition of $LiNO_3$ to the electrolyte. The $LiNO_3$ participates in the formation of a stable passivation film on the surface of the Li anode, which protects the dissolved polysulfides from chemically reacting with the Li anode. However, the capacity still fades with cycling, indicating the $LiNO_3$ could not eliminate the active material loss. Fluorinated compounds are thermodynamically unstable in contact with lithium metal and tend to chemically react with it. As a perfluorinated ether, TTE reacts with lithium forming a conjugated C=C bond and LiF. The formation of this composite layer on the Li anode surface acts as a physical barrier, thereby inhibiting the chemical and electrochemical reaction of polysulfides with the Li anode.

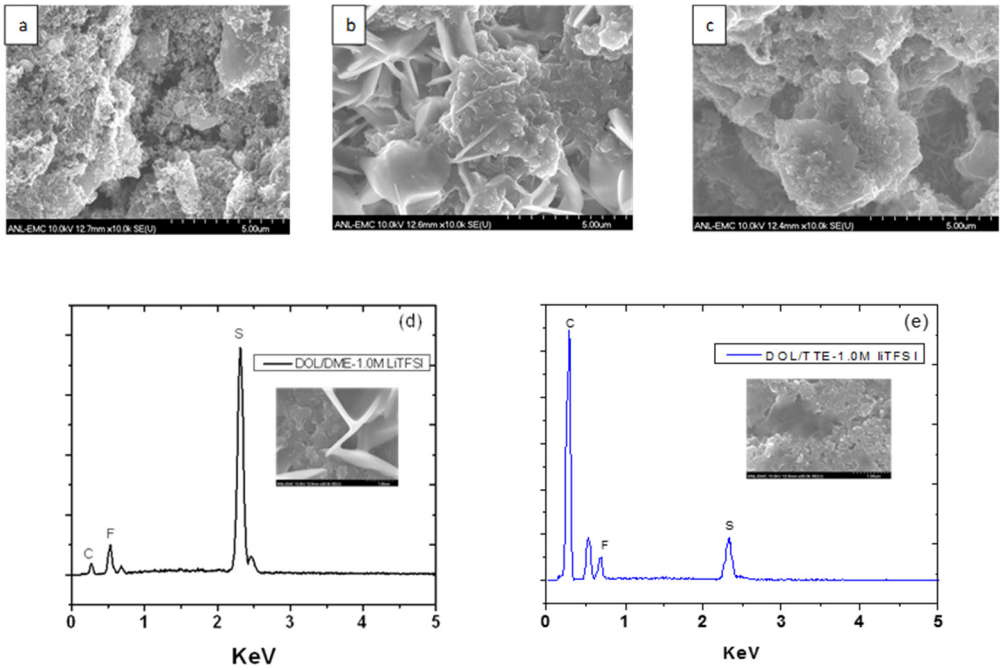


**Figure II-79: SEM images of (a) pristine sulfur electrode, (b) discharged sulfur electrode using 1.0 M LiTFSI DOL/DME, and (c) discharged sulfur electrode using 1.0 M LiTFSI DOL/TTE; EDS spectra of sulfur electrode at the first discharge using (d) 1.0 M LiTFSI DOL/DME and (e) 1.0 M LiTFSI DOL/TTE electrolytes**

We also determined the morphological changes of the sulfur electrode discharged in two electrolytes. Figure II-79(a) is a typical SEM image of the pristine sulfur/carbon electrode. After the first discharge in the baseline electrolyte, the surface of cathode had been deposited with large quantities of crystal-like discharge products (Figure II-79(b)) of insoluble lithium sulfides ($Li_2S$ and/or $Li_2S_2$). Further analysis of the deposit by energy-dispersive x-ray spectroscopy (EDS) revealed a sulfur-rich agglomeration, as shown in Figure II-79(d). However, when using the DOL/TTE fluorinated electrolyte, the discharged electrode showed morphology similar to the pristine cathode filled with fine discharged product particles/flakes hidden in the porous structure of the sulfur-carbon composite, as illustrated in Figure II-79(c). Additionally, much less lithium polysulfide deposition was detected from the EDS spectrum (Figure II-79(e)). These analysis results indicate that the SEI layer formation through reductive decomposition on the surface of the cathode suppressed the polysulfide dissolution and agglomeration of the discharged species, an observation that is supported by the improved specific capacity and superior CE for the fluorinated electrolyte versus baseline cell (Figure II-77(c) and (d)).

## Self-discharge improvement

A fundamental analysis reveals that the charge-discharge efficiency, redox shuttling phenomenon, and self-discharge are all facets of the same issue, which in principle could be solved by a single solution. In practice, $LiNO_3$ has become a mandatory additive in conventional DOL/DME-based electrolyte in order for Li-S cells to operate normally.The main function of $LiNO_3$ is to reduce shuttling of the soluble LiPS during charge-discharge cycles. Surface analysis shows that, in the presence of $LiNO_3$, a protective film composed $Li_xNO_y$ and $Li_mSO_n$ is generated on the surface of the lithium anode. However, $LiNO_3$ alone is still not able to completely eliminate the active material loss caused by shuttling, and repeated cycling destroys the protective film. Figure II-80(a) shows the self-discharge result of a Li-S cell with DOL/DME-1.0 M LiTFSI in the presence of 0.2 M $LiNO_3$. A 3.8% loss in discharge capacity was observed after 10 hour rest at room temperature, indicating much less self-discharge had occurred during the storage of the battery compared to the cell without $LiNO_3$ additive. However, when the 10 hour rest was performed at 55 °C, the capacity loss resulting from self-discharge increased to 8.6% (Figure II-80(b)), which is likely due to increased diffusion rate of LiPS and instability of the protective layer on the Li surface at elevated temperatures. In comparison, $LiNO_3$ was found to further suppress self-discharge in combination with the fluorinated electrolyte. As shown in Figure II-80(c), with the addition of 0.2 M $LiNO_3$ in the DOL/TTE-1.0 M LiTFSI electrolyte, only minor capacity loss (0.7%) was observed for the cell rested at room temperature. More surprisingly, negligible self-discharge was also evident when the cell was stored at fully charged state at 55 °C for 10 h, as shown in Figure II-80(d).

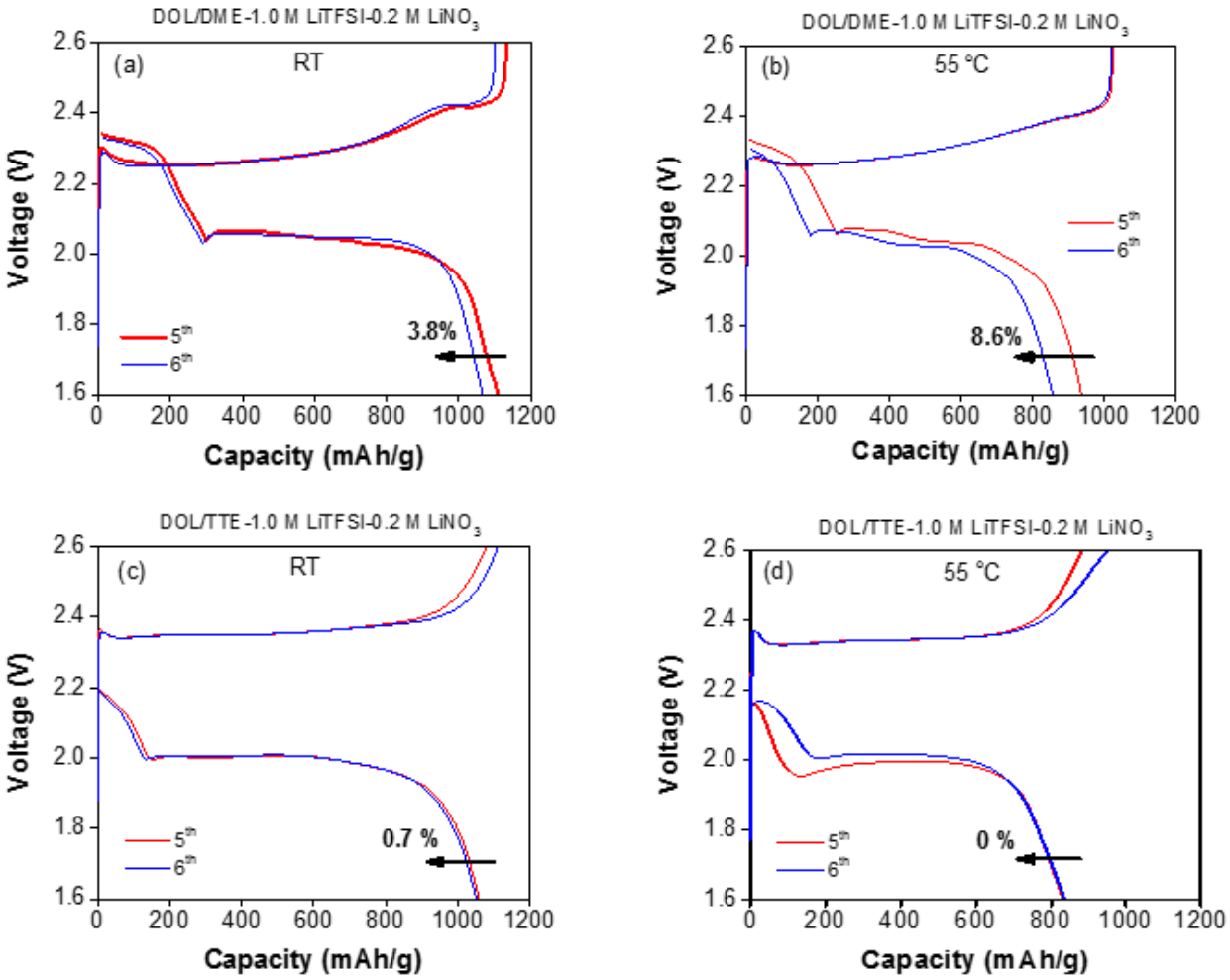


**Figure II-80: The 5th and 6th cycle voltage profile for Li-S cells with high-loading sulfur cathodes rested between the 5th charge and 6th discharge, with (a, b) DOL/DME-1.0 M LiTFSI+0.2 M $LiNO_3$ electrolyte and (c, d) DOL/TTE-1.0 M LiTFSI+0.2 M LiNO3 electrolyte rested at (a, c) room temperature and (b, d) 55 °C**

## TTE electrolyte cell mechanism study

The function mechanism was proposed in the schematic illustration of Figure II-81(a) and (b). The high solubility of polysulfides (PS) in the conventional DOL/DME solvent results in the diffusion of the PS species into the electrolyte and their reaction with the lithium anode causes severe shuttling phenomenon and loss of active materials. However, the PS intermediates have low solubility in the TTE electrolyte and tend to accumulate inside the electrode structure, thus the chances of its migration to the anode side and subsequent parasitic reaction with Li are extremely low. To confirm the effect of fluorinated solvent on the cell performance, solubility test was conducted by synthesizing 1.0 M of $Li_2S_x$ ($Li_2S_x$, x=8 based on stoichiometric amounts of $Li_2S$ and sulfur) in DOL/DME and DOL/TTE mixture solvents according to the method reported by Rauh et al. The images after 48 hours of agitation are shown in Figure II-82. $Li_2S_8$ completely dissolves in DOL/DME solvent and a dark-brown and viscous solution was obtained. However, less dissolution and more precipitate are observed for the DOL/TTE solvents by the lighter color of the mixture. The mixture solvent with the highest fluoroether concentration DOL/TTE=1:3 has the lowest solubility of polysulfides; however, it should be noted that the high ratio of DOL/TTE has a significant effect on the solubility of the LiTFSI salt. The low solubility of polysulfide and LiTFSI accounted for the poor cell performance of DOL/TTE=1:3 electrolyte.

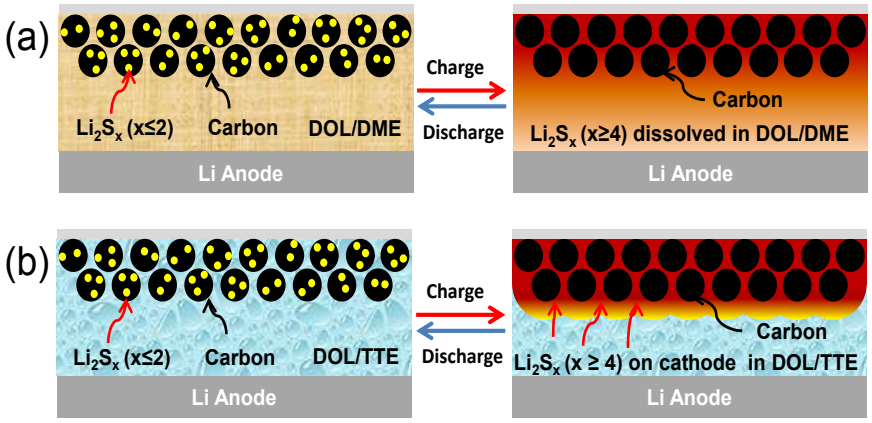


Figure II-81: Schematic illustration of discharge and charge process in Li-S battery with (a) baseline electrolyte DOL/DME-1.0 M LiTFSI and (b) fluorinated electrolyte DOL/TTE-1.0 M LiTFSI

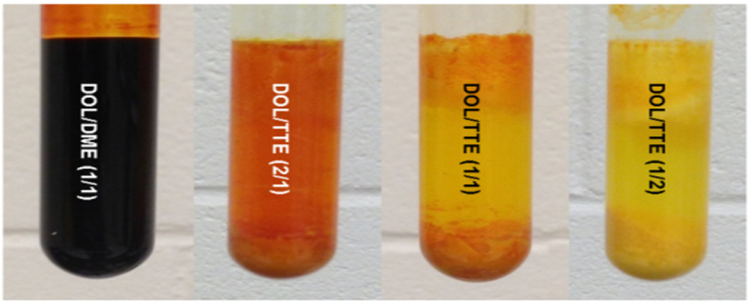


Figure II-82: Polysulfide solubility in fluorinated electrolyte solvents: 1.0 M Li2S8 (based on stoichiometric amounts of $Li_2S$ and sulfur) dissolved in baseline solvent DOL/DME (1/1) (left) and fluorinated solvents with different DOL/TTE volumetric ratios DOL/TTE (2/1) (second left), DOL/TTE (1/1) (second right) and DOL/TTE (1/2) (right)

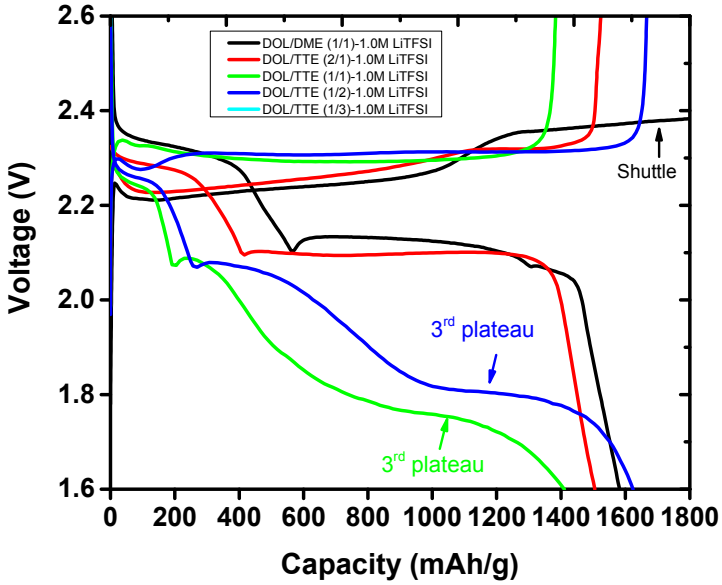


Figure II-83: The 1st charge and discharge voltage profiles for Li-S cell containing DOL/DME (1/1)-1.0 M LiTFSI and four fluorinated electrolytes with different DOL/TTE ratios 2/1, 1/1, 1/2 and 1/3

Figure II-83 shows the first charge/discharge voltage profiles of Li-S cells with different fluorinated electrolytes. Overpotential was observed in both high-order and low-order plateau from charge and discharge curves for the fluorinated electrolyte cells. This is caused by the lower ionic conductivity of the fluorinated electrolytes. Interestingly, for the TTE electrolyte cells, the contribution to the overall capacity from the high-order polysulfide reduction (the first plateau on discharge profile at ~2.3 V) becomes smaller with the increasing amount of TTE. For baseline cell, the contribution from the high-order plateau is 37.5% (600 out of 1600 mAhg-1), and this value decreases to 33.0% for DOL/TTE=2:1 (500 out of 1500 mAhg-1), 16.5% for DOL/TTE=1:1 (260 out of 1620 mAhg-1) and 14.2% for DOL/TTE=1:2 (200 out of 1400 mAhg-1). These results imply that the reduction reaction from elemental S to high-order PS is transient and the kinetics of the high-order PS further conversion to low-order ones is more favorable when the fluorinated electrolytes are present. This phenomenon is associated with the appearance of a 3rd "plateau", corresponding to the slope on the discharge profile as indicated by an arrow. Differential capacity profiles (dQ/dV) (not shown) confirmed this plateau is associated with the reductive decomposition of the fluoroether TTE on the surface of the sulfur/carbon particles during the discharge, forming a passivation layer as the so-called solid-electrolyte interphase (SEI). The SEI acts as a protection layer on the cathode surface and further mitigates the dissolution of the polysulfides thus enable the high reversibility of the sulfur redox reaction. This finding is consistent with the SEM observation which will be discussed later.

*Ex situ* analysis methods such as HPLC and UV-VIS spectroscopy were employed to characterize the active species in the electrolyte after cycling. The standard polysulfide samples of $Li_2S_4$ and $Li_2S_6$ with different molar concentrations were first measured by HPLC. Figure II-84 shows the HPLC chromatograms of standard $Li_2S_6$ samples with sulfur concentration of 3.0, 6.0, 12.5, and 50.0 mM. Three peaks were detected at retention times of 4.8-5.0, 5.8 and 6.1 min (major peak), corresponding to the elution of polysulfides with different chain length and size for $Li_2S_6$ reference sample. Since the major peak at 6.1 min is symmetrical and well-resolved, as is the baseline around this area, its position and integrated intensity at different concentrations were used to generate the calibration plot shown as the inset of Figure II – 19. Based on this highly linear plot, one can perform quantitative analysis of the polysulfide dissolution in the cycled baseline cell and the TTE-based electrolyte cell.

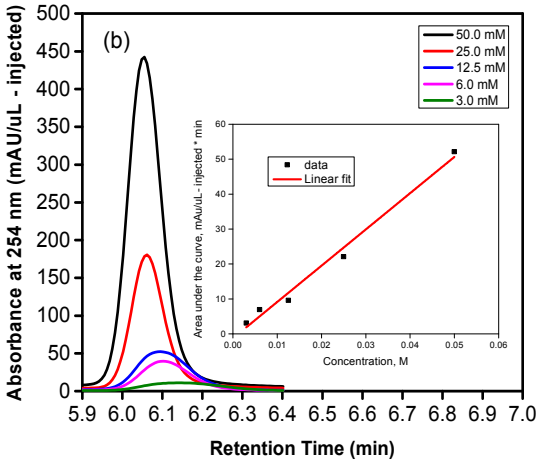


**Figure II-84: HPLC chromatograms of $Li_2S_6$ reference sample major peak at 6.1 min (inset for calibration plot). The concentration is normalized to sulfur**

The harvested baseline and fluorinated electrolyte from a Li-S cell cycled 10 times were analyzed by HPLC using the identical condition as the $Li_2S_6$ standard sample. As shown in Figure II-85, polysulfide peaks were observed for baseline and fluorinated electrolytes at 4.8, 5.2 and 6.1 min, indicating that the dissolved polysulfide species is close to $Li_2S_6$, not $Li_2S_4$. Actually, the major peak at 6.1 min is identical to that of the $Li_2S_6$ standard solution. Based on the peak intensity and integration area at 6.1 min, the concentration of the dissolved polysulfide in the cycled cells was calculated from the calibration plot. When cycled with the baseline electrolyte, the sulfur concentration is measured to be 12.5 mM, whereas it is only 8.0, 3.0 and 2.9 mM for the cells with DOL/TTE/LiTFSI electrolyte with solvent ratios of 1:1, 1:2, and 1:3, respectively. Thus, when the ratio of fluorinated solvent was increased, much lower concentration of polysulfide was generated, as well as much less diffusion of these species in the electrolyte. This finding serves as a direct evidence to understand the improved performance the Li-S cell in coulombic efficiency, sulfur utilization, and capacity retention with the fluorinated electrolyte.

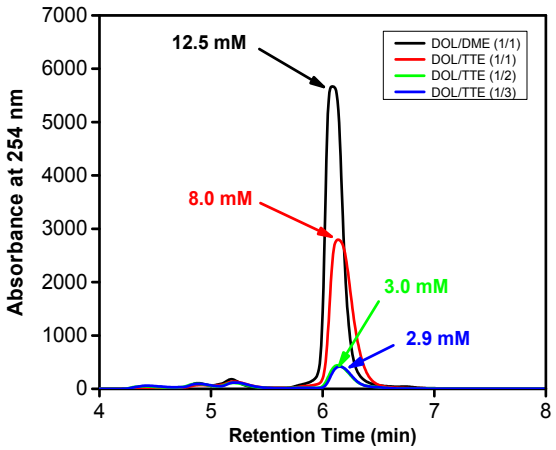


**Figure II-85: HPLC chromatograms of harvested electrolytes from Li-S cells after 10 cycles with DOL/DME (1/1)-1.0 M LiTFSI, DOL/TTE (1/1)-1.0 M LiTFSI, DOL/TTE (1/2) 1.0 M LiTFSI and DOL/TTE (1/3) 1.0 M LiTFSI**

## Sulfur cathode surface characterization

To further understand the effect of fluorinated solvents on the Li-S battery performance, we performed XPS analysis of the surface of cathodes retrieved from cycled cells. Figure II-86(a) shows the S2p binding energy of pristine and cycled sulfur electrodes in DOL/DME electrolyte. The S2p peaks at 164.4 eV and 165.7 eV are characteristic of S-S bonds of elemental S8 in the pristine cathode. After the first discharge, the S-S peak disappeared, and two new peaks emerged in the lower energy area at 162.6 and 163.8 eV, confirming the conversion of elemental S to S2- through electrochemical reduction with generation of the discharge product $Li_2S$ or $Li_2S_2$, and these peaks remain unchanged even in fully charged state, indicating the loss of the active material due to this irreversible reaction. However, for the electrode cycled in DOL/TTE electrolyte, the S2p peaks at 162.6 and 163.8 eV in the first discharge completely vanished at the first charge, as shown in the top curve in Figure II-86(b). This highly reversible process explains the high specific capacity and coulombic efficiency of the DOL/TTE-containing cell, as discussed in the electrochemical performance. The lower oxidation S2p peaks exist throughout the cycling and accumulate with cycling for the DOL/DME-containing cell (Figure II-86(c)); however, the electrochemical reversibility is maintained with the depth of cycling for the DOL/TTE-containing cell. No recognizable peaks appeared until the 20th cycle, as seen from Figure II-86(d), and the intensity of these S2p peaks was still small when DOL/TTE was used as electrolyte. This observation is in good agreement with the improved specific capacity and capacity retention of the DOL/TTE-containing cell.

The C1s, Li1s and F1s XPS spectra of sulfur cathodes at different charge and discharging cycles are shown in Figure II-87. In the pristine cathode, the C1s peak at 248.8 eV was attributed to the C-C, and peaks at 286.4 eV and 291.0 eV (Figure II-87(a) and (b)) were assigned to C-H and C-F bonds from the PVDF binder in the electrode. At the first discharge, the C1s peaks were covered by new species (C=O at 290.2 eV and CF2 at 293.4 eV) due to the SEI formation and the deposition of the discharge products on the electrode surface. Interestingly, for the DOL/TTE-containing cell, the binding energy of the C-F peak (CF2) has high intensity, and this peak does not disappear even at the fully charged state (Figure II-87(b)). In the Li1s spectra, the peak at 55.5 eV was assigned to the Li-S bonds from $Li_2S/Li_2S_2$ at the discharge state for the DOL/DME-containing cell (Figure II – 22(c)) and DOL/TTE-containing cell (Figure II-87(d)). However, in the charge state, this peak disappeared, and a new peak emerged at a shifted position at 56.2 eV, corresponding to the formation of the Li-F bond for the DOL/TTE-containing cell (Figure II-87(d)), whereas the peak remained unchanged in terms of position and intensity for the DOL/DME-containing cell (Figure II-87(c)). The LiF-rich SEI formed on the sulfur surface further improves the coulombic efficiency and capacity retention.

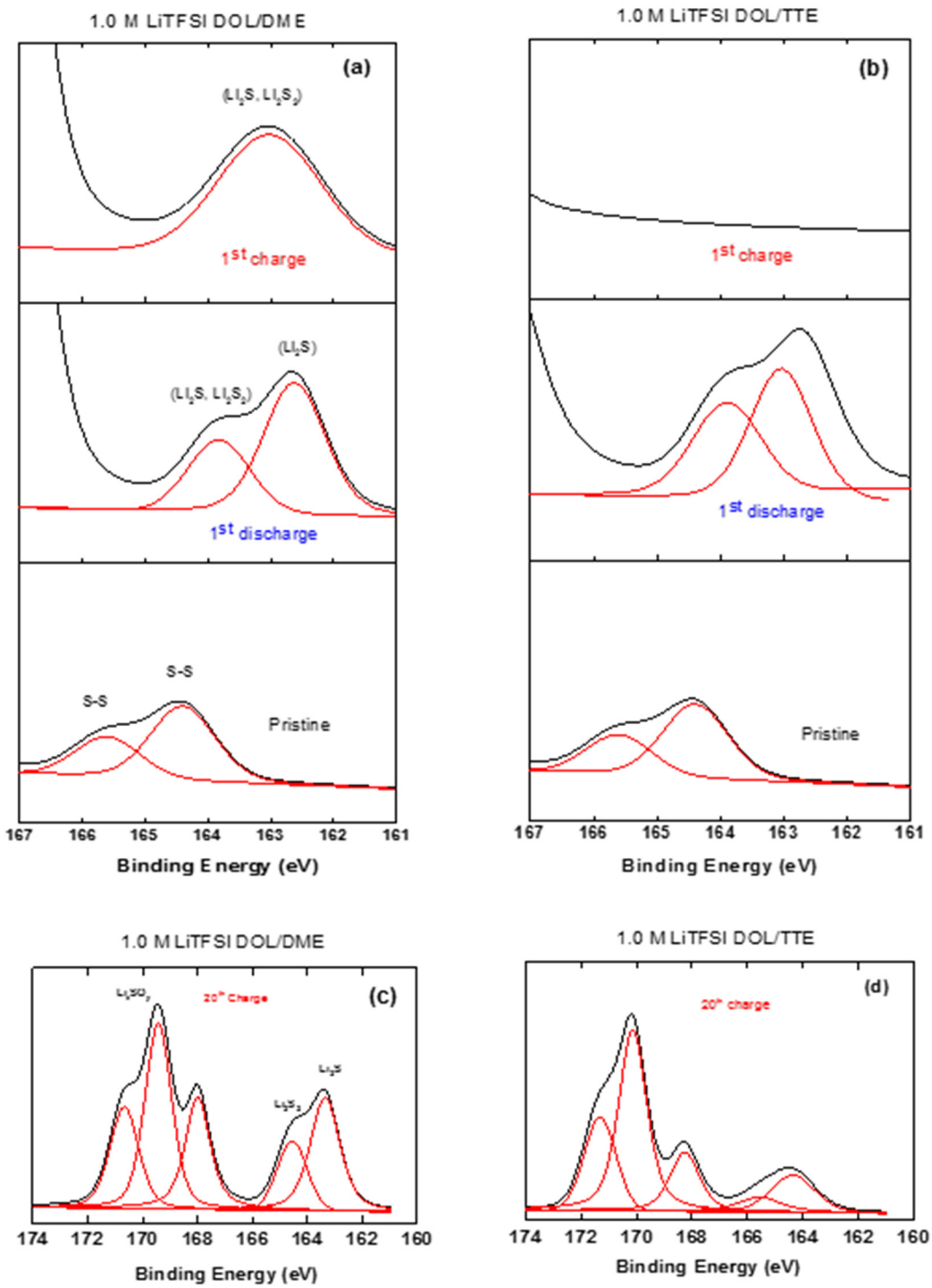


**Figure II-86: S2P XPS spectra of sulfur electrode at pristine state, the 1st discharge state and the 1st charge state with (a) 1.0 M LiTFSI DOL/DME (1/1) and (b) 1.0 M LiTFSI DOL/TTE (1/1); S2p XPS spectra of sulfur electrode at the 20th charge state with (c) 1.0 M LiTFSI DOL/DME (1/1) and (d) 1.0 M LiTFSI DOL/TTE (1/1)**

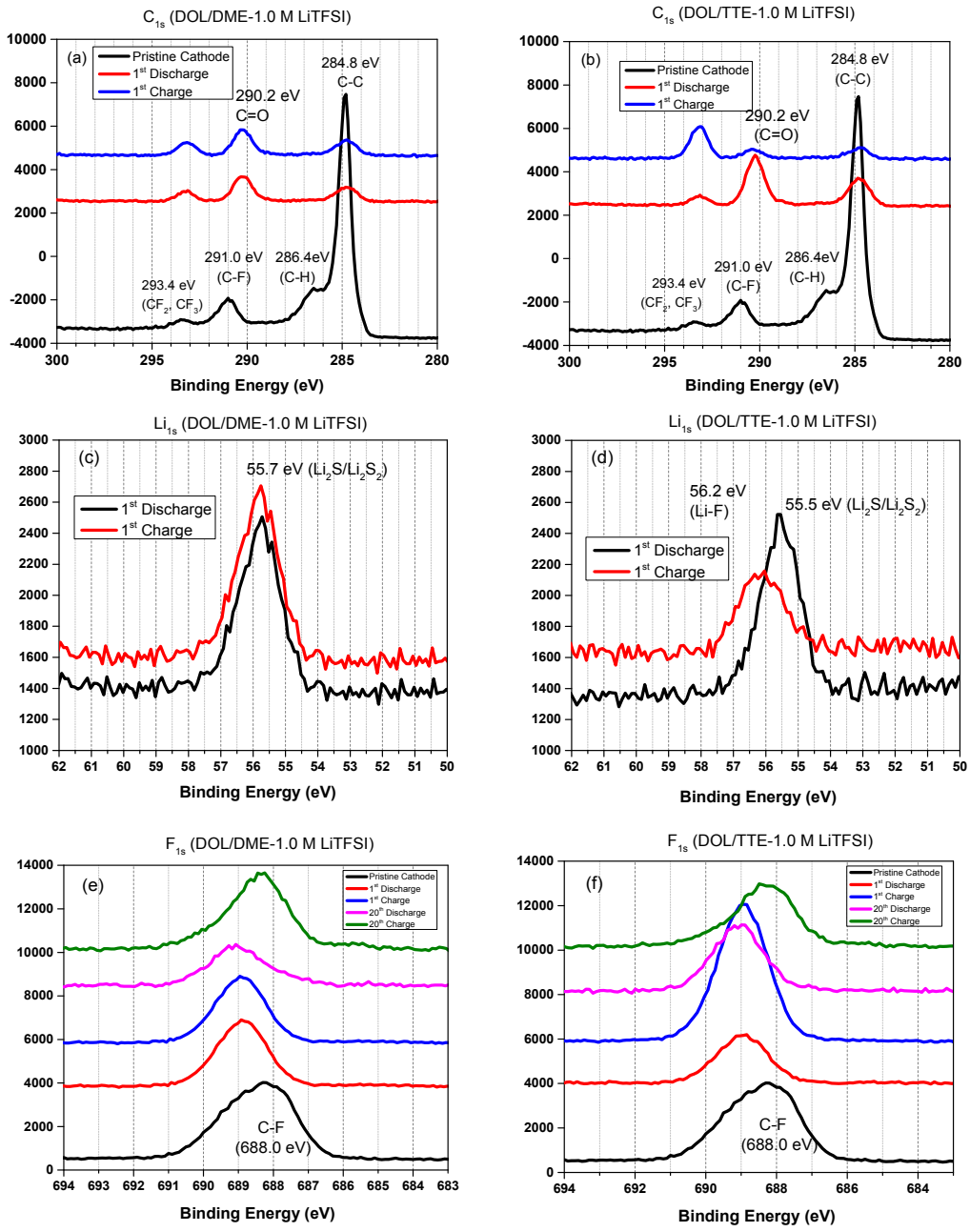


**Figure II-87: XPS spectra of sulfur cathodes at pristine state, the 1st discharge state, the 1st charge state, the 20th discharge state and the 20th charge state cycled with DOL/DME (1/1)-1.0 M LiTFSI electrolyte (a) C1s, (c) Li1s, (e) F1s and cycled with DOL/TTE (1/1)-1.0 M LiTFSI electrolyte (b) C1s, (d) Li1s, (f) F1s**

## Conclusions

Novel cathodes, anodes, and electrolytes have been investigated throughout the course of this project. During this fiscal year, nitrogen-doped graphene (NG) was experimented with as both a sulfur-confining cathode material and as a polysulfide-adsorbent coating on the separator. The thickness and mass loading of PSU-7 cathodes was optimized for use in pouch cells. Li powder (LiP) and Li foil with copper mesh anodes both demonstrated a greater than 1.5 Ah capacity. Between the two anode materials, more than 50 pouch cells were fabricated and delivered the Idaho National Laboratory (INL).

A deeper understanding of high performance Li-S battery with DOL/TTE fluorinated electrolyte was gained by using electrochemical methods and various analytical techniques such as HPLC, XPS, and SEM. The lithium polysulfide species generated in a Li-S cell with this electrolyte were quantitatively analyzed. The results

suggested that the improved performance of a Li-S cell with TTE as co-solvent is due to multiple reasons: (1) less solubility of high-order polysulfides as confirmed with solubility test and HPLC experiment mitigates the shuttle effect of polysulfide and promotes the reversible electrochemistry of insoluble $Li_2S/Li_2S_2$; (2) the SEI formation on the sulfur cathode by reductive decomposition of fluoroether further prevents the dissolution of the polysulfide and improves the sulfur utilization; and (3) the electrochemical/chemical reaction of fluoroether with lithium anode forms a protective layer acting as a physical barrier eliminating the parasitic reactions of dissolved polysulfides with lithium.

### Products

## Presentations/Publications/Patents

### Publications


1. Song, J. X., Gordin, M. L., Xu, T., Chen, S. R., Yu, Z. X., Sohn, H.S., Lu, J., Ren, Y., Duan, Y. H., Wang, D. H. Strong Lithium Polysulfide Chemisorption on Electroactive Sites of Nitrogen-Doped Carbon Enables High-Performance Lithium-Sulfur Battery Cathodes. Angewandte Chemie International Edition. (2015), 54(14), 4325. DOI: 10.1002/anie.201411109
2. Chen, S. R., Dai, F., Gordin, M. L., Yu, Z. X., Gao, Y., Song, J. X., Wang, D. H. Functional Organosulfide Electrolyte Promotes an Alternate Reaction Pathway to Achieve High Performance in Lithium–Sulfur Batteries. Angewandte Chemie International Edition, 2016, 55, 4231.
3. Sohn, H., Gordin, M. L., Regula, M., Kim, D. H., Jung, Y. S., Song, J. X., Wang, D. H. Porous Spherical Polyacrylonitrile-Carbon Nanocomposite with High Loading of Sulfur for Lithium-Sulfur Batteries. Journal of Power Sources, 2016, 302, 70.
4. N. Azimi, Z. Xue, I. Bloom, M. L. Gordin, D. Wang, T. Daniel, C. Takoudis, and Z. Zhang*. Understanding the Effect of Fluorinated Ether on the Improved Performance of Lithium-Sulfur Batteries. ACS Appl. Mater. Interfaces. (2015), 7(17), 9169-9177. DOI: 10.1021/acsami.5b01412.
5. Chenxi Zu, Nasim Azimi, Zhengcheng Zhang and Arumugam Manthiram. Insight into lithium-metal anodes in lithium-sulfur batteries with a fluorinated ether electrolyte. J. Mater. Chem. A, (2015), 3, 14864-14870.
6. Nasim Azimi, Zheng Xue, Libo Hu, Christos Takoudis, Shengshui Zhang, Zhengcheng Zhang*. Additive Effect on the Electrochemical Performance of Lithium-Sulfur Battery. Electrochim. Acta, (2015), 154, 205-210.
7. Nasim Azimi, Zheng Xue, Nancy Dietz Rago, Christos Takoudis, Mikhail Gordin, Jiangxuan Song, Donghai Wang, Zhengcheng Zhang*. Fluorinated Electrolytes for Li-S Battery: Suppressing the Self-Discharge with an Electrolyte Containing Fluoroether Solvent. J. Electrochem. Soc., (2015), 162 (1), A64-A68.


### Presentations


1. Wang, D. (Author Only), (November 2016). “DEVELOPMENT OF MATERIAL AND ELECTROLYTE FOR SULFUR BATTERIESS,” Materials Research Society Fall Meeting, Boston, USA, Invited. International.
2. Chen, S., Wang, D. (Presenter & Author), (October 2016). “High-Capacity Lithium-Sulfur Batteries at Low Electrolyte/Sulfur Ratios,” 230th Electrochemical Society (ECS) Meeting, Honolulu, USA, Accepted. National.
3. Wang, D. (Presenter & Author), (September 19, 2016). “DEVELOPMENT OF CATHODES AND ELECTROLYTE FOR HIGH PERFORMANCE LITHIUM-SULFUR BATTERIESS,” International Conference on Electrochemical Energy Science and Technology, Kunming, China, Invited. International.
4. Chen, S., Gao, Y., Wang, D. (Author Only), (August 24, 2016). “Functional Organosulfide Electrolyte for High Performance Lithium–Sulfur Batteries,” 252th ACS National Meeting Fall 2016, Philadelphia, USA, Invited. National.

5. Wang, D. (Presenter & Author), (July 2016). “Development of Functional Nanocomposite Materials for Energy Storage Applications,” 11th Sino-US Nano Forum, Nanjing University, Nanjing, China, Invited. International.
6. Song, J., Wang, D. (Author Only), (April 2016). “Advanced Sulfur Cathode Enabled by Highly Crumpled Nitrogen-doped Graphene Sheets for High-Energy-Density Lithium-Sulfur Batteries,” Materials Research Society Spring Meeting, Phoenix, USA, Accepted. International.
7. Chen, S., Dai, F., Gordin, M., Yu, Z., Gao, Y., Wang, D. (Author Only), (April 2016). “Functional Electrolyte Promotes an Alternate Reaction Pathway for High-Performance Lithium-Sulfur Batteries,” Materials Research Society Spring Meeting, Philadelphia, USA, Accepted. National.

## Patents

1. Wang, D. H., Chen, S., Dai, F. Liquid Electrolyte for Increasing Capacity and Cycling Retention of Lithium Sulfur Battery, US Utility Patent Application (14/108,094) and PCT Application (PCT/US2013/075481) 2013.
2. Wang, D. H., Song, J., Xu, T. Doped Carbon-Sulfur Nanocomposite Cathode for Lithium-Sulfur Batteries, US Utility Patent Application (13/938,527) and PCT Application (PCT/US2013/49870) 2013.

# II.C. Small Business Innovative Research (SBIR) Projects

**Brian Cunningham (SBIR Projects Manager)**
U.S. Department of Energy
Vehicle Technologies Office
1000 Independence Avenue, SW
Washington, DC 20585
Phone: 202-287-5686
E-mail: Brian.Cunningham@ee.doe.gov

## Objectives

Use the resources available through the Small Business Innovation Research (SBIR) and Small Business Technology Transfer (STTR) programs to conduct research and development of benefit to the Energy Storage effort within the Vehicle Technologies Program Office.

## Introduction and Approach

The Energy Storage effort of the Vehicle Technologies Office supports small businesses through two focused programs: Small Business Innovation Research (SBIR) and Small Business Technology Transfer (STTR). Both of these programs are established by law and administered by the Small Business Administration. Grants under these programs are funded by set aside resources from all Extramural R&D budgets; 3.0% of these budgets are allocated for SBIR programs while 0.45% for STTR grants. These programs are administered for all of DOE by the SBIR Office within the Office of Science. Grants under these programs are awarded in two phases: a 6-9 month Phase I with a maximum award of $150K and a 2 year Phase II with a maximum award of $1M. Both Phase I and Phase II awards are made through a competitive solicitation and review process.

The Energy Storage team participates in this process by writing a topic which is released as part of the general DOE solicitation. In FY12, the Energy Storage team decided to broaden its applicant pool by removing specific subtopics and allowing businesses to apply if their technology could help advance the state of the art by improving specific electric drive vehicle platform goals developed by the DOE with close collaboration with the United States Advanced Battery Consortium.

## Results

### Phase II Awards Made in FY 2016

Under the SBIR/STTR process, companies with Phase I awards that were made in FY 2015 are eligible to apply for a Phase II award in FY 2016.

Two Phase II grants were awarded in FY 2016 from four Phase I grants that were conducted in FY 2015.

**Novarials Corporation (Nashua, NH, 03062-1441):** Under this work, an ultrahigh safety battery separator technology will be developed that is a critical technology for manufacturing high safety and long term stability lithium ion batteries that are desired by electric vehicles, hybrid electric vehicles, and plug-in hybrid electric vehicles.

**SiILion, LLC (Boulder, CO, 80301-5465):** Despite the slow rate of improvement in lithium-ion technology, demand for a battery double the specific energy of current state-of-the-art (400 Wh/kg) is growing. To address this issue, this venture proposes to enable a safe, ~400 Wh/kg Si/Li-Mn-rich full-cell, compatible with the existing battery-manufacturing infrastructure, by utilizing a room temperature ionic liquid electrolyte.

## Phase I Awards Made in FY 2016

Five Phase I grants were awarded in the Summer of FY 2016.

**ADA Technologies, Inc. (Littleton, CO):** The growing demand for higher energy density and safer energy storage devices has prompted the search for next generation battery materials. ADA Technologies Inc. and partner propose to the development of a high energy and power density, safe, and cost competitive rechargeable lithium-ion battery suitable to meet various power needs.

**Coulometrics (Chattanooga, TN):** This project will develop state-of-the-art processes for the conversion of natural flake graphite into high quality lithium-ion battery (LIB) grade anode materials.

**Pneumaticoat Technologies LLC (Broomfield, CO):** This project will implement a low-cost, lean-manufacturing approach to providing safety and stability to lithium-ion battery materials using a nanotechnology-enabling coating solution. Expected outcomes are lower cost batteries, higher retained performance under extreme conditions, and a roadmap toward rapid commercialization and domestic production of next generation lithium-ion battery materials.

**Saratoga Energy Research Partners, LLC. (Berkeley, CA):** Developing a breakthrough process to manufacture low-cost, fast charging graphite – a key component of lithium-ion batteries – from carbon dioxide. This SBIR project will address the optimization of the process and demonstrate fast charging capability with different cathode materials.

**XG Sciences, Inc. (Lansing, MI):** Small, lightweight batteries storing increased energy are required for consumer products including electric vehicles, smartphones, e-bikes, and many other devices that enable the emerging mobile, connected society. XG Sciences will develop advanced silicon materials that store more energy than today's materials thereby enabling longer electric vehicle range and extended electronics runtimes.

# III. Battery Testing, Analysis, and Design

## III.A. Cost Assessments and Requirements Analysis

### III.A.1. BatPaC Model Development (ANL)

**Shabbir Ahmed, Principal Investigator**
**Kevin G. Gallagher, Paul A. Nelson, Naresh Susarla, Dennis W. Dees**
Argonne National Laboratory
9700 S. Cass Avenue
Argonne, IL 60439
Phone: 630-252-4553
E-mail: ahmeds@anl.gov

**David Howell, DOE Project Manager**
U.S. Department of Energy
Vehicle Technologies Office
1000 Independence Avenue, SW
Washington, DC 20585
Phone: 202-586-3148
E-mail: David.Howell@ee.doe.gov

Start Date: October 2012
End Date: October 2018

**Abstract**

BatPaC is a spreadsheet model that enables the design of lithium-ion battery packs for electric-drive vehicles using a range of selections and specifications (chemistry, power, energy, etc.) The model has been improved this year in terms of features such as charge time calculations and use of a blended cathode material, and fidelity though the setup of independent models to study the battery manufacturing process. These studies include the cathode manufacturing process, the cathode drying and solvent recovery process, and the formation cycling process. The results indicate that the cathode drying and recovery of the n-methyl pyrrolidone require a high energy demand because of the large amount of air that is heated in the process. The formation cycling process indicates opportunities for cost reduction through the use of fewer charge-discharge cycles and through the recovery and recycle of the discharged power.

#### Objectives

To develop and utilize efficient simulation and design tools for lithium-ion batteries to predict

- Overall and component mass and dimensions
- Cost and performance characteristics when manufactured in large volume

#### Accomplishments

- Developed an analytical expression, derived from experimental data and transport modeling, to calculate the optimum electrode loading.
- Modeled the production of NMC cathode material to estimate the energy use and cost of production.
- Modeled the cathode drying and NMP recovery process to estimate the energy use and cost contribution to the battery pack.
- Modeled operations of the Dry Room in the battery manufacturing plant to estimate the energy use and cost contribution to the battery pack.
- Conducted a preliminary assessment of the formation cycling step in the battery manufacturing plant to estimate the energy use and cost contribution to the battery pack.

- Released a new version of BatPaC with cost updates, more input options and generated results, and improved calculation methodologies.
  - Calculates the time required for charging
  - Adds the option to use a blended LMO-NMC cathode material
  - Reports the inventory of metals in the battery pack that can be potentially recovered for recycle

### Future Achievements

The features and fidelity of the BatPaC model will be improved by setting up independent models and studies of the steps in the manufacturing process, such as the formation cycle, the production of materials used in the pack, etc.

## Technical Discussion

### Background

The penetration of lithium-ion (Li-ion) batteries into the vehicle market has prompted interest in projecting and understanding the costs for this family of chemistries to electrify the automotive powertrain. Additionally, research laboratories throughout the DOE complex and various academic institutions are developing new materials for lithium-ion batteries every day. The performance of the materials within the battery directly affects the energy density and cost of the integrated battery pack.

### Introduction

A performance and cost model (namely, BatPaC) was developed at Argonne to design automotive lithium-ion batteries that can meet the vehicle specifications, and then to estimate the cost of manufacturing such a battery in large volume. It is the product of long-term research and development at Argonne through sponsorship by the U.S. Department of Energy.

Over a decade, Argonne has developed methods to design lithium-ion batteries for electric-drive vehicles based on modeling with Microsoft® Office Excel spreadsheets. These design models provided all the data needed to estimate the annual materials requirements for manufacturing the design batteries. This facilitated the next step, which was to extend the effort to include modeling of the manufacturing costs of the batteries.

The BatPaC model has been peer reviewed and is available on the web. It captures the interplay between design and cost of lithium-ion batteries for transportation applications. Moreover, BatPaC is the basis for the quantification of battery costs in U.S. EPA and NHTSA 2017-2025 Light-Duty Vehicle Technical Assessment. This assessment is then used to determine what mileage (i.e. CAFE) and $CO_2$ emission standards are optimal from a cost-benefit analysis.

### Approach

The battery pack design and cost calculated in BatPaC are based on projections of a 2020 production year and a specified level of annual battery production of 10,000-500,000. As the goal is to predict the future cost of manufacturing batteries, a mature manufacturing process is assumed. The model designs a manufacturing plant with the sole purpose of producing the battery being modeled. The assumed battery design and manufacturing facility are based on common practice today but it is also assumed that some problems have been solved to result in a more efficient production process and a more energy dense battery. Our proposed solutions do not have to be the same methods used in the future by industry. We assume the leading battery manufacturers, those having successful operations in the year 2020, will reach these ends by some means.

For a selected battery chemistry, BatPaC solves the governing equations to determine the size of each layer, cell, and modules that make up the battery pack that can meet the desired requirements for power and energy. This allows the calculation of the mass of each material, the volume of the components, and the heat removal needed during discharge. The cost of the pack is then estimated based on a predefined manufacturing process. Current effort is directed at:

- improving the design capability by considering additional relevant design constraints, e.g., coating thicknesses to reflect charge/discharge rates, etc.,
- reducing the uncertainty of model predictions by setting up independent models of the manufacturing process that include energy and cost breakdowns,
- updating the cost of the materials, and
- validating the results through discussions with manufacturers, and component developers.

## Results

**Charging Time:** The fastest rate at which a cell can be charged is constrained by the charger capacity, the maximum allowable current density (lithium deposition can occur at higher current (Gallagher, et al., 2016)), or the available cooling rate (to prevent the cell temperature from exceeding a maximum set value). Based on these three specifications, BatPaC calculates the shortest time needed to increase the state of charge (SOC) of the pack. Table III-1 compares three EV batteries with similar energy and power requirements, with respect to their charging time and cost, when the charger has a capacity of 135 kW. Battery1 with a 106-µm thick negative electrode requires 45 minutes to raise its SOC by 80% and the pack costs $10,090. Battery2 with a thinner (79 µm) negative electrode can achieve the same increase in SOC in 33 minutes, and costs $10,660. Both the batteries are limited from faster charging by the current density limit (4 mA/cm$^2$) set to avoid lithium deposition. Battery3 with a still thinner electrode (73 µm) can reduce the charging time by another 2 minutes only; faster charging is now constrained by the available cooling capacity of 6 kW.

### Table III-1: Charging Times Needed for EV Batteries with Different Electrode Thicknesses

| | Battery1 | Battery2 | Battery3 |
|---|---|---|---|
| Cathode / Anode | NMC622 / Gr | | |
| Energy storage, kWh | 79.4 | 79.4 | 79.4 |
| Capacity at C/3, Ah | 301 | 299 | 300 |
| Battery Power at 80% OCV, kW | 302 | 393 | 419 |
| Positive Electrode thickness, µm | 94 | 70 | 65 |
| Negative Electrode thickness, µm | 106 | 79 | 73 |
| Max. current density to avoid lithium deposition, mA/cm$^2$ | 4 | 4 | 4 |
| Initial battery temperature, °C | 15 | 15 | 15 |
| Max. allowed battery temperature, °C | 40 | 40 | 40 |
| Fast charge limiting condition | Li dep. | Li dep. | Temp. |
| Time to add 60% of SOC (15-75%) | 37 | 27 | 25 |
| Time to add 80% of SOC (15-95%) | 45 | 33 | 31 |
| Battery cost to OEM, $ | 10,090 | 10,660 | 10,840 |

**Production of Nickel Manganese Cobalt (NMC) Cathode Materials:** Considering the significant contribution of the cathode material to the cost of the battery pack, the production process for the NMC cathode material was studied to identify the cost drivers and challenges. The process, shown in Figure III-1 begins with the metal sulfate reacting with a carbonate $(Ni/Mn/Co)SO_4 + Na_2CO_3 = (Ni/Mn/Co)CO_3\downarrow + Na_2SO_4$ to co-precipitate the corresponding carbonates, in a continuous stirred tank reactor (CSTR). The precipitate is extracted by repeated filtration and washing. The final filter cake is then dried and mixed with lithium carbonate and fired in an oven to produce the lithiated NMC oxide ($Li_aNi_xMn_yCo_zO_2$).

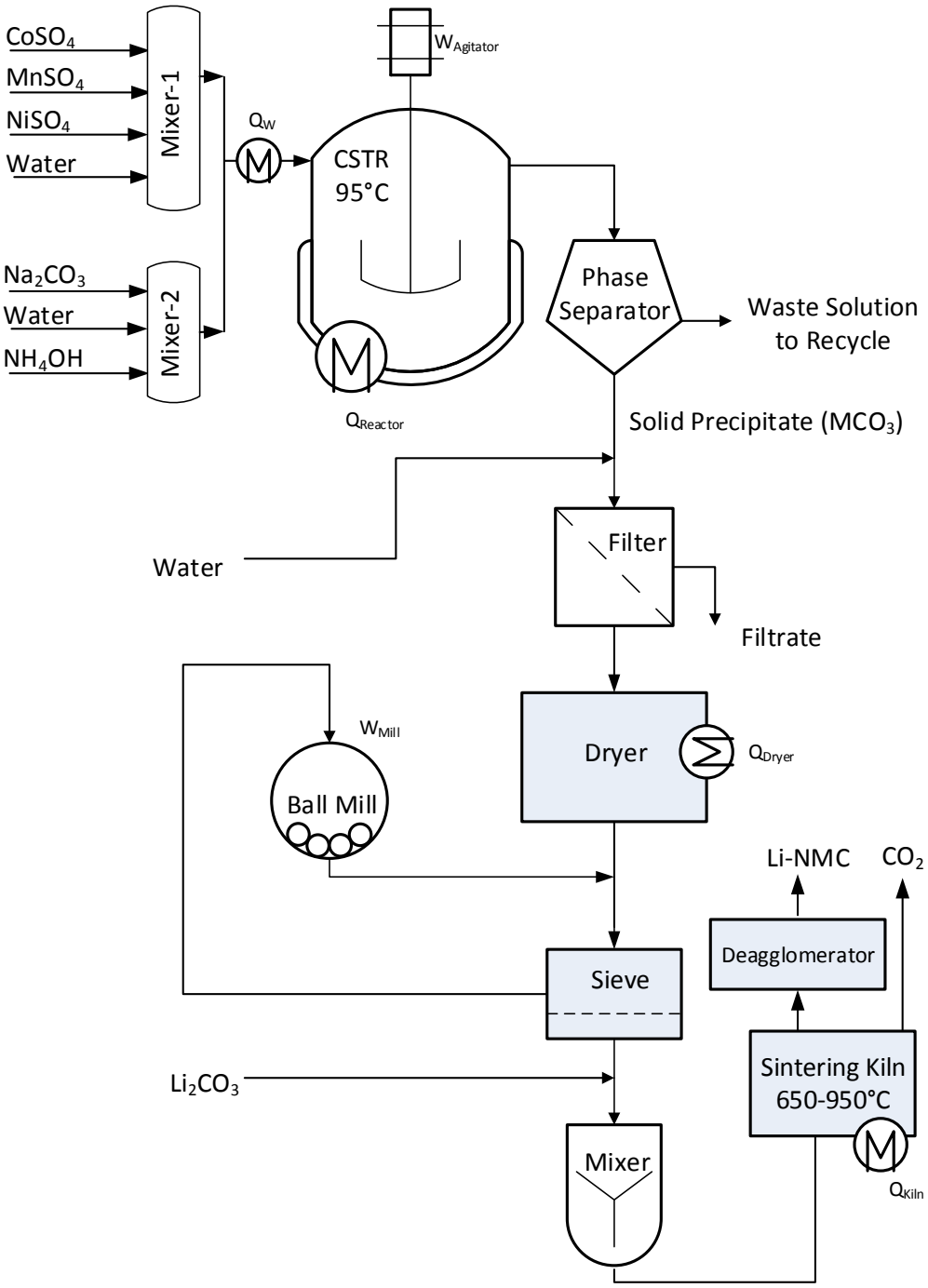


**Figure III-1: Schematic of a process for the production of NMC cathode materials using co-precipitation**

The process was simulated for a plant producing 6,500 kg/day and the results indicate that it consumes approximately 4 kWh per kg of NMC333 of energy, with more than 70% being consumed at the sintering furnace. The cost of the NMC333 production for the base case scenario was estimated to be ~$23 per kg. The raw materials represent more than 50% of the product cost. Figure III-2 shows the sensitivity of the product cost to a number of process parameters. It shows that the product cost is most sensitive to the cost of raw materials – a 20% change in the cost of raw materials affects the cost of production of the NMC333 by almost 14%.

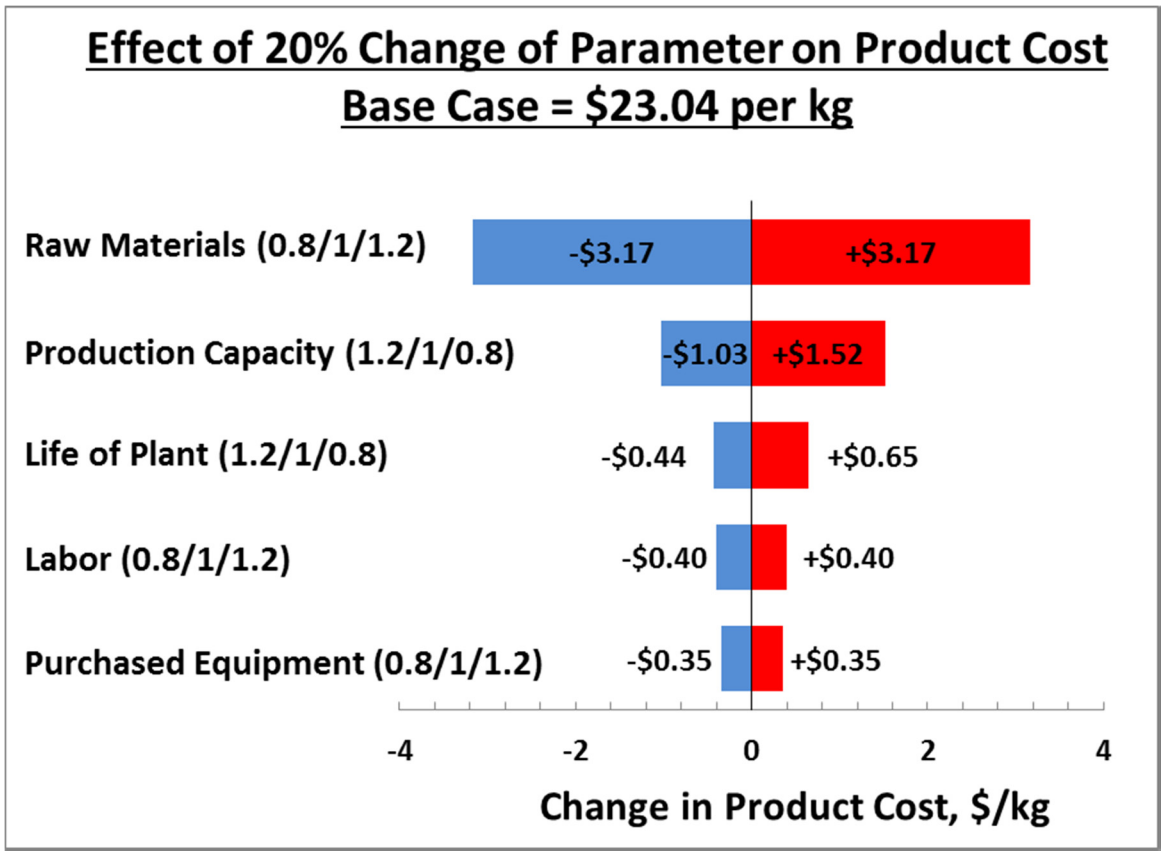


Figure III-2: Sensitivity of the cost of NMC333 (CO3 path) to 20% change in parameter values (6500 kg NMC333 per day)

Assuming the same manufacturing process, the model was exercised to compare the energy and cost of producing similar cathode materials with varying ratios of nickel, manganese, and cobalt, and are shown in Table III-2. Considering that cobalt is the most expensive metal in the material, it is found that the cost of the NMC decreases with decreasing cobalt content. The prices for the $NiSO_4$, $MnSO_4$, $CoSO_4$, $Na_2CO_3$, and $Li_2CO_3$ were assumed to be \$3.96, \$0.60, \$9.99, \$0.30, and \$7.90 per kg, respectively.

### Table III-2: The Energy and Cost of Producing NMC Cathode Materials Using the Coprecipitation Process

| Composition | Energy kWh per kg | Cost $ per kg |
|---|---|---|
| NMC333 | 3.88 | 23.04 |
| NMC622 | 3.83 | 22.14 |
| NMC532 | 3.81 | 21.41 |
| NMC811 | 3.85 | 21.47 |

**Cathode Drying and NMP Recovery:** The electrode-coated current collector is passed through the dryer to evaporate the liquid solvent (n-methyl pyrrolidone (NMP) in the cathode, water in the anode). The dryer stretches for several meters and carefully controls the temperature zones and air flow rates to ensure a drying rate that facilitates an electrode layer that is uniform, maintains the desired particle size and porosity (the porosity may be further reduced during calendaring downstream) and distribution. The NMP evaporated in the dryer is subsequently recovered and recycled, resulting in significant cost savings from the combination of avoided replacement cost and waste/emissions reduction. Figure III-3 shows the flow diagram for a NMP recovery process.

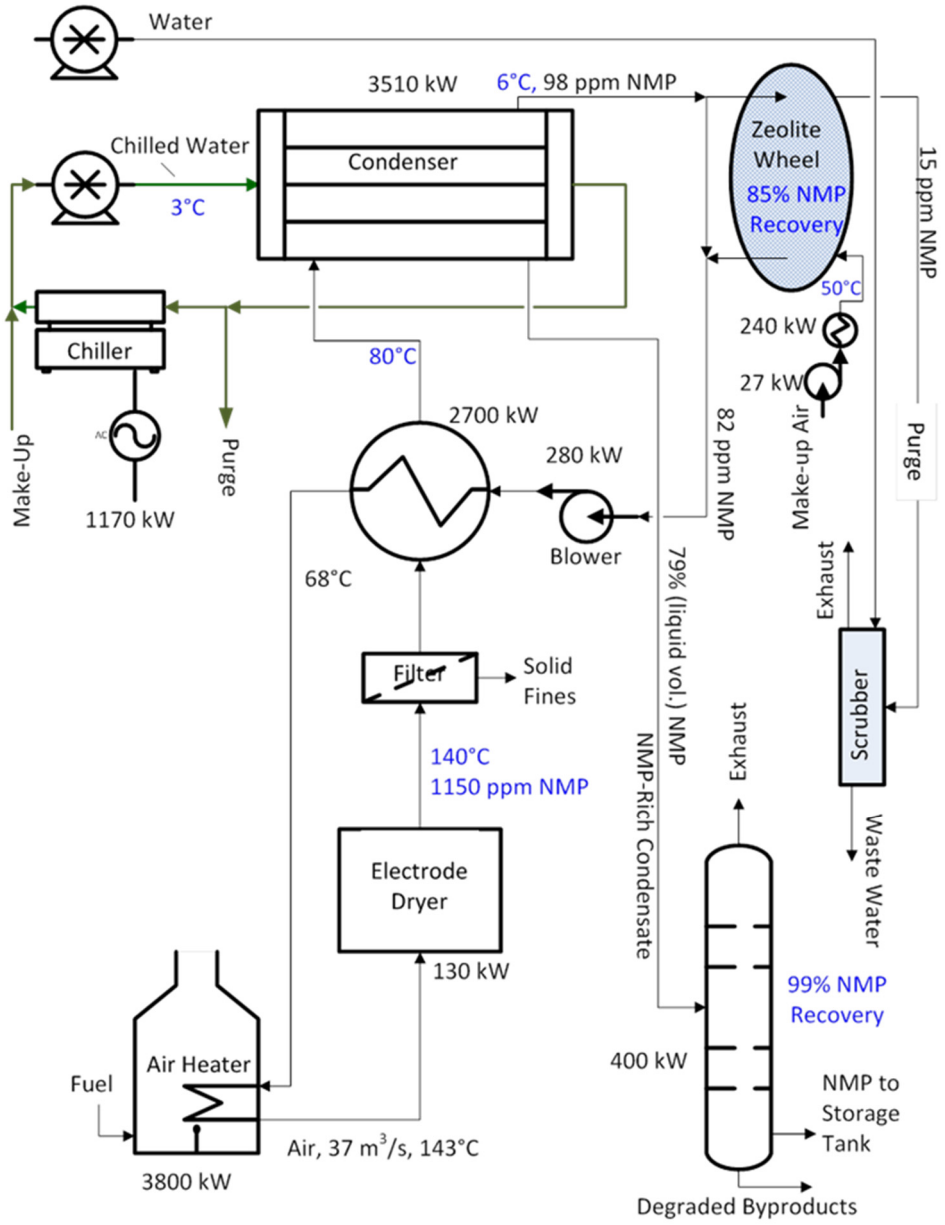


**Figure III-3: Process showing the drying and recovery of the cathode solvent NMP in a battery manufacturing plant (Base Case: 4.1x10$^6$ kg NMP evaporated per year)**

The energy demand rate for this process and set of input conditions is 1470 kW of electricity and 4381 kW of thermal energy, totaling to 5,851 kW (Ahmed, Nelson, Gallagher, & Dees, 2016). This translates to 421 kWh per battery pack and 10.2 kWh per kg of NMP. The total energy demand is nearly 45 times the energy needed to vaporize the NMP from the cathode. This high energy demand is due to the large amount of air that is passed through the dryer to ensure that the NMP concentration in the air, typically less than 1200 ppm, is sufficiently far from the NMP lower flammability limits (~1%) in air. Part of the sensible heat in the air is recovered in the air-air heat exchanger (located between the dryer and the condenser).

The cost of operations for the drying and recovery of the NMP was estimated at $2.60 per kg of NMP, clearly a significant savings from the purchase price of $3.20 per kg. The model helps to identify some of the areas where cost reductions are possible. These include the high capital cost of the distillation column and opportunities for cost reduction by enabling the use of higher concentration of NMP in the dryer (to lower the amount of air required in the dryer) without sacrificing safety, by optimizing the size of the air-air heat exchanger. Figure III-4 shows the results from a study of the tradeoff between the capital cost of the heat exchanger and the cost of energy usage. Using a larger heat exchanger enables more heat recovery, lowers the inlet temperature of the NMP-laden air entering the condenser, lowers the energy consumption for the process, and lowers the energy cost. However, the larger size of the heat exchanger increases the capital cost. The tradeoff study in the plot shows that the annualized cost of the operations for the drying and NMP recovery is lowest when the cooled air to the condenser is at 64°C (for the base case set of conditions).

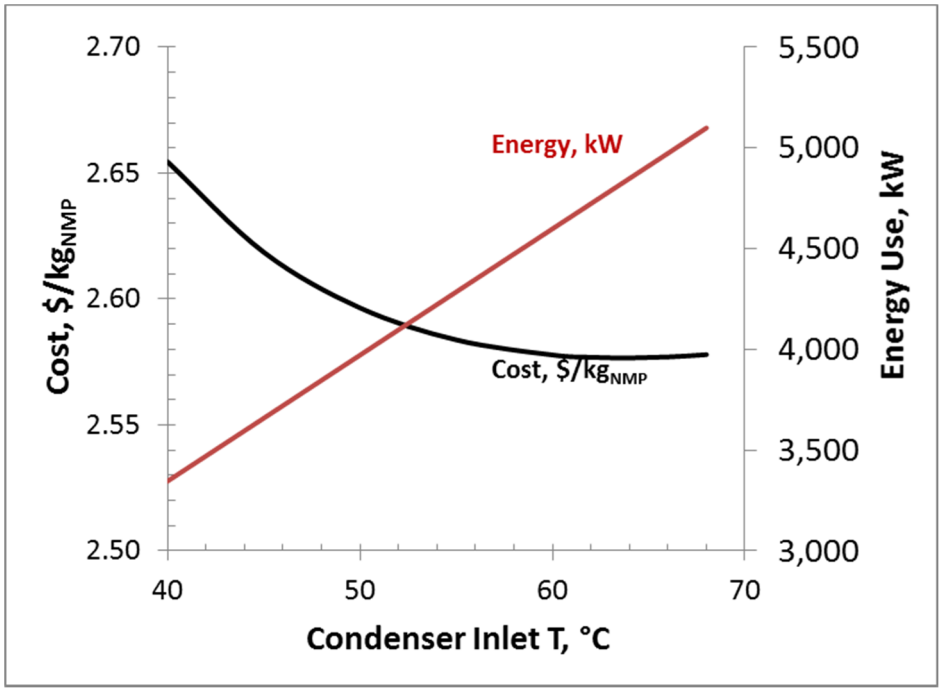


**Figure III-4: The effect of condenser inlet temperature on the cost of operations and the process energy demand (3.9M kg NMP recovered per year)**

**Dry Room Operations:** The dry room is a key part of the manufacturing process where cell assembly and electrolyte filling is carried out. The walls, floor and ceiling are designed to prevent leakage and maintain the very low humidity environment. The air quality (humidity and temperature) is maintained by flowing in an air stream that can remove the humidity and heat generated within the room or the moisture infiltration resulting from materials transfer to/from the room. The dry room contributes to the energy consumption, investment, and operations cost (Figure III-5). The dry room operations was studied with the help of a process model (Ahmed, Nelson, & Dees, Study of a dry room in a battery manufacturing plant using a process model, 2016).

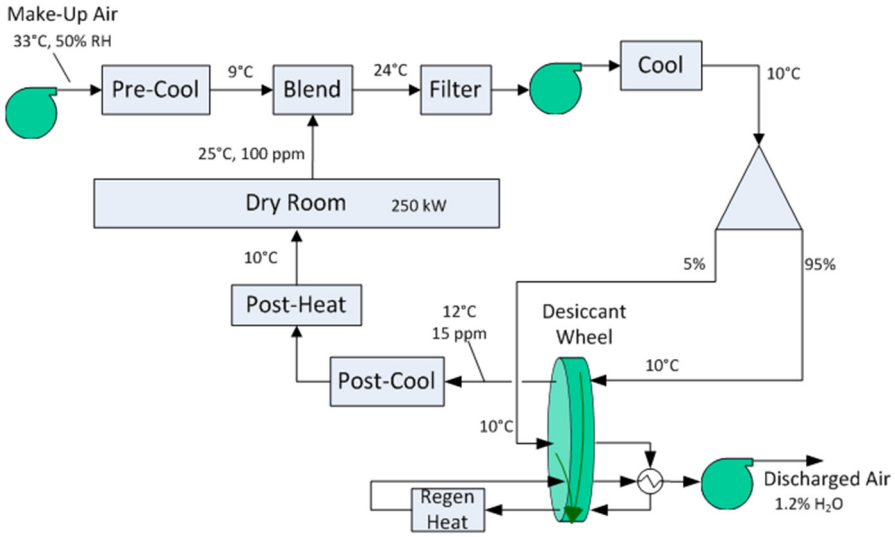


**Figure III-5: Schematic of the Air Processing for a Dry Room (16,000 m$^3$ volume)**

The study shows that for the baseline room size and process assumptions, approximately 9,600 kWh of energy is consumed per day, and contributes about $1,300 per m$^3$ of dry room space. The cost is affected by the heating and cooling, and moisture removal from the air stream; consequently the cost is sharply affected by the rate at which fresh/purge air is introduced/discharged. Increasing fresh/purge rate from 5% to 20% increases the energy demand by 62%, and cost by 10%.

**Formation Cycle:** The formation cycle process, a critical part of the cell manufacture, has a very significant impact on cell performance and durability. A simple set of charge-discharge cycles, as shown in Figure III-6 for a plant producing 100,000 packs per year of the 10 kWh PHEV (29 Ah cells) requires 3,600 MWh/year for charging. The resistive heat generated during the charge/discharge process is 240 MWh/year, and the energy released during the two discharge steps adds up to 1,900 MWh/year. Reducing the number of cycles and the rate and depth of charge/discharge will reduce the energy demand and cost considerably. Energy recovery and recycle can have a significant impact on the net power need from the grid, and depending on the price of electricity can have an impact on the cost contribution towards the cost of each battery pack. A process model is being set up to study these parameters more closely.

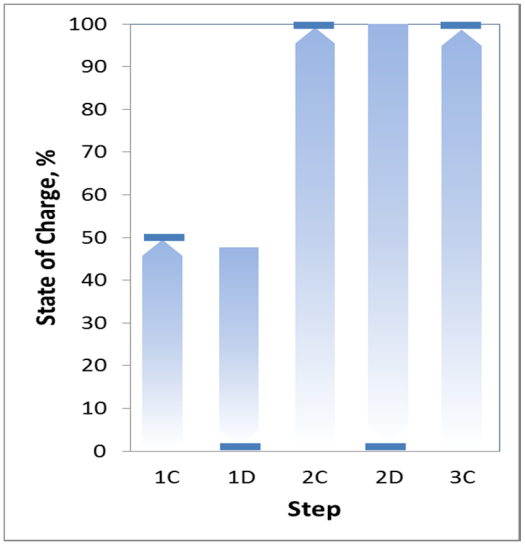


**Figure III-6: A charge-discharge cycle used to estimate the power demand during the formation cycling process (C-Charge, D-Discharge)**

## Conclusions

The BatPaC model has been improved to expand the capabilities and the fidelity of the calculations this past year. The new features and capabilities include

- inclusion of an analytical expression, derived from experimental data and transport modeling, to calculate the optimum electrode loading,
- inclusion of the option to use a blended LMO-NMC cathode material,
- revision/update of the default material prices based on modeling and communications with experts,
- estimation of the charging time required for specified constraints on charger capacity, maximum allowable current density, and the maximum allowable pack temperature,
- tabulation of the potentially recoverable materials that are used in the battery pack.

The fidelity of the model has been increased by developing independent models of the steps in the battery manufacturing process providing estimates of the energy usage and contributions toward the cost of the battery pack. These studies include the following.

- The production process of the NMC cathode materials, showing that the cost of the raw materials is a key cost factor in the price of the cathode material.
- The cathode drying and NMP recovery process model helps to quantify the savings potential from the recovery of NMP. This process appears to be the most energy intensive step in the plant.
- The dry room operations model helps to quantify the room volume, air change rate and their contribution to the cost of the battery pack.
- A preliminary assessment indicates that the energy usage during the formation cycling is significant, with opportunities for cost reduction.

### Products

A new version of BatPaC v.3.0 (http://www.cse.anl.gov/batpac/) was released in December 2015 to reflect many of the features and results mentioned above.

## Presentations/Publications/Patents

1. S. Ahmed, K.G. Gallagher, P.A. Nelson, N. Susarla, D.W. Dees, "BatPaC Model Development," presented at the 2016 DOE Vehicle Technologies Office Annual Merit Review and Peer Evaluation Meeting, Washington DC, June 6-10, 2016.
2. Gallagher, K.G., et al, "Optimizing Areal Capacities through Understanding the Limitations of Lithium-ion Electrodes," Journal of the Electrochem. Soc. 163(2) A138 (2016).
3. Ahmed, S., Nelson, P.A., Dees, D.W., "Study of a Dry Room in a Battery Manufacturing Plant using a Process Model," Journal of Power Sources 326 (2016) 490-497.
4. Ahmed, S., Nelson, P.A., Gallagher, K.G., Dees, D.W., "Energy Impact of Cathode Drying and Solvent Recovery during Lithium-ion Battery Manufacturing," Journal of Power Sources 322 (2016) 169-178.

### References


1. Ahmed, S., Nelson, P., & Dees, D. (2016). Study of a dry room in a battery manufacturing plant using a process model. *Journal of Power Sources*, 326, 490-497. doi:http://dx.doi.org/10.1016/j.jpowsour.2016.06.107.
2. Ahmed, S., Nelson, P., Gallagher, K., & Dees, D. (2016). Energy impact of cathode drying and solvent recovery during lithium-ion battery manufacturing. *Journal of Power Sources*, 322, 169-178.
3. Gallagher, K., Trask, S., Bauer, C., Woehrle, T., Lux, S., Tschech, M., Jansen, A. (2016). Optimizing Areal Capacities through Understanding the Limitations of Lithium-Ion Electrodes. *Journal of the Electrochemical Society*, 163(2), A138-A149.

# III.A.2. Battery Production and Recycling Materials Issues (ANL)

**Linda Gaines and Jennifer Dunn, Principal Investigators**
Argonne National Laboratory
9700 S Cass Avenue
Argonne, IL 60439
Phone: 630-252-4919; Fax: 630-252-3443
E-mail: lgaines@anl.gov

**David Howell**
U.S. Department of Energy
Vehicle Technologies Office
1000 Independence Avenue, SW
Washington, DC 20585
Phone: 202-586-3148
E-mail: david.howell@ee.doe.gov

Start Date: Spring 2008
End Date: Ongoing

## Abstract

### Objectives

- Examine material scarcity issues that may influence viability of automotive lithium-ion batteries.
- Characterize drivers of cradle-to-gate energy and emissions intensity of lithium-ion batteries and identify means for their reduction.
- Characterize lithium-ion battery recycling in the United States and abroad to identify the most promising recycling technologies as they evolve, barriers to recycling and influence of recycling on material scarcity.
- Engage with the international battery analysis community to exchange information, improve analysis, and formulate EV LCA results communication.
- Develop improved recycling process to maximize material recovery.
- Determine impact of battery reuse on recycling processes and economics.
- Formulate actions to address developing technical and institutional issues concerning used batteries.

### Accomplishments

- Compared critical material demand to supply out to 2050 for maximum penetration of EVs.
- Compiled information on local environmental burdens of metal production.
- Analyzed cradle-to-gate impacts of producing five new cathode materials and two new anode materials (Si, Li).
- Determined and characterized current production and recycling methods for lithium-ion batteries.
- Performed battery production and recycling lifecycle analysis to compare impacts and identify ideal recycling processes.
- Determined roles battery chemistry plays in both environmental and economic benefits of recycling.
- Identified institutional factors that can enable or hinder battery recycling.
- Presented and published analyses and recycling process comparison.
- Released update to GREET battery module, incorporating new active materials. In FY15 also updated nickel and graphite data in GREET.

- Participate in IEA HEV Task 19, SAE, and USCAR working groups.
- Convened experts' workshop on issues associated with lithium-ion battery recycling

### Future Achievements

- Integrate material and energy intensity of battery assembly in China through collaboration with Chinese universities and industry.
- Assess different criteria and frameworks for applying the lithium-ion battery module within GREET, or a derivative of it, towards an environmental certification or ranking system for automotive lithium-ion batteries in a manner similar to that of the EPEAT program that certifies PC and displays, imaging equipment, and televisions.
- Present different potential frameworks to a group of stakeholders at a workshop or through a webinar and develop the GREET-based tool for companies to use based on stakeholder feedback to carry out certification in FY18.
- Participate in IEA activities related to the assessment of environmental aspects and life cycle analysis of electrical vehicles through Task 30 of the Hybrid and Electric Vehicle Implementing Agreement, which is the extension of the previous task that Argonne supported, Task 19. Task 30 is called Assessment of Environmental Effects of Electric Vehicles.
- Refine detailed analysis of lithium-ion battery recycling processes and address economic feasibility.
- Address issues identified at stakeholders' workshop, such as process optimization, product specifications, and collection.

## Technical Discussion

### Background

The number of electric vehicles with lithium-ion batteries exceeded 400,000 in the United States in 2015 (per IEA) and with current policy support the EV population may grow significantly in the next several years. Lithium-ion batteries contain valuable cathode materials with cobalt, nickel, and lithium key among the metals they contain that, if not recovered from spent batteries, necessitates the mining of these metals and continues their depletion. Over the past several years, Argonne National Laboratory has sought to understand the energy and environmental impacts of producing lithium-ion batteries from cradle-to-gate and the potential avoidance of depleting metal stores through their recycling. The Greenhouse gases, Regulated Emissions, and Energy use in Transportation (GREET®) model contains a battery module that houses these analyses which are documented in several reports and peer-reviewed journal articles.

### Introduction

Examination of the production of batteries from raw material acquisition to assembly illuminates the stages of this supply chain that incur the greatest energy and environmental burdens. Recycling of material from spent batteries will be a key factor in alleviating potential environmental and material supply problems. We examine battery material production, battery assembly, and battery recycling processes that are available commercially now or have been proposed. Battery materials, assembly and recycling processes are compared on the basis of energy consumed and emissions, suitability for different types of feedstock, and potential advantages relating to economics and scale. We compare the potential of recycling processes to displace virgin materials at different process stages, thereby reducing energy and scarce resource use, as well as potentially harmful emissions from battery production. Although relatively few automotive batteries have been produced to date, viable processes will be required to recycle them when they are no longer usable. Secondary use of the batteries could delay return of material for recycling.

## Approach

In our initial work, we developed cradle-to-gate energy consumption and air emissions for electric vehicle batteries with and $LiMn_2O_4$ cathode. These data were incorporated into Argonne's GREET model and released in GREET1_2014. We also estimated the maximum reasonable demand for battery materials, based on extremely aggressive scenarios for the penetration of electric-drive vehicles. We combined vehicle demand growth with detailed battery designs and looked at how lithium demand might grow world-wide. We also estimated how much material could be recovered by recycling, thus reducing demand for virgin materials. We determined that cumulative world demand for lithium to 2050 would not strain known reserves. Although cobalt supplies, and possibly those of nickel as well, could become significant constraints by 2050, the envisioned move away from chemistries containing those elements would obviate potential problems.

Now, life cycle analysis (LCA) of batteries with other cathode materials based on detailed process data is being used to further identify potential environmental roadblocks to battery production, and to compare energy savings and emissions reductions enabled by different types of recycling processes. Analysis of recycling processes revealed cathode recovery as a key to process economic viability for low-Co cathodes. The cathode materials that are the focus of current work are lithium cobalt oxide ($LiCoO_2$), lithium iron phosphate ($LiFePO_4$), nickel manganese cobalt ($LiNi_{0.4}Co_{0.2}Mn_{0.4}O_2$), and an advanced cathode that has been the subject of research at Argonne, $0.5Li_2MnO{\cdot}0.5LiNi_{0.44}Co_{0.25}Mn_{0.31}O_2$ (LMR-NMC). The anode paired with each of these cathode materials is typically graphite, although we have also developed an analysis for silicon and pure lithium anodes. In FY16, we added material and energy flows for the production of nickel cobalt aluminum ($LiNi_{0.8}Co_{0.15}Al_{0.05}O_2$), an important cathode material, in GREET. Table III-3 contains the energy and GHG intensity of the different cathode and anode materials in GREET.

**Table III-3: Cradle-to-Gate Energy and GHG Intensity in the GREET Model [1,2]**

| Cathode or Anode Material | Cradle-to-Gate Energy Intensity (MJ/kg) | Cradle-to-Gate GHG Intensity (kg/kg) |
|---|---|---|
| LCO prepared hydrothermally ($LiCoO_2$) | 320 | 23 |
| LCO prepared with a solid state method | 180 | 13 |
| NCM ($LiNi_{0.4}Co_{0.2}Mn_{0.4}O_2$) | 140 | 9.9 |
| LMR-NMC ($0.5Li_2MnO_3{\cdot}0.5LiNi_{0.44}Co_{0.25}Mn_{0.31}O_2$) | 140 | 10 |
| LFP prepared hydrothermally ($LiFePO_4$) | 60 | 4.0 |
| LMO ($LiMn_2O_4$) | 40 | 3.6 |
| LFP prepared with a solid state | 40 | 2.6 |
| Silicon | 1000 | 55 |
| Lithium | 160 | 12 |
| Graphite | 90 | 5.3 |
| NCA ($LiNi_{0.8}Co_{0.15}Al_{0.05}$) | 167.8 | 11.7 |

## Results

### Battery Production

Roughly half of battery mass consists of materials (Cu, steel, plastics, Al) that have been extensively documented in previous analyses. Therefore, our focus was on the active battery materials that are not as well-characterized, and their fabrication into finished cells. Our earliest work emphasized production of the raw materials and their conversion to active materials. Our focus then shifted to component manufacture and battery assembly, which must be repeated even if recycled materials are used.

Argonne's life cycle analysis (LCA) of lithium-ion batteries is based upon a model of lithium-ion battery assembly that Nelson et al. (2011) developed. This peer-reviewed model provides an inventory of battery components and describes the equipment and steps involved in assembling these components into a battery at a manufacturing facility. Total energy for the manufacturing stage of overall battery production from cradle-to-gate is estimated to be on the order of 5-10 MJ/kg, compared to over 130 MJ/kg for the material production (all steps that precede manufacturing) for a battery with a $LiMn_2O_4$ cathode. Therefore, recycling has the potential to save a very large fraction of the total battery production energy. Energy intensity of assembly is strongly dependent upon throughput because the dry room, which is energy-intensive to operate, likely consumes a relatively even amount of energy regardless of throughput. A low throughput yields a high energy intensity. In a mature industry, we expect that a battery assembly facility would operate closer to capacity, reducing the energy intensity of battery assembly.

Based on our analysis, recycling does provide energy conservation benefits and reduces the local impacts of metal recovery and purification. Recycling is even more beneficial when cathode materials contain nickel or cobalt. Cathode materials with these metals have higher cradle-to-gate energy consumption and greenhouse gas (GHG) emissions than $LiMn_2O_4$ (30 MJ/kg $LiMn_2O_4$). The greater energy intensity of cobalt and nickel-containing cathode materials is evident when the cradle-to-gate energy consumption for different cathode materials are compared side-by-side as in Table III-3. In the case of $LiCoO_2$, the recovery and purification of the metal dominates the overall energy consumption of producing this cathode material.

### Battery Recycling

Stakeholders at the Argonne battery recycling workshop agreed on several points that require additional work. Although recycling technologies have been demonstrated, basic process R&D is needed to determine the optimal recycling method for each lithium-ion chemistry, especially lower cobalt cathode materials. For such materials, it appears that direct recycling, still only demonstrated at bench scale, offers the only real prospect of being economically feasible, but a segregated feed stream would be required. For any process, the goal is to maximize the yield of valuable materials at a lower recycling cost. Optimized processes would then require demonstration on a larger scale, but this might not be sufficient because manufacturers are skeptical about putting recycled material back into batteries. Therefore, we need to develop product specifications that recycled materials must meet. Furthermore, there is not yet enough material available to support full-scale infrastructure for collection and processing. There should be enough material from consumer electronics, but those batteries are generally not getting collected, let alone recycled. The potential for restrictive government regulations also hinders recycling business development, so the industry could consider pre-emptive self-regulation. Challenges to be faced for lithium-ion battery recycling are shown in Table III-4, with suggestions on how they can be addressed.

**Table III-4: Challenges for Lithium-Ion Battery Recycling**

| Challenge | R&D needed to address |
|---|---|
| **Long-term performance of some recycled materials is not proven** | Long-term testing |
| **There is no standard chemistry or design** | Convergence of chemistries and designs<br>Flexible processes<br>Design for recycling<br>Automation |
| **There are no regulations, so restrictive ones could be imposed** | Fashioning regulations that will protect health and safety without hindering recycling |
| **Many of the constituents have low market value** | Process development to recover multiple high-value materials |
| **Low value of mixed streams, prevention of fires and explosions** | Effective labeling and sorting |

## Engagement in the International Energy Agency Hybrid and Electric Vehicle (EV) Implementing Agreement - Task 19: Life Cycle Assessment (LCA) of Electric Vehicles

Argonne has engaged in Task 19 (Life Cycle Assessment of Electric Vehicles) since 2012. The task closed at the end of 2015 in FY16. Over those three years, the task, for which Argonne served as Vice Chair, held five workshops to bring together international experts in EV LCA for discussion around key data and methodology issues that influence EV LCA results and their communication to policy makers and other stakeholders. The first meeting was held in Braunschweig, Germany in 2012 on the topic of LCA Methodology and Case Studies. At this workshop, Argonne delivered two presentations, one on the overall treatment of EV LCA in GREET as a key note talk and one on the well-to-wheels analysis of plug-in hybrid electric vehicles as a case study for the United States. Other case studies presented included those of Belgium and Austria. Argonne hosted the second workshop in the spring of 2013 regarding material and energy flows in the production of EVs with a focus on automotive lithium-ion batteries. Talks were provided by several industry associations including those of aluminum, copper, and steel. Furthermore, the United States Geological Survey provided a presentation on the materials flow of mineral commodities. Argonne's presentation covered energy consumption and greenhouse gas emissions during automotive lithium-ion battery production. It was recognized that data for the production of key materials used in production of EVs, including those of cathode materials used in batteries, still merit development and improvement. The third workshop was held in Switzerland in October 2013 and covered the end of life of EVs and its treatment in EV LCA. The fourth workshop, on the topic of electricity production and infrastructure, was held in Spain in the fall of 2015. Experts participated from Portugal, Belgium, Germany, Austria, Spain, and the United States. At this workshop, Argonne presented the results of an analysis of current and future electricity consumption modelling for EVs in the United States. This meeting featured a discussion of several key topics including connecting additional renewable electricity and loading strategies of EVs, environmental effects of current and future electricity production, vehicle-to-grid analysis in LCA, and the modeling of electricity production for EVs. A capstone workshop for the task was held in Vienna in 2015. It was attended by 20 people from Germany, Austria, Spain, Switzerland, and the United States. Argonne's presentation at this workshop updated attendees on Argonne's analysis of lithium-ion battery production and recycling over the past three years. Other presentations covered lightweighting, critical materials in EVs, and a literature review of over 100 studies on EV LCA. As a result of this task, a visiting scholar from the German Aerospace Center (DLR) spent three months at Argonne in 2015 to collaborate on a paper to document the conclusions of this task and to assess EV LCA GHG emissions (current and future) in selected countries to show how potential benefits of EV adoption vary by location. This manuscript, under review, highlights key unknowns in EV LCA and assessment of potential benefits of deployment including fuel economy as a function of driving cycle and local conditions, likely future populations of EVs in various countries, and how the electric grid will evolve over time.

A new task under the same IEA Implementing Agreement, called Task 30: Assessment of Environmental Effects of Electric Vehicles has been started. Workshops for this task will cover EV effects on air quality, water availability and quality, and waste and land use. The first workshop on water availability and quality influences of EVs is scheduled for January 2016 in Austria. Argonne will present its analysis of water consumption of EVs.

## Conclusions

This project has evaluated the contribution of lithium-ion batteries of life-cycle electric vehicle GHG emissions and concluded that this influence is dependent on battery chemistry and, furthermore, on whether a battery assembly facility is operating at capacity, in which case the battery cradle-to-gate GHG intensity is lower than when a facility has throughput well below its capacity. Furthermore, recycling has the potential to significantly reduce both demand for raw materials and energy and environmental impacts of battery production. However, technical and economic barriers must be overcome before recycling will be available on a large scale. Through engagement with IEA tasks on EV LCA as well as through publications and presentations, Argonne has disseminated its research results in this area.

## Products

## Presentations/Publications/Patents


1. Gaines, L. “Lifecycle Analysis of Lithium-ion Batteries and End-of-Life Issues.” Battery Show 2016 (September 2016).
2. Gaines, L. “Lifecycle Analysis of Lithium-ion Batteries and End-of-Life Issues.” EPRI ENV-Vision Conference. Washington, D.C. (May 2016).
3. J.B. Dunn, Gaines, L., Gallagher, K., Kelly, J. C. “Life cycle analysis summary for automotive lithium-ion battery production and recycling.” TMS2016, February 14-18, 2016. Nashville, TN.
4. J. B. Dunn, “Life Cycle Analysis of Automotive Lithium-Ion Battery Production and Recycling.” IEA Hybrid and Electric Vehicle Implementing Agreement Task 19 Workshop Five. Vienna, Austria November 13, 2015.
5. Gaines, L. (2014), The Future Of Automotive Lithium-Ion Battery Recycling: Charting A Sustainable Course, Sustainable Materials and Technologies http://dx.doi.org/10.1016/ j.susmat.2014.10.001
6. Dunn, J.B., James C., Gaines, L., Gallager, K. “Material and Energy Flows in the Production of Cathode and Anode Materials for Lithium Ion Batteries,” Argonne National Laboratory, report no. ANL/ESD-14/10 Rev (2015).
7. Dunn, J.B., Gaines, L., Kelly, J. C., James, C., Gallagher, K.G. (2015) “The significance of Lithium-ion batteries in electric vehicle life-cycle energy and emissions and recycling’s role in its reduction.” Energy and Environmental Science, doi: 10.1039/C4EE03029J
8. “The Future of Automotive Lithium-Ion Battery Recycling: Charting a Sustainable Course,” poster for TRB 2015 Annual Meeting (January 2015).
9. Benavides, P. B., Dai, Q., Sullivan, J., Kelly, J. C., Dunn, J. B. “Material and Energy Flows Associated with Select Metals in GREET2: Molybdenum, Platinum, Zinc, Nickel, Silicon.” Argonne National Laboratory, report No. ANL/ESD-15/11 (2015).
10. “Life Cycle Analysis Summary for Automotive Lithium-Ion Battery Production and Recycling,” paper for 2016 TMS Annual Meeting (February 2016).
11. Lithium-Ion Battery Environmental Impacts, in Lithium-Ion Batteries: Advances and Applications, Elsevier (2014) (book chapter).
12. Life Cycle Assessment of Electric Vehicles – Key Issues of Task 19 of the International Energy Agency (IEA) on Hybrid and Electric Vehicles (HEV), G. Jungmeier, J.B. Dunn, A. Elgowainy, L. Gaines, S. Ehrenberger, E.D. Özdemir, H.J. Althaus, R. Widmer, Transport Research Arena 2014, Paris (paper).

## References


1. Dunn, J.B., James C., Gaines, L., Gallager, K. “Material and Energy Flows in the Production of Cathode and Anode Materials for Lithium Ion Batteries,” Argonne National Laboratory, report no. ANL/ESD-14/10 Rev (2015).
2. Benavides, P. T., Dai, Q., Kelly, J., Dunn, J. B. “Addition of nickel cobalt aluminum (NCA) cathode material to GREET2” Argonne Technical Memo. https://greet.es.anl.gov/publication-NCA-Cathode-2016.

# III.A.3. Battery Leasing & Standardization for Medium-Duty Hybrid Electric Vehicles (NREL)

**Kenneth Kelly, Principal Investigator**
National Renewable Energy Laboratory
15013 Denver West Parkway, MS 1633
Golden CO 80401
Phone: 303-275-4465
E-mail: kenneth.kelly@nrel.gov

**Brian Cunningham, DOE Program Manager**
U.S. Department of Energy
Vehicle Technologies Office
1000 Independence Avenue, SW
Washington, DC 20585
Phone: 202-287-5686
E-mail: brian.cunningham@ee.doe.gov

Start Date: October 2014
End Date: December 2015

## Abstract

### Objectives

Identify strategies that will increase the adoption rate of fuel efficient hybrid electric vehicles (HEVs) in commercial medium-duty (MD) fleets by reducing the payback period for the HEV relative to a conventional vehicle.

### Accomplishments

Key technical accomplishments from previous fiscal years (FY15) were reported in the FY15 Annual Report. **The accomplishment for FY16 include:**

- The latest (beta-version) of Argonne National Laboratory's BatPaC (Battery Performance and Cost) modeling tool was obtained and used to confirm and enhance earlier calculations involving the cost impacts of standardization strategies.
- Additional BatPaC simulations were completed to evaluate the cost impact of varying the number of cells per module as well as the cell capacity (Ah), including the number of cells per pack.
- Additional research was completed to determine the cost of battery packs to vehicle OEMs, including warranties and integration of thermal management systems (air cooling for MD HEV packs).
- A more detailed evaluation of cost components was completed for the identified standardization strategies and range of production volumes, including fixed, variable, and investment costs.
- Additional interviews were conducted with vehicle OEMs, hybrid component suppliers, and fleet managers to confirm vehicle specifications and operational costs associated with the total cost of ownership (TCO) model.
- The completed Milestone Report entitled: "Battery Ownership Model: Medium Duty HEV Battery Leasing & Standardization - - Simulate MD HEVs with standardized batteries and evaluate economics of leased and owned battery scenarios" was published December 2015.

### Future Achievements

This project was ***completed in FY16*** with the publication of the Final Milestone Report referenced above. Several potential follow-on activities were identified in the milestone report, including:

- Expand analysis beyond Class 5 delivery vehicles to Class 4-7 vehicles and additional vocations.
- Expand design space beyond HEV to also include PHEV and EV.
- Perform analysis of HEV powertrain with goal of minimizing cost while maintaining or improving performance. This may include the use of COTS components.
- Employ TCO model to investigate impact of a wider range of parameters on total cost of ownership (e.g., maintenance cost reduction, use of synthetic lubricants and fluids, battery second life application impacts on residual value).
- Identify common battery requirements across Class 4-7 PHEV, EV, HEV vehicle platforms in order to increase MD battery annual sales to greater than 10,000 batteries per year. Total Class 4-7 market segment is 150k vehicle per year annual sales, 10k HEVs per year is a reasonable 7% of this segment.
- Extend analysis to include other powertrain components for which a cost reduction might result from a broader range of applications.

## Technical Discussion

### Background

In summer of 2014, principals at Eaton discussed with DOE VTO that standardization and leasing batteries could make the fledging medium-duty (MD) HEVs more cost attractive and perhaps revive the USA market. DOE VTO provided guidance to NREL to focus its Battery Ownership subtask to investigate the economics of leasing standardized battery packs for medium duty HEVs. Over the last 15 months, we performed preliminary analysis and interacted with industry to collect necessary information for assessing the merit of leasing standardized batteries for MD HEVs. We found that economics of leasing may be better than owning batteries but depending on how much standardization could reduce the incremental cost of HEVs compared to conventional diesel vehicles. We then started to identify battery standardization strategies and how it could impact cost.

The focus of the work in this report was to further quantify the cost benefits of standardized batteries for MD HEVs. We decided to draw on the experience of Ricardo experts who have done a battery standardization study for the California Energy Commission. Interim results of the joint effort by Ricardo and NREL were shared with DOE and Eaton via web meeting on December 23, 2015. After the web meeting, an additional total cost of ownership analysis was added for the final milestone report.

### Introduction

Medium-duty HEVs used by commercial vehicle fleets are selling in limited numbers due to (i) present low fuel prices and (ii) high incremental cost of the HEV technology relative to a conventional powertrain. These two factors contribute to long payback times for the HEV technology.

Data from NREL's FleetDNA project indicate that a conventional delivery truck achieves around 7 miles per gallon (mpg) on average, while the same vehicle with an HEV powertrain achieves 8.2 mpg on average [1]. This has the following implications for an HEV with a $15,000 net incremental cost (extra cost minus government incentives) to achieve simple payback compared to a conventional vehicle:

- At $2.50/gallon diesel fuel prices, an HEV delivery truck would need to drive ≥30,000 miles/year or more to pay for itself over its 10-year lifetime.
- At $3.50/gallon diesel, the average forecast for 2018-2020 [2], the HEV delivery truck would need to
  - Drive ≥22,000 miles/year to pay for itself in 10 years, or
  - Achieve fuel efficiency ≥15 mpg and drive 22,000 miles/year or more to pay for itself in 3 years.

In these scenarios, the payback period can be cut in half if the HEV incremental cost is reduced from $15,000 to $7,500, which may be possible with future cost reductions for batteries and other HEV technologies. HEV payback period can also be strongly influenced by the business model of battery direct ownership versus battery leasing.

To shorten the payback period and increase HEV adoption rates in fleets, two focus areas for this analysis are to (i) evaluate the economics of a battery leasing business model for fleets and (ii) reduce battery costs through standardization.)

## Approach

The team leveraged multiple toolsets including NREL's FleetDNA database, FastSim vehicle simulator, and Battery Lifetime Analysis and Simulation Tool (BLAST) suite; Argonne National Laboratory's Battery Performance and Cost (BatPaC) model; and Ricardo's Total Cost of Ownership (TCO) model. Major elements of the project included:

- Assessment of MD HEV delivery truck market, interviews with industry experts, and analysis of battery requirements.
- Evaluation of economics of battery leasing versus direct ownership.
- Identification of standardization strategies that show most promise to reduce battery upfront cost and thus reduce the incremental cost of HEV technology in the MD commercial delivery truck space.

## Results

### MD HEV Market Assessment and Battery Requirements Analysis

Market analysis indicates production volumes of MD HEVs will remain relatively low through 2020. This study focuses on Class 6 trucks. The projected number of 2015 U.S. full-year new registrations of Class 6 trucks (all vocations) was 51,900 [3]. Based on several years of sales data from 2007 to 2013, HEVs represent a small portion of overall Class 6 truck annual sales—only around 900 vehicles per year [4-7]. With present market conditions, we forecast MD HEV annual production over the 2015 to 2020 timeframe will range from 1,000 to 4,400 vehicles per year [8].

The incremental cost of MD HEVs is still quite expensive due to low production/sales numbers and the need to cover non-recurring engineering (NRE) design costs. The typical incremental cost of a Class 6 HEV is around $27,000, however this is partly offset by federal, state, and local incentives totaling about $19,000 (Table III-5). Incremental cost of the technology is expected to come down in the future, but so are the incentives. Based on this, net incremental costs are forecast to range from $15,000 at present to $7,500 in the future.

To determine battery design requirements, the team performed analysis of vehicle drive cycles from the NREL FleetDNA database and selected a representative cycle for vehicle simulation. FastSim vehicle simulations were run for some 60+ hypothetical HEV designs. The simulations indicated a 45 kW battery yields optimal fuel economy for the Class 6 truck. The BLAST simulation tool showed lithium-ion battery lifetime to be a strong function of total energy, which impacts the depth of discharge experienced by the battery during the HEV drive cycles. To achieve a 10-year, 200,000-mile total lifetime requires a battery with total energy of 1.8 to 2.5 kWh.

**Table III-5: Incremental Cost of HEV Drive Systems and Incentives in the MD Market Segment**

| Application | Incremental Cost | Battery Type | Typical Incentive Funding/Voucher | References |
|---|---|---|---|---|
| Class 6 package delivery truck | $35k | Lithium-ion | $15k | 8 |
| Class 6 package delivery truck | $21k | Lithium-ion | $15k | 9 |
| Class 5 package delivery truck | $12k | Nickel metal hydride | $18k | 4,10 |
| Class 6 HEV | $12k-$40k | Lithium-ion | $15k-$30k | 4 |

### Preliminary Analysis of Battery Leasing Versus Direct Ownership

A spreadsheet model was created to perform a preliminary analysis of battery leasing versus direct ownership from both the lessee and lessor perspectives [13]. The analysis found that a battery leasing company (lessor) could achieve a 10% return on equity (ROE) with a lease price of $177/month. A 10% ROE implies that the net worth of the lease at year 10 is equal to the compounded value of the initial capital outlay at year 0. Other assumptions included a $5,100 battery cost, 1.33 markup, 10-year battery life with linear depreciation, 39.3% taxes on net revenues and $100/year/battery general and administrative costs. The lease price is sensitive to these baseline assumptions:

- Eliminating the corporate income tax reduces the lease price from $177/month to $132/month.
- Reducing the battery cost by 15% reduces the lease from $177/month to $151/month.
- Reducing the battery markup from 1.33 to 1.1 reduces the lease from $177/month to $166/month.

The analysis furthermore found that 15% ROE for the lessor is not viable, as it raises the battery lease price too high, from $177/month at 10% ROE to $260/month at 15% ROE.

For the fleet owner (lessee), monthly fuel savings of operating an HEV compared to a conventional vehicle range from $50/month at 12,000 miles/yr and $2.50/gal fuel to $175/month at 30,000 miles/yr and $3.50/gal fuel. Under the battery leasing arrangement, the lessee also no longer has to pay upfront the $5,100 x 1.33 markup cost of the battery, but still may bear other HEV incremental costs for the electric motor and inverter. As an example, avoiding the upfront battery cost generates an additional $189/month savings over the 3-year period in simple terms. (Other HEV incremental costs, heavily dependent on future HEV production volumes, NRE costs, and government incentives can reduce this savings by 10% to 100%.)

To summarize, the business model for the battery leasing company allows them to achieve a reasonable 10% ROE over 10 years. The fleet owner benefits over the initial 3 years to the tune of $40/month to $170/month. The downside is that the fleet owner does not own the battery after 3 years.

### Evaluation of Battery Standardization Strategies

Building off of recent analysis of battery standardization for commercial plug-in HEV and electric vehicle designs [12], Ricardo performed an analysis of battery standardization strategies for commercial Class 6 HEV batteries using the BatPac model from Argonne National Laboratory. Eight categories of strategies were considered:

1. Module housings, bus bar, attachments
2. Module voltages
3. Electrode dimensions
4. Communications
5. Current collectors
6. Safety systems

7. Module stack interface, heating/cooling, heat conductors
8. Interface for power transfer

Within each category, a relative cost curve was derived to estimate the impact of production volume on cost. In some categories, such as metal stampings for module housings, the cost versus production volume falls steeply due to high tooling costs. In other categories, such as printed circuit boards, the cost versus production volume falls only slightly, indicating that the cost is less sensitive to production volume due to highly automated production processes that can efficiently produce the device even at low numbers.

At low production volumes of 1,000 battery packs per year (Figure III-7), all but one of the strategies (standardized communications interface) results in a battery cost increase. At around 10,000 battery packs produced per year, five of the strategies become viable (i.e., cost of implementing strategy approximately equal to savings), the most advantageous being standardizing module housings, bus bars, and attachments. This strategy is estimated to reduce battery pack cost by 17%. At 50,000 battery packs produced per year, the standardized module housing, bus bar, and attachment strategy may reduce battery pack cost by 36%. The results are further summarized in Table III-6.

It is apparent from this analysis that significant battery pack cost reductions are not achieved until annual production volumes reach 10,000 to 50,000 battery packs per year. But the annual production rate of all commercial MD delivery trucks—hybrids and non-hybrids—is presently only around 50,000 vehicles per year. This suggests two methods to achieve cost reductions:

1. Hybridize a significant portion, >20% of commercial MD vehicles, which may require significant government incentives, or
2. Identify and use battery cells and modules that are already produced in significant volumes, >50,000 packs per year, in some other application such as light-duty HEVs.

### Table III-6: Percentage Cost Savings or Cost Increase from Each Standardization Strategy at Different Annual Battery Pack Production Volumes

| Standardization Approach | Cost savings or penalty (% of delivered cost of battery to vehicle OEM) for indicated production volumes (batteries/year) | | | | |
|---|---|---|---|---|---|
| | 1,000 | 5,000 | 10,000 | 50,000 | 100,000 |
| Module Housings, Bus Bar, Attachments | -89.80 | -0.20 | 16.84* | 35.75* | 39.34* |
| Module Voltages | -24.12 | -0.19 | 4.40* | 9.90* | 11.60* |
| Electrode Dimensions | -5.10 | -0.43 | 1.41* | 5.29* | 6.81* |
| Communications | 2.22* | 2.30* | 2.41* | 3.42* | 5.05* |
| Current Collectors | -0.26 | -0.23 | -0.20 | 0.24* | 1.17* |
| Safety Systems | -0.39 | -0.04 | 0.03* | 0.12* | 0.17* |
| Module Stack Interface, Heating/Cooling, Heat Conductors | -111.42 | -41.60 | -25.80 | -4.75 | 1.16* |
| Interface for Power Transfer | -32.46 | -17.78 | -14.89 | -10.73 | -6.10 |

* Standardization strategies that produce cost savings at the indicated production volume.

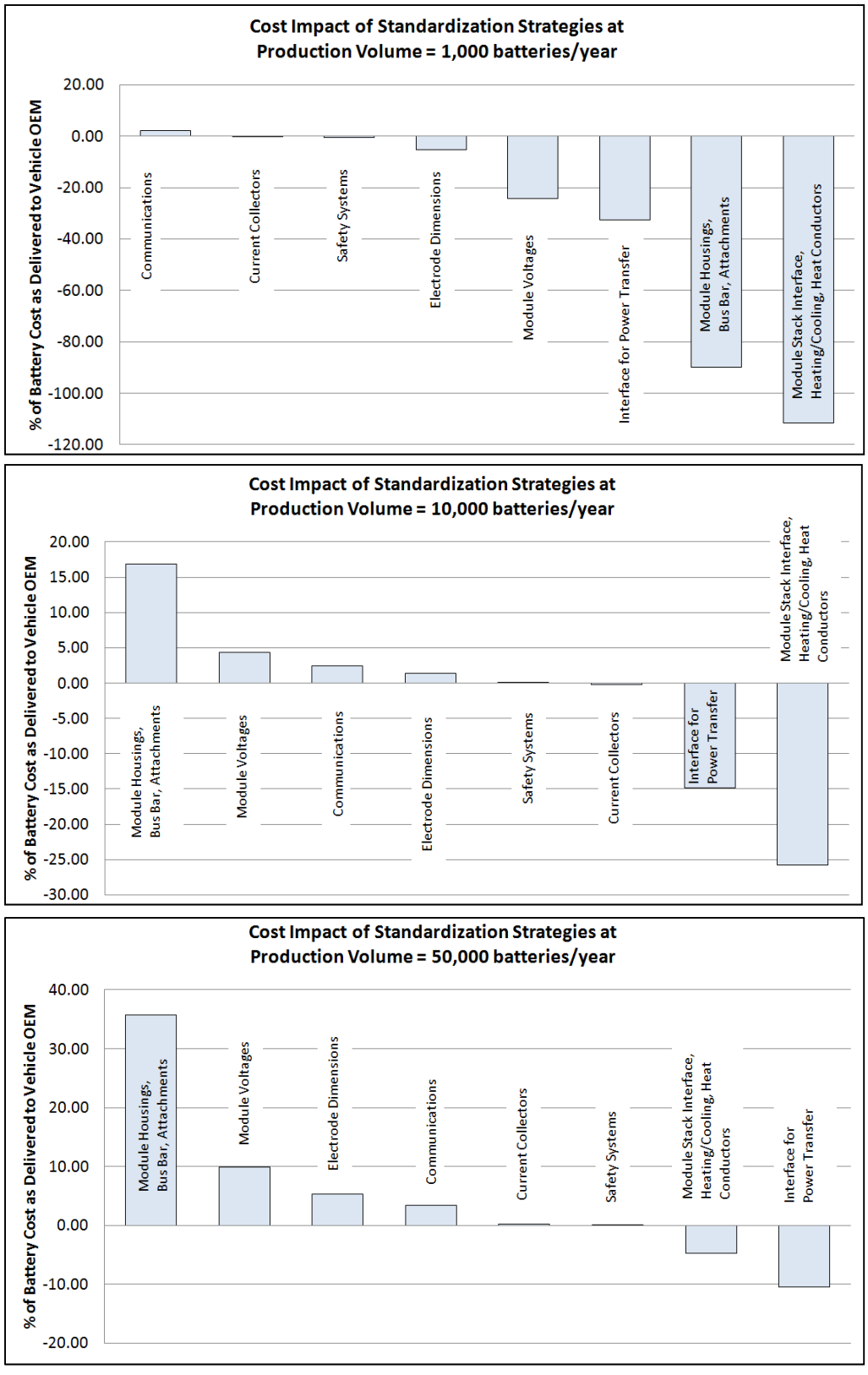


**Figure III-7: Impact of individual standardization strategies on battery cost (positive is cost reduction), NREL Milestone Report**

## Conclusions

Commercial MD Class 6 trucks are presently produced and sold at rates of around 50,000 vehicles per year. With present market conditions, HEVs are only expected to account for 2-9% of this segment. But in order for the battery costs to come down, battery packs must be produced at numbers of 10,000 to 50,000 per year or greater. Without significant government incentives to push hybridization, a possible path forward for MD vehicle original equipment manufacturers (OEMs) to bring down battery costs is to build business arrangements with light-duty vehicle OEMs to purchase battery modules similar to those used in their light-duty HEVs, which are already produced at high volumes.

Presently, commercial MD HEVs achieve about 17% greater fuel economy compared to conventional MD vehicles. With further optimization, this could be improved to 25-40%, which is similar to light-duty HEVs. This improved fuel economy, if it can be achieved with low HEV incremental cost, would shorten the payback period for MD HEVs.

A preliminary analysis of the battery leasing business model indicates that it can indeed shorten the payback period for MD HEVs. A battery leasing company could achieve a reasonable 10% return on equity. Whether the battery leasing strategy can shorten the payback period to less than 3 years greatly depends on the incremental cost of the HEV technology and government incentives.

An analysis methodology has been developed to evaluate the impact of a range of battery standardization strategies. The analysis models have been populated with vehicle duty cycles, battery requirements, and cost data, and a preliminary analysis has been conducted on a range of strategies. In the remaining 3 months of the study, the team will review results with industry to obtain feedback on the analysis, refine the analysis, and establish best paths forward. A final technical report will be published in FY 2016.

## Products

### Presentations/Publications/Patents (APR_Gray Shaded_Heading)

1. Kelly, K. Smith, J. Cosgrove, B. Prohaska, A. Pesaran, J. Paul, M. Wiseman, “Milestone Report: “Battery Ownership Model: Medium-Duty HEV Battery Leasing & Standardization - Simulate MD HEVs with standardized batteries and evaluate economics of leased and owned battery scenarios” December 2015 NREL-DOE Milestone Report, DOE-NREL AOP WBS 1.1.2.409)

## References


1. Burton, J., Walkowicz, K., Sindler, P., and Duran, A., “In-Use and Vehicle Dynamometer Evaluation and Comparison of Class 7 Hybrid Electric and Conventional Diesel Delivery Trucks,” SAE Int. J. Commer. Veh. 6(2):545-554, 2013, doi:10.4271/2013-01-2468. SAE Paper No. 2013-01.
2. Annual Energy Outlook 2014, U.S. Energy Information Administration.
3. Clinton, P., Commercial Truck Registrations, Work Truck Magazine, September 3, 2015.
4. Lyden, S., The Latest Developments in Hybrid-Electric Medium-Duty Trucks, TruckingInfo, March 2014.
5. Cornils, H., Hybrid Solutions for MD Commercial Vehicles, ERC Symposium, University of Wisconsin, June 10, 2009.
6. Busdiecker, M., Technology Potential of Commercial Vehicle Transmissions, Heavy-Duty Vehicle Efficiency Technical Workshop, San Francisco, October 22, 2013.
7. Parish, R., et. al., Demand Assessment of First-Mover Hybrid and Electric Truck Fleets, CALSTART High Efficiency Truck Forum (HTUF), October 2012.
8. K. Kelly, K. Smith, J. Cosgrove, B. Prohaska, A. Pesaran, J. Paul, M. Wiseman, “Battery Ownership Model: Medium-Duty HEV Battery Leasing & Standardization,” September 2015 NREL-DOE Milestone Report, DOE-NREL AOP WBS 1.1.2.409.
9. California Air Resources Board, Hybrid Truck & Bus Voucher Incentive Project (HVIP), Making the Case for Hybrid and Electric Trucks and Buses, https://www.californiahvip.org/making-the-case, Accessed September 12, 2015.

10. Interviews with vehicle OEMs (step vans), battery manufacturers (lithium-ion), government vehicle purchase incentive program administrators, and hybrid-electric drive system component manufacturers and suppliers, September 2-28, 2015.
11. California Air Resources Board, Hybrid Truck & Bus Voucher Incentive Project (HVIP), Hino Motors Model 195h Delivery Truck with Parallel Hybrid System, Package Delivery, California HVIP Voucher Amount, https://www.californiahvip.org/docs/HVIP_Year4_EligibleVehicles.pdf, accessed September 17, 2015.
12. Paul, J., Bogen, M, Liss, J, Holmes, J, Sohnen. 2014. The Market Impact of Standardized Design in PEV Commercial Battery Pack Purchase and Disposal. California Energy Commission (CEC). Public Interest Energy Research (PIER) Project Number CEC-PIR-12-005. CEC document number not yet assigned, expected publication date: January 2016.
13. Neubauer, A. Pesaran, "FY15 Milestone: Medium-Duty Hybrid Electric Vehicle Battery Leasing Scoping Analysis," December 2014 NREL-DOE Milestone Report, DOE-NREL AOP WBS 1.1.2.409.

# III.B. Battery Testing

## III.B.1. Battery Performance and Life Testing (ANL)

**Ira Bloom, Principal Investigator**
**John Basco, Panos Prezas, David Robertson**
Argonne National Laboratory
9700 South Cass Avenue
Argonne, IL 60439
Phone: 630-252-4516
E-mail: ira.bloom@anl.gov

**Samuel Gillard, DOE Program Manager**
U.S. Department of Energy
Vehicle Technologies Office
1000 Independence Avenue, SW
Washington, DC 20585
Phone: 202-287-5848
E-mail: samuel.gillard@ee.doe.gov

Start Date: October 2013
End Date: September 2018

**Abstract**

### Objectives

- Provide DOE, USABC, and battery developers with reliable, independent and unbiased performance and life evaluations of cells, modules and battery packs.
- Benchmark battery technologies which were not developed with DOE/USABC funding to ascertain their level of maturity.

### Accomplishments

- Tested battery deliverables from many developers. (See Table III-7.)
- Compare EV battery test protocols used in the US and in China (Argonne lead; in progress).

### Future Achievements

Testing has been shown to be a useful way to gauge the state of a developer's technology and to estimate the life of a battery.

For the future, we plan to:

- Continue testing HEV, PHEV, EV, and 12V S/S contract deliverables.
- Continue acquiring and benchmarking batteries from non-DOE sources.
- Aid in refining standardized test protocols.
- Upgrade and expand test capabilities to handle increase in deliverables.
- Complete the fast-charge experiment.
- Begin testing deliverables using recycled materials.
- Explore other possibilities for test protocol comparison and standardization with Europe, Japan and China.

**Table III-7: List of Battery Deliverables Tested**

| Developer | Application | Status |
|---|---|---|
| JohnsonControls, Inc. | PHEV20<br>PHEV20 | Complete<br>Complete |
| Optodot | EV | Complete |
| Navitas | EV<br>EV | On-going<br>complete |
| XALT | EV | On-going |
| Leyden | 12-V S/S | On-going |
| Maxwell | 12-V S/S | On-going |
| 24M | EV<br>EV<br>EV | On-going<br>On-going<br>On-going |
| ANL/J. Zhang | EV | Complete |
| SiNode | EV<br>EV | On-going<br>On-going |
| 3M | EV | Complete |
| Tiax | EV<br>EV | Complete<br>On-going |
| Wildcat | EV-like | On-going |
| LG | PHEV40 | On-going |
| Seeo | EV | Complete |

## Technical Discussion

### Background

The objective of this work is to provide reliable, independent, and unbiased evaluations of battery performance and life. The evaluations serve as progress measures for US DOE and USABC projects.

### Introduction

Batteries are evaluated using standard tests and protocols which are transparent to technology. Two protocol sets are used: one that was developed by the USABC [1-3], and another which provides a rapid screening of the technology. The discussion below focuses on results obtained using the standard protocols.

### Approach

The batteries are evaluated using standardized and unbiased protocols, allowing a direct comparison of performance within a technology and across technologies. For those tested using the USABC methods, the performance of small cells can be compared to that of larger cells and full-sized pack by means of a battery scaling factor [1, 2].

## Results

As electric vehicles become more acceptable to them, the consumers would want all aspects of owning and driving an EV to be similar to that of an internal-combustion-engine-powered automobile. This includes "refueling," that is, charging the battery. In general, most automotive traction batteries are charged in 1 to 3 h. In contrast, refueling an automobile usually takes on the order of 6 to 10 min. Additionally, the charging of the battery does not have be 100%, but can be a partial charge.

In a previous report [4], we showed the effects of fast-charging 18650-sized cells containing an NMC-based chemistry. Here, using two sets of cells, we showed the effects of the USABC fast-charge test (FC) [3] and constant-current charging (CC) using charge rates ranging from 1- to 6-C. For reference, the cycling profiles used in the work are shown in Figure III-8.

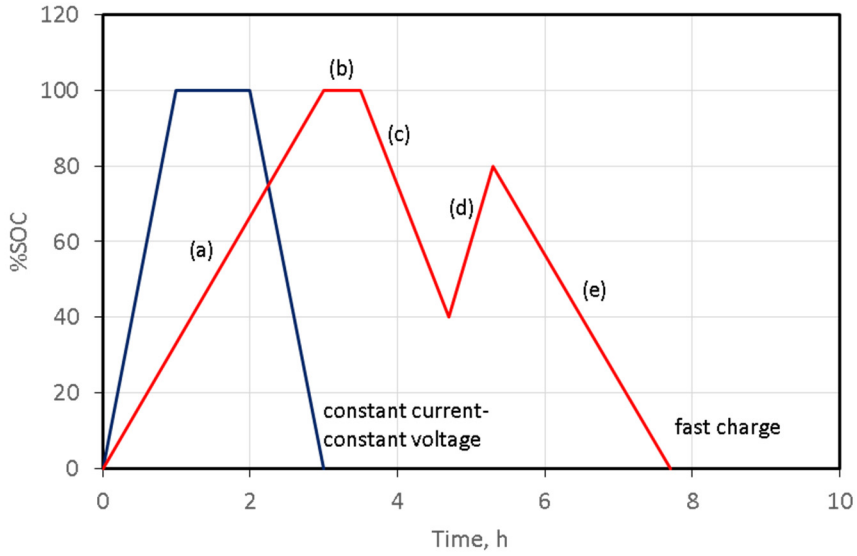


**Figure III-8: Cycling profiles used in the fast-charge tests. The segments represent (a) C/3 charge to 100% SOC; (b) 30-min rest; (c) C/3 discharge to 40% SOC; (d) fast charge to 80% SOC; and (e) C/3 discharge to 0% SOC. The fast-charge step shown in this particular profile used twice the simulated overnight rate, 2C/3**

With cycling, the resistance of the CC and FC cells, for example, increased. This is shown in Figure III-9 and Figure III-10. Examining the figures shows an apparent contradiction. In Figure III-9, the CC cells appear to display faster resistance increase than the FC cells. On the other hand, Figure III-10 shows exactly the opposite; the FC cell display the faster resistance increase. Thus, the central question is, how should the data be presented?

One way to remove the time-base ambiguity is to plot $\Delta R$ vs. $R_{N-1}$. The effect of this transform is shown in Figure III-11 and Figure III-12. Based on the slopes of the lines shown in these figures, the FC cells display faster resistance increase than the CC cells, which is consistent with post-test findings [5]. Post-test examination showed that there was damage (delamination) to the anode laminate, which increased with charge rate in the CC cells. The damage pattern to the anode in the FC did not display a pattern. There was extensive delamination at all charge rates.

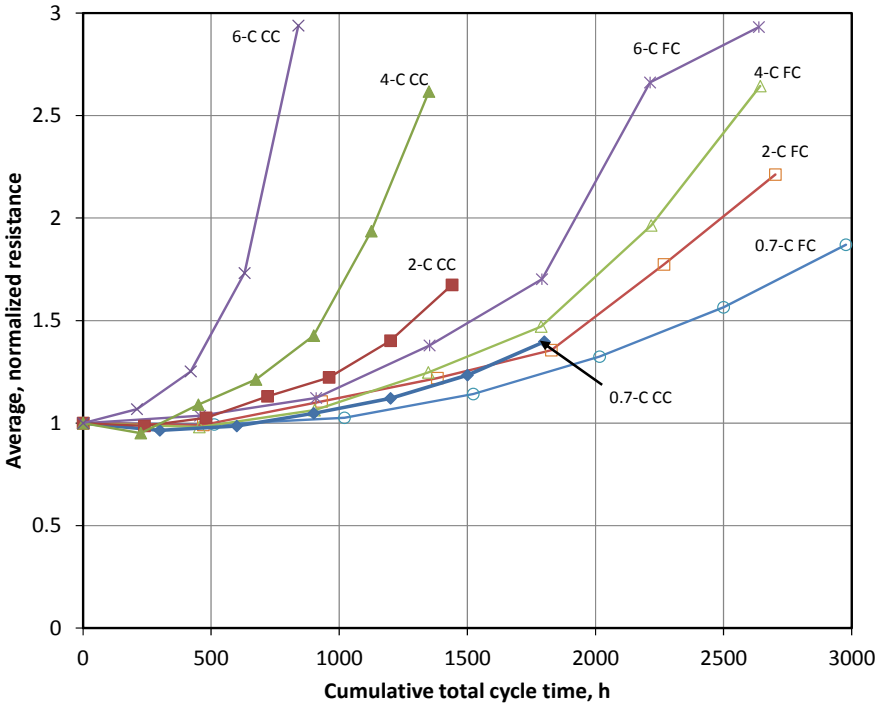


Figure III-9: Average, normalized resistance vs. cumulative total cycle time

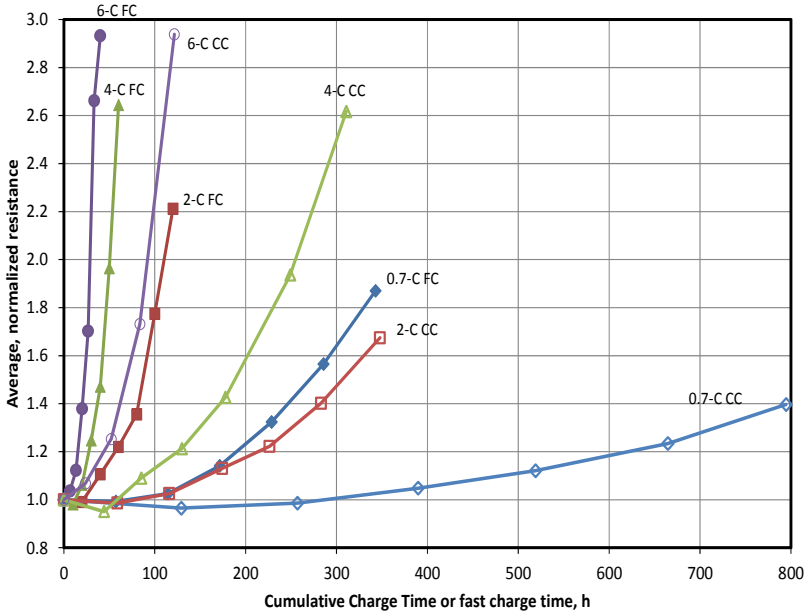


Figure III-10: Average, normalized resistance vs. cumulative charge or fast-charge time

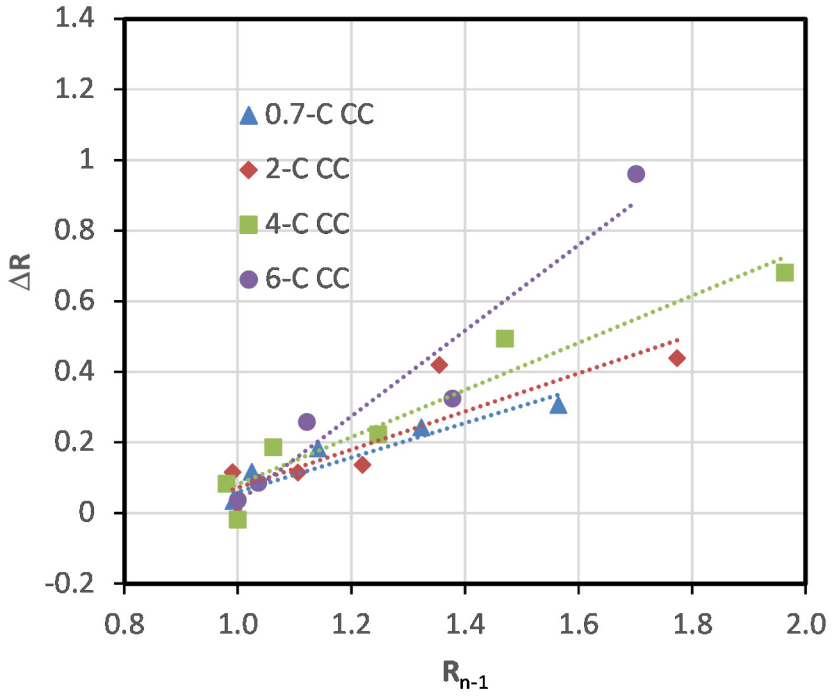


Figure III-11: ΔR vs. $R_{N-1}$ for the CC cells

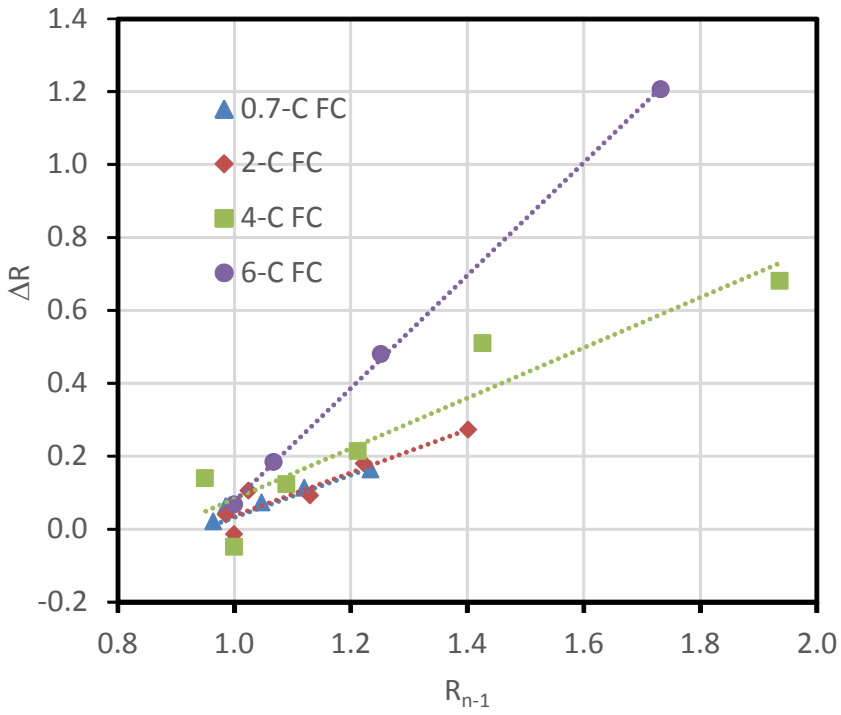


Figure III-12: ΔR vs. $R_{N-1}$ for the FC cells

## Conclusions

Charging at high rates caused performance decline in lithium-ion cells. Representing the resistance data as ΔR vs. $R_{N-1}$ plots was shown to be a viable method to remove the ambiguity inherent in the time-based analyses of the data. Comparing the ΔR vs. $R_{N-1}$ results, the change in resistance was proportional to charge rate in both the CC and FC cell data, with the FC cells displaying a greater rate of change.

## List of Abbreviations

12-V S/S: 12-V start/stop hybrid

HEV: hybrid electric vehicle

PHEV: plug-in hybrid electric vehicle

EV: electric vehicle

USABC: United States Advanced Battery Consortium (DOE, GM, Chrysler and Ford)

NMC: $Li(Ni,Mn,Co)O_2$

SOC: state of charge

ANL: Argonne National Laboratory

RPT: reference performance test

DST: dynamic stress test, see reference 3.

## Products

## Presentations/Publications/Patents

1. Presentation at the 2016 DOE Annual Merit Review, Washington, DC, June 2016.
2. "A Comparison of US and Chinese EV Battery Testing: An Interpretation," D. Robertson, I. Bloom, J. Christophersen, T, Bennett, F. Wang and S. Liu, 11th US-China EV and Battery Technology Workshop, Denver. CO, April 24-26, 2016.
3. "Performance Effect of Fast Charging Lithium-Ion Cells," Panos D. Prezas, John K. Basco, Tien Q. Duong and Ira Bloom, 18th International Meeting on Lithium Batteries, June 19-24, 2016, Chicago, IL, Poster P1-435.
4. "A Comparison of Battery Testing Protocols: Those Used by the US Advanced Battery Consortium and Those Used in China," David C. Robertson, Jon P. Christopherson, Taylor Bennett, Lee Walker, Fang Wang, Shiqiang Liu, Bin Fan, and Ira Bloom, J. Power Sources, 306 (2016) 268-273. DOI: 10.1016/j.jpowsour.2015.12.004
5. "Effect of Fast-Charging of Lithium-Ion Cells: Performance and Post-Test Results," Panos Prezas, Limhi Somerville, Paul Jennings, Andrew McGordon, John K. Basco, Tien Q. Duong, and Ira Bloom, SAE Technical Paper series, paper #2016-01-1194 (2016).
6. "Effect of Fast Charging on Lithium-Ion Batteries," I. Bloom, P. Prezas, J. K. Basco, L. Somerville and T. Duong, The Battery Show and Conference, Novi, MI, September 13-15, 2016.

## References


1. FreedomCAR Battery Test Manual for Power-Assist Hybrid Electric Vehicles, DOE/ID-11069, October 2003.
2. FreedomCAR Battery Test Manual for Plug-In Hybrid Electric Vehicles, June 2010.
3. Electric Vehicle Battery Test Procedures Manual, Revision 2, January 1996.
4. 2014 DOE Annual Report, Section IV.B.1.
5. Panos Prezas, Limhi Somerville, Paul Jennings, Andrew McGordon, John K. Basco, Tien Q. Duong, and Ira Bloom, SAE Technical Paper series, paper #2016-01-1194 (2016).

# III.B.2. Electrochemical Performance Testing (INL)

**Matthew Shirk, Principal Investigator**
Idaho National Laboratory
P.O. Box 1625
Idaho Falls, ID 83415
Phone: 208-526-7216; Fax: 208-526-3150
E-mail: matthew.shirk@inl.gov

**Samuel Gillard, DOE Program Manager**
U.S. Department of Energy
Vehicle Technologies Office
1000 Independence Avenue, SW
Washington, DC 20585
Phone: 202-287-5849
E-mail: samuel.gillard@ee.doe.gov

Start Date: September 2015
End Date: August 2018

## Abstract

### Objectives

- Provide high fidelity science-based performance and life testing, analysis, modeling, reporting, and support related to electrochemical performance.
- Develop test methods and analysis procedures for advanced vehicle electrochemical energy storage systems in conjunction with the U.S. Advanced Battery Consortium (USABC).

### Accomplishments

- Performance and life testing for
  - USABC: 232 Cells and 1 Pack
  - Benchmark: 77 Cells
  - 2011 FOA: 87 Cells
  - ARRA: 8 Cells
  - Applied Battery Research (ABR): 63 Cells
- Publications and Test Procedure Manual Development
  - Development of 'Battery Test Manual for 48 Volt Mild Hybrid Electric Vehicles' for the USABC and is publicly available on their website.
  - Published the article 'A comparison of battery testing protocols: Those used by the U.S. advanced battery consortium and those used in China' in the *Journal of Power Sources*.

### Future Achievements

- Continued testing support for USABC and Benchmark programs
  Performance and Life Testing focusing on EV, PHEV, and 12VS/S applications
- Test manual publication
  'Battery Test Manual for 48 Volt Mild Hybrid Electric Vehicles'
- Enhanced Durability, Reliability, and Safety testing procedures
  - Vibration
  - Fast Charge

## Technical Discussion

### Background

The Battery Test Center at Idaho National Laboratory has been supporting the evolution of electrified transportation through high-quality, independent testing of electrical energy storage systems for more than 30 years. Test methods and techniques are continuously improved to offer data on relevant metrics as vehicle applications progress.

### Introduction

Advancing electrified powertrain transportation, such as EV, PHEV, and HEV technologies, has the potential to increase energy security through reduction of US dependence on foreign oil. The INL Battery Test Center (BTC) is a world leader in science-based performance testing and assessment of advanced electrochemical energy storage technologies, primarily for automotive applications. The BTC at INL has been designated by DOE as a core capability and the lead test facility for supporting USABC through testing activities. The development of batteries and other energy storage devices requires validation testing from an independent source to accurately characterize the performance and life capability against the established USABC technical targets for EVs, PHEVs, 12V Start/Stop, HEV, and other emerging electric drive system applications.

### Approach

High quality testing, validation, and analysis of electrochemical energy storage systems are critical for the advancement of technologies that enable widespread deployment of electric vehicles. The INL BTC has over 20,000 square feet of laboratory space and is equipped with over 700 test channels for advanced energy storage testing at the cell-level (e.g., up to 7V, 300A), module-level (e.g., up to 65V, 250A), and pack-level (e.g., 500-1000V, 500A). The test equipment can be programmed to perform any test profile while simultaneously monitoring constraints such as voltage, current and temperature limits. Batteries and other energy storage devices are typically subjected to a test sequence while housed inside thermal chambers to ensure consistent and repeatable results. To enhance performance testing and modeling capabilities the thermal chambers operate over a broad temperature range (e.g., -70°C to 200°C).

Successful performance testing and accurate life modeling are highly dependent on the accuracy of the acquired test data. The INL BTC has developed advanced calibration verification and uncertainty analysis methodologies to ensure that voltage, current, and temperature measurements are within the tolerance specified by the test equipment manufacturer (e.g., 0.02% of the full scale). These measured test parameters are subsequently used in various mathematical combinations to determine performance capability (e.g., resistance, energy, power, etc.) INL has also quantified the error associated with these derived parameters using the accuracy and precision of the relevant measured parameter (e.g., voltage) to ensure high-quality and repeatable results and meaningful presentation.

The INL BTC capability has also been enhanced with additional equipment for advanced characterization of battery technologies. For example, a Ling Dynamic Systems V8-640 SPA56k shaker table (installed in FY13) was utilized for one USABC programs to non-destructively test reliability and cell robustness. Unconventional and untested cell designs are the key drivers behind the interest in using a vibration system to perform additional non-destructive characterization testing at INL. The shaker table is equipped with both safety shielding and thermal control chambers and is co-located with battery test equipment to allow performance testing immediately before and after the vibration testing has occurred.

### Results

The INL BTC continues to test articles of various sizes and configurations using standardized test protocols. Table III-8 and Table III-9 summarize the testing activities under the USABC and Benchmarking Programs, respectively, for FY16. The purpose of the USABC testing activities is to evaluate a candidate technology against specified targets (EV, HEV, PHEV, 12V S/S.) and, where applicable, previous generations of test articles from the same manufacturer. The purpose of the Benchmark Program is to evaluate devices that do not have existing contracts in place, but have technologies of interest to VTO. In some cases, a Benchmark Program is also used to validate newly developed test procedures and analysis methodologies.

## Table III-8: Articles Tested for USABC

| Developer | Application | Deliverable Type | Number of Articles Tested | Status at Year End |
|---|---|---|---|---|
| Amprius | EV | Cells | 20 | Complete |
| Entek | PHEV | Cells | 36 | Complete |
| Envia | EV | Cells | 14 | Complete |
| Leyden | EV | Cells | 9 | Complete |
| LG Chem | HEV | Cells | 10 | Ongoing |
| | PHEV | Pack | 1 | Complete |
| | PHEV | Cells | 10 | Complete |
| | 12V Stop/Start | Cells | 12 | Ongoing |
| | EV | Cells | 12 | Complete |
| | 12V Stop/Start | Cells | 15 | Ongoing |
| | PHEV | Cells | 23 | Ongoing |
| Nohms | PHEV | Cells | 15 | Ongoing |
| Saft | HEV | Cells | 14 | Ongoing |
| | 12V S/S | Cells | 12 | Complete |
| | 12V S/S | Cells | 15 | Complete |
| | 12V S/S | Cells | 15 | Ongoing |

## Table III-9: Articles Tested for Benchmark

| Developer | Application | Deliverable Type | Number of Articles Tested | Status at Year End |
|---|---|---|---|---|
| EIG | 12V S/S | Cells | 20 | Ongoing |
| Hydro-Québec | HEV | Cells | 13 | Complete |
| LG Chem | PHEV | Cells | 10 | Ongoing |
| ORNL | EV | Cells | 12 | Ongoing |
| Sanyo | PHEV | Cells | 16 | Complete |
| Toshiba | EV | Cells | 3 | Ongoing |

Table III-10 and Table III-11 summarize the INL testing activities associated with the 2011 FOA cell development programs and the ARRA manufacturing programs, respectively, for FY16. The 2011 Advanced Cells and Design Technology for Electric Drive Batteries FOA program focuses on developing high performance cells for electric drive vehicles that significantly exceed existing technology, in both cost and performance. Technologies addressed include those for EV, PHEV, and HEV applications; the INL focus in FY16 was on PHEV cells (87 cells with advance materials were evaluated). The ARRA program, 2009 Electric Drive Vehicle Battery and Component Manufacturing Initiative, focuses on battery and battery material manufacturing plants and equipment for advanced vehicle batteries. Final deliverables from manufacturing lines were evaluated to confirm performance in line with manufacturer claims.

**Table III-10: Articles Tested for 2011 FOA**

| Developer | Application | Deliverable Type | Number of Articles Tested | Status at Year End |
|---|---|---|---|---|
| Applied Materials | PHEV | Cells | 15 | Complete |
| | PHEV | Cells | 15 | Ongoing |
| ANL/Miltec UV | PHEV | Cells | 9 | Ongoing |
| One-D Materials | EV | Cells | 16 | Complete |
| Penn State | PHEV | Cells | 32 | Complete |

**Table III-11: Articles Tested for ARRA Projects**

| Developer | Application | Deliverable Type | Number of Articles Tested | Status at Year End |
|---|---|---|---|---|
| LG Chem | EV | Cells | 8 | Complete |

The purpose of the Applied Battery Research (ABR) program is to assess core performance, cycle life and accelerated calendar life of advanced lithium-ion cell chemistries. Table III-12 summarizes the INL ABR testing activities in FY16. Testing is underway on the baseline cell chemistries with interim deliverables scheduled to be shipped to INL in early FY16. The testing will benchmark the performance capability of the cells relative to the established PHEV-40 or EV targets. Typically, 12 cells are subjected to life testing, with 3 cells undergoing cycle-life aging at 30°C and nine cells undergoing calendar-life aging (3 each at 30, 40, and 50°C). All cells are initially characterized with constant current discharges at the C/1, C/2 and C/3 rates, an HPPC test, a 48-hr stand test, and impedance spectroscopy measurements. During life testing, the cells are periodically interrupted by RPTs at 30°C to track degradation rates compared to the targets.

**Table III-12: Articles Tested for ABR**

| Developer | Application | Deliverable Type | Number of Articles Tested | Status at Year End |
|---|---|---|---|---|
| ANL | PHEV | Cells | 12 | Ongoing |
| | EV | Cells | 12 | Ongoing |
| Envia | PHEV | Cells | 12 | Ongoing |
| | EV | | 12 | Ongoing |
| Farasis | EV | Cells | 3 | Complete |
| Penn State | EV | Cells | 12 | Ongoing |

In summary, 465 articles were on-test at INL's BTC throughout FY16. 205 of those articles completed testing during the year, while 260 were continuing life testing at the close of the year. This is summarized in Table III-13

**Table III-13: Summary of All Articles Tested in FY16**

| Status at Year End | Number of Articles |
|---|---|
| Completed | 205 |
| Ongoing | 260 |
| Total | 465 |

Utilizing recent capability enhancements for durability, reliability, and safety testing, cells with novel electrode structures were subjected to the vibration test protocol specified in UN-ECE R100. This procedure is used to evaluate the safety of rechargeable energy storage systems. Cell voltage and temperature are monitored during and after the vibration test. Commercial EV cells were subjected to the same protocol, and cycle-life aged using the USABC EV Dynamic Stress Test. To support future work, the SAE J2380 protocol, 'Vibration Testing of Electric Vehicle Batteries', referenced in previous USABC EV manuals, was also performed on commercial EV cells, followed by cycle-life aging. Data from vibration testing utilizing the UN ECE-R100 vibration test procedure are shown in Figure III-13. The vibration protocol benchmarking and evaluation work continues into FY17.

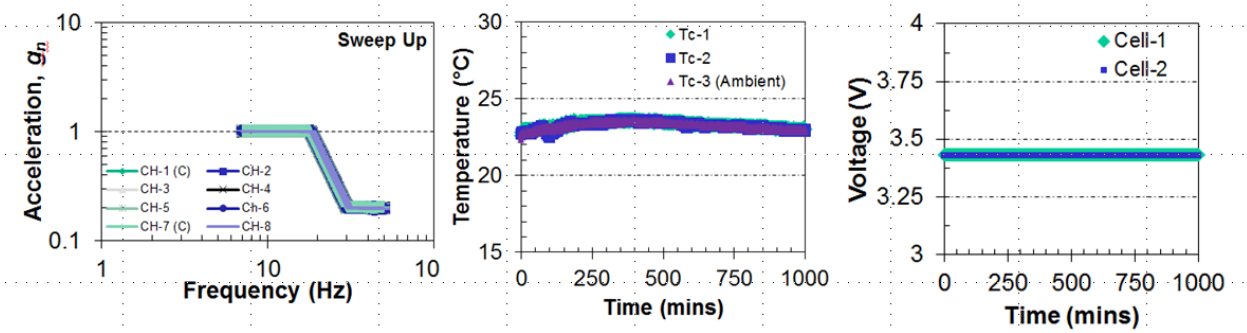


**Figure III-13: Data from vibration testing utilizing the UN ECE-R100 vibration test procedure**
*Credits: INL*

## Conclusions

Battery performance and life testing is critical to the successful adoption and implementation of advanced electric vehicles. The INL BTC is a DOE core capability well equipped to conduct accelerated aging protocols on battery technologies of various sizes and shapes while ensuring high quality, repeatable results and serve as an independent source of science-based performance assessment for DOE, the automotive industry, and battery developers. As such, testing on key programs funded through the Vehicle Technologies Office of DOE was conducted. A total of 465 devices were tested in FY16. In FY17, INL plans to continue this level of support for multiple programs with broad support for USABC, Benchmarking and the ABR programs in particular, having completed support of 2011 FOA and 2009 ARRA programs. In addition to testing and life modeling, INL will also continue developing and refining standard test protocols and analysis procedures in collaboration with USABC. In particular, the development and publication of a test manual for 48V mild hybrid EVs will be finalized and published during FY17. Additional activities to be expanded in FY17 include enhanced durability, reliability, and safety testing of key deliverables from USABC programs including the vibration assessment of new chemistries and currently being developed cell formats.

## Products

### Presentations/Publications

1. “Impacts of Fast Charging at the Cell and Vehicle Level” Eric J. Dufek, Matt Shirk, Randy Bewley and Ryan Jackman, 2016 Battery Show (Sept. 13, 2016), Novi, MI.
2. David C. Robertson, Jon P. Christophersen, Taylor Bennett, Lee K. Walker, Fang Wang, Shiqiang Liu, Bin Fan, Ira Bloom, A comparison of battery testing protocols: Those used by the U.S. advanced battery consortium and those used in China, Journal of Power Sources, Volume 306, 29 February 2016, Pages 268-273, ISSN 0378-7753.

# III.B.3. Battery Safety Testing (SNL)

**Leigh Anna M Steele, Principal Investigator**
Sandia National Laboratories
P. O. Box 5800, Mail Stop 0614
Albuquerque, NM 87185-0614
Phone: 505-844-9290; Fax: 505-844-6972
E-mail: lsteele@sandia.gov

**Samuel Gillard, DOE Program Manager**
U.S. Department of Energy
Vehicle Technologies Office
1000 Independence Avenue, SW
Washington, DC 20585
Phone: 202-287-5849
E-mail: Samuel.Gillard@ee.doe.gov

Start Date: October 2015
End Date: September 2016

## Abstract

### Objectives

- Serve as an independent abuse test laboratory for DOE and USABC.
- Abuse testing in accordance with the USABC abuse testing manual.
- Successful testing of all deliverables from developers under USABC contracts.
- Evaluate single point failure propagation in batteries.
- Short circuit current evaluation during failure propagation in battery strings.
- Provide testing data to support modeling efforts developed by NREL.
- Study thermal runaway of cells at various states of charge.
- Provide mechanical testing support to develop and validate mechanical models for EV batteries through CAEBAT program.
- Provide abuse testing support for ABR Post Test program.

### Accomplishments

- Successful testing of cell and module deliverables through USABC contracts including
  - SEEO (TAP)
  - Maxwell (12V SS)
  - LG Chem (12V SS)
  - Envia (aged cells and EV)
  - Amprius (EV)
  - NHOMS (Electrolyte)
- Stood up large scale testing capability at Sandia's burn site and successfully completed testing of USABC modules.
- Performed multi-cell pack propagation testing with alternative designs (electrical configuration and connections, failure points within pack, and air gaps).
- Developed and validated testing method to analyze short circuit current between cells during failure propagation.

- Completed thermal testing of fresh cells at various states of charge.
- Testing data produced for constrained single cell and pack level mechanical crush testing for USCAR-CSWG/CAEBAT.
- Supported post-test analysis program with batteries overcharged at various states.
- Provided separator testing using SNLs Separator Evaluation Platform (SEP) for DOE contractor Miltech to determine extent of shutdown for various ceramic coated materials.

### Future Achievements

- Abuse testing cells and batteries for upcoming USABC deliverables and new contracts.
- Propagation testing of batteries with increasing levels of designed passive and active thermal management (leverage industry partnerships) to demonstrate the effectiveness of engineering controls to mitigate propagation in batteries.
- Investigate laser induced short circuit failure mechanism.
- Work with both SNL and NREL modeling experts to develop a predictive failure propagation model.
- Dynamic mechanical testing of batteries and model validation to demonstrate battery crashworthiness (USCAR, NREL, CAEBAT).
- External analysis of battery during thermal runaway (gas analysis, heat flux, and pressure release).
- Support testing for post-test analysis of cells to determine degradation mechanisms from cell overcharging: ORNL and ANL as part of ABR.

## Technical Discussion

### Background

Safety issues associated with lithium-ion cells are independent of any other performance or cost metric and may have a negative impact on the public perception of these technologies for transportation. As a result of this issue, abuse tolerance of energy storage devices is identified as a barrier in USABC and DOE battery development programs. Sandia is tasked with the safety testing for this portfolio using our knowledge and understanding of failure modes within lithium-ion battery technology, which has been identified as a core capability for DOE. Abuse testing includes electrical, thermal, and mechanical insult which is carried out for all types of chemistries, designs, packaging and systems for PHEV/EV applications. The suite of testing is performed in Sandia's Battery Abuse Testing Lab (BATLab) for cell and module level testing and the burn site for larger module and pack level testing. The BATLab also houses battery calorimetry to aid in testing support needs.

The goals include providing independent abuse testing support for DOE and USABC according to testing manuals to gain insight into research challenges that are areas of interest to the battery community. Included in those interests are understanding how single cell or cell group failures propagate and how the primary drivers impact battery design. This has been coupled with quantifying possible short circuit currents that evolve during failure propagation scenarios. Development of predictive modeling capabilities to better understand battery failures through mechanical stresses and propagation are also being evaluated in conjunction with the other national lab partners.

### Introduction

Abuse tests are designed to determine safe operating limits for HEV\PHEV energy storage devices. The tests are performed to yield quantitative data on cell\module\pack response to allow determination of failure modes and help guide developers toward improved materials and designs. Standard abuse tests with defined start and end conditions are performed on all devices to allow comparison of different cell chemistries and designs. New tests and protocols are developed and evaluated to more closely simulate real-world failure conditions.

When scaling from cell to the battery level, a detailed understanding of cell interactions provides insight into safety performance. Single point failures from a cell or group of cells can be initiated by a number of triggers including an internal short circuit, misuse or abuse, or a component failure at the battery or system level. Propagation of that single failure event (regardless of the initiation trigger) through an entire battery, system, or vehicle is an unacceptable outcome to ensure EV battery safety. Our work focuses on evaluating the propagation of a single cell thermal runaway event through a battery using a variety of design considerations. In addition, we are working to analyze short circuits as a result of failure propagation. Testing and validation of these values is underway.

While robust mechanical models for vehicles and vehicle components exist, there is a gap for mechanical modeling of EV batteries. The challenge with developing a mechanical model for a battery is the heterogeneous nature of the materials and components (polymers, metals, metal oxides, liquids). Our work will provide some empirical data on the mechanical behavior of batteries under compressive load to understand how a battery may behave when a vehicle crash occurs. This work is performed in collaboration with the U.S. Council for Automotive Research (USCAR) and Computer Aided Engineering of Batteries (CAEBAT). This work is discussed in further detail in the annual report submitted by NREL. Additional modeling efforts lie in being able to better predict failure propagation within larger battery systems. Sandia is providing testing support to better aid in thermoelectrical model development at NREL and SNL.

Many development efforts directed toward improving safety performance are designed and evaluated using cells at full charge. However, it is important to understand how battery state of charge (SOC) affects thermal runaway profiles. Our work is directed toward understanding the effects that the SOC has on heating rates during runaway, using calorimetry techniques and quantifying the "tipping point" where SOC trades off with safety performance and a significant heating rate increase is observed, to help identify when a thermal response will be more energetic.

Materials characterization to better understand batteries that have undergone abusive conditions is of interest. Partnering with Argonne National Lab (ANL) and Oakridge National Lab (ORNL) through the Post Test Analysis Program for ABR includes building of cells with known materials (ORNL), overcharge testing to various states (SNL), and the post-test analysis of the cells (ANL).

## Approach

Abuse tolerance tests evaluate the response to expected abuse conditions. The goals of abuse and safety testing include a) test to failure of energy storage devices and documentation of conditions that caused failure, b) systematic evaluation of failure modes and abuse conditions to be achieved using destructive physical analysis (DPA), c) quantitative measurements of cell/module response, d) document improvements in abuse response, and e) new abuse test procedure that more accurately determine cell performance under most probable abuse conditions. Electrical (overcharge/overvoltage, short circuit, over discharge/voltage reversal, and partial short circuit), mechanical (controlled crush, penetration, blunt rod, drop, water immersion, mechanical shock and vibration) and thermal abuse (thermal stability, simulated fuel fire, elevated temperature storage, rapid charge/discharge, and thermal shock cycling) cover the main categories of possible conditions evaluated. These techniques are applied to USABC deliverables and the results reported to DOE and USABC.

Research and development batteries used for propagation and short circuit current evaluation are based on COTS $LiCoO_2$ 18650 and LFP 18650 (designed for energy) and 26650 (designed for power) cells. Cell failure and thermal runaway are initiated by a mechanical nail penetration into a single cell at various locations within a pack and with several architectural designs.

## Results

**Battery Abuse Testing.** In FY16, Sandia's standard abuse testing practices were collected in a manual for the USABC and will be published in a publicly available report on their website. This will be used in conjunction with the USABC abuse testing manual that underwent a review this year. The actual USABC testing results are protected information and prohibited from public release. However, representative data is shown below for a commercial-off-the-shelf (COTS) cell purchased on the open market with the corresponding gas analysis data collected during the runaway event.

Overcharging a battery beyond 100% SOC is a common abuse test performed on all cell deliverables. Typically, the cell is overcharged at a 1C rate with an end condition of 250% SOC or failure (whichever occurs first). During the test, battery temperature and voltage are monitored as well as the current being supplied to the battery. Figure III-14 shows an example of overcharge data for a COTS 10Ah Li-$CoO_2$ pouch cell that was overcharged at a 10A.

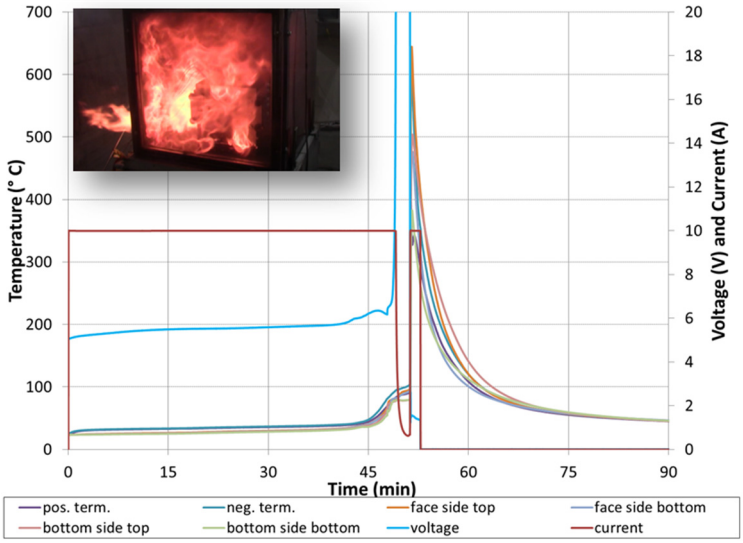


**Figure III-14: Representative cell temperatures and voltage during a 1 C overcharge test of a 10 Ah Li-$CoO_2$ pouch cell**

The cell undergoes ~90% overcharge (50 min) before thermal runaway occurs. Battery skin temperatures reach >600 °C. Ancillary capabilities during abuse testing include FTIR analysis to monitor gas products that evolve during cell vent and runaway. Figure III-15 shows representative gas data collected during the overcharge test with the main components observed being electrolyte vapor and combustion products.

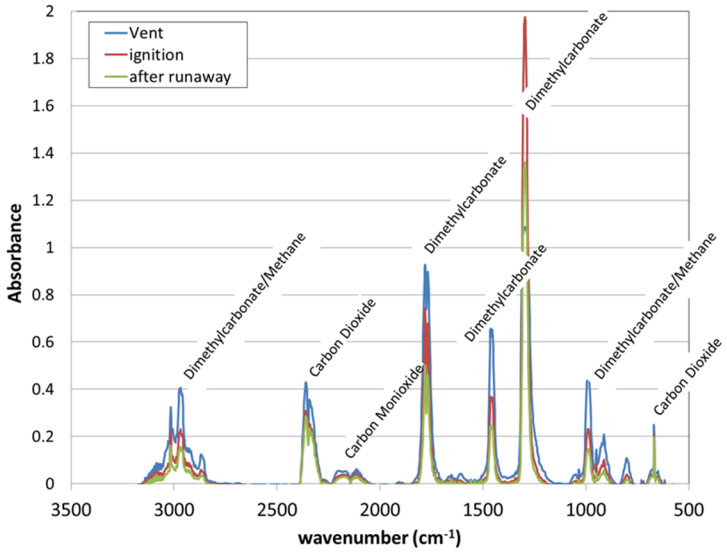


**Figure III-15: FTIR gas analysis collected real-time during overcharge testing showing DMC and combustion gasses**

**Propagation Testing with Alternative Designs**. A number of studies evaluating response of single cells to field and abusive failures have been conducted at Sandia, however less attention has been paid to how a battery system responds to the energetic failure of a constituent cell. A single cell failure may be a relatively rare occurrence, but the consequence of that failure can be significantly greater if these failures propagate through the entire battery. To study this further, we have tested a series of small batteries constructed with COTS cells to investigate how failure point, battery electrical configuration, and passive thermal management (air gap) impacts propagation.

In our experimental work, batteries consisting of 2.2 Ah $LiCoO_2$ cylindrical COTS cells were constructed in parallel (1S10P) and series (10S1P) configurations. These were stacked together in a pyramid shape to allow for the maximum battery surface area contact with one another to aid in thermal transfer. We previously investigated failures of a single cell located at the interior of the pack. Building on these results, we wanted to determine the possible difference in failure propagation with an exterior initiation point. Complete propagation through the battery was achieved in the parallel configuration within 1-6 minutes and the peak temperatures were >700°C. The series configuration resulted in a range of responses including limited propagation (cells next to failure point engaged) to complete propagation. Representative data for an exterior initiation point in a 1S10P (full propagation) and 10S1P (limited propagation) are shown in Figure III-16. These results are consistent with what was observed for the interior cell failure point suggesting electrical configuration has a larger impact on propagation than the failure point for this battery type.

The impact of battery architecture in the form of electrical connections was explored. Packs using 26650 LFP COTS cells were assembled in a 1S10P configuration using either nickel tabbing or a robust copper bus bar. Mechanical insult was performed on the central cell of the pack to initiate a failure point. The pack with the nickel tabbing showed no evidence of propagation due to the nickel being unable to carry the currents between cells during failure. However, using the same cells, complete propagation occurred in the case with the bus bar. This suggests that pack design impacts the ability for propagation to occur. Figure III-17 shows the results of both tests.

Both passive and active thermal management can be engineered into pack design to help reduce the effects of single cell failures propagating. We focused on using passive management through an air gap. A gap of 2-4mm was applied during the assembly of a 1S10P 18650 COTS pack. Spacers were added to ensure the gap remained uniform (as shown in Figure III-18).

Again, failure was initiated through mechanical insult of the central cell. At the 2 mm distance, complete propagation through the pack was achieved within 4 minutes. Increasing the distance to 4 mm eliminated propagation completely. The skin temperatures of the neighboring cells do see 100-200°C, however no cells besides the failure point exhibit thermal runaway. Representative data from both tests are shown in Figure III-19. Adding these types of thermal management could drastically reduce the impact the extent of propagation battery assemblies.

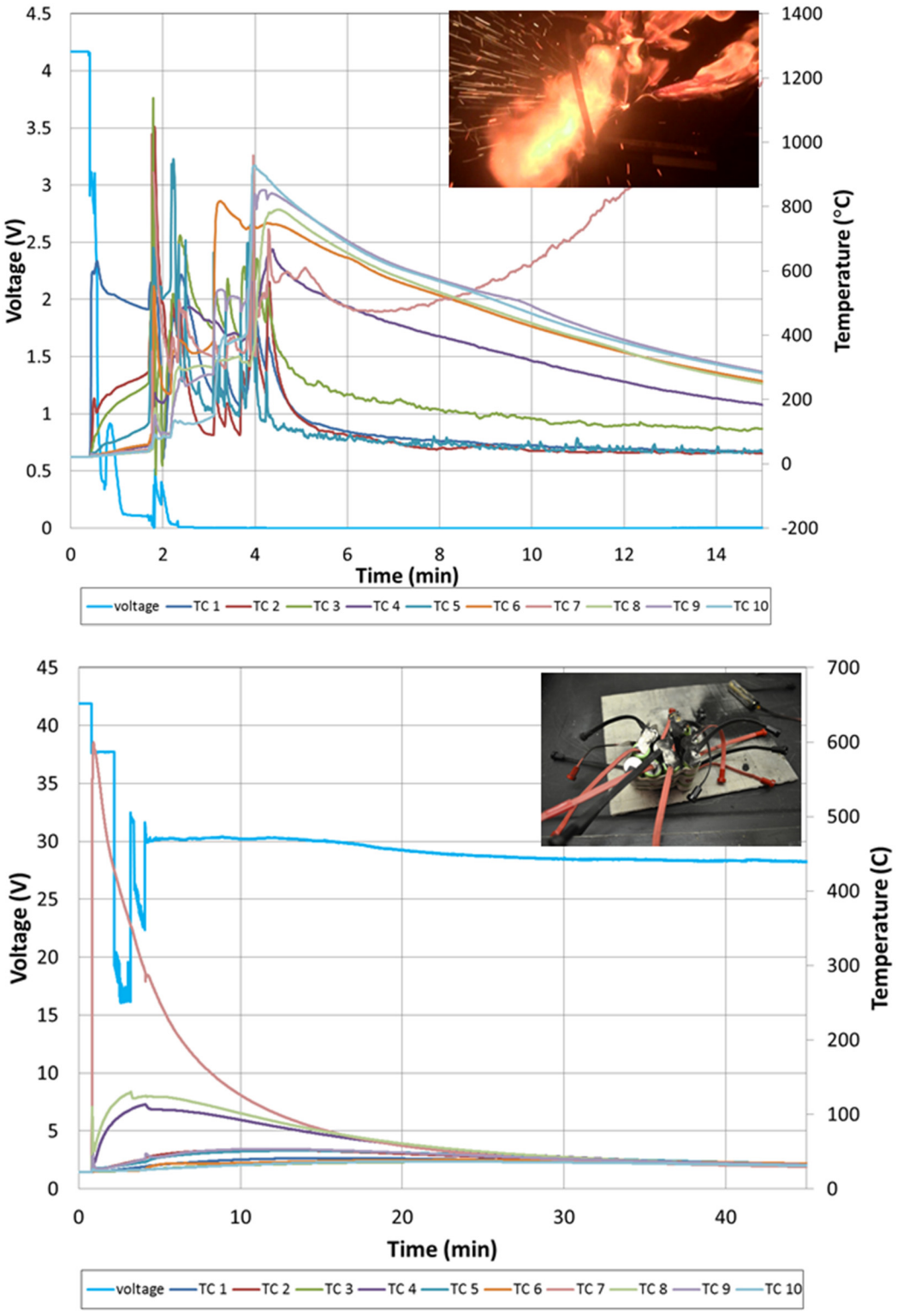


**Figure III-16: Representative data from edge cell initiation point for a failure propagation test in a 1S10P pack showing full propagation (upper) and in a 10S1P pack showing limited propagation (lower)**

A)

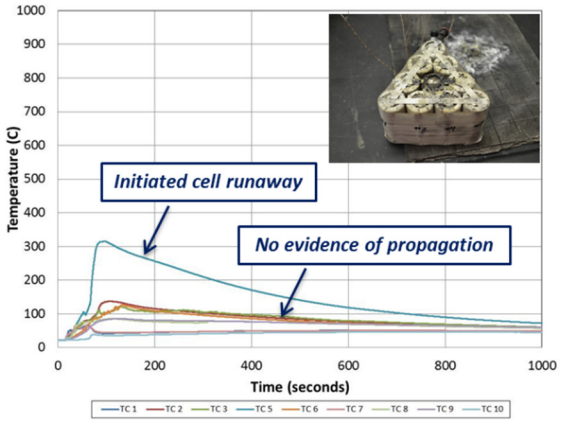


B)

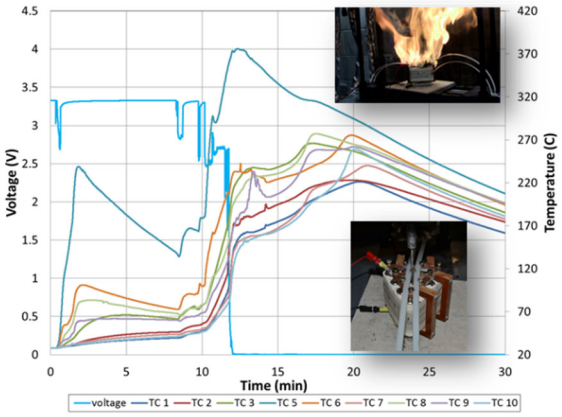


**Figure III-17: A) Cell temperatures during a propagation test of a 1S10P LFP battery connected with Ni tab, B) cell temperatures and pack voltage during a propagation test of a 1S10P LFP battery with cells connected using a copper bus bar**

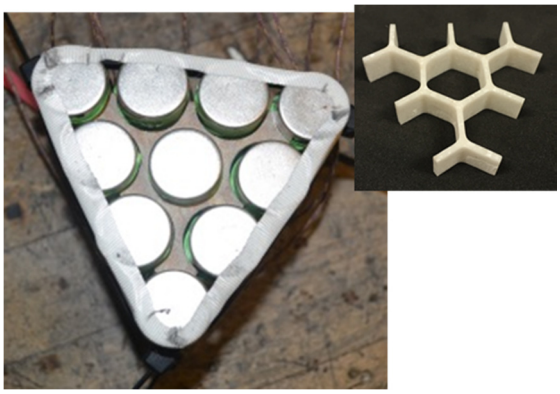

**Figure III-18: 3D printer spacers used to apply air gaps between cells for propagation testing**

A)

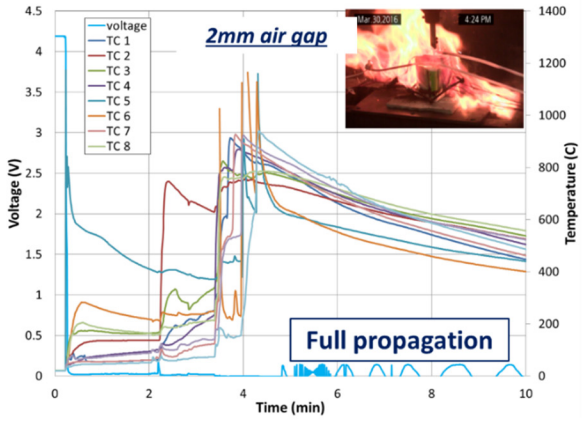


B)

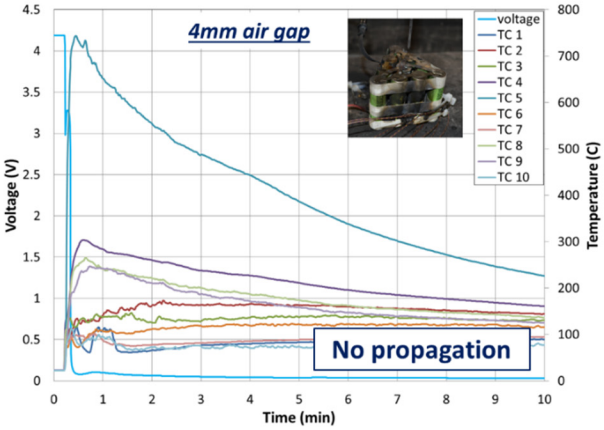


**Figure III-19: Cell temperatures and voltage during a failure propagation test of a 1S10P $LiCoO_2$ battery with A) 2 mm air gap and B) 4 mm air gap**

The results obtained from failure propagation testing are currently being incorporated into multiscale thermoelectrical simulations at NREL and SNL and we plan to work with both teams to further develop and validate this predictive capability in FY17.

**Test Development to Quantify Short Circuit Current during Failure Propagation**. As realized during previous failure propagation testing, high short circuit currents from non-abused cells discharging into the failure point exist. Sandia has developed a method to quantify these currents and validated the test setup for a variety of cells. Two cell strings using COTS 2.2Ah $LiCoO_2$ 18650, 1.5Ah LFP 18650, or 2.6Ah LFP 26650 were assembled in a 1S2P configuration in the testing apparatus shown in Figure III-20.

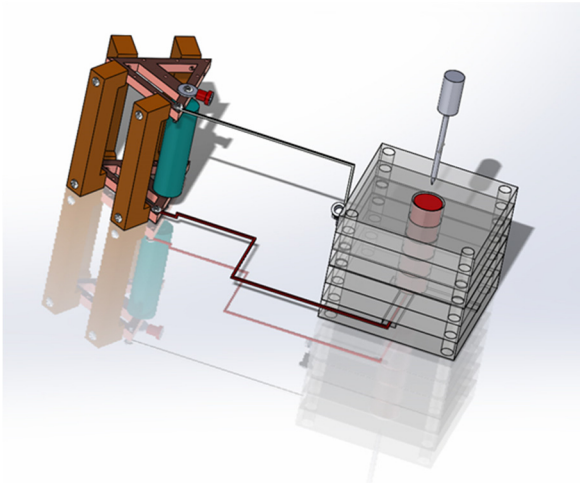

**Figure III-20: Schematic for 1S2P setup bridged by constantan wire to measure short circuit current during failure propagation**

The cells were joined using constantan wire of know resistance to allow for current measurements between cells to be obtained. Mechanical insult of cell 1 (right) was performed while cell 2 (left) remained untouched, allowing for the cell to discharge through the electrical connections of the string. Data for each cell type is shown in Figure III-21 (2.2Ah 18650), Figure III-22 (1.5Ah 18650), and Figure III-23 (2.6 Ah 26650). Upon failure of cell 1, cell 2 was allowed to discharge its capacity through the bridge to cell 1. The energy output measured during the discharge was 1.14W for $LiCoO_2$ (18650), 6.24W for LFP (18650), and 95W for LFP (26650) while peak currents across the bridge reached 37A, 30A, and 90A respectively. It is important to note that for high rate cells designed for power (LFP 26650), the short circuit power is significantly greater (1-2 order of magnitude) than that for a cell that is designed for energy (LFP 18650) or different chemistry ($LiCoO_2$ 18650).

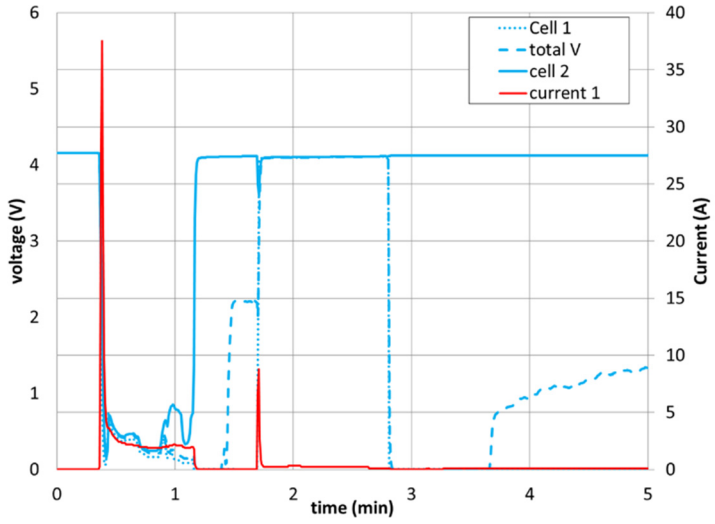


**Figure III-21: String current across bridge and voltage measured during the failure propagation test for A) $LiCoO_2$ 18650**

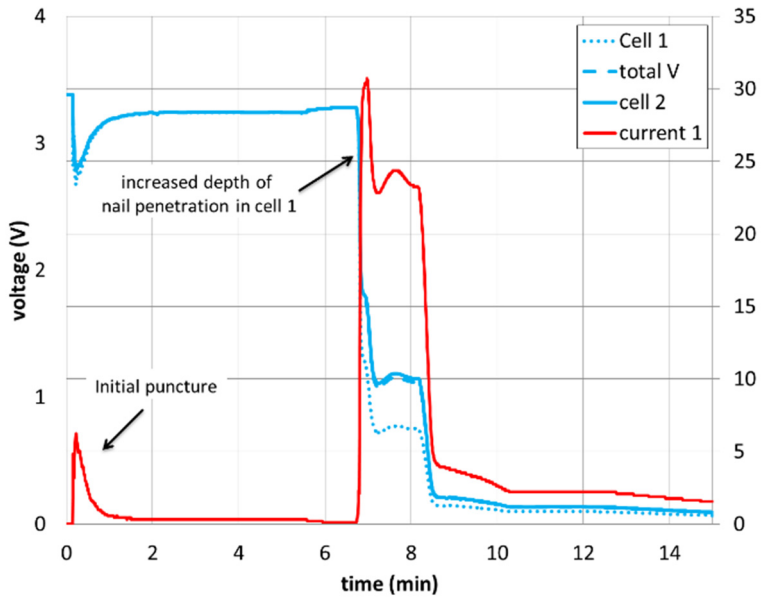


Figure III-22: String current across bridge and voltage measured during the failure propagation test for LFP 18650

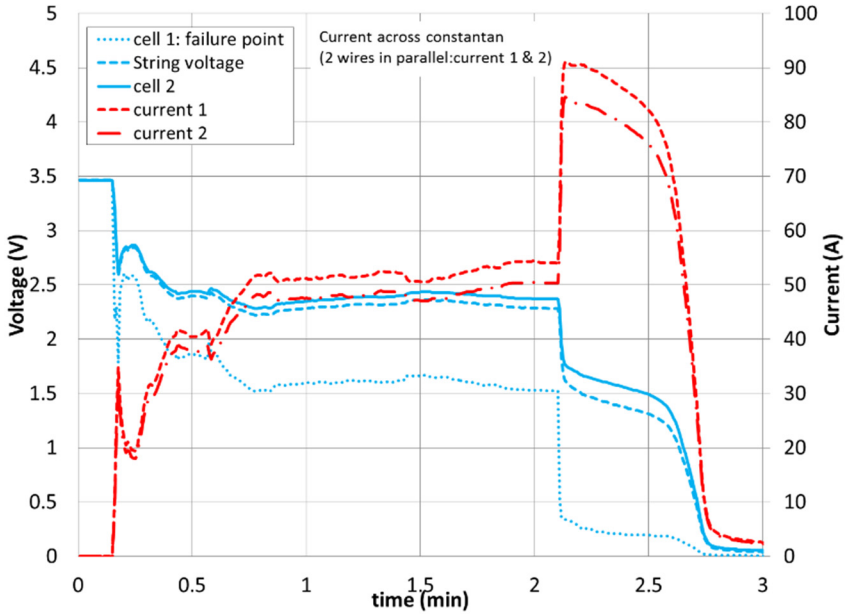


Figure III-23: String current across bridge and voltage measured during the failure propagation test for LFP 26650 in 1S2P configuration

We plan to continue to improve this testing method and apply it to more complex cell strings and electrical configurations in hopes to better quantify the impact of short circuit current during failure propagation in the next level of assemblies.

**Mechanical Testing.** Sandia is providing mechanical testing support to the VTO CAEBAT program to set boundary parameters for mechanical models and to validate predictions made by the numerical models. Further details are available in the annual report submitted by NREL.

**State of Charge Effect on Thermal Runaway.** While significant attention has been paid to cell safety at full charge (100% SOC) to help anticipate worst case scenarios during a failure, there is interest in understanding how a cell failure, in particular thermal runaway profiles, may change with state of charge. This includes quantifying the "tipping point" where a significant heating rate increase is observed to help identify when a thermal runaway response will be more energetic.

A systematic study of how battery SOC effects thermal runaway profiles was investigated using COTS NMC cells (Sanyo) set at 20-100% SOC in 20% increments. Figure III-24 shows accelerating rate calorimetry data for a representative cell at each SOC evaluated.

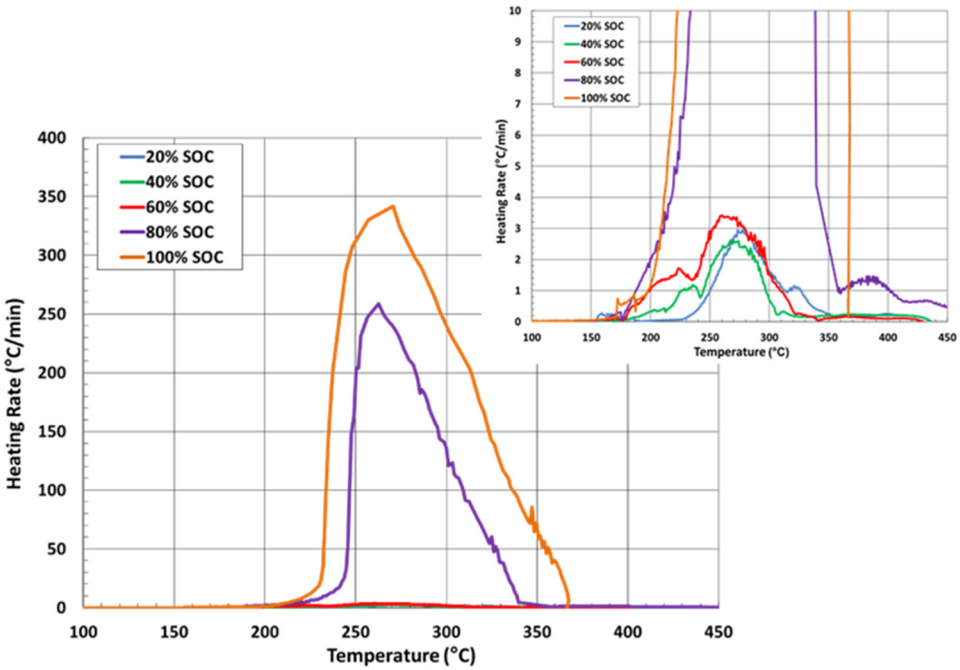


**Figure III-24: Heating rate data obtained from battery calorimetry on COTS NMC cells set at various states of charge from 20-100%. Inset shows a zoomed in image to help identify unset temperature of the runaway as well as the amplitude for the lower heat release rate reactions**

The peak heating rate of the cell at 100% SOC is ~325 °C/min with an estimated runaway enthalpy of ~78 kJ/Ah, while the cell at the lowest SOC (20%) had a peak heating rate of 3 °C/min and a runaway enthalpy of ~20 kJ/Ah. While this trend of a less energetic runaway for the lower states of charge is expected, the SOC has a larger impact on runaway and had not been evaluated previously for this cell. Peak heating rates during runaway are similar for the lower states of charge (20-60%) then drastically increase by 400-500x at 80% and 100%SOC as shown in total energy output (W) in Table III-14. In addition, the onset of thermal runaway shifts right (to a higher temperature) as the %SOC decreases.

### Table III-14: Energy Output Observed as a Function of SOC

| %SOC | KJ | KJ/Ah | W | W/Ah |
|---|---|---|---|---|
| 20 | 19.5 | 20.4 | 4.64 | 18.6 |
| 40 | 23.9 | 31.0 | 4.14 | 8.27 |
| 60 | 25.7 | 34.3 | 5.37 | 7.17 |
| 80 | 31.0 | 47.8 | 406 | 406 |
| 100 | 25.5 | 78.0 | 536 | 426 |

## Conclusions

Development and testing of higher energy, larger format cells and modules continues for USABC developers to meet the DOE EV goals. We provide a means to field the most inherently safe chemistries and designs to help address the challenges in scaling up lithium-ion technologies of interest. This has required careful control and monitoring of tests with the potential of high energy release as well as standing up a larger facility at SNL

to support module level testing this FY. This has provided critical information to cell developers to aid in the development of increasingly abuse tolerant cell chemistries and module designs. This independent testing is also necessary to perform objective evaluations of these various designs and chemistries by DOE and by US automobile manufacturers. SNL has completed abuse testing support for all USABC deliverables to date.

Understanding battery design effects on failure propagation was investigated this FY including failure point, electrical configuration, design architecture, and passive thermal management. All aspects proved to have an impact on the extent of propagation. Large short circuit currents were noticed during propagation testing that impacted the extent of propagation. We developed and validated a method to quantify discharge currents using COTS cells of different sizes and chemistries. Initial testing was completed on 2 cell strings in a 1S2P configuration using constantan bridge wires of known resistance to obtain current.

Having better predictive models for battery failures continues to be of interest to the battery community. SNL provides the testing support and data to help build and validate these models with other national lab partners through the CAEBAT VTO program. Additional abuse testing support for the VTO post mortem program started during this fiscal year. Initial overcharging tests of cells manufactured by ORNL to various states were achieved and post-test analysis of the cells is being done by ANL.

Evaluation of SOC impact on thermal runaway was performed using battery calorimetry. For the selected COTS cell, lower SOC (20-60%) showed linear heating rates that peak at 2-3°C/min. The tipping point for the thermal runaway profile was realized at 80 - 100% SOC where the peak heating rate was 250-350°C/min respectively. The interplay between state of charge and thermal runaway is well documented, but not necessarily well understood. For these tests, peak heating rate increases dramatically with SOC at high levels of charge, with the most notable change from 60 -80% SOC. However, even at low states of charge there is still energy available to contribute to a thermal runaway. This may have an impact in well insulated systems or during the failure of a multi-cell system.

## Products

### Presentations/Publications


1. J. Lamb et. al. “Understanding lithium ion safety through abuse testing”, the First International Battery Safety Workshop, Munich, Germany (2015 August)
2. J. Lamb et. al. “Recent Safety and Abuse Testing at SNL” The Battery Show, Novi, MI (September 2015)
3. J. Lamb et. al. “Determination of Battery Stability with Advanced Diagnostics” 228th ECS meeting, Phoenix, AZ (October 2015)
4. USABC TAC, November 2015
5. C. J. Orendorff, “Quantifying Thermal Runaway by Battery Calorimetry and Opportunities for Improvement” Interagency Power Group (IAPG) Safety Panel meeting, Feb. 2016
6. USABC TAC, February 2016
7. USABC TAC, May 2016
8. 2016 DOE Annual Peer Review Meeting Presentation
9. J. Lamb et. al. “Advances Towards Inherently Safe Lithium-Ion Batteries” Advanced Automotive Battery Conference, Detroit MI (June 2015)
10. USABC TAC, July 2016
11. “Failure propagation in multi-cell lithium-ion batteries” Lamb et Al., JPS vol 283, pp. 517-523 (2015)
12. “Studies on the Thermal Breakdown of Common Lithium-ion Battery Electrolyte Components” Lamb et Al., JECS vol 162, pp. A2131-A2135 (2015).
13. J. Lamb et. al. “Looking at the relationship of total energy and thermal runaway” Prime 2016, Honolulu, HI, October 2016.

# III.B.4. Battery Thermal Analysis and Characterization Activities (NREL)

**Matthew Keyser, Principal Investigator**
National Renewable Energy Laboratory
15013 Denver West Parkway
Golden, CO 80401
Phone: 303-275-3876; Fax: 303-275-4415
E-mail: matthew.keyser@nrel.gov

**Samuel Gillard, DOE Program Manager**
U.S. Department of Energy
Vehicle Technologies Office
1000 Independence Avenue, SW
Washington, DC 20585
Phone: 202-287-5849
E-mail: samuel.gillard@ee.doe.gov

Start Date: October 1, 2015
End Date: September 30, 2021

## Abstract

### Objectives

- Thermally characterize battery cells and evaluate thermal performance of battery packs provided by USABC developers.
- Provide technical assistance and modeling support to USDRIVE/USABC and developers to improve thermal design and performance of energy storage systems.
- Quantify the impact of temperature and duty-cycle on energy storage system life and cost.

### Accomplishments

- Obtained cells/modules from various USABC battery partners including LGCPI, Envia, Maxwell, Saft, and Seeo.
- Obtained infrared thermal images of cells provided by USABC battery developers and identified any areas of thermal concern.
- Used NREL's unique calorimeters to measure heat generation from cells and modules under various charge/discharge profiles in order to design the appropriate thermal management system.
- Obtained thermal and electrical performance data of cells under HEV, PHEV and EV power profiles.
- Presented results of cell thermal characterization and pack thermal evaluation at USABC/battery developers review meetings.

### Future Achievements

Long-life, high-performance battery packs are critical components in efforts to overcome mounting energy and environmental challenges. NREL's research can make a huge difference in the marketplace and society by:

- Providing information needed to make reliable, safe, and affordable batteries for EDVs.
- Increasing consumer confidence in EDVs and breaking down barriers to mass-market adoption.
- Developing or validating novel and effective battery management systems to extend the life of EDV batteries.
- Reducing emissions of greenhouse gases while increasing independence from oil imports.

## Technical Discussion

### Background

While EDVs promise to reduce America's need for imported oil and consequent greenhouse gas emissions, designing high-performance, cost-effective, safe, and affordable energy-storage systems for these cars can present challenges, especially in the critical area of battery thermal control. As manufacturers strive to make batteries more compact and powerful, knowing how and where heat is generated becomes even more critical to the design of effective thermal-management systems. NREL's thermal characterization activities provide developers, manufacturers and OEMs with the knowledge necessary to assure that batteries are designed to perform strongly, last a long time, and operate at maximum efficiency.

Understanding and controlling the temperature of battery systems is necessary for the successful operation of EDVs. The chemistries of many advanced energy-storage devices—such as lithium-based batteries—are very sensitive to the operating temperature. High temperatures degrade batteries faster while low temperatures decrease their power and capacity, affecting vehicle range, performance, and cost. Understanding heat generation in battery systems—from the individual cells within a module, to the inter-connects between the cells, and across the entire battery system—is imperative for designing effective thermal-management systems and battery packs.

### Introduction

The operating temperature selection is critical to achieving the right balance between performance, cost, and life for both lithium-ion batteries and ultracapacitors. At NREL, we have developed unique capabilities to measure the thermal properties of cells and evaluate thermal performance of battery packs (air or liquid cooled). We also use our electro-thermal finite element models to analyze the thermal performance of battery systems in order to aid battery developers with improved thermal designs.

### Approach

NREL has measured the thermal properties of the cells and batteries with many different chemistries (lead acid, NiMH, and many versions of lithium cells) through heat generation, heat capacity, and infrared thermal imaging; conducted performance thermal testing of battery and ultracapacitor modules and packs; analyzed the thermal performance of cells and modules; and developed thermal models. Researchers perform thermal testing, analysis, and modeling (1) to assist DOE/USABC battery developers in designing cells/modules/packs for improved thermal performance, and (2) to evaluate and validate the thermal performance of cell/module/pack deliverables from DOE/USABC battery developers and suppliers.

Testing and evaluating cells, modules, and packs is critical to the integration of battery systems into advanced vehicles. NREL's equipment can benchmark how changing the design of the cell using a different cathode, anode, current collector, electrolyte, additive, or separator affects the overall performance of the cell. The information garnered from these tests helps battery and advanced vehicle manufacturers improve their design, while providing critical data for development of thermal management systems that will reduce the life-cycle cost of battery systems. Using NREL's unique R&D 100 Award-winning calorimeters and infrared thermal imaging equipment, we obtain thermal characteristics of batteries and ultracapacitors developed by USABC battery developers and other industry partners. NREL supports the Energy Storage Technical Team by participating in various work groups such as the LG CPI, Envia, Maxwell, Saft, and Seeo USABC Working Groups.

### Results

#### Calorimeter Testing

Figure III-25 shows the efficiency of cells tested in FY15/FY16 at NREL at a calorimeter temperature of 30°C. The lithium ion cells were fully discharged from 100% SOC to 0% SOC under a C/2, C/1, and 2C currents. It should be noted that the cells in the figure are for both power and energy cells and have been developed for the

HEV, PHEV, EV, and/or the 12 Volt Start/Stop programs within USABC. The figure shows that most of the lithium-ion cells, A-E, are very efficient over this cycling regime – typically greater than 94% for a 2C discharge. Cells F and G, experimental chemistries, show a slightly lower efficiency as compared to many of the other cells tested at NREL. DOE and USABC are developing these new chemistries to improve energy density, power density, cycle life and/or cost benefits. NREL's calorimeter is useful in identifying these outliers but can also help determine if the inefficiency is due to chemistry or cell design.

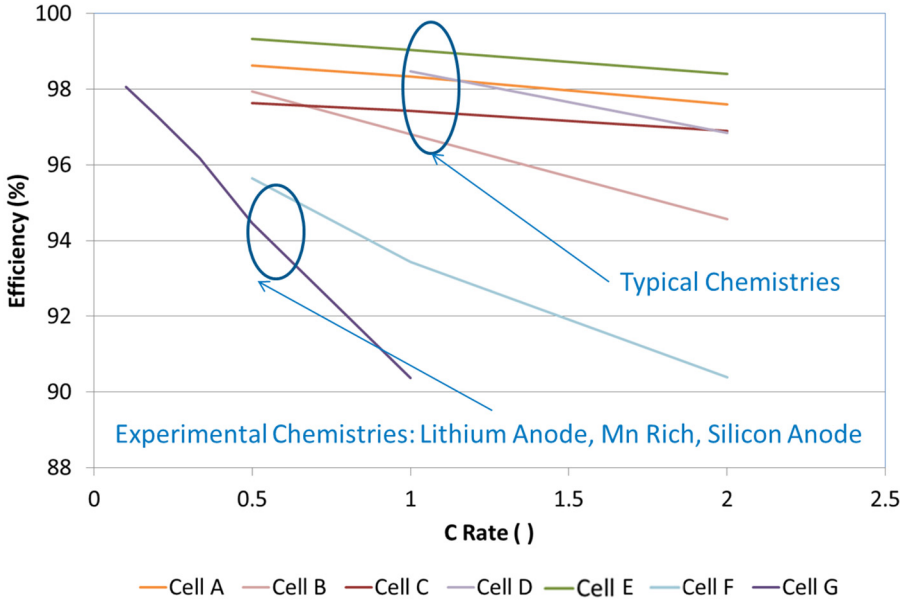


**Figure III-25: Efficiency of cell tested at 30 °C in NREL's calorimeter during FY15/FY16**
*Caption Credits/Source: NREL - Matt Keyser*

Figure III-26 shows the efficiency of a cell under a constant current discharge from 100% to 0% SOC. NREL has tested three versions of the cell from the same manufacturer and the graph compares/contrasts the efficiency as a function of temperature. As expected, the efficiency increases as the temperature increases. Furthermore, each successive generation of the cell shows improvements in efficiency. Of particular note, the efficiency at 0°C for the latest version of the cell, version 3, is equivalent to the 30°C efficiency of the first version of the cell. NREL's calorimeters can determine whether or not the changes that are being made to the cell such as new electrolytes, additives, conductive binders, etc. are having a positive impact on the cell's performance.

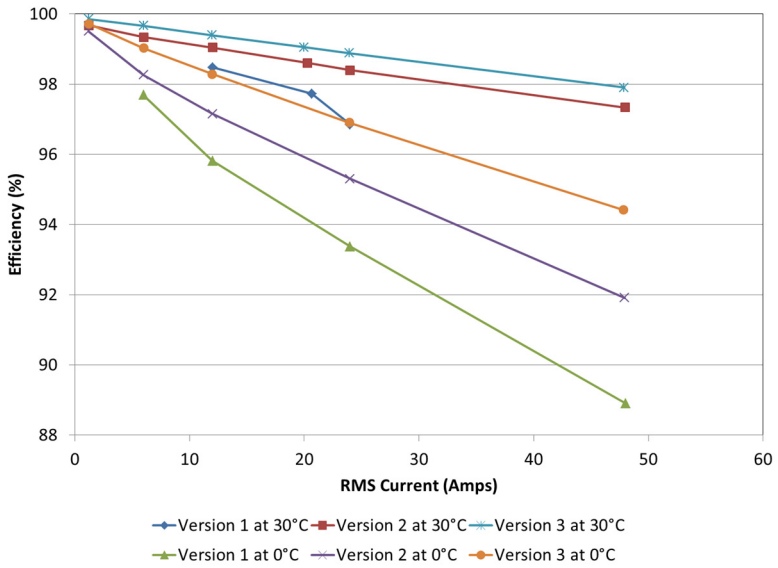


**Figure III-26: Efficiency of different versions of a manufacturer's cell tested at 30 °C and 0 °C in NREL's calorimeter**
*Caption Credits/Source: NREL - Matt Keyser*

NREL's calorimeters are designed to be accurate enough to measure the electrochemical response from batteries under test. Figure III-27 shows the entropic heat generation rates of two versions of a LTO cell tested at 30°C. The cells in this figure were cycled over their entire depth of discharge range at a very low current – minimizing the current decreases the joule heating of the cell and allows for the entropic heat signature to be assessed. As shown in the figure, the cells undergo endothermic and exothermic heat generation over the cycling range. The primary differences in the heat signatures from the two versions of the cell are due to the electrochemical changes to the anode and cathode. Thus, the latest version of the cell, version 3, shows a more significant endothermic response at the beginning of the regen and discharge. Typically, LTO cells do not undergo phase transitions during cycling but changing the chemistry will alter the heat signature of the cell and could have an effect on the cycle life of the cell.

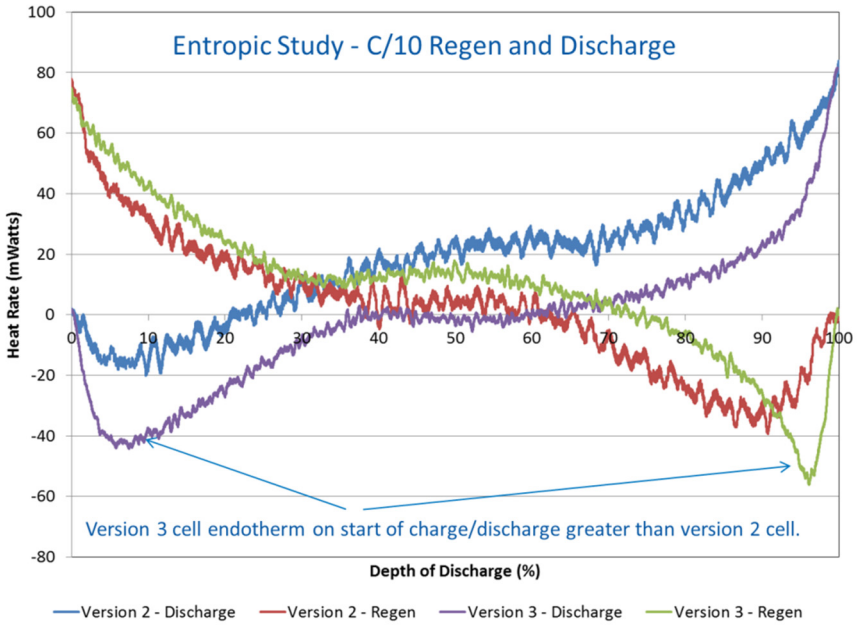


**Figure III-27: Entropic response to LTO cells tested at 30 °C in NREL's calorimeter**
*Caption Credits/Source: NREL - Matt Keyser*

Figure III-28 shows the calorimeter response to a cell undergoing a full discharge at varying discharge rates from 100% to 0% SOC. As expected, the heat rate increases as the current increases. However, the C/2 and C/1 discharge currents show an endothermic response at the beginning of the test - the cell response is endothermic if the heat rate is below zero and exothermic if the heat rate is above zero. An endothermic response within the cell can only be attributed to the electrochemistry of the cell. As indicated above, the entropic changes within a cell can typically only be seen by the calorimeter under very low discharge rates - less than C/10. However, the cell below shows these entropic changes even at a discharge current of C/1. As a result, the heat efficiency of the cell at these low rates is close to 100% - however, nothing is free. The regen efficiency will be lower than the discharge efficiency leading to a roundtrip efficiency much less than 100%.

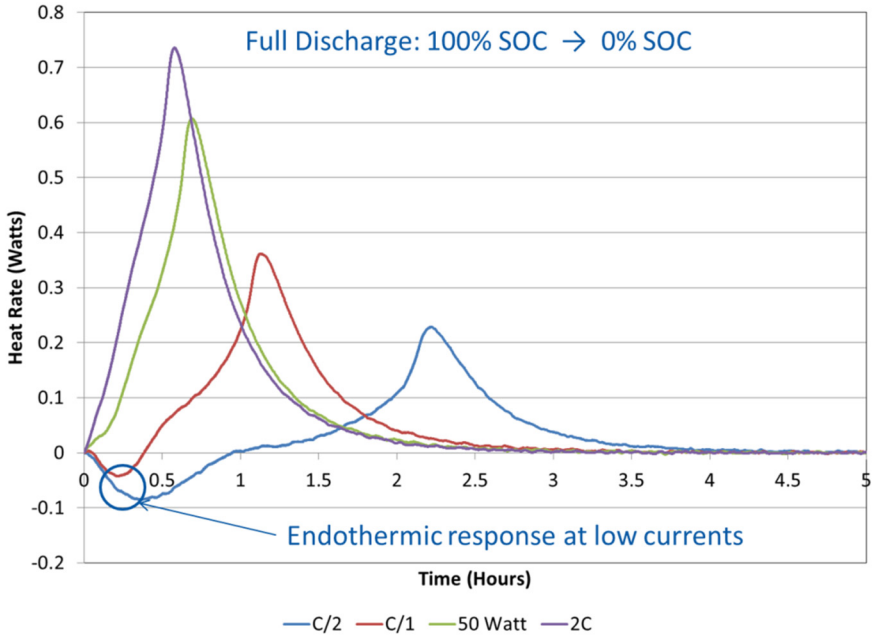


**Figure III-28: Calorimeter response to cell tested at 30 °C in NREL's calorimeter**
*Caption Credits/Source: NREL - Matt Keyser*

When testing a cell to size the thermal management system, it is imperative to test the cell according to how it will be used. Figure III-29 shows the calorimeter response to an EV cell undergoing a DST cycle as well as a US06 cycle at two power levels. The average efficiency over the DST usage profile is approximately 95.3% at 30°C. However, the efficiency drops to 91.1% when applying a full power US06 cycle. The data provided by the calorimeter will allow the battery manufacturer and OEM to size their thermal management systems so as to limit the maximum operational cell temperature while ensuring that the battery pack meets their specific cycle life specifications.

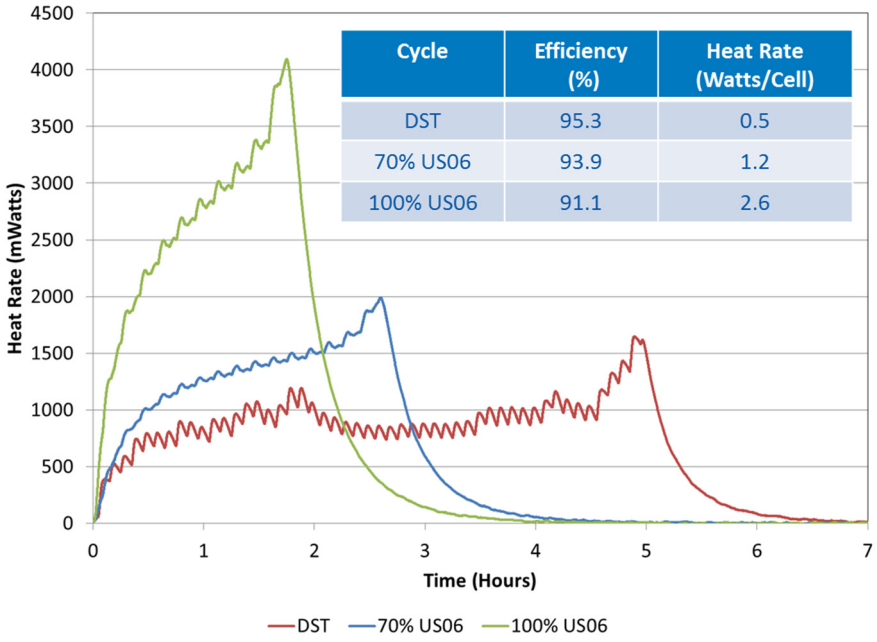


**Figure III-29: Calorimeter heat response to cell tested under different drive cycles at 30 °C in NREL's calorimeter**
*Caption Credits/Source: NREL - Matt Keyser*

## Infrared Imaging of Cells

NREL performs infrared (IR) thermal imaging of battery manufacturer's cells to determine areas of thermal concern. We conduct IR thermal imaging under a set of prescribed procedures and environments to minimize the error from different sources such as reflective cell surfaces, radiation from surrounding surfaces, and cooling from the power cables attached to the cell. NREL combines the IR imaging equipment with a battery cycler to place the cells under various drive cycles, such as a US06 charge depleting cycle for a PHEV, to understand the temperature differences within the cell. We then make recommendations to the battery manufacturers and USABC on how to improve the thermal design of the cell to increase its cycle life and safety.

Figure III-30 shows a lithium battery module at the end of a 2C discharge. Each IR image has a temperature spread associated with it – by decreasing the temperature spread from 12°C to 4°C a visual reference can be used to determine where the heat is preferentially generated within the module. For this module, the heat generation is biased towards the bottom and side of the module. The unique heat signature is due to the thermal management system for the module as well as the interconnects. During the IR imaging, we also assess the temperature uniformity across the volume of the module. When the module temperature is not uniform and consistent, the individual cells age differently affecting the cycle life of the module. NREL is working with battery developers to understand how temperature non-uniformities affect the efficiency and cost of the cell over its life.

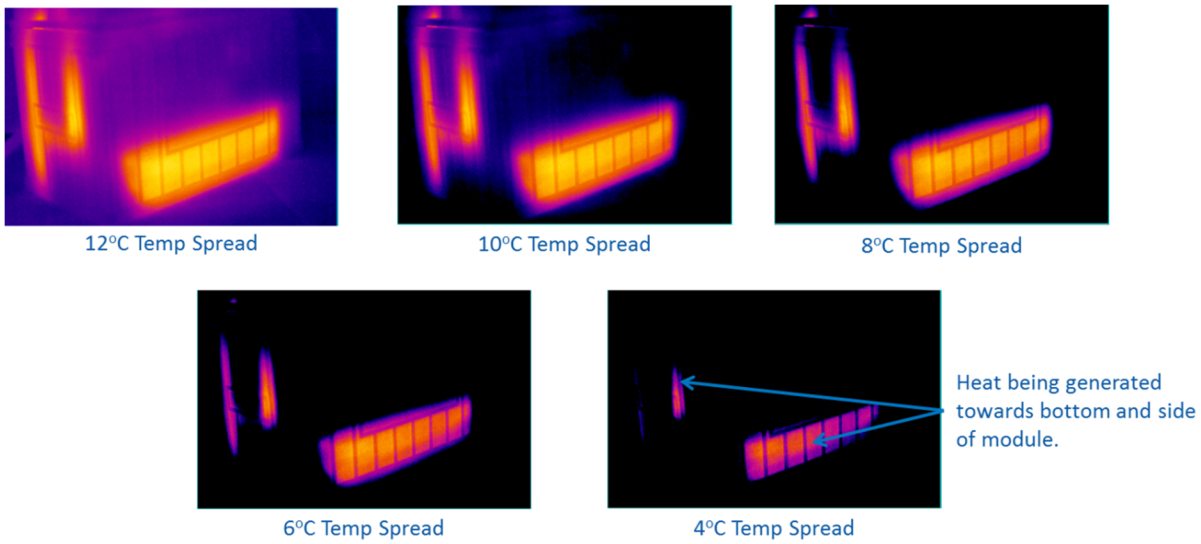


**Figure III-30: Infrared image of lithium battery module at the end of a 2 C discharge**
*Caption Credits/Source: NREL - Matt Keyser*

## Conclusions

NREL has thermally tested cells, modules, and/or packs from LG CPI, Envia, Maxwell, Saft, and Seeo during FY16. We've provided critical data to the battery manufacturers and OEMs that can be used to improve the thermal design of the cell, module, pack and their respective thermal management systems. The data included heat generation of cells under typical profiles for PHEV, EV, and 12 Volt Start/Stop applications, which is essential for designing the appropriate sized battery thermal management system. During the thermal imaging of the cells, we identified areas of thermal concern and helped the battery developers improve the thermal design of their cells. In FY17, NREL will continue to thermally characterize cells, modules, packs for USABC, DOE, and USDRIVE.

### Products

## Presentations/Publications/Patents

1. 2016 DOE Annual Merit Review
2. Quarterly meeting presentation to the battery working group and manufacturer.

### References

1. Design and Analysis of Large Lithium-Ion battery Systems, Santhanagopalan, et al, Artech House, 2014.

# III.C. Battery Analysis and Design Activities

## III.C.1. Computer Aided Battery Engineering Consortium (NREL/ANL/SNL)

**Ahmad Pesaran**
National Renewable Energy Laboratory (NREL)
15013 Denver West Pkwy
Golden, CO 80401
Phone: 303-275-4441; Fax: 303-275-4415
E-mail: ahmad.pesaran@nrel.gov

**Brian Cunningham, DOE Program Manager**
U.S. Department of Energy
Vehicle Technologies Office
1000 Independence Avenue, SW
Washington, DC 20585
Phone: 202-287-5686
E-mail: brian.cunningham@ee.doe.gov

Start Date: October 1, 2015
End Date: September 30, 2018

### Abstract

### Objectives

- In consortium with Argonne National Laboratory (ANL), Sandia National Laboratory (SNL) and Texas A&M University (TAMU), develop advanced modeling capabilities that help industry accelerate development of electric-drive vehicles (EDVs) and their batteries.
- Document and publish new numerical methods to reduce computation time of multiscale multidomain (MSMD) 3-D battery electrochemical-thermal simulations by 100-1000 fold.
- Integrate those fast running models with optimization software to identify electrochemical model parameters from experimental data for NMC523 and graphite electrodes from ANL Cell Analysis, Modeling and Prototyping (CAMP) facility.
- Use microscopy and tomography at ANL to characterize the microstructure of $Ni_{0.5}Co_{0.3}Mn_{0.2}$ (NMC523) and graphite porous electrodes with varying thickness, recipe and calendaring condition.
- With TAMU and ANL, identify and elucidate critical factors of electrode microstructure influencing performance and lifetime using microstructural analysis, stochastic reconstruction, homogenization and direct numerical simulation of electrochemical physics on the complex 3-D geometry.
- With SNL, build experimentally validated simulation tools to predict the thermal-runaway behavior of lithium ion cells after a crash-induced crush, including rate-dependent mechanical failure of individual cell components coupled with electrical, thermal and electrochemical reactions.
- At SNL, obtain quasi-static test data from cells and cell strings under mechanical constraint, followed by computer tomographic (CT) scan of abuse-tested batteries to parameterize mechanical models. Use off-axis quasi-static crush testing of cell strings to validate model predictions.
- Partner with the USCAR Crash Safety Work Group (CSWG) to evaluate models, obtain feedback, and ensure they meet the needs of crash safety engineers.
- Implement crash abuse models in ANSYS/Fluent and LS-DYNA using user-defined functions, expanding upon the approach developed by NREL in the first two phases of CAEBAT.

## Accomplishments

- Benchmarked and documented new GH-MSMD model, achieving 100-1000 fold speedup in electrochemical simulation, spanning particle, electrode, cell and module length scales.
- Quantified the effects of thickness and porosity on the electrochemical performance of NMC523 oxide-based positive electrodes and graphite-based negative electrodes.
- Extracted effective diffusion coefficients of Li in the ANL graphite and NMC523 baseline electrodes using galvanostatic intermittent titration technique (GITT).
- Collected FIB-SEM data to resolve the microstructure of ANL NMC523 baseline electrode, with 34 μm coating and 34% porosity.
- Developed fractal-based criterion for image segmentation of microstructure tomography images to isolate different available phases.
- Developed algorithms to abstract electrode microstructures in terms of porous electrode properties – porosity, tortuosity of pore phase, electronic conductivity of solid phase and interfacial area.
- Developed a novel method to stochastically reconstruct the secondary phase (conductive additive + binder) in an imaged electrode structure containing active material and pore phases only.
- Studied the effects of active material, binder and conductive additive ratios on electrochemical performance of a half cell.
- Developed a multiscale mechanical modeling framework that links properties measured at the electrode scale to failure under mechanical crush at the cell level. The framework simultaneously couples mechanics with electro-chemical-thermal physics for thermal runaway prediction.
- Conducted component-level mechanical characterization experiments for measuring model parameters.
- Performed pack level mechanical crush tests on both fully charged and discharged packs and evaluated failure behavior using CT imaging.
- Conducted mechanical tests at the single-cell level to determine the behavior of cells in multiple orientations with respect to deformation rate and cell temperature.
- Studied short circuit behavior by measuring thermal response and cell resistance during short tests.
- Led test workgroup coordinating tests and sharing data amongst CAEBAT projects.

## Future Achievements

- Develop recommended identification procedure for electrochemical-thermal models versus experimental data.
- Characterize model for NMC523 and graphite electrodes of varying thickness and at varying temperatures. Track performance degradation by evolving parameters in macro-homogeneous model.
- Identify the effects of calendaring and electrolyte filling on electrode microstructure.
- Obtain FIB-SEM and/or X-ray tomography images and reconstruct microstructure of electrodes with different porosities and thicknesses.
- Perform direct numerical simulation of electrode microstructure geometry to elucidate reaction inhomogeneity, transport limitations and their impact on performance and lifetime.
- Identify dominant microstructural properties and correlate with performance of battery electrodes.
- Validate mechanical abuse models using SNL cell- and pack-level crush abuse test data.
- Based on the initial comparison between the model predictions and test data further refine single cell test methods, including off-axis and three point bend testing conditions and compare results from dynamic testing apparatus at dynamic deformation rates.
- Train technical participants from industry on the use of the validated crush abuse models.

## Technical Discussion

### Background

The U.S. Department of Energy has established goals for EDV batteries that, if achieved, will make those vehicles directly competitive with conventional vehicles in the marketplace. Electric vehicle battery pack cost goals for 2020 are $125/kWh (compared to $268/kWh in 2015) and performance goals are 237 Wh/kg, 1000 deep cycles and 15-year calendar life [1]. Complementing other battery research and development efforts, computer models are widely recognized throughout industry as valuable tools for reducing the cost and time of product development, improving manufacturing processes, and optimizing designs.

Predictive simulation of performance and abuse response of large-scale battery systems is challenging. The device response of a battery results from complex nonlinear interactions amongst material characteristics, design variables, and environmental, operational, and abuse conditions. The multiscale nonlinear nature of battery physics critically affects the device behavior as the size of a battery increases. Without understanding the interplays among the interdisciplinary physicochemical processes occurring across the varied scales, it is costly to design long-lasting, high-performing, safe, large batteries. Complex physics and long computation time hinder the adoption of computer aided engineering models in the design of battery electrodes and large-format battery cells and systems. Lacking adequate software tools, the battery and auto industries have typically followed a "build-test-break" product development cycle.

### Introduction

The U.S. Department of Energy's Computer Aided Engineering for Electric Drive Vehicle Battery (CAEBAT) program has supported development of modeling capabilities to help industries accelerate mass-market adoption of EDVs and their batteries. In support of the CAEBAT program, NREL previously developed the multiscale multidomain (MSMD) model, overcoming challenges in modeling the highly nonlinear multiscale response of battery systems [2]. The MSMD model introduces separate model domains at particle, electrode, and cell levels, while tightly coupling physics across the scales. Under the previous CAEBAT project, NREL further developed a simulation framework that captures the propagation of thermal events following mechanical impact from a single cell across a multi-cell module.

For the present CAEBAT-3 project, NREL teamed with experts from labs and academia to improve upon the current state of EDV battery modeling. The project builds upon state-of-the-art modeling tools developed in the first and second phases of CAEBAT at NREL, stochastic reconstruction and mesoscale simulation capabilities at TAMU, and leverages experimental capabilities for electrode fabrication/characterization and mechanical abuse at ANL and SNL, respectively. The project is organized into three technical thrust areas: (1) improving computational efficiency and applicability of electrochemical models, (2) addressing technical gaps in mechanical abuse simulation, and (3) characterization and simulation of electrode microstructure.

**1) Computational efficiency**

Disparate battery physics occur at a range of length scales. The typical multiscale modeling approach requires time-consuming nested iterations to iterate various length-scale submodels to self-consistency. For CAEBAT-2, NREL-led teams developed an innovative GH-MSMD framework, which evolved from the MSMD modularized architecture, improving computational speed by 100-1000 times while retaining the accuracy and modularity. Identification of electrochemical model parameters remains a major bottleneck for industry to adopt electrochemical models into their design process. Identification is inherently difficult because battery characterization is intrinsically solving an under-determined problem. In addition, the physicochemical nature of a battery evolves with degradation. A combined testing and numerical approach is desired that reduces the burden of electrochemical model characterization, identification and validation.

**2) Mechanical abuse**

The coupled mechanical-electrical-chemical-thermal (MECT) models developed under CAEBAT-2 enabled the team to identify technical gaps in the area of battery safety that needed to be resolved for the broader community to adopt these models. In the previous year's report, we demonstrated simulation capabilities across multiple form factors for individual cells (e.g., prismatic vs pouch cells, wound vs stacked, cylindrical

vs prismatic). These models are chemistry agnostic and leverage the battery module available from ANSYS developed under CAEBAT-1.

State-of-the-art constitutive models for battery laminates are oversimplified and do not capture the physics adequately. Porosity and multiple thin layers result in significant stiffening in the compressive stress-strain response of the cells. Currently, there is inadequate understanding of failure propagation across multiple layers within the cell and across multiple cells in a module. There are few established test methods to identify the worst possible outcome of a battery subjected to crush. Under this effort, we identify a set of experimental test procedures for mechanical evaluation of lithium-ion cell components and cells, and a modeling approach that the industry can use to assess the combined mechanical-electrochemical-thermal response of lithium-ion batteries subjected to mechanical crush.

**3) Microstructure**

Microstructure simulation is a new topic area added for the present CAEBAT-3 program. Today's battery software tools cannot predict the behavior of new electrode designs without first building and experimentally testing prototype electrodes. Those macro-homogeneous models rely on adjustable properties such as tortuosity to tune the model to match data. As such, they are not predictive. To date there is no validated tool accounting for stochastic variation in particle morphology; variation in amounts of inert binder and conductive additive; and calendaring process. This hinders application of CAE models in the electrode design process. Accurate models of mesoscale processes on realistic electrode architecture would be of great value to improve understanding of electrode inhomogeneity, performance limitations and degradation processes.

Several challenges exist. Physics at the mesoscale, e.g., transport of lithium-ions through binder, are not completely understood. Measurement of microstructure architecture requires multiple experimental techniques to resolve fine and coarse features of the electrode. Images obtained from scanning electron microscopy and tomography experiments must be stitched together to reconstruct the 3-D architecture. At the spatial resolution of tomography experiments, pore and active material phases (which are larger material volumes) are readily available, while the other species, e.g., conductive additives, are too small to be resolved accurately. Thus, the secondary phase (binder + conductive additives) needs to be reconstructed for simulation. Validation of microstructure models requires characterization of multiple electrode thicknesses and porosities to verify a generalizable simulation tool.

## Approach

### 1) Computational efficiency

The GH-MSMD model uses time-scale separation and variable decomposition to eliminate layers of nested iteration, but retains the modular framework architecture that is critical to battery behavior simulations (Figure III-31). Fast electronic charge balance is differentiated from the processes related to slow ionic movements. The method is being published in a forthcoming manuscript [3]. The fast-running model, capturing all relevant physics of battery performance, is ideally suited for electrochemical parameter estimation. In the present project, GH-MSMD is nested within a nonlinear least squares algorithm and the algorithm is given access to iteratively adjust model parameters. Leveraging DOE Advanced Battery Research (ABR) program developments, model parameters are identified for graphite and NMC523 electrodes fabricated at ANL's CAMP facility. GITT experiments on baseline thin electrode specimens in half-cell format are used to establish open-circuit potential and diffusivity of Li in active material. The cells use a Gen II electrolyte that was previously characterized. Given half-cell and electrolyte-transport data, the model is validated with full cell test data. ANL pouch cells with 300 mAh capacity are used to measure the response of a full battery for constant current discharge, hybrid pulse power characterization (HPPC) and drive cycle electrical load profiles.

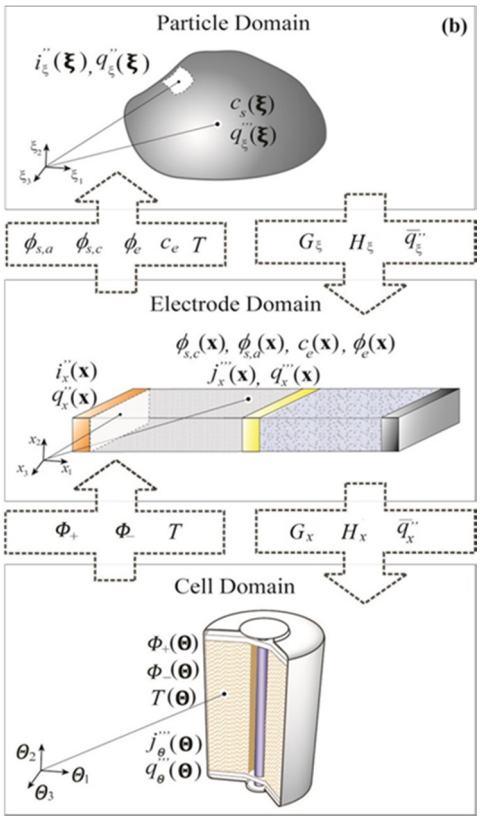


Figure III-31: Modular domain structure of GH-MSMD model

## 2) Mechanical abuse

NREL developed a multi-scale model capable of studying the interactions between mechanical failure and battery cell performance, through incorporation of temperature evolution from multiple sources (mechanical heat, Joule heat and electrochemical heat) and determination of the short resistance from the results of the mechanical failure simulation as a function of time.

The model predicts the location of failure initiation during a mechanical crush test. Figure III-32 shows the scheme for the simultaneously coupled model. At the macro-scale, the model is homogeneous with a uniform element size as shown in the representative volume element of the battery cell, which is a stacking of anode, separator and cathode. A volume-average based homogenization model is introduced to analyze the actual deformation and failure of each component. On the other hand, the mechanical model is coupled with an electrochemical-thermal model in micro-scale to transfer failure status of separator layer, to predict the electrical short circuit resistance and to simulate the consequential electrical/thermal responses (current increase and drop, voltage drop and thermal runaway). The model is implemented in the commercial finite element software LS-DYNA through a user-defined material model. Mechanical testing is performed at the component, individual cell and cell-string levels to identify material constitutive relationships and parameters.

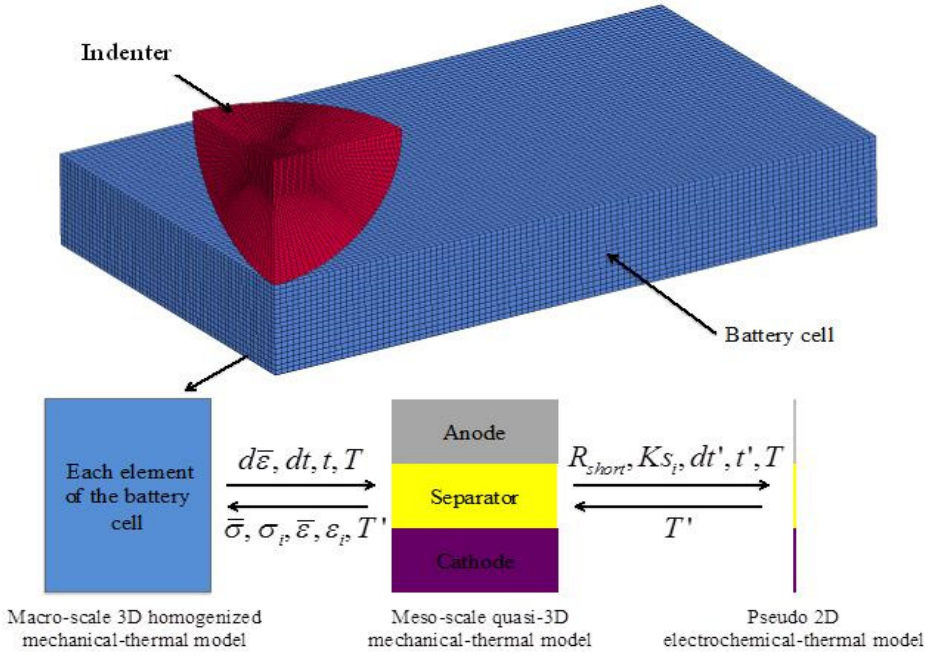


**Figure III-32: Multi-scale simultaneously coupled mechanical electrochemical-thermal modeling framework for mechanical abuse of lithium-ion cells**

### 3) Microstructure

While the electrochemical physics of lithium-ion batteries are relatively well understood, most models of those physics rely on homogenization assumptions that ignore microstructural details in favor of producing a fast model that can be tuned to a small set of electrode test data. Homogenized models reasonably extend test data to other charge/discharge conditions, but are unable to predict electrode response prior to actually building and characterizing a physical test specimen. Without tuning, homogenized models are unable to predict transport limitations and localized utilization of active materials that limit performance and lifetime.

Figure III-33 provides an overview of the microstructure modeling task. In addition to electrochemical characterization, ANL is conducting FIB-SEM studies and tomography measurements in its Advanced Photon Source (APS) user facility to map the 3-D architecture of electrodes. From this data, TAMU is extracting detailed geometry and computational mesh for simulation. As tomography experiments are unable to separately identify binder and conductive additive phases, TAMU has developed stochastic reconstruction algorithms that artificially grow the secondary phase amongst the active material primary phase.

The 3-D reconstructed architecture serves several purposes. Standalone simulations of ionic and electronic transport quantify effective transport properties for macro-homogeneous models. Microstructure analysis quantifies distributions of pore and particle sizes, including aggregates of particles that impede electrode utilization. Full electrochemical simulations are developed and carried out on high performance computers.

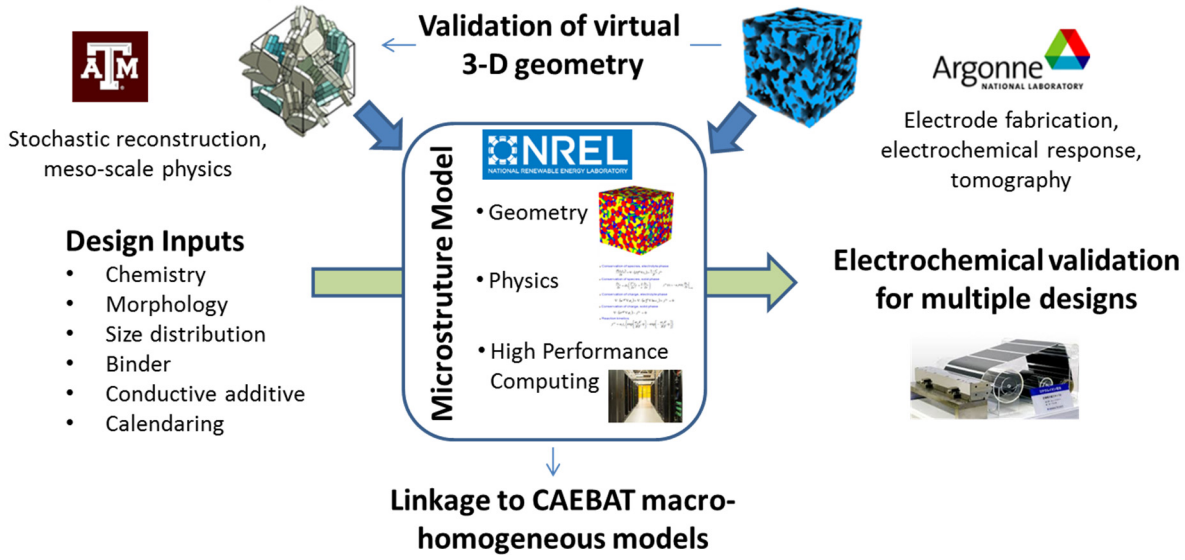


Figure III-33: Microstructure modeling task and roles at NREL, TAMU and ANL

## Results

### 1) Computational efficiency

#### GH-MSMD documentation

The modular, efficient MSMD battery simulation model was previously introduced by NREL to aid the scale-up of lithium-ion material and electrode designs to complete cell and pack designs, capturing electrochemical interplay with 3-D electronic current pathways and thermal response. A forthcoming manuscript [4] describes significant computational efficiency improvement to the MSMD model using a separation of time-scales principle to decompose model field variables. The GH-MSMD decomposition provides a quasi-explicit linkage between the multiple length-scale domains and thus reduces time-consuming nested iteration when solving model equations across the multiple domains. In addition to particle-, electrode- and cell-length scales treated in the previous work, the GH formulation extends to bus bar- and multi-cell module-length scales. The GH-MSMD model achieves 100-1000 times speedup compared to baseline MSMD models, making it well suited for parameter identification, performance evolution studies, design optimization and real-time control.

#### Electrochemical model identification and validation

Positive and negative electrodes were fabricated and characterized at the ANL CAMP facility. The positive electrode comprises a coating of NMC523 oxide, C-45 carbon and polyvinylidene fluoride (PVdF) binder in a 90:5:5 weight ratio of on a 20 µm thick Al current collector. The negative electrode comprises a coating of A12 graphite, C-45 carbon, and PVdF binder in a 92:2:6 weight ratio on a 10 µm thick Cu current collector [5]. The diffusion coefficient of $Li^+$ ions in intercalation oxides has important implications for the charge and discharge rate of electrodes. Figure III-34 present values of diffusion coefficients extracted from GITT data for the baseline NMC523 electrodes. Values of diffusion coefficients on the order of 5E-12 $cm^2/s$ are estimated for x = 0.1 to 0.9 where x refers to the estimated number of lithium in the active material at the given state of charge. Diffusivities ranging from 5E-10 to 1E-12 $cm^2/s$ [6,7] have previously been estimated for NMC523 and are likely linked to assumptions made regarding the active surface areas in the electrodes. Our diffusion coefficients use BET-measured specific surface area of 0.28 $m^2/g$.

Open circuit potential is taken from the rest portions of the GITT experiment. With solid diffusivity and OCP properties identified, a GH-MSMD particle-domain model is fit to the data to extract final reference values of diffusivity, exchange current density and film resistance. Similar experiments and model fitting procedure are carried out for the graphite electrode in half cell configuration. Full cell tests are underway at NREL on 300 mAh pouch cells from CAMP combining the graphite and NMC523 electrodes. Full cell data will be used to

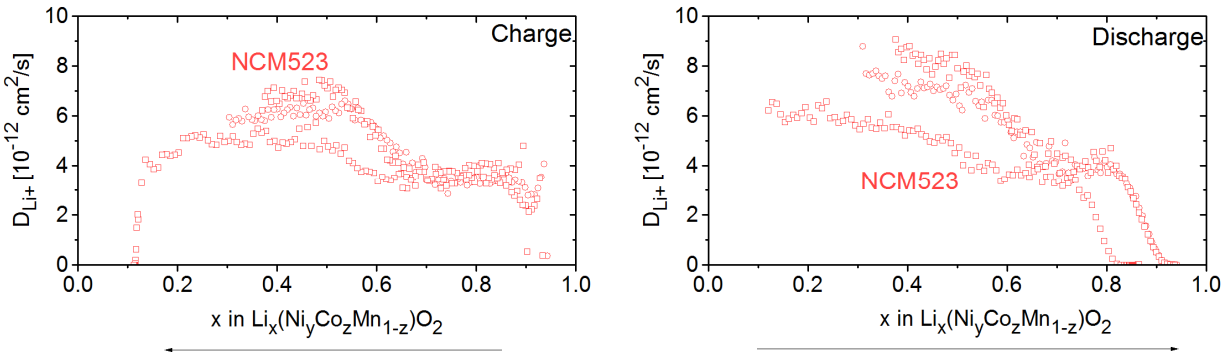


**Figure III-34: Diffusion coefficient of Li+ in NMC523 electrodes on charge and discharge extracted using GITT. Each figure contains three separate tests terminated at 4.2, 4.4, and 4.5 V, respectively. Arrow indicate the direction of progression of extraction on charge and insertion on discharge**

validate GH-MSMD electrode-domain models. Future achievements will evaluate the extent to which the model extends to thicker electrode designs that utilize the same active materials. Thicker electrodes are more energy dense and cheaper to manufacture, however suffer from performance limitations. Models optimizing energy, cost and performance must correctly capture the mesoscale performance limitations of thick electrodes.

**Effect of electrode porosity and thickness on electrochemical performance**

NMC523 electrodes of thicknesses 106, 140, and 160 µm were fabricated without calendaring; these electrodes displayed final porosities on the order of 50%. From these electrodes a sub-section was cut and calendared to thicknesses of 88, 108, and 129 µm, respectively, resulting in porosities on the order of 37%. The data from these electrodes were compared with data from the baseline NMC523 electrode, which has a coating thickness and porosity of 34 µm and 34%, respectively. Similarly, graphite electrodes of thicknesses 140, 173, and 205 µm were fabricated without calendaring: these electrodes displayed final porosities on the order of 51%. Subsequent calendaring on a portion of the electrodes resulted in thicknesses of 120, 141, and 175 µm, respectively, and porosities on the order of 37%.

The fabricated electrodes were electrochemically characterized at rates ranging from C/20 to 2C in half-cells containing either NMC523 or graphite as the working electrode, a lithium-foil counter electrode, Celgard 2325 separator and 1.2 M LiPF6 in EC:EMC (3:7 by weight) electrolyte. All electrochemical cycling tests were performed at 30°C using a MACCOR Series 4000 Test System. Electrode porosity and thickness have a synergistic effect on the lithiation and delithiation capacities of lithium-ion electrodes. In Figure III-35, data from NMC523 electrodes charged at a slow rate of C/10 followed by discharge at C/10 or 1C rates are shown.

With some expected scatter, one can see from Figure III-35a, b that at a given electrode thickness and applied C-rate, electrodes with high porosities generally show higher discharge capacities. Figure III-35c highlights the discharge profiles of two NMC523 electrodes with comparable thicknesses of ~107 µm at the same applied current of 181 mA/g (1C rate). It is evident that the higher porosity electrode ($\varepsilon = 47\%$) discharges at a higher potential, thus promoting a higher end gravimetric capacity/energy at the cut-off voltage of 3.0 V compared to an electrode calendared to $\varepsilon = 38\%$. Similar trends are observed for the graphite electrodes where higher porosities and lower thicknesses result in better utilization of the electrode active material, especially at high C-rates.

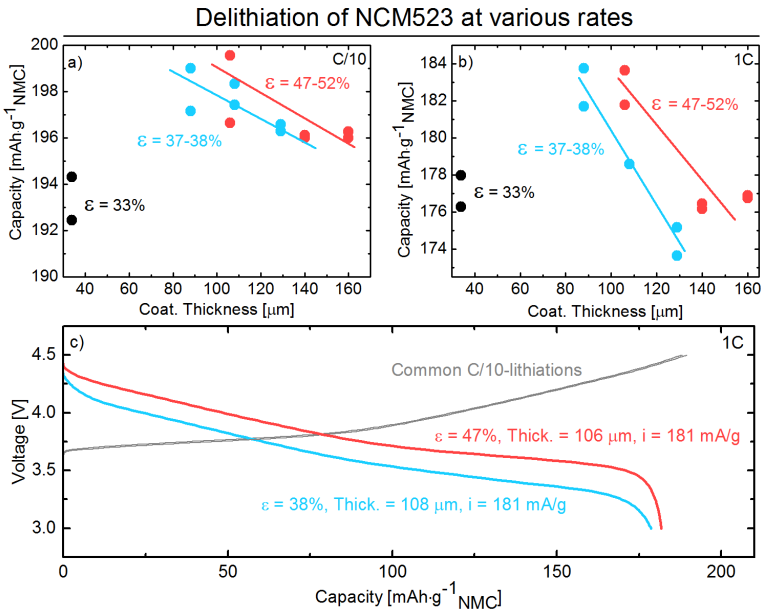


**Figure III-35: Summary of half-cell NMC523||1.2 M LiPF6 in EC/EMC||Li capacities at (a) C/10 and (b) 1 C rates as a function of electrode thickness and porosity. For a given electrode thickness and applied specific current, oxide-lithiation (discharge) capacities increase with higher porosities especially at high currents. (c) 1C discharge capacity as a function of cell voltage for electrodes that have a similar thickness but different porosities (38% and 47%). The discharge potential profile is higher for the 47% porosity electrode, which indicates a lower electrode impedance**

## 2) Mechanical abuse

A single element benchmark study is conducted to verify the model developed above. We start with a numerical verification of the macro-meso mechanical homogenization method, followed by a preliminary case study for a short circuit induced by compression of the cell. We also present a parametric study on the effect of short resistance. The thickness of the macro element, anode, separator and cathode are 180 μm, 85 μm, 25 μm and 70 μm, respectively. The in-plane size of the element is 0.5 mm.

### Verification of mechanical homogenization model

A linear elastic case is presented considering the electrodes and separators all exhibit isotropic elasticity. We assume that the cathode and anode both have a Young's modulus of 40 GPa, and that the Young's modulus of separator is 4 GPa. The Poisson's ratios of all components are set to 0.3. Two loading conditions, in-plane tension and through-thickness compression, are studied using the macro-meso model (named as the multiscale model) that has only one element and compared with the actual model with multiple layers (named as multilayer model) that has three elements each representing one of the components. The strain and stress profiles are plotted and compared, as shown in Figure III-36. As seen from the results, the multiscale model predicts the stress/strain responses accurately for the in-plane tensile loading condition, which has been known to be the primary failure condition of the separator layer. For the through-thickness compression case, some discrepancy of the predicted stress/strain is observed with errors less than 20%. Overall, the multiscale model exhibits acceptable accuracy in predicting the mechanical deformation of the battery cell and cell components.

The current multiscale model provides a generic framework for studying the mechanical and coupled mechanical-electrochemical-thermal responses. The individual pieces of the model, e.g., the mechanical homogenization approach, electrochemical model and correlation of short resistance can be further enhanced using more sophisticated models when available.

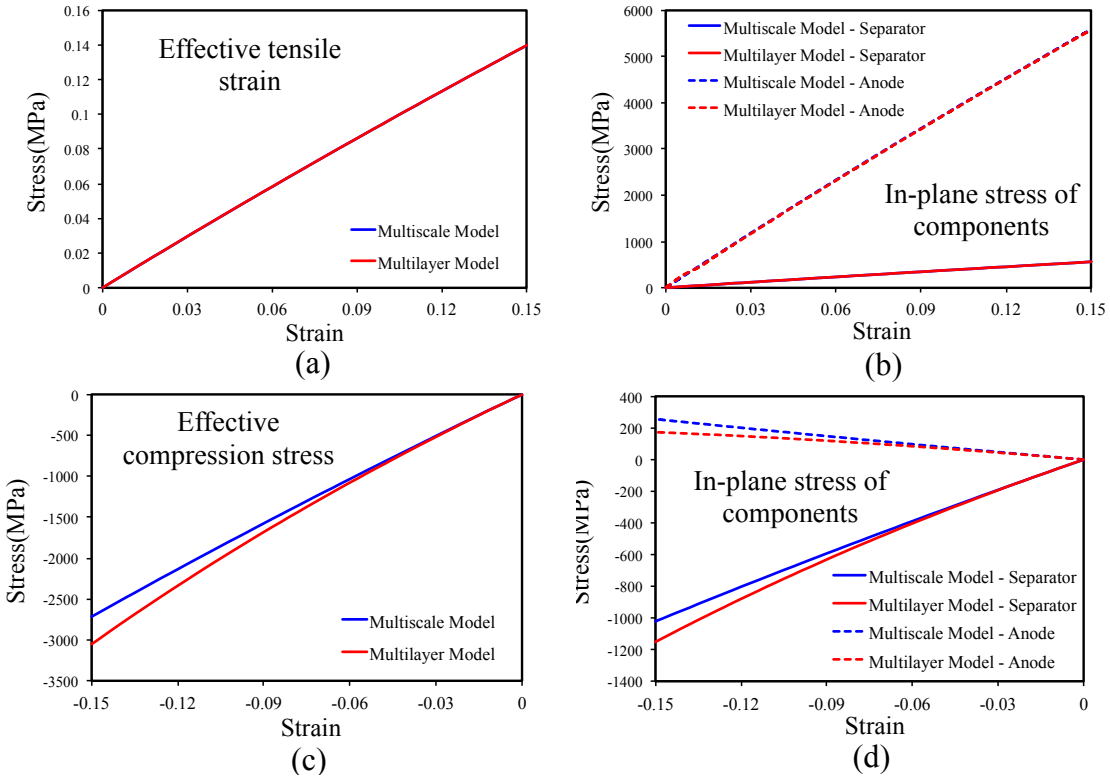


**Figure III-36: Comparison of numerical results for multiscale model and multilayer model: (a) effective in-plane tensile strain under in-plane tension, (b) in-plane stress of separator and anode under in-plane tension, (c) effective through-thickness compression stress under through-thickness compression and (d) in-plane stress of separator and anode under though-thickness compression**

### Single cell parameterization

Mechanical testing was performed on single cells at SNL to parameterization models under development. This has included multiple orientations of mechanical deformation as well as external short circuit results to provide internal resistance and worst-case short circuit behavior information. The mechanical behavior of single cells is evaluated both into the face of the cell and through the edge with a cylindrical impactor. Single cells are also evaluated as a function of deformation rate and cell temperature (Figure III-37).

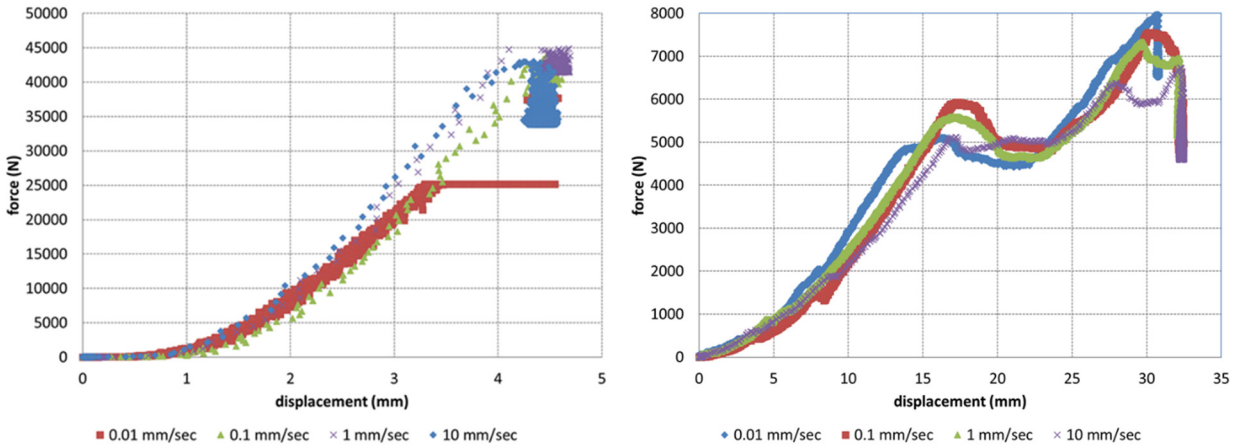


**Figure III-37: Impact of deformation rate on cells crushed into the face (left) and edge (right) of a single cell. This shows the impact of strain rate on the compaction (left) and buckling (right) of the electrode layers within a single cell**

Crushing through the face primarily focuses on the compaction of electrode layers as force is applied and shows little change as the deformation rate is increased. Buckling of the electrode layers is the primary mode of failure when crushing through the edge, and Figure III-37 (right) shows some change to the behavior of cells

as the deformation rate is increased. Initial buckling is observed at 12-17 mm of total displacement, (observed in the figure where the force reaches a local maximum and begins to decrease) with this point increasing as the deformation rate is increased. The impact of temperature as a single cell is crushed into the face showed that the force needed for equivalent deformation generally decreased as the cell temperature is increased.

**Short circuit test and simulation**

External short circuit data was collected to provide insight both to the potential short circuit behavior the 5-Ah commercial cells might exhibit during a vehicle collision and to determine the internal resistance of the cells. External loads of 1 mOhm and 10 mOhm were applied for 1 hour. The initial 9 seconds of the test were monitored at a 1kHz collection rate to better observe the behavior of the cells during the initial transient period. Cell resistances were estimated to be around 12-13 mOhm for both sets of cells.

The short experiment was replicated in simulation. In our simulations, for a uniform through-thickness compression of the element, we assign a failure compressive strain of 0.8 for the separator layer. A constant loading rate of 0.00015 mm/s is applied and the displacement holds following by the failure of separator layer. Figure III-38 shows the voltage, current density and temperature profiles against the strain history of the separator layer. As we can see, during the initial stage before the short circuit, there is a slight decrease in the cell voltage from 4.113 V to 4.107V. Followed by the failure of separator, an instantaneous drop of voltage is observed due to the sudden increase in the current density from 0.012 A/m3 to 5.26 A/m3. Subsequent gradual decrease of cell voltage and leveling off of the current density are consistent with the experimental observations during mechanical abuse tests. On the other hand, the temperature increases continuously after the short due to the increasing contributions from the Joule heating energy and the electrochemical reaction energy. The internal resistances for the cell prevent any further discharge below 2.8V for the parameter set chosen for the electrochemical model. Also, since we assumed adiabatic boundary conditions, there is no thermal conduction of the heat away from the single element and so the temperature remains constant after complete discharge.

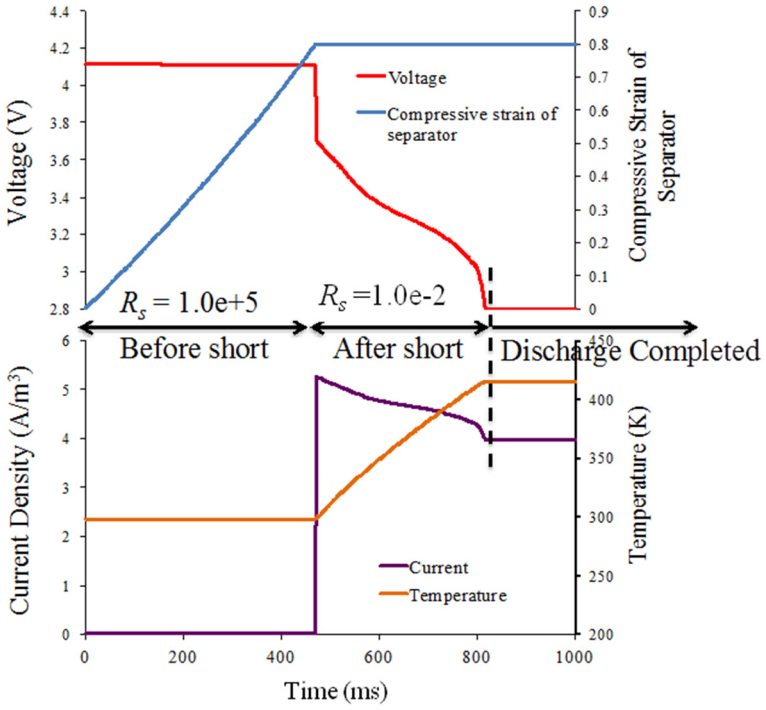


**Figure III-38: Simulated voltage, current density and temperature versus strain profile of the separator during a compressive load during a short-circuit test in which the drop in resistance of the short was limited to 10 mOhm**

**Pack-level mechanical evaluation**

SNL performed crush testing on 12 cell packs constructed by stacking commercial-off-the-shelf 5 Ah pouch cells together in a close-packed configuration. CT imaging was performed post-crush to better understand internal deformations. Mechanical testing of these packs included both a strict compaction of the pack through the longest pack dimension perpendicular to the cell electrodes, and a cylindrical impactor affecting 4 cells

within the center of the pack with force applied parallel to the cell electrodes. These configurations excite different failure modes with compaction of the electrode layers in the first case and buckling of the electrode layers in the second.

This is performed on both fully charged cells to determine the pack level failure response and discharged cells to better understand the mechanical deformation process. Figure III-39 shows the results of the cylindrical buckling test on fully charged cell strings. Approximately twice the force is required to drive the fully charged pack to failure in the electrode layer compaction case compared to the buckling case. Post-test CT images of the fully discharged pack (Figure III-40) indicate how buckling propagates through the cells as a result of the cylindrical impactor. Buckling causes significant damage to the electrode layers. Electrodes pull apart in some regions and become compacted in others. Comparison of multi-cell test results against model results will be performed during the next fiscal year. Future work will also include publication of methods to measure model parameters at the component level that will serve as input to the approach outlined above.

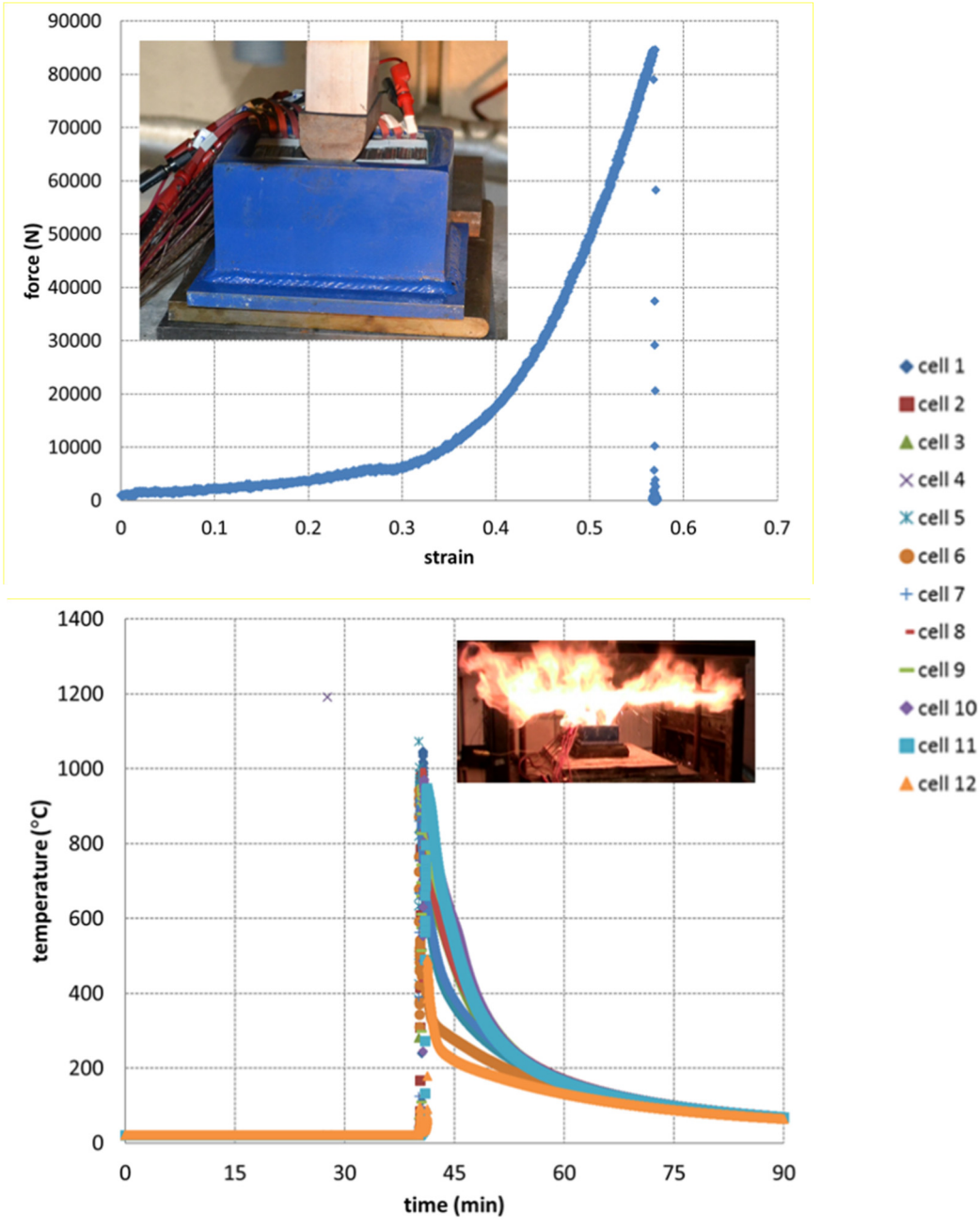


Figure III-39: 12 cell central pack crush with cylindrical impactor on a fully charged pack

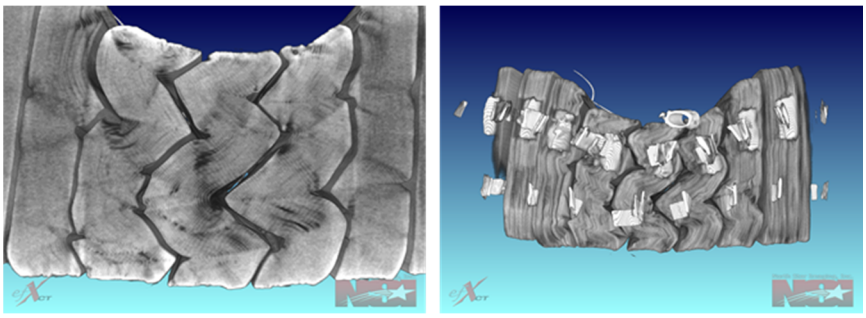

Figure III-40: CT scan performed after deformation of fully discharged 12 cell pack

## 3) Microstructure

### FIB-SEM microscopy

FIB-SEM tomograms of the baseline NMC523 electrode were collected to map the three dimensional architecture of the electrodes (Figure III-41). The FIB-SEM was performed with 20 nm sectioning thicknesses, over approximately 0.6 µm of the electrode cross-section, which is sufficient to resolve the mesoscale structure of the carbon-binder network and its distribution with respect to the oxide particles. In Figure III-41b, a machine learning classifier built into the FIJI software package is trained to segment the various phases (active $LiNi_{0.5}Co_{0.2}Mn_{0.3}O_2$, pores, and carbon-binder phases). The segmentation of phases will later be used in reconstructing the electrode architecture for the three dimensional modeling efforts.

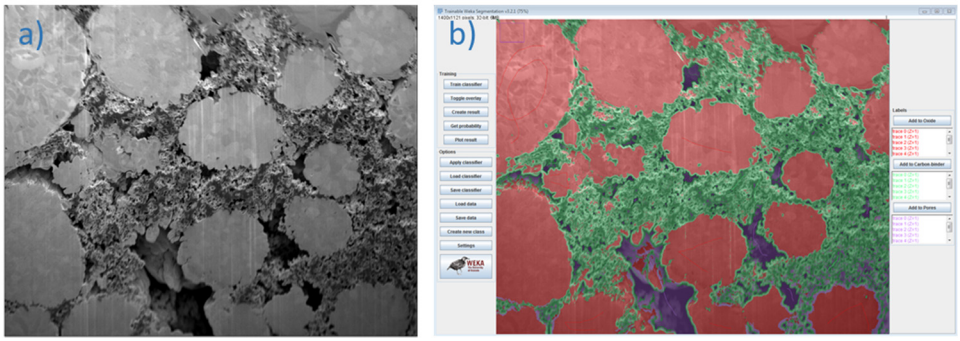


Figure III-41: (a) FIB-SEM cross-section image of the baseline NMC523 electrode showing large oxide particles, carbon-binder conductive network, and pores. (b) Example of phase segmentation with the WEKA machine learning classification algorithm. The color scheme is as follows: NMC523 oxide (red), carbon-binder network (green), pores (purple)

### Fractal image segmentation and secondary phase reconstruction

Complementing FIB-SEM characterization, x-ray tomography characterization experiments are underway. Tomography experiments provide images of intensity distribution in the bulk of the electrode volume that must be segmented and reconstructed into a 3-D geometry. The intensity value at a particular spatial location (x, y, z) relates to the material phase present. For an n-bit image, intensity values range from 0 to $2^n$-1, while in a composite lithium-ion battery electrode four phases are present: pore, active material, binder and conductive additive. Thus, these $2^n$ values have to be appropriately mapped onto four phases. This step is known as image segmentation. To automate this step we have developed a fractal-based criterion for image segmentation to intuitively segment the available tomography data.

Fractal dimension generalizes the concept of length (distance between two points) for an arbitrary geometry. The Euclidean distance measures the straight line distance, while most of the objects in real world have curved and intricate surfaces. The fractal dimension is a metric of these non-linear features. As the window of observation is decreased, small scale features also become available, and correspondingly the measured fractal dimension changes. The measured value converges when sufficient resolution is achieved. Combined with a region merging segmentation algorithm, the process of stochastic image reconstruction is efficiently automated (Figure III-42).

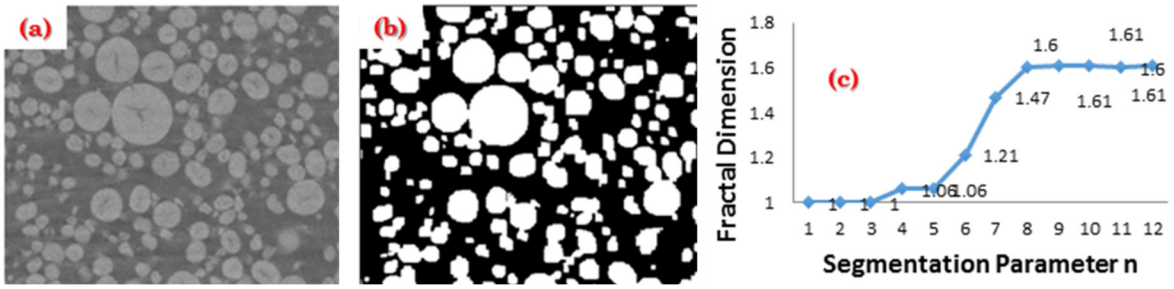


**Figure III-42: (a) Original tomographic image, (b) segmented image based on fractal criterion, (c) fractal dimension converges as the segmentation parameter is increased**

*Tomographic image source: Ebner et al., 2013, Adv. Energy Materials 3 (845).*

Both the amount and local arrangement of the secondary phase significantly affect the electrode-scale microstructural properties. Thus, relative amounts of active material, binder and conductive additive will strongly influence the electrochemical performance of electrodes. At the spatial resolution of tomography experiments, pore and active material phases (which represent larger material volumes) are readily available, while the size of other species, e.g., conductive additives, is very small to be resolved accurately. Thus, the secondary phase (binder + conductive additives) needs to be reconstructed. We have come up with a stochastic regeneration method for the secondary phase based on an energy criterion.

Deposition of the secondary phase takes place preferentially at active material/pore interface and especially in nooks and crannies of the active material network. This specificity is related to difference in energy reduction upon deposition at different spatial locations. This physics is utilized to stochastically add secondary solid phase in the active material network provided by segmented tomography data or stochastically reconstructed microstructures. From experimental electrode composition, the amount of secondary phase is known. Multiple deposition cycles are repeated until one achieves the desired amount. For each of these cycles, first the entire electrode structure is scanned to explore interfacial sites where future secondary phase deposition can take place. Then an energy landscape is formed while accounting for the fact that deposition of secondary phase on active material is fundamentally different than that on pre-deposited secondary phase. Using random numbers, different deposition sites are chosen based on this energy landscape, which leads to newly deposited sites. The preference of secondary phase deposition can be tuned to achieve different deposition structures for the same amount of secondary phase addition, which in turn leads to significantly different porous media properties.

Described in the manuscript [3], once these different electrodes are generated to explore the variation of active material loading, amount of secondary phase and porosity, they are subsequently characterized in terms of corresponding electrode microstructural properties. These abstracted values are later on utilized to perform cell level electrochemical performance simulations using a cell sandwich model based on porous electrode theory. Nickel manganese cobalt oxide ($Ni_{0.33}Mn_{0.33}Co_{0.33}$) is used as representative active material for all the computations, while polyvinylidene fluoride (PVDF) as binder and acetylene black as conductive additive.

When a secondary phase (of conductive additive and binder domain) is added, it reduces the available active material/electrolyte contact, thus lowering down the electrochemical active area which represent sites for Li intercalation. Thus, entry of Li into active material is partially blocked.

Figure III-43 shows impact of secondary phase on electrode effective properties where the tendency of secondary phase to deposit on itself (rather than on the primary phase) is quantified by weight parameter, w. With more secondary phase self-deposition, pore/active material interfacial area increases while the secondary phase/pore area decreases (Figure III-43c). Similar variations are also present on tortuosity and electronic conductivity values (Figure III-43d). The cathode active material in lithium-ion batteries is usually an inferior conductor of electricity. Hence, as secondary phase deposits more on itself, the long range percolation pathways reduce, which leads to reduced conductivity. On the other hand, more self-deposition leads to more restricted transport in the pore phase, which leads to greater tortuosity for more self-deposition.

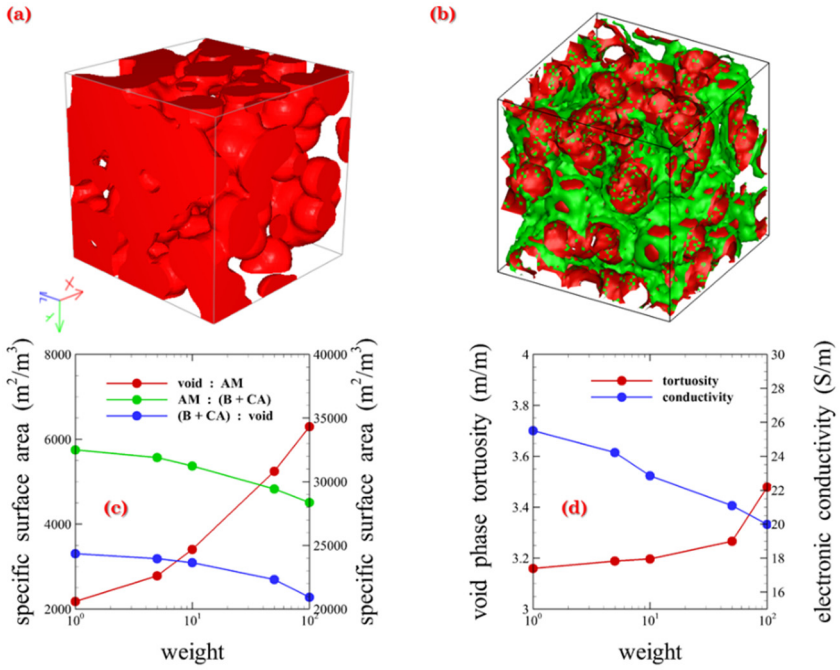


**Figure III-43: Secondary phase addition and microstructure characterization. (a) Original structure containing active material and pore phase (b) solid/pore interface where red represents active material and green the secondary phase. Variation of microstructural properties (c) specific surface area, (d) tortuosity and electronic conductivity as a function of weight factor accounting for preference of secondary phase to deposit on itself**

Figure III-44 shows the impact of active material:secondary phase weight fraction on electrochemical performance of Li|NMC half cells. For each of these electrodes, the porosity is kept constant at 30%. As the amount of active material increases, it leads to increase in electrochemically active area as the area covered by secondary phase decreases. On the other hand, since the active material does not have enough electronic conductivity, the electronic conductivity of the cathode deteriorates as active material:secondary phase ratio increases. These two opposing factors can bring about a non-monotonic variation in cell performance as active material loading is varied (Figure III-44a). This is observable if electronic conductivity of the composite electrode drops below the corresponding ionic conductivity of the electrolyte. Thus, this non-linear trend is observed for low conductivity conductive additive: binder phase, i.e., 0.2:1 and not for 0.8:1. Once enough electronic percolation is achieved, the performance limitation stems from ion blockage effect and leads to inferior performance of cathode with more percentage of secondary phase as shown on Figure III-44b.

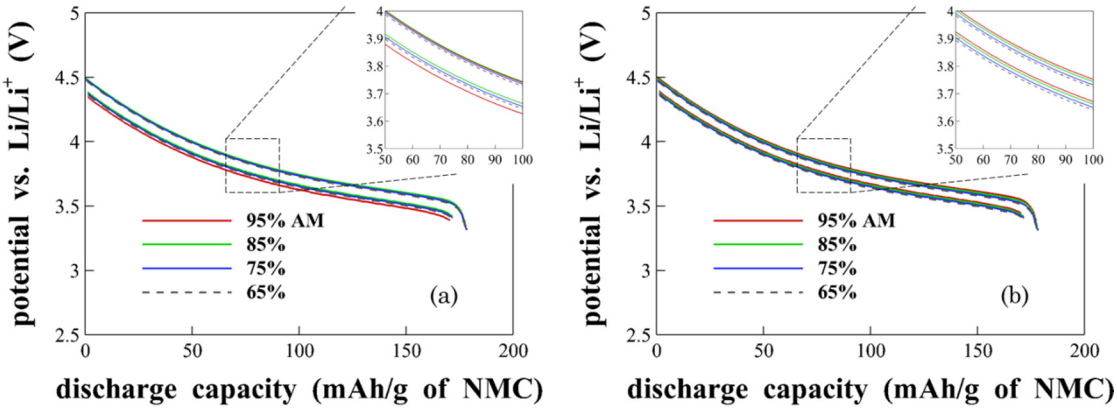


**Figure III-44: Effect of active material:secondary phase ratio on electrochemical performance of Li|NMC half cells. The percentages represent weight fraction of active material available. The lower family of curves correspond to 2 C operation while the upper set is for 0.5 C. (a) High and (b) low electronic conductivity case using 0.2:1 and 0.8:1 conductive additive:binder ratios, respectively**

### Statistical analysis and homogenization

Given a microstructure's reconstructed geometry, several algorithms have been developed and are under evaluation for their ability to accurately quantify surface area, volume fraction, material connectivity, isotropy, tortuosity, and similar properties. Figure III-45 shows pore sizes as distributed throughout the electrode, with pore size indicated by both color and circle size. It is found that the large pore sizes are more likely to occur at the front of the electrode neighboring the separator and at the back of the electrode neighboring the current collector. This is intuitive, as fewer particles can occupy a cross section of electrode at these boundaries. As a result, it is expected that ionic tortuosity will be large in the middle of the electrode and smallest at the edges. This spatial distribution is not captured in macro-homogeneous models and its impact on electrochemical performance will be investigated.

### Direct numerical simulation

Complementing homogenization calculations, the team is developing full electrochemical simulations of the 3-D electrode architecture. Multiple software platforms were evaluated for their ability to efficiently simulate electrochemical physics, with extensibility to add additional physics in the future. The FEniCS open-source finite element code was selected due to its abilities to scale to a massively parallel high-performance computing environment and also quickly accept new physics as the model is enhanced. Preliminary electrochemical simulations have been carried out using FEniCS on sample microstructure geometries. As 3-D data become available from upcoming tomographic experiments, the so-called direct numerical simulation model will be employed to investigate the impact of microstructure on performance, performance limitations, and inhomogeneity of battery electrodes. The model will be validated for multiple electrode designs from ANL of varying thickness. The validated model will serve as a virtual prototyping tool to optimize and enhance the performance and durability of next generation electrodes.

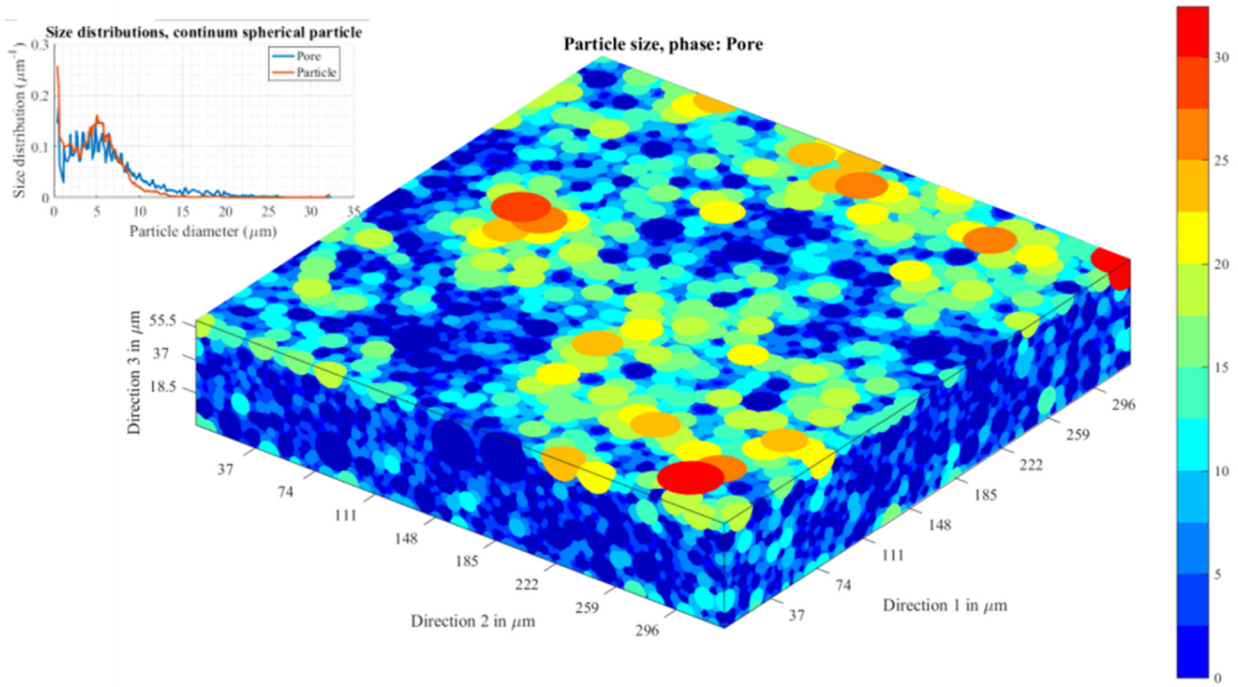


Figure III-45: Microstructure pore size analysis using continuum algorithm

## Conclusions

A new GH-MSMD multiscale electrochemical battery model platform was developed, validated and documented [3]. Compared to previous approaches, the quasi-explicit GH method reduces computation time by 100-1000 fold, greatly improving the usefulness of electrochemical models in computer-aided engineering processes. The model was coupled with optimization software to identify electrochemical model parameters from test data. A recommended model identification approach is under development using graphite/NMC523 half-cell data from ANL ABR program. Following validation with thin electrode samples, the models will be

evaluated for thick electrodes. Thick electrodes increase energy density and reduce battery cost, but can suffer from performance limitations.

Experimental studies at ANL show that higher porosities and lower thicknesses result in better utilization of the active material, especially at high rates, for both NMC523-based positive and graphite-based negative electrodes. Initial FIB-SEM data reveals the complex microstructure of the NMC523 baseline electrodes. Efforts are underway to thoroughly image the three dimensional architecture of the many electrodes using X-ray tomography and electron microscopy techniques. These electrode architectures will then be correlated with the electrochemical performance providing valuable information for the computational modeling efforts.

TAMU developed a fractal-based image segmentation algorithm that provides a consistent, automated approach to image segmentation. Lacking precise microscopy techniques to map binder and conductive additive geometry, TAMU further developed a stochastic reconstruction method to artificially grow the secondary phase on active material geometry available from tomographic images. Mesoscale modeling of these reconstructions shows the electrochemical performance of the cells is an intricate function of electrode porosity and recipe (active material:binder:conductive additive ratio). As conductive additive is increased in the recipe and electronic conductivity of the composite electrode is higher than corresponding ionic conductivity of the electrolyte, performance becomes limited due to secondary phase blocking electrochemical active area, as well as electrolyte phase transport. This substantially affects high C-rate operation of lithium-ion cells. Microstructure analysis shows distributions of pore and particle phases—not accounted for in macro-homogeneous models—whose impact will be quantified through direct numerical simulation of electrochemistry on the 3-D microstructure geometry.

For prediction of battery thermal response to mechanical abuse in case of vehicle crash, we presented a multi-scale simultaneously coupled mechanical-electrochemical-thermal modeling framework, implemented in commercial software LS-DYNA with a user-defined material model. The model enables a combination of computational efficiency and accurate modeling of failure location. The mechanical model is coupled with the electrochemical-thermal model at the microscale through exchange of displacement, temperature, and other field variables. A single element numerical verification study is presented. From the preliminary numerical results, we verify the accuracy of the multiscale mechanical model, and demonstrate the capability of the model to predict mechanical abuse induced short-circuit behavior and the effect of short resistance. To extend the current model to a multi-cell simulation, we need to address continuity and boundary equations for the electrochemical model.

Mechanical failure behavior was evaluated experimentally at SNL on both 12-cell packs and single cells. This has been done to provide both an experimental understanding of how modules can fail during a mechanical crush event, and to provide parameterization and validation for model development efforts. Twelve-cell string testing shows that pack level failure when the force is applied through the face of the pouch cells is caused largely by compaction and fracturing of the electrode layers, while a force applied to the sides of the cell buckles the electrode layers leading to widespread deformation of the cells. The buckling failure mode requires significantly less force to cause a significant failure event compared to face compression.

## Products

### Presentations/Publications/Patents

1. A. Mistry, A. Verma, R. Mukherjee and P. P. Mukherjee, “Image-based reconstruction and statistical characterization of Lithium-ion battery electrode microstructure”, Electrochemical Society Spring Meeting (ECS Spring 2016), San Diego, CA, May29-June 2 (2016).
2. C. Zhang, S. Santhanagopalan, M.A. Sprague, A. Pesaran, “Simultaneously coupled mechanical-electrochemical-thermal simulation of lithium-ion cells,” ECS Transactions 72(24):9-19, Sept. 2016.

## References


1. Howell, D., Cunningham, B., Duong, T, Faguy, P., Overview of the DOE VTO Advanced Battery R&D Program, Annual Merit Review, June 6, 2016.
2. G.-H. Kim, K. Smith, K.-J. Lee, S. Santhanagopalan, and A. Pesaran, J. Electrochem. Soc., 158, A955–A969 (2011).

3. G.-H. Kim, K. Smith, J. Lawrence-Simon, C. Yang, Efficient and Extensible Quasi-Explicit Modular Nonlinear Multiscale Battery Model: GH-MSMD, accepted.
4. A. Mistry, D. Juarez-Robles, M. Stein IV, K. Smith and P. P. Mukherjee, "Analysis of long range interactions in lithium-ion battery electrodes," Journal of Echem. Energy Conversion and Storage (2016).
5. Gilbert, J. Bareño, T. Spila, S.E. Trask, D.J. Miller, B.J. Polzin, A.N. Jansen, D.P. Abraham, "Cycling behavior of NMC523/Graphite lithium-ion cells in the 3-4.4 V Range", J. Electrochem. Soc. 164 (2017)
6. Amin, R. and Y.-M. Chiang, Characterization of Electronic and Ionic Transport in $Li_{1-x}Ni_{0.33}Mn_{0.33}Co_{0.33}O_2$(NMC333) and $Li_{1-x}Ni_{0.50}Mn_{0.20}Co_{0.30}O_2$(NMC523) as a Function of Li Content. Journal of the Electrochemical Society, 2016. 163(8): p. A1512-A1517.
7. Wei, Y., et al., Kinetics Tuning of Lithium-ion Diffusion in Layered $Li(Ni_xMn_yCo_z)O_2$. J Am Chem Soc, 2015. 137(26): p. 8364-7.

# III.C.2. Consortium for Advanced Battery Simulation (CABS)

**John A. Turner, Group Leader, Computational Engineering and Energy Sciences**
Oak Ridge National Laboratory
1 Bethel Valley Road
Oak Ridge, TN, 37831-6164
Phone: 865-241-3943
E-mail: turnerja@ornl.gov

**Brian Cunningham, Battery R&D Technology Manager**
U.S. Department of Energy
Vehicle Technologies Office
1000 Independence Avenue, SW
Washington, DC 20585
Phone: 202-287-5686
E-mail: brian.cunningham@ee.doe.gov

Start Date: October 1, 2015
End Date: September 30, 2018

## Abstract

This report includes four distinct projects. The first two projects, "New experimental protocols" and "Improved property data" were present in last year's CABS section of the Annual Progress Report. This year, two additional projects have been incorporated which were elements of an industry-led project that was unable to proceed in its original form. Due to synergies in project goals and alignment between institutions and staffing between those projects and CABS, they have been integrated into CABS. Those additional projects are as follows:

- Implementing micro-structural models to extend the CAEBAT I simulation technology length scale coverage (LBNL): This project was a component of an industry-led project that was unable to proceed in its original form.
- Implementing micro-structural models to extend the CAEBAT I simulation technology length scale coverage (SNL): This project was also a component of an industry-led project that was unable to proceed in its original form.

Due to synergies in project goals and alignment between institutions and staffing, those projects have been integrated into the CABS project. Accordingly, the FY16 accomplishments are reported here (under their respective subheadings).

## Objectives

CABS objectives can be grouped into four major areas and this report will use these throughout.

- Develop new experimental protocols for characterization of deformation and failure of lithium-ion cells as well as properties of cell components.
- Obtain new experimental property data (mechanical, electrochemical, thermal) to support modeling and validation.
- Deliver new microstructural modeling tools and homogenized models for electrode design.
- Continuous improvement of VIBE/OAS, the software environment developed and deployed under CAEBAT 1 - Enhanced physics capability and improved computational efficiency.

## Accomplishments

We list both milestones, each of which is documented upon completion by a memo and accompanying report, along with data and/or software, and additional accomplishments, often supporting future milestones.

- New experimental protocols
  - Milestone I.1: Report on experimental techniques supporting models.
  - Milestone E.2: Demonstration of single side indentation test with incremental deformation to determine faulting in spirally wound, wound prismatic, and stacked electrodes in hard case.
- Experimental property data
  Measured tracer diffusion in electrolyte solution by pulsed field gradient nuclear magnetic resonance spectroscopy.
- Microstructure data and modeling
  - Milestone E.1: Used X-ray microtomography to obtain three-dimensional microstructures of pristine electrodes, uncalendered and calendered. Reconstructions were processed into surface meshes.
  - Compared macro-homogenous porous electrode-based battery model to microscale model.
- Improved computational efficiency of VIBE/OAS
  - Milestone C.1: Baseline performance profile of VIBE/OAS/AMPERES.
  - Milestone I.2: Deployment of VIBE/OAS with enhanced extensibility and hybrid models resulting in a 2x speedup in time to solution.

### Future Achievements

- New experimental protocols
  Milestone E.4: Release data from mechanical deformation tests to the community.
- Improved property data
  Milestone E.3: Measure multicomponent diffusivities from pulsed field gradient nuclear magnetic resonance spectroscopy and by an approach combining microfluidics and inductively coupled plasma optical emission spectroscopy.
- Microstructure data and modeling
  - Milestone I.3: Construct 3D meshes of electrodes using reconstructions from micro-tomography, including cycled electrodes.
  - Associate microstructure information of electrodes of different thickness with electrochemical behavior.
- Continuous improvement of VIBE/OAS
  - Milestone C.2: Validated constitutive models and failure criteria for electrode materials and spirally wound, wound prismatic, and stacked electrodes under indentation.
  - Milestone I.4: Demonstrate ability of VIBE/OAS to simulate onset of short-circuit due to mechanical abuse informed by microstructure.
  - Milestone I.5: Deployment of VIBE/OAS with integrated multiscale capability.

## Technical Discussion

### 1. New Experimental Protocols

#### Background

CABS is an integrated partnership between Oak Ridge National Laboratory (ORNL), Lawrence Berkeley National Laboratory (LBNL), and Sandia National Laboratories (SNL). LBNL provides data for properties and validation of microstructure models. SNL performs high-resolution microstructure simulations. ORNL develops and performs new mechanics experiments, develops homogenized, layer-resolved, and microstructure models, and deploys software components through VIBE/OAS while enhancing its extensibility and improving computational performance through implementation of new hybrid/adaptive methods and other numerical improvements. ORNL serves as the lead institution, performing overall management.

We report on the four focus areas of the project (experimental protocols, property data, microstructure modeling, and VIBE/OAS development and deployment) in the following sections.

The report for Milestone I.1 summarized experimental techniques available to address mechanical and electrochemical behavior of the lithium-ion cell and cell components and active materials. The scope of experiments can be divided in general by four criteria:

- Determination of material properties for model input
- Determination of geometric features of electrodes (microstructure reconstruction) for meshing
- Validation of models
- Experiments defining failure mode of cells under mechanical abuse

## Introduction

### Experimental Characterization of Electrode Materials and Cell Components

As a part of development of the experimental protocols, we performed an exhaustive search on available experimental techniques to determine the microstructure of electrodes, mechanical properties of lithium-ion cell components and electrode materials, as well as electrochemical and transport properties. The results of this review were summarized in the Milestone I.1 Report. After preliminary testing, some techniques were eliminated or postponed for future exploration as necessary. One of these was the resonant ultrasound spectroscopy (RUS). While the initial experiments with $LiCoO_2$ thin films demonstrated a proof of principle, the method's requirements on sample geometry appeared to be very restrictive. The following are the experimental characterization techniques found essential for the project that we are extensively using to obtain the properties of cells, cell components, and electrode materials. The majority of the mechanics experiments and results will be summarized in the future Milestone E.4 report.

- X-Ray Micro CT
- PFG NMR and micro-fluidics
- Grid nano-indentation
- Compression of cell components
- Tension of cell components
- Single side indentation of the cell

### Experimental Characterization of Deformation and Failure

In order to study deformation and failure mechanisms, mechanical indentation tests on single cells, cell stack and cell pack have been conducted. Similar abuse tests such as crushing, pinching, dropping and impact were able to identify the final failure conditions. However, since the cells underwent thermal runaway as a result, there was not much evidence left to examine. In order to understand what happened to the materials inside the cells, we carried out incremental indentations of the cells in aluminum cans. Multiple steps were used to stop the indentation at various stages and the hard case aluminum cans were able to retain the deformation after the tests. Post-mortem analysis using cross-section imaging and x-ray tomography were performed. The onset of layers folding and the final failure indentation depth have been identified. Finite element analysis model was used to simulate indentations at two loading rates. The simulated load vs. displacement curve matched very well with experimental results.

It should be mentioned that no short was observed when the medium size cell was subjected to out-of-plane compression between two flat plates by the time the load exceeded 60 kN [3]. This suggests that uniform compression of cell layered structure will not lead to separator failure and short circuit and that presence of shear and tensile strains is necessary to trigger battery failure. In the current project, we plan to further investigate the failure mechanisms of the jelly-roll by doing controlled incremental indentation of the cells and performing cross-sectioning to observe internal distribution of strain. Previous experiments [4] on spherical indentation of prismatic cells revealed rather complex internal mechanisms of strain accommodation

(Figure III-46). Multiple fault lines running at approximately 45$^{o}$ can be observed indicating low shear strength of the jelly-roll. In addition due to in-plane constraint, folding of the electrodes can be seen.

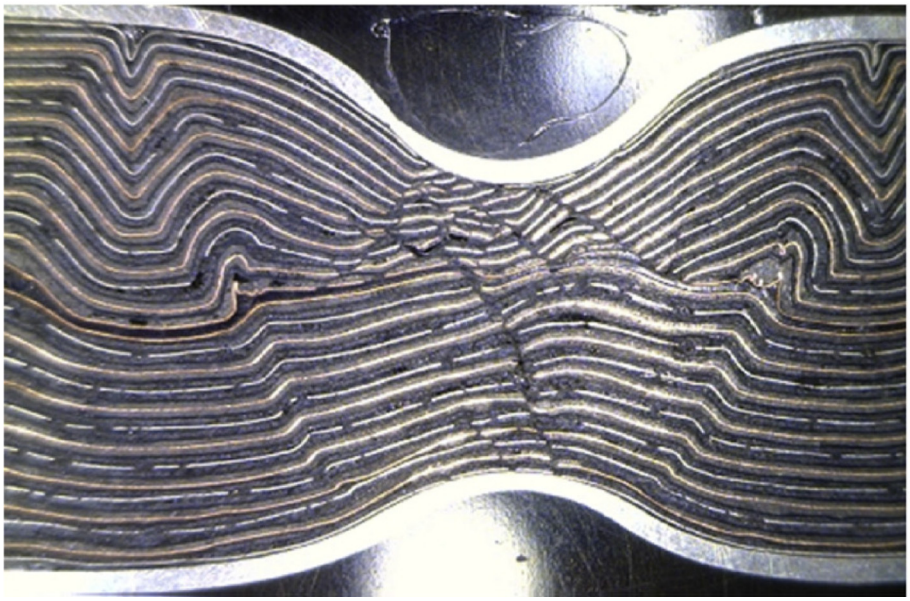

**Figure III-46: Internal shear faults and folding of electrodes in a prismatic cell under pinch test [4]**

This preliminary work identified the faults and studied the effect of the indenter size [4]. We will pursue this research further by studying the formation of the faults from the onset of indentation. Multiple companion specimens will be used for this purpose and incremental indentation will be performed. Prismatic cells are enclosed in a hard case which preserves the internal configuration once the load is removed. Small prismatic cells will be used and each will be mounted in epoxy and cross-sectioned to reveal the internal deformation. A spherical tip will be used; experiments with pressing cylindrical bar across the cell are also envisioned to create two-dimensional deformation. Further studies may involve indentation of a cell on a backing with appropriate stiffness representing the effective stiffness of cell strings. Such a backing can be made out of clay, similar to ballistics testing.

## Approach

Lithium-ion cells for small electronic appliances were used in single-side indentation tests. An opened cell is shown in Figure III-47. The cells are 650-670 mAh in capacity. The cells were cycled 11 times using 250 mA constant current and 4.2V. All cells exhibited typical performance of LCO even after a few years in storage. The homemade mechanical load frame has an actuator driven by a servomotor and a 2000 lb. load cell measures the indentation force. We used a ½ in diameter indenter and two indentation speeds of 0.01”/min and 0.05”/min. A series of cells were indented with increments of 0.01” and 0.02”. One set of the indented cells was cut in half, back filled with epoxy and polished for cross-section imaging. We also explored the x-ray tomography and scanned one cell that was shorted by pinching. The remaining cells will be scanned with a new system at ORNL before cutting.

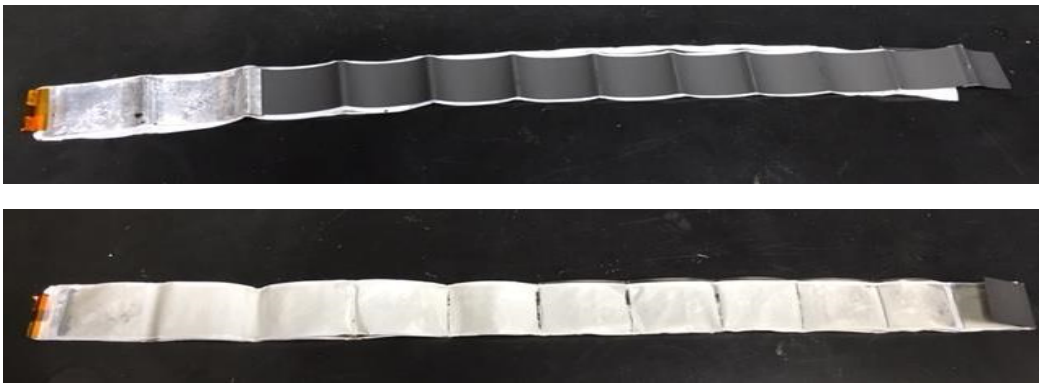

Figure III-47: Opened jelly-roll showing 11 repeated layers

## Results

In order to induce short circuit, one cell was indented at 0.05”/min and the results are shown in Figure III-48. At a depth of approximately 2.8 mm, the load limit of the actuator was reached (1200 lb.). No short circuit was detected by monitoring cell voltage. The rest of the tested cells all have smaller indentation depths.

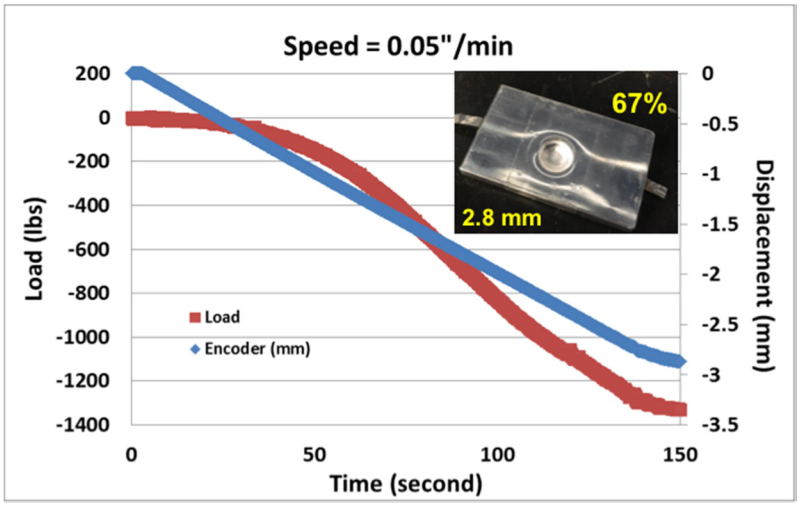


Figure III-48: First cell tested at 0.05 ”/min

In Figure III-49, cells are shown after indentation. The cells were tested in two groups: Group 1 at 0.01”/min and four cells were indented at 0.02” (0.5 mm), 0.04” (1.0 mm), 0.06” (1.5 mm) and 0.08” (2.0 mm), and Group 2 had seven cells and were tested at 0.05”/min with 0.01” steps. Figure III-50 shows the load and displacement vs. time of the 4 cells tested at 0.01”/min. Each test tracked previous results very well indicating high repeatability of the response to indentation. The high cell-to-cell consistency allowed us to use multiple cells for the incremental indentation tests.


Figure III-49: Incremental indentation of cells

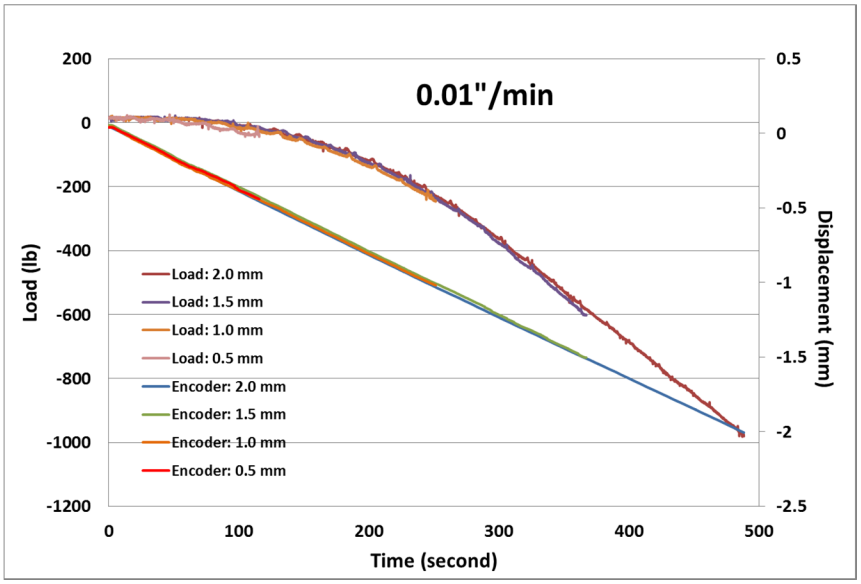


Figure III-50: Load and Displacement as a function of Time of 4 cells at 0.01 ”/min

Figure III-51 shows the results of 7 cells indented at the rate of 0.05”/min. The load curves also tracked each other and are highly repeatable. The indenter was reversed at the same speed and the recoveries of the load were also very similar. When the load vs. displacement curves of the two speeds are plotted together; they did not show any strong dependency on the loading rate. This is consistent with the assumption in our FEA simulation that the Load vs. Displacement is rate independent.

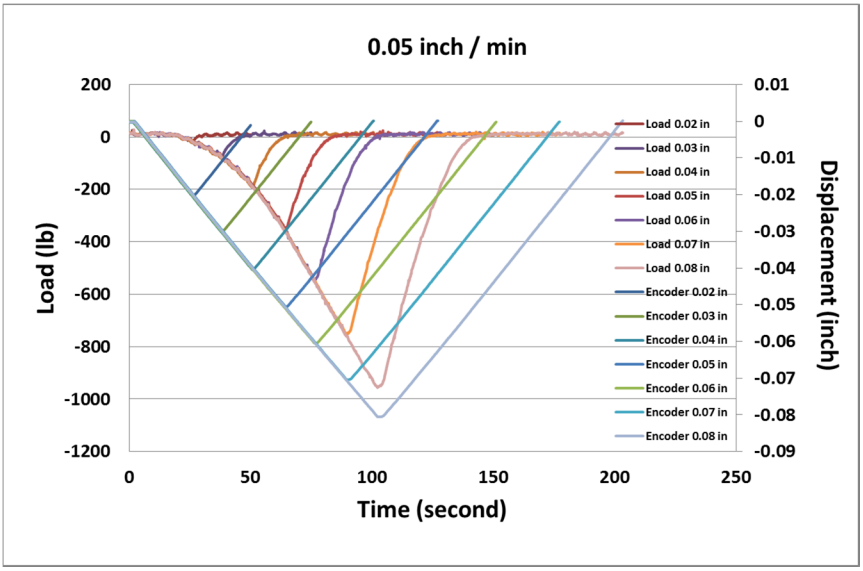


Figure III-51: Load and Displacement as a function of Time of 7 cells at 0.05 ”/min

The next task was to examine the layer movements from the cross-section images. As the indentation depth increased, more layers started to get compressed. The layer folding did not happen until the last sample with 2.75 mm depth. This was experimental confirmation that using the constituent model is reliable in the early stages of mechanical deformation. The final failure associated with folding and cracking of layers occurs just before and after 2.75 mm. Figure III-52 shows high-resolution image of the deformed and folding of layers. One observation was that the anode layers were compressed much more than the cathode layers. This is consistent with the mechanical properties measured on separate components. The graphite anodes showed very different behavior from the LCO materials in the cathodes.

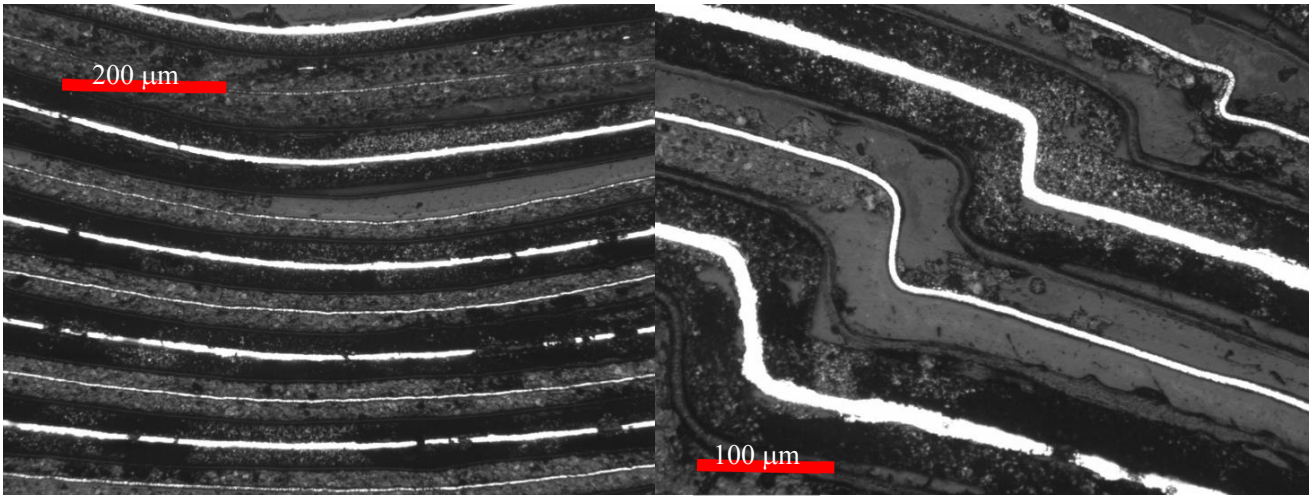


Figure III-52: High-resolution images of deformation and folding

Non-destructive techniques are useful in examining internal damages. X-ray tomography has been used for demonstration shown in Figure III-53. In this particular shorted cell after pinching, the cracking, folding and sliding of the layers can be clearly seen.

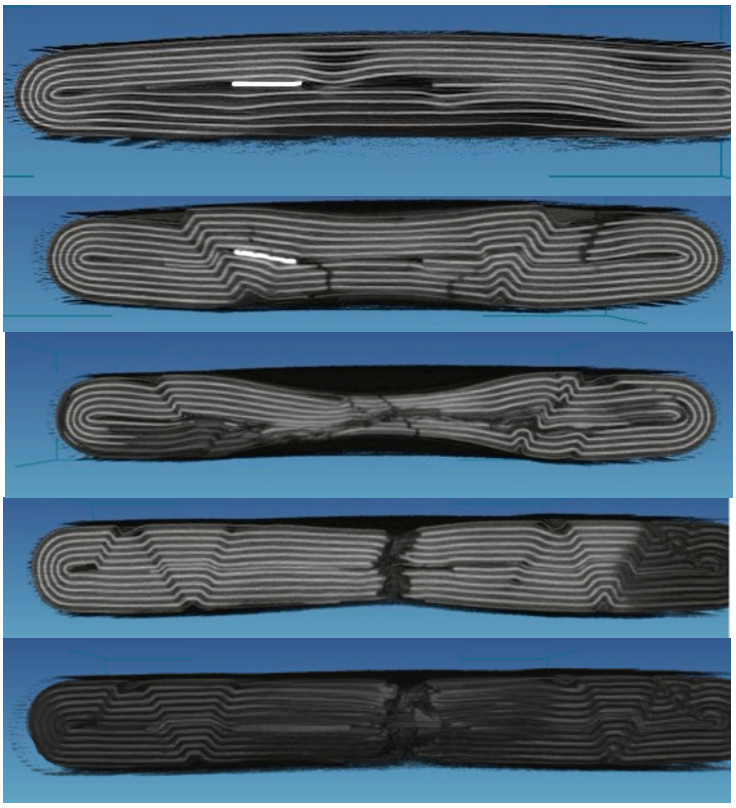

Figure III-53: X-ray tomography of a pinched cell

## Conclusions

Preliminary indentation tests were carried out to incrementally study the deformation of the lithium-ion cells. Follow-on tasks will include further isolation of the final failure and utilization of x-ray tomography.

## References


1. Takahashi, Y., Kijima, N., Dokko, K., Hishizawa, M., Uchida, I., Akimoto, J., Structure and electron density analysis of electrochemically and chemically delithiated LiCoO2 single crystals, J Solid State Chem 180 (2007), 313-321.
2. Wang, D., Wu, X., Wang, Z., Chen, L., Cracking causing cyclic instability of LiFePO4 cathode material, J Power Sources 140 (2005), 125-128.
3. Sahraei, E., Meier, J., Wierzbicki, T., Characterizing and modeling mechanical properties and onset of short circuit for three types of lithium-ion pouch cells, J Power Sources 247 (2014), 503-516.
4. Wang, H., Simunovic, S., Maleki, H., Howard, J.N., Internal configuration of prismatic lithium-ion cells at the onset of mechanically induced short circuit, J Power Sources 306 (2016), 424-430.


# 2. Property Data

## Background

One goal of the CABS project is to produce accurate battery models providing high spatial resolution. Such models rely on accurate property information. Within CABS, the Srinivasan group provides the relevant accurate physical information for incorporation into these detailed models.

These models require high-resolution spatial domains, which can be obtained from electrode microstructure data. The first task of the Srinivasan group was to obtain such data from uncalendered and calendered

electrodes supplied by teammates at ORNL. The resulting microstructure information was provided for use by teammates at SNL in high-resolution simulations.

As another example, accurate transport parameter values paired with concentrated solution theory are vital to the accuracy of battery simulations [1], particularly under demanding use cases. However, diffusion coefficients reported for these battery electrolyte solutions, as measured by electrochemical methods, range over almost two orders of magnitude for a given concentration. This variation might be the consequence of complications that arise in common electrochemical experimental setups, such as convection, side reactions, or bubble formation. Within CABS, the Srinivasan group provides concentration-dependent electrolyte solution transport parameters for use in electrochemical simulations.

Macro-homogeneous, or "macroscale," battery models, originally developed by Professor John Newman, have a long history of providing qualitative predictions of battery behavior at low computational cost. However, detailed information about electrode microstructure is missing from these models, and the models typically diverge from experimental observations at high rates of charge/discharge. This project will improve those macroscale models by incorporating microscale information.

## Introduction

Three-dimensional electrode microstructure information was needed to construct spatial domains for use in the high-resolution electrochemical simulations by teammates at SNL. The Srinivasan group applied hard X-ray microtomography [2] to obtain this microstructure information because this technique is non-destructive and allows one to interrogate samples that are soaked in electrolyte solution. It was decided that samples soaked in solution were likely to be more representative than dry samples of electrodes in real batteries. In order to perform this imaging work, a custom sample holder was designed and fabricated.

For the planned battery simulations by teammates at ORNL and SNL, to provide accurate results, accurate transport parameter values paired with concentrated solution theory will be needed to account for the large concentrations gradients that can develop during battery operation. However, diffusion coefficients reported for these battery electrolyte solutions range over almost two orders of magnitude for a given concentration. This variation might be the consequence of complications that arise in common electrochemical experimental setups, such as convection, side reactions, or bubble formation; indeed, early attempts by the Srinivasan group to use a restricted diffusion method produced unreliable results. For this reason, the Srinivasan group has chosen to explore non-electrochemical approaches to transport property measurement, focusing on methods based on nuclear magnetic resonance (NMR) and microfluidics.

Traditional macroscale battery models involve spatial averaging, which reduces computational requirements, at the cost of a loss of spatial detail. This project will modify traditional macroscale battery models with microscale information in order to improve predictive capabilities. Previous work in the Srinivasan group has included electrochemical experiments along with the development of a corresponding pseudo-2D macroscale model. Leading up to this project, X-ray microtomography was performed on the same electrode material as used in the electrochemical experiments. The work performed over the past year has involved the construction of a microscale model based on this microtomography data and corresponding to the earlier electrochemical experiments and macroscale model.

## Approach

The positive electrodes were prepared by slurry casting on 15 µm thick aluminum foil using the slot-die coater at the ORNL Battery Manufacturing Facility (BMF). The active material was $LiNi_{0.5}Mn_{0.3}Co_{0.2}O_2$ (NMC532), and the slurry composition was in wt% NMC/PVdF/carbon black 90/5/5. The as-cast coating thickness (dry) was measured as 87 µm with gravimetric areal loading of 16.67 mg/cm2. Electrodes were calendered at ORNL to reduce porosity to five levels: 0.5 (light compaction), 0.4, 0.3, 0.23, and 0.18. The representative SEM images of electrode cross-sections show significant material compaction and particle penetration into current collector under calendering (Figure III-54).

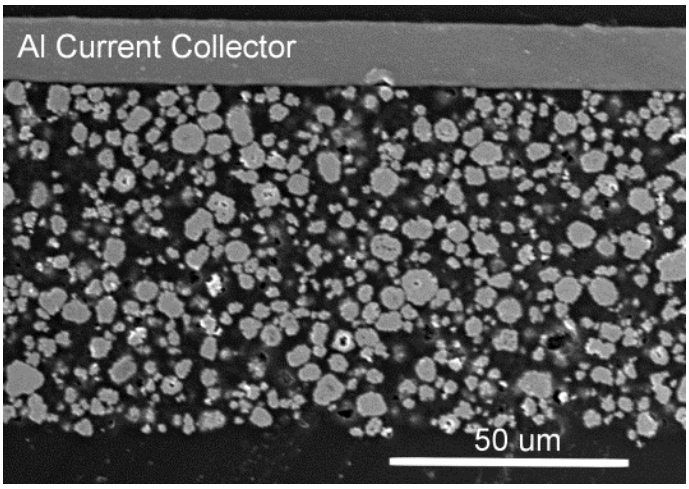


(a)

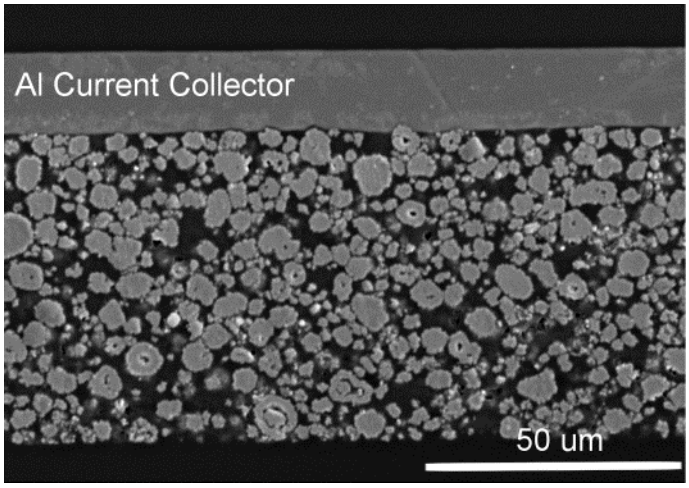


(b)

**Figure III-54: SEM of cross-sections of NMC(532) electrodes (a) as cast with 53% porosity, and (b) calendered to 30% porosity**

Electrode sample disks with 1/16 inch diameters were extracted from laminates provided by ORNL with a hammer-driven punch. In order to image these electrode samples when wet with electrolyte solution using hard X-ray microtomography, a custom sample holder was designed and fabricated (see Figure III-55). Polymer binder swells when immersed in electrolyte solution, so the sample holder was designed to apply light pressure to keep the samples from warping. For efficient use of time, the sample holder was also designed to accommodate multiple samples for simultaneous scanning. Microtomography was performed at the beamline 8.3.2 at the Advanced Light Source (ALS), with the help of beamline scientist Dula Parkinson.

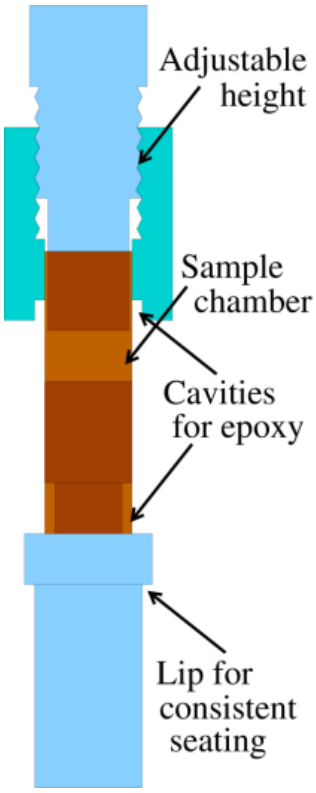


Figure III-55: Diagram of custom X-ray tomography sample holder

Solutions of lithium hexafluorophosphate ($LiPF_6$) in a mixture of ethylene carbonate and diethyl carbonate (EC/DEC), 1:1 by mass, were prepared at concentrations of 0.1 M, 0.25 M, 0.5 M, 0.75 M, 1 M, 1.25 M, and 1.5 M in an argon-filled glovebox at Lawrence Berkeley National Laboratory (LBNL). These were shipped to EMSL for analysis by pulsed field gradient (PFG) NMR [3]. NMR and PFG-NMR experiments were performed for these solutions by EMSL's Kee Sung Han at a range of temperatures (0°C, 10°C, 20°C, 30°C, and 40°C), tracking 1H, 7Li, and 19F. These provided tracer diffusion coefficient values for EC and DEC, and lithium ions ($Li^+$) and hexafluorophosphate ions ($PF_6^-$). A theoretical relationship connecting these tracer diffusivities to concentrated solution theory parameters needed for use in electrochemical simulations was then derived. In addition to the PFG-NMR data, corresponding activity coefficient data is needed to make use of this relationship.

A second non-electrochemical approach using microfluidics to measure diffusion coefficients [4] of $LiPF_6$ in EC/DEC is also under development. Two $LiPF_6$ electrolyte solutions of different concentration will be injected into a Y chip microchannel (Figure III-56), which will allow $LiPF_6$ to diffuse from one solution to the other. At the other end of the microchannel, the flow is separated into two outputs, and samples collected from these outputs will be analyzed with ICP-OES to measure $LiPF_6$ concentration. Changes with respect to the original concentrations indicate diffusion along the width of the microchannel. A COMSOL model combining laminar flow and concentrated solution theory will be applied to calculate diffusion coefficients based on the measured concentration changes.

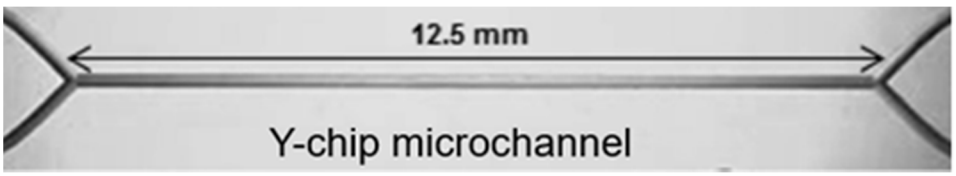


Figure III-56: Picture of Y microchannel chip

Microtomographic reconstructions previously collected from the same electrodes used in electrochemical experiments and modeled through macroscale simulation were processed with semi-automated pipeline to produce pairs of interlocking surface meshes. This pipeline made use of custom programs, Fiji/ImageJ [5], and

Avizo. Each pair consisted of a mesh surrounding an active material phase and a mesh surrounding all other regions (pore, conductive additive, and binder), thought to be soaked with electrolyte solution. Volume fractions were chosen to match those estimated from macroscopic measurements. These meshes were loaded into STAR-CCM+ and incorporated into a virtual battery domain, as shown in Figure III-57. Electrochemical simulations were performed, based on equations that are essentially identical to those used in the macroscale model, but before spatial averaging.

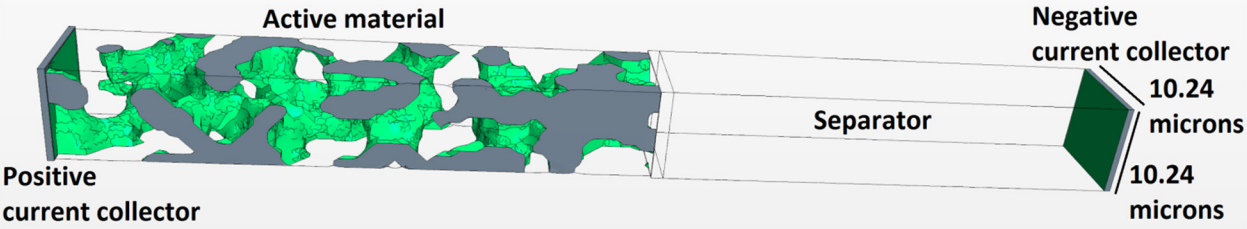


Figure III-57: Battery microscale simulation domain

## Results

The meshes constructed from X-ray microtomography of the ORNL electrodes suggested that neighboring active material particles are fused together and sometimes far from spherical (Figure III-58), which is unrealistic. Unfortunately, the level of noise in these measurements was found to be an obstacle to more highly-resolved spatial domains. In FY17, alternative imaging options that might produce less noisy data will be considered.

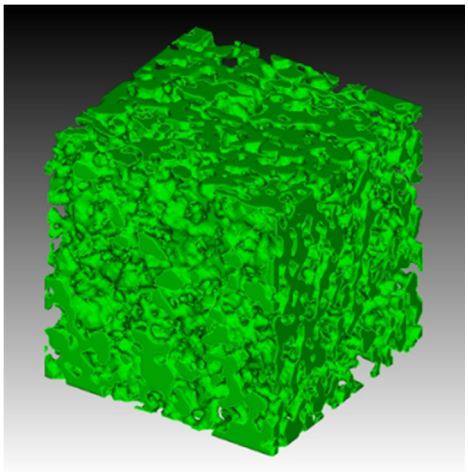

Figure III-58: Reconstruction of uncalendered electrode

Shown in Figure III-59 are the tracer diffusion coefficient values for of $Li^+$, $PF_6^-$, EC and DEC as functions of temperature and concentration, as measured by PFG-NMR. All four species show higher values at higher temperature, as one might expect due to increased thermal agitation, and at lower concentration, as one might expect if ion-ion interactions are relatively strong. The tracer diffusion coefficient values for EC and DEC are very similar, and slightly larger than that of $PF_6^-$, which is in turn larger than that of $Li^+$. This suggests that EC and DEC can be modeled as a single species, and that $Li^+$ has a larger solvated structure than does $PF_6^-$.

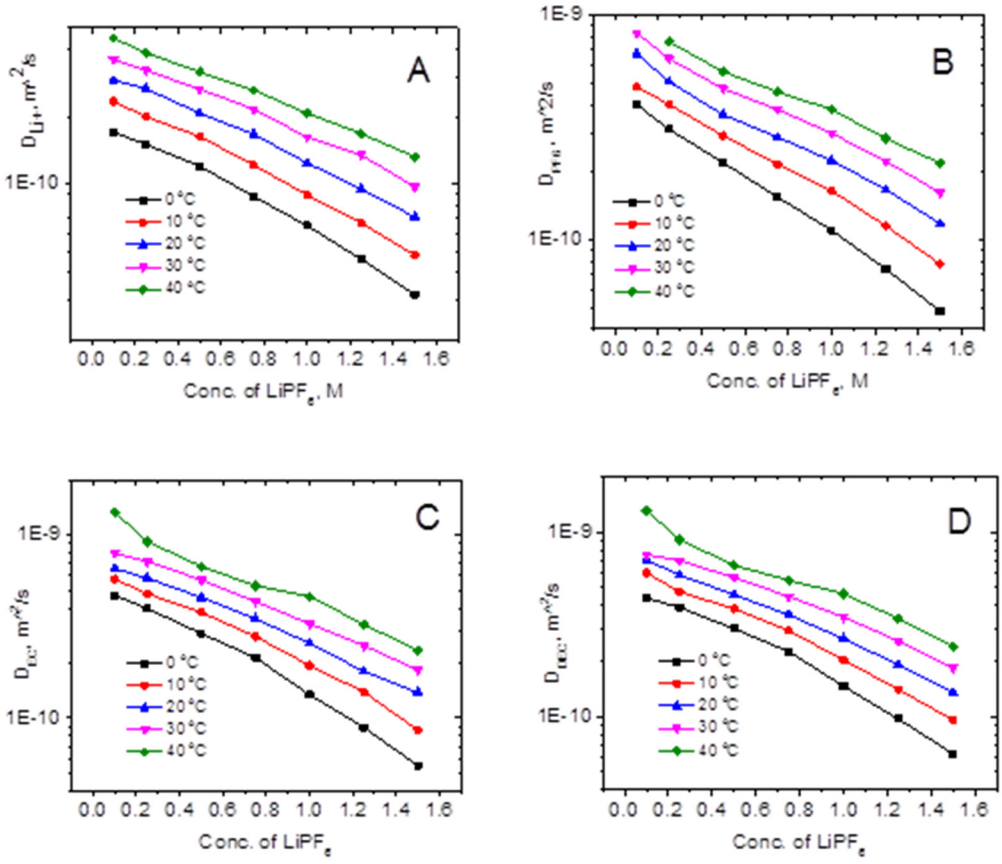


**Figure III-59: Concentration and temperature dependence of tracer diffusion coefficient of $Li^+$ (A), $PF_6^-$ (B), EC (C), DEC (D).**

The microfluidic diffusivity experiments will require accurate measurements of salt concentration. It has been determined that inductively coupled plasma optical emission spectroscopy (ICP-OES) will be suitable for measuring these differences.

Discharge curves from corresponding macroscale and microscale simulations are shown in Figure III-60. Corresponding curves show initial agreement but later diverge, leading to very different capacities. Further analysis suggested that this disagreement comes from two main sources: also in Figure III-60, it is seen that even during a 1C discharge, the interior of the active material was underutilized, because the surface area in the spatial domain was much lower than that in a comparable macroscale simulation, or which would be expected if the particles did not appear "fused." This led to high current density, early surface saturation, and early end of discharge. Better resolved particle surfaces are needed to eliminate this problem. At higher rates, the microscale model overpredicted capacity because solution-phase transport was less limiting than in the macroscale model. A tortuosity analysis of the pore space (Figure III-60) suggested that the tortuosity used in the macroscale simulation was too high. Since the effective diffusivity used in the macroscale simulation led to fairly realistic results, the combination of the macroscale and microscale simulation has suggested that the intrinsic diffusion coefficient is likely to be in error. This finding highlights the need for improved diffusivity measurements, like those planned for CABS.

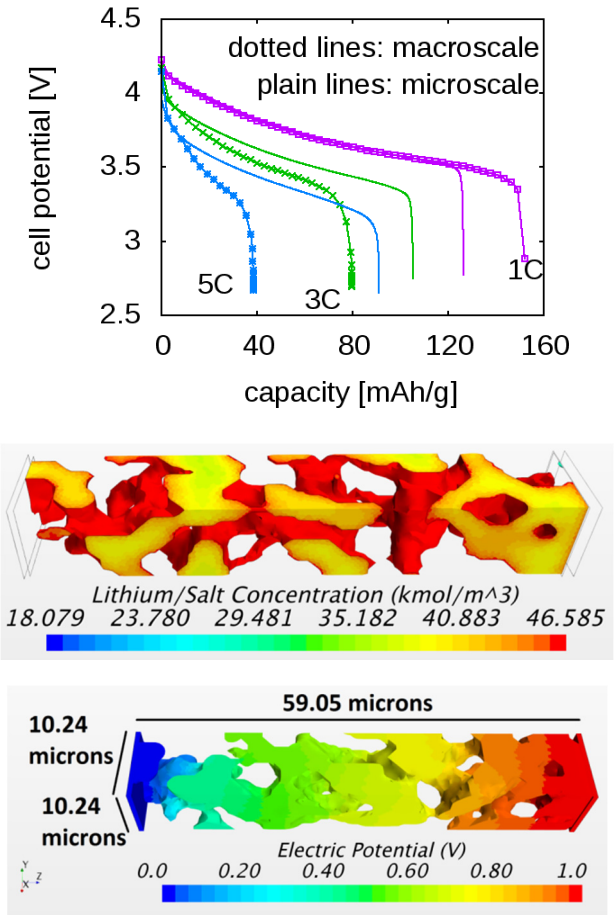


**Figure III-60: (Top): discharge curves from macroscale and microscale simulation, (Middle): Lithium concentration in active material at end of 1 C discharge, and (Bottom): Pore diffusion simulation**

## Conclusions

Within CABS, the Srinivasan group is providing physical information to be used as the basis for electrochemical simulations. Work in FY17 has included X-ray microtomography of electrodes provided by ORNL, conversion to surface meshes used for the construction of simulation domains, tracer diffusivity measurements in electrolyte solution by PFG-NMR, development of a relationship between these tracer diffusivities and the multicomponent diffusivities needed by concentrated solution theory, as well as preparation for upcoming diffusivity measurements using microfluidics and ICP-OES. In FY17, the transport properties of $LiPF_6$ will be further analyzed, completing the measurements needed to obtain multicomponent diffusivities by the two different non-electrochemical approaches.

A microscale simulation on spatial domains generated from X-ray microtomography data and corresponding to an existing macroscale model and electrochemical experiments has been developed. Comparison with the macroscale model and experimental results suggests that further experimental work is needed in order for microscale models without tuning parameters to yield better results than macroscale models with tuning parameters. This will be partially addressed through the planned work of the Srinivasan group within CABS project. In FY17, information extracted from X-ray microtomography images of electrodes of different thickness will be associated with results from electrochemical tests of batteries incorporating these electrodes.

## References

1. J. Newman, D. Bennion, and C. W. Tobias, Adv. In Electrochem. Electrochem. Eng., 5, 87 (1967)
2. J. C. Elliot and S. D. Dover, Journal of Microscopy, volume 26, issue 2, 211-213 (1982)
3. E. O. Stejskal and J. E. Tanner, J. Chem. Phys. 42, 288 (1965)

4. N. Milozic, M. Lubej, U. Novak, P. Znidarsic-Plazl, and I. Plazl, Chem. Biochem. Eng. Q., 28 (2) 215-223 (2014)
5. C. A. Schneider, W. S. Rasband, and K. W. Eliceiri, Nature methods, 9(7): 671-675 (2012)

## 3. Microstructure Modeling

### Background

The packing of electrode particles (e.g., NMC for vehicle technologies) at the mesoscale (e.g., hundreds of particles) strongly influences battery performance. The nature of the packing governs transport pathways for ions (through the electrolyte) and for electrons (through the active material). As the particles swell and shrink during operation due to lithiation-induced density changes, the electrical conductivity evolves. Mechanical stresses also evolve, potentially leading to particle slip and fracture. The conductive binder phase plays a critical role in both of these processes, mitigating stress generation and shifting electron transport pathways. Mesoscale simulations can be used to study these processes, and with this project we seek to develop this simulation process and workflow.

### Introduction

Mesoscale (100s of particles) electrochemical-thermal-mechanical models and simulations of NMC cathodes are an important outcome of the CABS project. While the mathematical model formulation for these mesoscale simulations is well established [1, 2, 3], these simulations also require (1) calibrated parameterization of the mathematical model, and (2) mesostructure geometries on which to perform the simulations. This work was performed in FY16.

### Approach

Mesoscale properties for NMC are primarily gathered from the literature. Key references are Amin [4], Smekens [5], de Vasconcelos [6], and Kam [7]. NMC mesostructure image data is obtained from Ebner [8] and reconstructed using the process described by Roberts [1].

### Results

A complete set of NMC mesoscale simulation properties was obtained from the literature, and the full set is detailed in our C.1.1 milestone report. Using the image data from Ebner [8], we were able to create a computational reconstruction and mesh of a representative NMC pack and prepare it for simulation. A visualization of this 3D reconstruction is found in Figure III-61.

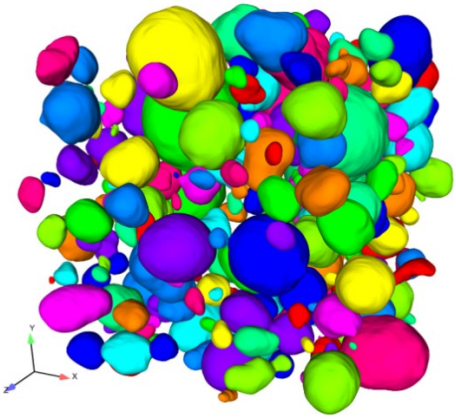

**Figure III-61: 3D visualization of a small domain of NMC particles, with particles separated to allow anisotropic representation and binder placement**
*Source data from Ebner (2013)*

It is also important to verify the numerical implementation of mesoscale models. An important part of this is solution verification, which helps one understand the required mesh resolution to accurately capture the physics. This can be studied for the capture of geometrical parameters (volume, surface area, contact area) and physical properties (effective conductivity, effective elastic modulus, tortuosity). A highlight of this study is found in Figure III-62, with a full set of results being prepared for publication.

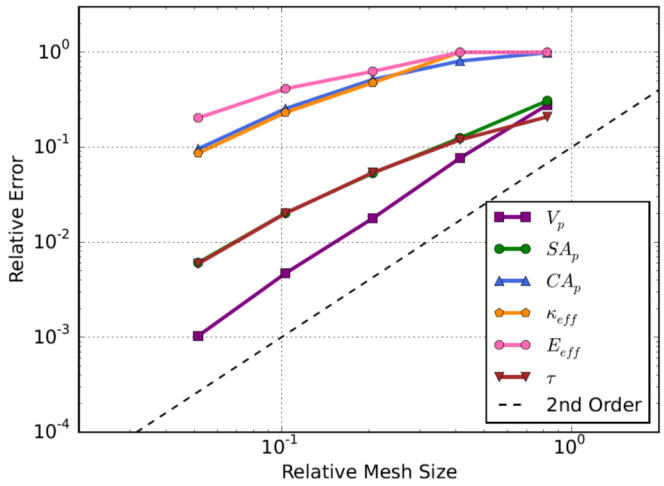


**Figure III-62: Solution verification (mesh refinement) of mesoscale simulations for both geometrical and physical properties showing an approach to ideal second-order convergence**

## References


1. S. A. Roberts, V. E. Brunini, K. N. Long, and A. M. Grillet, "A Framework for Three-Dimensional Mesoscale Modeling of Anisotropic Swelling and Mechanical Deformation in Lithium-Ion Electrodes," J. Electrochem. Soc., vol. 161, no. 11, pp. F3052–F3059, 2014, doi: 10.1149/2.0081411jes.
2. H. Mendoza, S. A. Roberts, V. E. Brunini, and A. M. Grillet, "Mechanical and Electrochemical Response of a LiCoO2 Cathode using Reconstructed Microstructures," Electrochimica Acta, vol. 190, pp. 1–15, 2016, doi: 10.1016/j.electacta.2015.12.224.
3. S. A. Roberts, H. Mendoza, V. E. Brunini, B. L. Trembacki, D. R. Noble, and A. M. Grillet, "Insights into lithium-ion battery degradation and safety mechanisms from mesoscale simulations using experimentally-reconstructed mesostructures," J. Electrochem. Energy Convers. Storage, 2016, doi: 10.1115/1.4034410.
4. R. Amin and Y.-M. Chiang, "Characterization of Electronic and Ionic Transport in $Li_{1-x}Ni_{0.33}Mn_{0.33}Co_{0.33}O_2$ (NMC333) and $Li_{1-x}Ni_{0.50}Mn_{0.20}Co_{0.30}O_2$ (NMC523) as a Function of Li Content," J. Electrochem. Soc., vol. 163, no. 8, pp. A1512–A1517, Jan. 2016, doi: 10.1149/2.0131608jes.
5. J. Smekens, J. Paulsen, W. Yang, N. Omar, J. Deconinck, A. Hubin, and J. Van Mierlo, "A Modified Multiphysics model for Lithium-Ion batteries with a $Li_xNi_{1/3}Mn_{1/3}Co_{1/3}O2$ electrode," Electrochimica Acta, vol. 174, pp. 615–624, Aug. 2015, doi: 10.1016/j.electacta.2015.06.015.
6. L. S. de Vasconcelos, R. Xu, J. Li, and K. Zhao, "Grid indentation analysis of mechanical properties of composite electrodes in Lithium-ion batteries," Extreme Mech. Lett., doi: 10.1016/j.eml.2016.03.002.
7. K. C. Kam, A. Mehta, J. T. Heron, and M. M. Doeff, "Electrochemical and Physical Properties of Ti-Substituted Layered Nickel Manganese Cobalt Oxide (NMC) Cathode Materials," J. Electrochem. Soc., vol. 159, no. 8, pp. A1383–A1392, Jan. 2012, doi: 10.1149/2.060208jes.
8. M. Ebner, F. Geldmacher, F. Marone, M. Stampanoni, and V. Wood, "X-Ray Tomography of Porous, Transition Metal Oxide Based Lithium Ion Battery Electrodes," Adv. Energy Mater., vol. 3, no. 7, pp. 845–850, 2013, doi: 10.1002/aenm.201200932.

## 4. Continued Improvement of Virtual Integrated Battery Environment (VIBE)/ Open Architecture Software (OAS)

### Background

The Virtual Integrated Battery Environment (VIBE) is an open architecture platform for battery simulation that integrates software from industry, academia and national labs. Algorithmic and software design improvements can improve VIBE's computational efficiency, enabling faster simulation of rapid discharge of cells under various abuse and electrical short scenarios and drive cycles of battery pack.

### Introduction

Open Architecture Software (OAS) is a component-based framework implemented in Python [1]. The framework provides a set of services for components such as data/file management, resource and task management and configuration management. The simulation driver contains the global time loop and dictates the order in which components are called. Each component internally can utilize own time stepping algorithm where the order of execution is dictated by the data dependencies among the components. The core of the framework runs as a single Python process, and each component is spawned as separate processes that invoke underlying physics code. The framework services control the various software components through component adapters. The components update the battery state through state adapters. The battery state is the minimal digital description of the battery in space and time. The OAS framework, along with physics and support components and the adapters constitute the Virtual Integrated Battery Environment (VIBE).

In our approach, a multi-dimensional representation of battery is discretized independently for different transport phenomenon. Multi-material interfaces are kept intact without assumptions of homogeneity. A detailed description of the technique can be found in reference [2]. Two models for electrochemical behavior were used. The first model, known as Newman-Tiedemann-Gu (NTG) model, describes the overall characteristics of the cell without resolving local kinetics of electrochemical reactions or the internal concentration and potential gradients within the cell-sandwich. The NTG model has been widely used in cell and pack-level thermal modeling due to simplicity of its implementation. The second implemented model for electrochemistry is based on porous electrode theory. The corresponding component within the framework is called DualFoil. The model employs one-dimensional description of the lithium-ion transport from the negative electrode and into the positive electrode. Thermal transport and Laplace equation for charge transport are solved using AMPERES, an unstructured 3D Finite Element (FE) code developed at ORNL. Given the different spatiotemporal scale of electrochemical and thermal transport, the simulations are conducted at respective scales using operator-splitting method so that we have an efficient computational scheme to solve the coupled problem. The electrochemistry model requires a more refined discretization along the thickness of the cell compared to the thermal transport where a coarser discretization is sufficient.

We anticipated two main time consuming stages. The first includes exchanging the information between the different discretizations and models. The component adapters exchange the volume-averaged data via the battery state. Hence a significant portion of the component task is computing these averages at each time step. The second involves reinitializing the physics-based components by their solution from the previous time-steps. For 3D representations, this restart process includes building of element connectivity and degree of freedom map. For small problems, the computer time for initialization is negligible whereas for simulations of battery packs with thousands of degrees of freedom, initialization introduces significant overhead at each time integration step.

### Approach

For simulations of battery packs with thousands of degrees of freedom, initialization becomes significant. Each of the physics-based component is wrapped in a python driver with a light interface that plugs into the OAS framework. Each component is invoked during time marching inside the main simulation driver. Stepping through simulation time loops involves complete execution of the underlying code. Implementation of a server/client mode will avoid stopping and re-initializing components. This entails launching underlying physics-based component as a daemon instead of end to end invocation at each time step. The python wrapper translates calls from simulation driver into messages to the code daemon. This allows the physics components unchanged with minor changes to the interface. Time-stepping proceeds whenever the battery state is updated

and continues until the end of the simulation. The battery state server will reside in memory, which will allow VIBE components to update and retrieve solution data without file-based communication. This is an essential feature for flexible plug-and-play, and will benefit all OAS compliant components.

## Results

In order to measure the improvement in performance, a test case was used in which four pouch cells are connected in parallel to form a battery module (4P). No cooling fins were placed between the cells in this model. Simulations were conducted using symmetric cooling to the module surfaces with a convective heat transfer coefficient of 35 W $m^{-2}$ $K^{-1}$. A 5C constant current discharge boundary condition results in temperature distribution with maximum value of 327 K at the core of the module. The mesh consists of approximately 150,000 FE nodes and 308 zones in the whole module thus resolving each current collector.

The simulation completed nine global time steps till end of discharge. At each time, the physics based components restart from the previous state. We profiled the physics based components and respective python adapters such as state adapters tasked with preparation of input and processing of output from the components.

Profiling of the simulation using VIBE with the new continuous execution mode of the Electrical, Thermal components based on AMPERES demonstrated a 49% reduction in total simulation time (approximately 2x speedup in simulation performance).

## References


1. S. Allu, S. Kalnaus, S. Simunovic, J. Nanda, J. A. Turner, and S. Pannala, A three-dimensional meso-macroscopic model for Lithium-ion intercalation batteries, Journal of Power Sources, vol. 325, pp. 42–50, Sep. 2016. doi:10.1016/j.jpowsour.2016.06.001.
2. H. Zhou, K. An, S. Allu, S. Pannala, J. Li, H. Z. Bilheux, S. K. Martha, and J. Nanda, Probing Multiscale Transport and Inhomogeneity in a Lithium-Ion Pouch Cell Using *in situ* Neutron Methods, ACS Energy Letters, pp. 981–986, Oct. 2016. doi:10.1021/acsenergylett.6b00353.


## Products

## Presentations/Publications/Patents


1. S. Allu, S. Kalnaus, S. Simunovic, J. Nanda, J. A. Turner, and S. Pannala, A three-dimensional meso-macroscopic model for Lithium-ion intercalation batteries, Journal of Power Sources, vol. 325, pp. 42–50, Sep. 2016. doi:10.1016/j.jpowsour.2016.06.001.
2. H. Zhou, K. An, S. Allu, S. Pannala, J. Li, H. Z. Bilheux, S. K. Martha, and J. Nanda, Probing Multiscale Transport and Inhomogeneity in a Lithium-Ion Pouch Cell Using *in situ* Neutron Methods, ACS Energy Letters, pp. 981–986, Oct. 2016. doi:10.1021/acsenergylett.6b00353.
3. H. Wang, S. Simunovic, H. Maleki, J. N. Howard, and J. A. Hallmark, Internal configuration of prismatic lithium-ion cells at the onset of mechanically induced short circuit, Journal of Power Sources, vol. 306, pp. 424–430, Feb. 2016. doi:10.1016/j.jpowsour.2015.12.026.
4. A. Kumar, S. Kalnaus, S. Simunovic, S. Gorti, S. Allu, and J. A. Turner, Communication — Indentation of Lithium-ion Pouch Cell: Effect of Material Homogenization on Prediction of Internal Short Circuit, Journal of The Electrochemical Society, vol. 163, no. 10, pp. A2494–A2496, Sep. 2016. doi:10.1149/2.0151613jes.
5. K. Higa*, S.-L. Wu*, D. Y. Parkinson, Y. Fu, V. Battaglia, and V. Srinivasan, “Macroscale vs. Microscale Simulation of Porous Battery Electrodes,” 229th Meeting of the ECS, #209, San Diego, CA, June 2016. *These authors share equal credit for this work. Part of this work was funded through the Battery Materials Research program.
6. S. A. Roberts, B. L. Trembacki, H. Mendoza, K. N. Long, V. E. Brunini, A. M. Grillet, “Mesoscale Modeling of Lithium-Ion Battery Electrodes: Computational Requirements and the Role of Polymeric Binders.” 229th Electrochemical Society Meeting, San Diego, CA, May 2016.
7. S. A. Roberts, H. Mendoza, V. E. Brunini, B. L. Trembacki, D. R. Noble, and A. M. Grillet, “Insights into lithium-ion battery degradation and safety mechanisms from mesoscale simulations using

experimentally-reconstructed mesostructures," J. Electrochem. En. Conv. Stor, 13(3), 031005 (2016). DOI: 10.1115/1.4034410.

# III.C.3. Development and Validation of a Simulation Tool to Predict the Combined Structural, Electrical, Electrochemical and Thermal Responses of Automotive Batteries (Ford Motor Company)

**Dr. James Marcicki, Principal Investigator**
Ford Motor Company
Product Development and Strategy Analytics
15403 Commerce Drive South
Dearborn, MI 48120
Phone: 313-845-2489
E-mail: jmarcick@ford.com

**Adrienne Riggi, DOE Program Manager**
National Energy Tech Lab
3610 Collins Ferry Road
P.O. Box 880
Morgantown WV 26507-0880
Phone: 304-285-5223
E-mail: adrienne.riggi@netl.doe.gov

Start Date: January 1, 2016
End Date: December 31, 2018

## Abstract

### Objectives

Develop and validate a simulation tool to predict the combined structural, electrical, electrochemical and thermal (SEET) response of automotive batteries to crash-induced crush and short circuit, overcharge, and thermal ramp, and validate it for conditions relevant to automotive crash.

### Accomplishments

- Automotive grade lithium-ion cells were selected and purchased, and initial component testing conducted.
- An analysis of existing models and input parameters was completed.
- Basic assumptions for the model were formulated.
- A test matrix was developed for cell-level software validation experiments, and a test site selected.
- A preliminary version of the software was developed and demonstrated for external short circuit and crush leading to internal short circuit scenarios. Multiphysics behavior is coupled to the mechanical models, including the localization of current density and corresponding temperature response.
- Techniques such as the use of layered solid elements and macro scale meshes were developed to reduce simulation complexity, and demonstrated significant reductions in calculation times.

### Future Achievements

- Complete multiphysics framework and enhanced material models.
- Identify and obtain required model inputs for both project cell types to complete input database.
- Integrate solvers into Alpha version model.
- Formulate development assumptions for the Beta version model.
- Select and build hardware for use in the Beta model validation.
- Create multiphysics solvers and material models for the Beta model.

## Technical Discussion

### Background

The use of lithium-ion batteries in electric drive vehicles is becoming increasingly important, and understanding the behavior of these high-energy batteries in crash situations is a major effort in the industry. Ford Motor Company has long been involved in this area and has expertise in vehicle safety analyses and crash modes. In this project, Ford Motor Company, along with its partner Oak Ridge National Laboratory (ORNL), will develop and validate a simulation tool with unprecedented fidelity to predict the combined structural, electrical, electrochemical, and thermal response of automotive batteries to crash-induced crush and short circuit. Previously, Ford conducted related battery abuse simulation projects with ORNL, NREL, and the Livermore Software Technology Corporation (LSTC). Ford also recently completed a three-year, $4.2M battery safety performance project funded by the Department of Transportation (DOT/NHTSA) featuring over 200 discrete lithium-ion cell-string, module, and pack experiments, testing such abusive conditions as short circuit, overcharge, and crush. These data will guide simulation tool development and provide simulation case studies, and the working knowledge of test site capabilities will ensure the quality of new validation experiments performed in the project. Ford also built significant experience related to battery modeling software development as a participant in prior Department of Energy (DOE) funding opportunities.

The ORNL team is experienced in developing multiphysics software models. It has developed the CAEBAT Open Architecture Software (OAS) - a modular and extensible software infrastructure that supports multiple modeling formulations and computer codes. These computational models couple the physical phenomena governing lithium-ion batteries, including electrochemistry, electronic transport, heat transport, and mechanics. The coupling strategies can range from one-way coupling, where the results from one physics model are provided to another, to fully-implicit nonlinear coupling where all the physics models are solved simultaneously. The overall computational suite, named Virtual Integrated Battery Environment (VIBE), has been used to optimize and design novel thermal management solutions for pouch cells through an ARPA-E project, study cell and cell-string failure under mechanical abuse for a DOT/NHTSA project, and for other battery simulations. ORNL is also investigating the use of composite modeling elements to reduce computational complexity and time.

The expected benefits of the simulation tool are to reduce development time and cost by reducing the number of physical prototypes required, and improve the abuse response of battery systems. A better understanding of potential failure modes should lead to safer batteries and optimized protection systems. The development of simulation tools should also enable a design process for batteries that mirrors other automotive components that rely heavily on computer-aided engineering (CAE) analysis for guidance in the early stages of design.

### Introduction

This is the first year of a three-year project to develop a practical simulation tool for predicting battery abuse response. The project plan including major constituents and progression based on case studies is shown in Figure III-63.

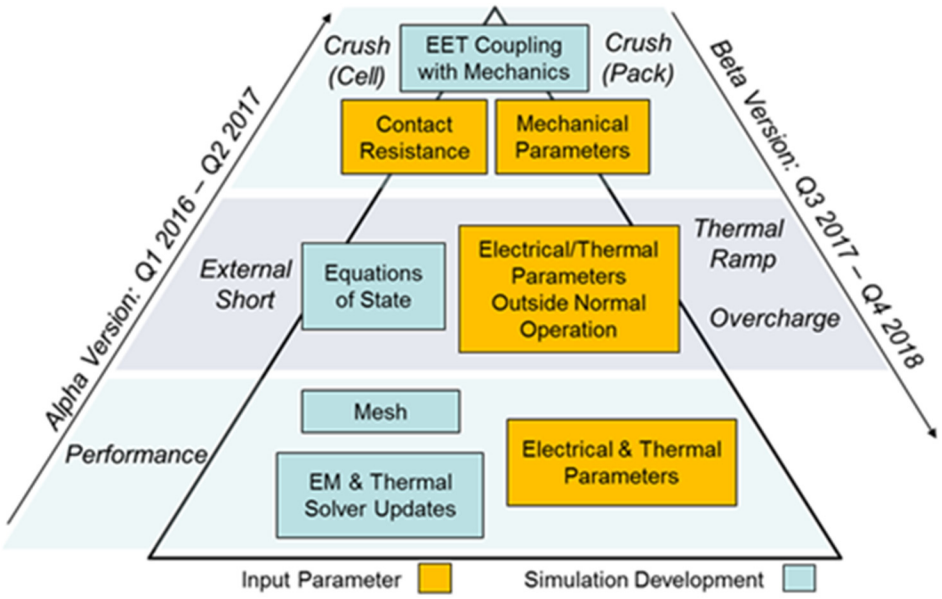


**Figure III-63: Project schematic showing major constituents and progression of the Alpha and Beta versions**

The first half of the project is focused on developing an Alpha version of the model. This includes developing new, battery-specific keywords within LS-DYNA, identifying electrical, thermal, and mechanical input parameters, validating the model for performance situations where the cells are cycling in their intended operating mode, demonstrating preliminary abuse simulations for external short and crush, and enhancing the composite element formulations within LS-DYNA to provide accurate representations of battery material mechanics. Importantly, one-way coupling mechanisms linking the structural response to the electrical and thermal response have been implemented, and initial simulation predictions have been compared to test results from previous studies to confirm that the solvers are directionally accurate. Physical testing of full cells will begin in the second year for model validation, and further testing of cell components will be conducted to determine critical physical parameters for the model.

## Approach

- Develop innovative material constitutive models and finite element method (FEM) element formulations that capture the mechanical response of cell components, including the case material, electrodes, separator, and their interactions with electrolyte.
- Clearly identify the required input parameters for the new constitutive models, FEM element formulations, and exothermic, electrochemical reaction state equations governing multiphysics phenomena during crush-induced electrical short, thermal ramp, and overcharge conditions.
- Design and execute a test matrix encompassing automotive crash strain rates, at a number of kinetic energy levels and physical orientations likely to occur during vehicle impacts.
- Develop integrated modeling tools which demonstrate high-fidelity predictions of the onset of thermal runaway from the experimental test matrix using commercially available cells, module, and packs, spanning multiple chemistries relevant to automotive applications.
- Maintain high-fidelity predictions while exploring methods to reduce the computational complexity of the model, and deliver a practical tool that is integrated with ORNL's OAS, for a broad customer base within automotive product development.

## Results

During the first three quarters of the first year, two types of automotive grade lithium-ion cells were selected and purchased to support model validation activities. A test matrix was established and a test site selected.

Tensile and compressive testing of cell components is roughly 80% complete. This testing is being carried out to establish the model input database needed to simulate the cell response. Cell teardowns have been conducted

to generate test samples, including dogbone samples for tensile testing and disks for compression. In general, the first cell separator tensile response is isotropic within the bounds of experimental repeatability, while the second cell separator exhibits a strong orientation dependence. Both cell types exhibit a 10 – 15% decrease in failure strain going from 0.01/s to 0.1/s strain rates, but otherwise qualitatively similar tensile responses. The electrode tensile data show a relatively brittle response, which indicates that the interaction between the coating and metal current collector produces a strain localization effect. All compressive tests are qualitatively similar, with observable increases in the slope of the force-displacement response with increasing compression. The test data has been used to select and parameterize material models for the separator mechanical response incorporated into cell-level simulations. The experimental procedures are illustrated in Figure III-64.

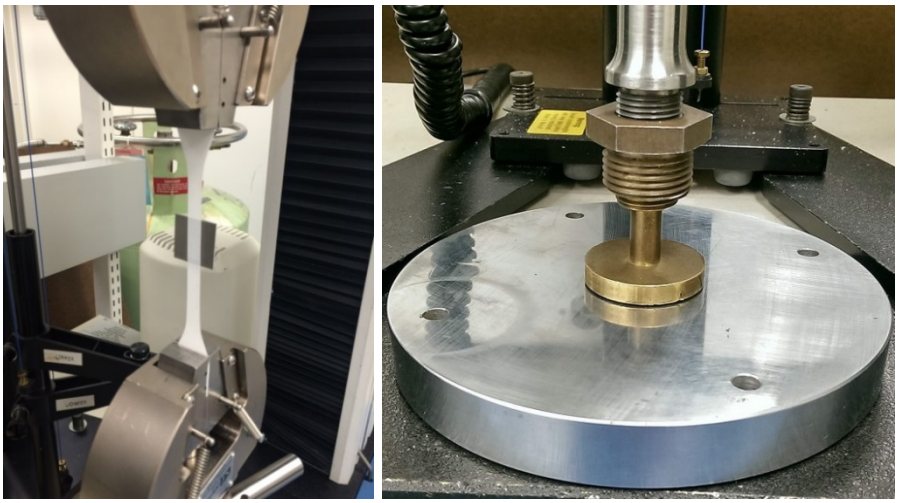

**Figure III-64: Separator tensile test (left) and compression test (right)**

Analyses of existing models and formulations of assumptions helped direct further development of the model. Battery multiphysics models have been developed within the LS-DYNA thermal and electromagnetism solvers. The battery model relies upon a spatially distributed equivalent circuit model that is implemented as illustrated in Figure III-65. The input parameters are dependent on state of charge, temperature and current direction, and coupling mechanisms are in place between the electrical, thermal, and structural solvers. The contact algorithms for detecting mechanical contact and quantifying contact resistance have been updated to be compatible with the new battery keywords. Preliminary models were demonstrated for external short circuit and internal short circuit case studies that include basic characteristics representative of crash events. For example, the mechanical time scale occurs much faster than the electrical and thermal consequences, so the simulation first uses explicit time integration, then freezes the structural response and performs implicit time integration.

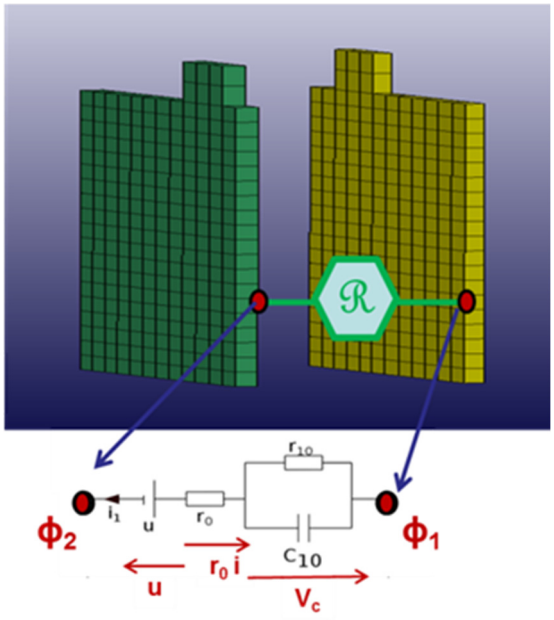


Figure III-65: Integration of spatially distributed, equivalent circuit battery models with finite element models in LS-DYNA

In the first case study, a conducting metal rod moves into contact with the tabs to initiate an external short circuit. Once the contact is initiated, the discharge begins and the cell voltage begins to decrease as energy is removed. The heat generated by the cell is mapped to the LS-DYNA thermal solver to compute the distributed temperature rise. The resistance of the short is automatically computed based upon the conducting path geometry and assigned conductivity. The setup and thermal fringe plots are summarized in Figure III-66. Additional work is planned to better quantify and model the contact resistance at the interfaces between parts.

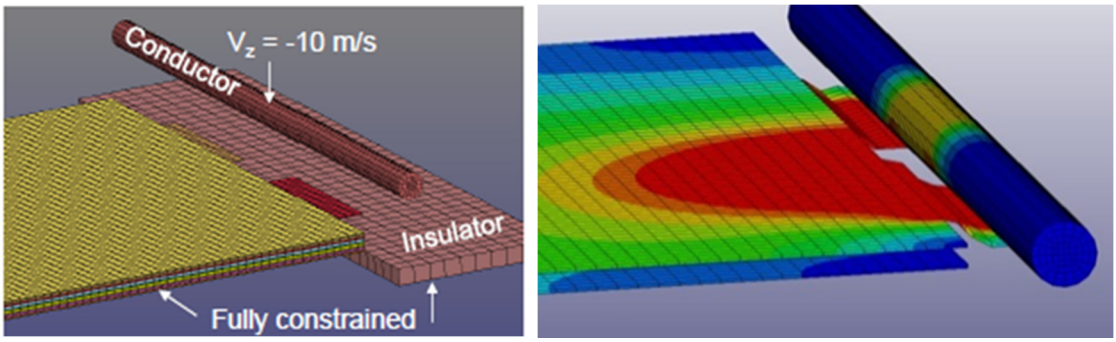


Figure III-66: Model setup for a mechanically-induced external short circuit, and thermal fringe response after contact is initiated (red is warmer, blue is colder)

A second case study has been conducted for cell crush leading to internal short circuit. A spherical indenter of 75 mm radius is brought into contact with the broad face of the cell, along its midsection. Once the compression across any unit cell exceeds a pre-defined failure threshold, the equivalent circuit models in that area are replaced with resistive constraints and discharge through those shorted areas begins. The resistive heat generated by current flow through the short, as well as the resistive and entropic heat sources of the still functional areas of the cell, are mapped to the thermal solver. The mechanical and thermal fringe plots are shown in Figure III-67.

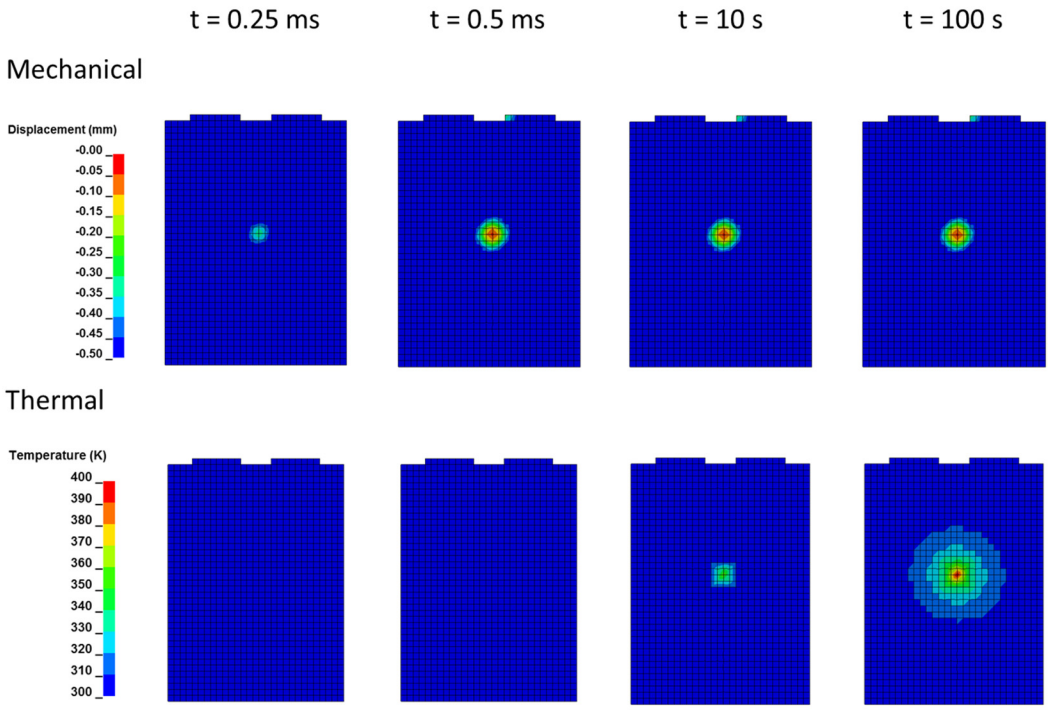


**Figure III-67: Cell crush mechanical and thermal simulation output, demonstrating the solver capability and separation of time scales**

Progress was also made in exploring meshing strategies to reduce complexity and computation time. A factor of 10 reduction in simulation time was achieved with minimal loss of accuracy by moving from a Meso (where all unit cells are resolved) to a Macro mesh (where only one representative unit cell is modeled). The Macro mesh is expected to enable external short circuit simulations of large-scale hardware, since it drastically reduces the element count per cell and therefore requires fewer computations per time step. A 10C discharge simulation was conducted to compare the model types, which demonstrated minimal impact on model accuracy.

We have benchmarked and validated the 3D coupled electro-chemical and thermal transport simulation of a single pouch battery with 17 cathode layers with the experimental values published in the literature on NMC. This demonstrated the speed up of the variable order adaptive time-stepping algorithms on parallel architecture systems. The simulation results show reduced time to computing a constant current discharge by an order of magnitude when compared to LSTC under-development alpha version of the software, which motivated LSTC to revisit their time integration algorithm for the new battery keywords. The enhancements enabled significantly larger time steps without introducing stability issues, removing the battery-specific time step as a limitation in most practical cases.

Another approach to reducing computation time is by using layered solid elements. The purpose of incorporating multiple layers into a single element is to enable upscaling of battery cell model while still preserving the dependence of deformation on its composition and structure. Modeling of individual layers explicitly by separate finite elements is computationally feasible only for small scale analysis. In order to implement kinematics characteristic of layered solids with repeated layer pattern, we are using solid element assemblies as templates and benchmarks to compare with layered solid developments. The use of layered elements and macro-scale meshes were both shown to significantly reduce computational requirements, and further development in these areas is underway. A new formulation for layered element has been developed by LSTC and ORNL that enables upscaling of the cell structure while accounting for different materials in the cell. The solid element assembly, layered solid, and the corresponding material models and properties are shown in Figure III-68 and Table III-15, respectively. The close match of through-thickness compression between an assembly of solid elements and the corresponding layered solid element in Figure III-69 illustrates how the upscaling can be achieved.

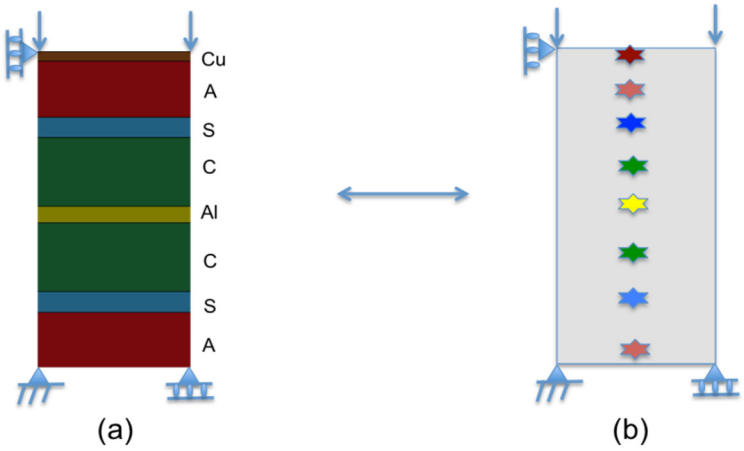


Figure III-68: Cell layer model. (a) Solid element assembly, 8 elements, (b) layered solid, 1 element, 8 integration points

## Table III-15: Cell Layer Material Models, Thickness and Properties

| Component | Material Model | Thickness (mm) | Elastic Modulus (GPa) |
|---|---|---|---|
| Copper Foil (Cu) | Mat-24 | 0.011 | 110 |
| Anode (A) | Mat-63 | 0.065 | 0.465 |
| Separator (S) | Mat-24 | 0.024 | 0.5 |
| Cathode (C) | Mat-63 | 0.080 | 0.55 |
| Aluminum Foil (Al) | Mat-24 | 0.019 | 70 |

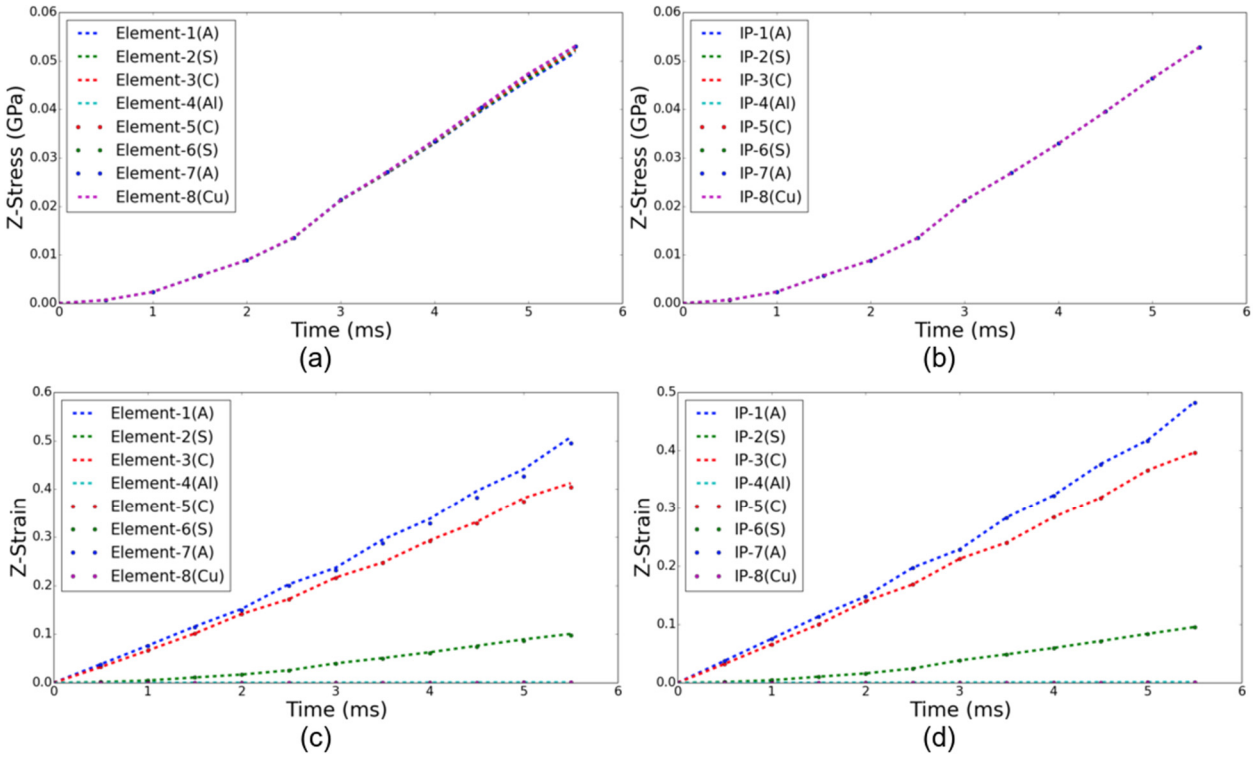


Figure III-69: Cell layer model. (a) Solid element stress distribution, 8 elements, (b) layered solid stress distribution, 1 element, 8 integration points, (c) Solid elements strain, (d) layered element strain

## Conclusions

The first year has been successful with the project on track and all milestones accomplished. A test matrix was developed for the cells, and a test site selected. A preliminary version of the software has been developed and demonstrated for external short circuit and crush leading to internal short circuit scenarios. Techniques such as the use of layered solid elements and macro scale meshes were developed to reduce simulation complexity, and demonstrated significant reductions in calculation times. In the coming year, validation experiments will be performed and simulations will be carried out to confirm the model predictions align with physical experiments.

### Products

## Presentations/Publications/Patents

1. The PI gave a presentation at the 229th ECS Meeting in San Diego, CA, on June 1, 2016.
2. The PI presented a poster on this project at the Department of Energy Annual Merit Review on June 7, 2016.
3. Two papers were presented on this project at the 14th International LS-DYNA Users Conference in Dearborn, MI, on June 13, 2016.
4. The PI gave a presentation at the 16th Annual Advanced Automotive Battery Conference in Detroit, MI, on June 15, 2016.